

Synthesis and characterisation of ferrocenylalkoxy-functionalised
polyphosphazenes for biomedical applications

A thesis submitted in accordance with the requirements for the degree
Philosophiae Doctor

in the
Department of Chemistry
Faculty of Natural and Agricultural Sciences

at the
University of the Free State

by
Maheshini Govender

Supervisor
Dr. E. Müller

Co-supervisor
Prof. J. C. Swarts

January 2020

In remembrance of
Visvanathan Govender
(1950 – 2014)

Abstract

A series of known ferrocene-containing alcohols of the type $\text{Fc}(\text{CH}_2)_m\text{OH}$, where $m = 1, 2, 3$, and 4 and $\text{Fc} = \text{Fe}^{\text{II}}[(\eta^5 - \text{C}_5\text{H}_5)(\eta^5 - \text{C}_5\text{H}_4)]$, were obtained in multiple synthetic steps and characterised with the aid of infra-red (IR) spectroscopy and ^1H nuclear magnetic resonance (NMR) spectroscopy.

A series of new poly[*tris*(2,2,2-trifluoroethoxy)(ferrocenylalkoxy)phosphazene] derivatives, - $[(\text{P}(\text{OCH}_2\text{CF}_3)_2=\text{N})-(\text{P}(\text{OCH}_2\text{CF}_3)(\text{O}(\text{CH}_2)_m\text{Fc})=\text{N})]$ - with $m = 1, 2, 3$, or 4 , were also synthesised in yields of 11.6 %, 13.5 %, 12.2 %, and 10.3 %, respectively. All synthesised ferrocenylalkoxy-functionalised polyphosphazenes were characterised with IR spectroscopy, and ^1H , ^{19}F , and ^{31}P NMR spectroscopy.

Gel permeation chromatography (GPC) was used to determine number average molecular masses relative to poly(methylmethacrylate) standards for the new poly[*tris*(2,2,2-trifluoroethoxy)-(ferrocenylalkoxy)phosphazene] derivatives; they were determined to be 6307 ($m = 1$), 3410 ($m = 2$), 7421 ($m = 3$), and 3310 ($m = 4$) daltons respectively. Increasing monomer to initiator ratios of $\text{Cl}_3\text{P}=\text{N}(\text{SiMe}_3):\text{PCl}_5 = 33:1$, 50:1 and 100:1 generated polymer molecular masses of 126 554, 168 475, and 213 731 daltons respectively against polystyrene standards.

Dilute solution viscometry measurements were used to determine the Mark-Houwink constants “a” and “K” for poly[*tris*(2,2,2-trifluoroethoxy)(ferrocenylalkoxy)phosphazenes] in the equation $[\eta] = KM_{\text{vis}}^a$; “a” was determined to be 0.87 and “K” was determined to be 0.0000634 dl/gm.

X-ray photoelectron spectroscopic (XPS) analyses of the synthesised ferrocenylalkoxy-functionalised polyphosphazenes resulted in elemental compositions of $\text{P}_{2.0}\text{N}_{2.1}\text{O}_{4.2}\text{F}_{7.8}\text{C}_{9.4}\text{H}_x\text{Fe}_{0.7}$ (theoretical $\text{P}_2\text{N}_2\text{O}_4\text{F}_9\text{C}_{17}\text{H}_{17}\text{Fe}$), $\text{P}_{2.0}\text{N}_{2.0}\text{O}_{3.4}\text{F}_{9.3}\text{C}_{5.6}\text{H}_x\text{Fe}_{0.6}$ (theoretical $\text{P}_2\text{N}_2\text{O}_4\text{F}_9\text{C}_{18}\text{H}_{19}\text{Fe}$), $\text{P}_{2.0}\text{N}_{2.1}\text{O}_{3.7}\text{F}_{9.0}\text{C}_{6.7}\text{H}_x\text{Fe}_{0.7}$ (theoretical $\text{P}_2\text{N}_2\text{O}_4\text{F}_9\text{C}_{19}\text{H}_{21}\text{Fe}$) and $\text{P}_{2.0}\text{N}_{2.1}\text{O}_{2.3}\text{F}_{7.4}\text{C}_{3.9}\text{H}_x\text{Fe}_{0.5}$ (theoretical $\text{P}_2\text{N}_2\text{O}_4\text{F}_9\text{C}_{20}\text{H}_{23}\text{Fe}$) for ferrocenylalkoxy chain lengths of $m = 1, 2, 3$, and 4 , respectively. XPS cannot measure hydrogen and the lower than expected carbon content is amongst others ascribed to the evaporation of cyclopentadienyl fragments that are liberated during irradiation while the analysis takes place. The full width at half maximum value for phosphorus and nitrogen photoelectron lines (P 2p and N 1s) were observed to be directly proportional to the alkyl chain length of the ferrocenylalkoxy groups. Results were consistent with greater polymer conformation flexibility in polymers with longer ferrocenylalkoxy side chain lengths.

An electrochemical study of the poly[*tris*(2,2,2-trifluoroethoxy)(ferrocenylalkoxy)phosphazene] derivatives resulted in ferrocenyl formal reduction potentials of $E^{\circ} = 23.5, -24.5, -35.5$, and -51.1 mV versus FcH/FcH^+ for $m = 1, 2, 3$, and 4 respectively. Electrochemical reversibility (expressed as a function of ΔE_p values) for this redox process was found to decrease as the alkyl chain length on the ferrocenylalkoxy groups increased. Chemical reversibility of these ferrocenyl-based redox processes were observed to be directly proportional to the alkyl chain length of the ferrocenylalkoxy groups implying that as the alkyl chain length increased, the ferrocenyl

redox processes became more chemically reversible. The i_{pc}/i_{pa} ratios for poly[*tris*(2,2,2-trifluoroethoxy)(ferrocenylalkoxy)

phosphazenes], with alkyl chain lengths of $m = 1, 2, 3$, and 4 , were determined to be $0.288, 0.387, 0.676$, and 0.839 respectively at a scan rate of 100 mV s^{-1} .

UV/Vis spectroscopy was used to investigate the kinetics of hydrolysis of poly[*tris*(2,2,2-trifluoroethoxy)(ferrocenylmethoxy)phosphazene] into 2,2,2-trifluoroethanol, ferrocenylmethanol, phosphates and ammonia. Pseudo first order reaction conditions were used whereby THF polymer solutions with a polymer concentration of 2.377 mM were allowed to react with THF solutions with an H_2O content of 18.51 M . Kinetic results are consistent with three equivalents of 2,2,2-trifluoroethanol being cleaved first from the polymeric main chain followed by hydrolysis of the ferrocenylmethoxy group. Observed pseudo first order rate constants are 2.0×10^{-4} and $1.29 \times 10^{-4}\text{ s}^{-1}$ respectively. The remaining polymer main chain fragments then isomerises and recoils into a new folding pattern. Finally, the remaining polymer main chain fragments hydrolyse to $(\text{NH}_4)_3\text{PO}_4$ with $k_{\text{obs}} = 2.6 \times 10^{-6}\text{ s}^{-1}$. The second order rate constant for this main chain hydrolysis is $1.38 \times 10^{-7}\text{ M}^{-1}\text{s}^{-1}$. Increasing the concentration of water from 18.52 M to 27.28 M increased the rate of main chain hydrolysis by an order of magnitude.

Differential scanning calorimetry (DSC) was utilised to evaluate the thermal properties of poly[*bis*(2,2,2-trifluoroethoxy)phosphazene] and poly[*tris*(2,2,2-trifluoroethoxy)(ferrocenylalkoxy) phosphazene] derivatives. Poly[*bis*(2,2,2-trifluoroethoxy)phosphazene] exhibited thermoplastic properties with indications of thermal cracking of the polymer main chain after multiple heating and cooling cycles. A glass transition temperature of 220 K was estimated. The onset melting temperature of this polymer was $68.46\text{ }^{\circ}\text{C}$. DSC thermograms for poly[*tris*(2,2,2-trifluoroethoxy)-(ferrocenylalkoxy)phosphazene] derivatives exhibited melting temperatures at 38.3 ($m = 1$), 42.4 ($m = 2$), 70.1 ($m = 3$), and $38.7\text{ }^{\circ}\text{C}$ ($m = 4$) respectively. Phase separation between higher and lower molecular mass fractions of poly[*tris*(2,2,2-trifluoroethoxy)(ferrocenylbutoxy)phosphazene] was also observed.

Cytotoxicity studies for all poly[*tris*(2,2,2-trifluoroethoxy)(ferrocenylalkoxy)phosphazene] derivatives against a human HeLa cervical cancer cell line resulted in half maximal inhibitory concentrations (IC_{50}) of 18.24 ($m = 1$), 40.15 ($m = 2$), 67.85 ($m = 3$), and $59.09\text{ }\mu\text{M}$ ($m = 4$) respectively. The IC_{50} value of cisplatin under the same conditions was $1.21\text{ }\mu\text{M}$. It is concluded that polyphosphazenes are successful in acting as drug delivery devices, although cisplatin is $15 - 50$ times more effective.

Keywords : polyphosphazene, ferrocene, gel permeation chromatography, Mark-Houwink, electrochemistry, hydrolysis kinetics, cytotoxicity.

Opsomming

'n Reeks bekende ferroseenbevattende alkohole, $\text{Fc}(\text{CH}_2)_m\text{OH}$ met $m = 1, 2, 3$, en 4 en $\text{Fc} = \text{Fe}^{\text{II}}[(\eta^5 - \text{C}_5\text{H}_5)(\eta^5 - \text{C}_5\text{H}_4)]$, is in veelvuldige stappe gesintetiseer en ook gekarakteriseer met behulp van infrarooispektroskopie en ^1H kernmagnetiese resonansspektroskopie.

'n Reeks nuwe poli[*tris*(2,2,2-trifluoroetoksie)(ferrosielalkoksie)fosfaseen] derivate, $-[(\text{P}(\text{OCH}_2-\text{CF}_3)_2=\text{N})-(\text{P}(\text{OCH}_2\text{CF}_3)(\text{O}(\text{CH}_2)_m\text{Fc})=\text{N})]$ - met $m = 1, 2, 3$, en 4 , is ook gesintetiseer met opbrengste van 11.6 , 13.5 , 12.2 , en 10.3% onderskeidelik. Alle gesintetiseerde ferrosielalkoksie-gefunksionaliseerde polifosfasene is gekarakteriseer met infrarooispektroskopie, asook ^1H , ^{19}F , en ^{31}P kernmagnetiese resonansspektroskopie.

Jelpermeasiekromatografie is gebruik om die getal-gemiddelde molekulêre massas vir die nuwe poli[*tris*(2,2,2-trifluoroetoksie)(ferrosielalkoksie)fosfaseen] derivate relatief ten opsigte van poli(metielmetakrielaat) standarde as 6307 ($m = 1$), 3410 ($m = 2$), 7421 ($m = 3$), en 7421 daltons ($m = 4$) onderskeidelik te bepaal. Variasies in monomeer tot iniseerder verhoudings van $\text{Cl}_3\text{P}=\text{N}(\text{SiMe}_3):\text{PCl}_5 = 33:1$, $50:1$ en $100:1$ tydens die sintese van poli[*tris*(2,2,2-trifluoroetoksie)-(ferrosielbutoksie)fosfaseen] het polifosfasene met molekulêre massas van onderskeidelik $126\ 554$, $168\ 475$, en $213\ 731$ daltons relatief ten opsigte van polistireen standarde gelewer.

Viskositeitsmetings met verdunde oplossings is gebruik om die Mark-Houwink konstantes "a" en "K" in die vergelyking $[\eta] = K\bar{M}_{\text{vis}}^a$ vir poli[*tris*(2,2,2-trifluoroetoksie)(ferrosielalkoksie)fosfaseen] te bepaal. Die waarde vir "a" is gevind as 0.6809 terwyl "K" as $0.00007251\ \text{dl/gm}$ bepaal is.

X-straalfotoelektron spektroskopiese (XFS) ontledings van die gesintetiseerde ferrosielalkoksie-gefunksionaliseerde polifosfasene het elementanalise resultate van $\text{P}_{2.0}\text{N}_{2.1}\text{O}_{4.2}\text{F}_{7.8}\text{C}_{9.4}\text{H}_x\text{Fe}_{0.7}$ (teoreties $\text{P}_2\text{N}_2\text{O}_4\text{F}_9\text{C}_{17}\text{H}_{17}\text{Fe}$), $\text{P}_{2.0}\text{N}_{2.0}\text{O}_{3.4}\text{F}_{9.3}\text{C}_{5.6}\text{H}_x\text{Fe}_{0.6}$ (teoreties $\text{P}_2\text{N}_2\text{O}_4\text{F}_9\text{C}_{18}\text{H}_{19}\text{Fe}$), $\text{P}_{2.0}\text{N}_{2.1}\text{O}_{3.7}\text{F}_{9.0}\text{C}_{6.7}\text{H}_x\text{Fe}_{0.7}$ (teoreties $\text{P}_2\text{N}_2\text{O}_4\text{F}_9\text{C}_{19}\text{H}_{21}\text{Fe}$) en $\text{P}_{2.0}\text{N}_{2.1}\text{O}_{2.3}\text{F}_{7.4}\text{C}_{3.9}\text{H}_x\text{Fe}_{0.5}$ (teoreties $\text{P}_2\text{N}_2\text{O}_4\text{F}_9\text{C}_{20}\text{H}_{23}\text{Fe}$) vir ferrosielalkosiekettinglengtes van $m = 1, 2, 3$, en 4 onderskeidelik gelewer. XFS kan nie waterstof meet nie, terwyl die lae koolstofinhoude toegeskryf is onder andere aan verdamping van siklopentadienielfragmente wat vrykom tydens bestraling gedurende die analise. Die volwydte by halfmaksimumwaardes vir die fosfor en stikstof fotoelektronlyne ($\text{P } 2\text{p}$ en $\text{N } 1\text{s}$) is direk eweredig aan die kettinglengte van die ferrosielalkoksiegroepe. Resultate was in ooreenstemming met 'n groter polimeer konformasieveranderingskapasiteit vir langer ferrosielalkoksiesykettinglengtes.

Tydens 'n elektrochemiese studie van die poli[*tris*(2,2,2-trifluoroetoksie)(ferrosielalkoksie)fosfaseen] derivate is die ferrosiel formele reduksiepotensiale onderskeidelik as $E^{\circ\prime} = 20.2$, -19.4 , -42.3 , en $-51.1\ \text{mV}$ vs. FcH/FcH^+ vir $m = 1, 2, 3$, en 4 gemeet. Elektrochemiese omkeerbaarheid vir hierdie redoksprosesse (uitgedruk as 'n funksie van ΔE_p waardes) neem af namate die alkielkettinglengte van die ferrosielalkoksiegroepe toeneem. Chemiese omkeerbaarheid van die ferrosiel-gebasseerde redoksprosesse is direk eweredig aan die alkielkettinglengte van die

ferrosenielalkoksiegroepe menende dat, soos die alkielkettinglengte toeneem, word ferrosenieloksidasie meer chemies omkeerbaar. Die i_{pc}/i_{pa} verhoudings vir hierdie redoksproseses is gemeet as 0.288 ($m = 1$), 0.387 ($m = 2$), 0.676 ($m = 3$), en 0.839 ($m = 4$) onderskeidelik tydens 'n skandeertempo van 100 mV s^{-1} .

UV/Vis spektroskopie is gebruik om die kinetika van hidrolise van poli[*tris*(2,2,2-trifluoroetoksie)(ferrosenielmetoksie)fosfaseen] na 2,2,2-trifluoroetanol, ferrosenielmetanol, fosfate en ammoniak te ondersoek. Pseudo eerste-orde reaksietoestande is gebruik deur 'n THF polimeer oplossings met polimeer konsentrasies van 2.377 mM met THF oplossings met 'n H_2O inhoud van 18.51 M te laat reageer. Kinetiese resultate is in ooreenstemming met die aanvanklike vrystelling van drie ekwivalente 2,2,2-trifluoroetanol vanaf die polimetriese hoofketting gevolg deur die hidroliese van die ferrosenielmetoksiegroepe. Waargenome pseudo eerste-orde tempokonstantes was 2.0×10^{-4} en $1.29 \times 10^{-4} \text{s}^{-1}$ onderskeidelik. Hierna isomeriseer en hervou die oorblywende polimeriese hoofkettingfragmente in 'n nuwe vroupatroon. Laastens hidroliseer die oorblywende polimeriese hoofketting fragmente na $(\text{NH}_4)_3\text{PO}_4$ met $k_{obs} = 2.6 \times 10^{-6} \text{s}^{-1}$. Die tweede-orde tempokonstante vir hierdie finale proses is $1.38 \times 10^{-7} \text{M}^{-1} \text{s}^{-1}$. 'n Toename in waterkonsentrasie vanaf 18.52 M tot 27.28 M lei tot 'n tienvoudige verhoging in reaksiesnelheid.

Differensiële skanderingskalorimetrie (DSK) is gebruik om temperatuurprofiële van die gesintetiseerde poli[*bis*(2,2,2-trifluoroetoksie)fosfaseen] en poli[*tris*(2,2,2-trifluoroetoksie)-(ferrosenielalkoksie)fosfaseen] derivate te bepaal. Poli[*bis*(2,2,2-trifluoroetoksie)fosfaseen] het termoplastiese eienskappe en indikasies van termiese kraking van die polimeerhoofketting is met veelvuldige verhitting- en afkoelsiklusse waargeneem. 'n Glasovergangstemperatuur van 220 K is geprojekteer. Die smeltpunt van hierdie polimeer is 68.46°C . DSK termogramme van poli[*tris*(2,2,2-trifluoroetoksie)(ferrosenielalkoksie)fosfaseen] derivate het smeltpunte van 38.3 ($m = 1$), 42.4 ($m = 2$), 70.1 ($m = 3$), and 38.7°C ($m = 4$) onderskeidelik uitgewys. Faseskeiding tussen groter en kleiner molekulêre massa fraksies van poli[*tris*(2,2,2-trifluoroetoksie)(ferrosenielbutoksie)fosfaseen] is ook waargeneem.

Sitotoksiese studies op alle poli[*tris*(2,2,2-trifluoroetoksie)(ferrosenielalkoksie)fosfaseen] derivate teen 'n menslike HeLa servikale kancersellyn het op halfmaksimale inhiberende konsentrasies (IC_{50}) van 18.24 ($m = 1$), 40.15 ($m = 2$), 67.85 ($m = 3$), en $59.09 \mu\text{M}$ ($m = 4$) gedui. Die IC_{50} waarde van cisplatin onder soortegelyke kondisies is $1.21 \mu\text{M}$. Die gevolg trekking wat gemaak is, is dat polifosfasene wel suksesvol as geneesmiddeldraer teen kanker gebruik kan word.

Kernwoorde: polifosfaseen, ferroseen, jelpermeasiekromatografie, Mark-Houwink, elektrochemie, hidroliese kinetika, sitotoksiteit.

Table of Contents

| | |
|---|-----------|
| List of Structures | a |
| List of Abbreviations and Units | d |
| Introduction and Aims | 1 |
| 1.1 Introduction | 1 |
| 1.2 Aims | 3 |
| References | 4 |
| Literature Survey | 5 |
| 2.1 Introduction | 5 |
| 2.2 Polyphosphazenes | 5 |
| 2.2.1 Thermal Ring-opening Polymerisation | 6 |
| 2.2.2 Living Cationic Polymerisation | 9 |
| 2.2.3 Functionalisation of poly(dichloro)phosphazenes | 12 |
| 2.2.4 Metallocene-containing polyphosphazenes | 14 |
| 2.2.5 Poly(organo)phosphazenes in biomedical applications | 16 |
| 2.3 Ferrocene | 18 |
| 2.3.1 Biomedical applications | 18 |
| 2.3.2 Synthesis of ferrocene-containing alcohols | 20 |
| 2.4 Viscometry | 23 |
| 2.5 Gel Permeation Chromatography | 25 |
| 2.6 X-Ray Photoelectron Spectroscopy | 27 |
| 2.7 Electrochemistry | 29 |
| 2.7.1 Cyclic Voltammetry | 29 |
| 2.7.2 Cyclic voltammetry of ferrocene | 30 |
| References | 33 |
| Results and Discussion | 37 |
| 3.1 Introduction | 37 |
| 3.2 Synthesis | 38 |
| 3.2.1 Ferrocenylmethanol, 3. | 38 |
| 3.2.2 2-Ferrocenylethanol, 9. | 40 |

| | |
|---|------------|
| 3.2.3 3-Ferrocenylpropanol, 13. | 42 |
| 3.2.4 4-Ferrocenylbutanol, 16. | 47 |
| 3.2.5 Trichloro(trimethylsilyl)phosphoranimine, 19. | 48 |
| 3.2.6 Poly(dichlorophosphazene), 20. | 50 |
| 3.2.7 Poly[<i>bis</i> (2,2,2-trifluoroethoxy)phosphazene], 21. | 53 |
| 3.2.8 Poly[<i>tris</i> (2,2,2-trifluoroethoxy)(ferrocenylalkoxy)phosphazene] complexes | 55 |
| 3.3 Gel Permeation Chromatography | 62 |
| 3.4 Viscometry | 64 |
| 3.5 X-ray Photoelectron Spectroscopy | 69 |
| 3.5.1 Poly(dichlorophosphazene), 20. | 69 |
| 3.5.2 Poly[<i>bis</i> (2,2,2-trifluoroethoxy)phosphazene], 21. | 71 |
| 3.5.3 Poly[<i>tris</i> (2,2,2-trifluoroethoxy)(ferrocenylalkoxy)phosphazene] complexes 22 - 25 | 74 |
| 3.6 Cyclic Voltammetry | 81 |
| 3.7 Kinetics of hydrolysis | 86 |
| 3.8 Differential Scanning Calorimetry (DSC) | 92 |
| 3.9 Cytotoxicity | 99 |
| References | 104 |
| Experimental | 107 |
| 4.1 Introduction | 107 |
| 4.2 Materials | 107 |
| 4.3 Spectroscopic Measurements | 107 |
| 4.4 Synthesis of ferrocene derivatives | 108 |
| 4.4.1 Ferrocene carboxaldehyde | 108 |
| 4.4.2 1-Ferrocenylmethanol | 109 |
| 4.4.3 Sodium-1-ferrocenylmethoxide | 110 |
| 4.4.4 <i>N,N</i> -Dimethylaminomethylferrocene | 110 |
| 4.4.5 <i>N,N,N</i> -trimethylaminomethylferrocene iodide | 111 |
| 4.4.6 Ferroceneacetonitrile | 111 |
| 4.4.7 Ferroceneacetic acid | 112 |
| 4.4.8 2-Ferrocenylethanol | 112 |
| 4.4.9 Sodium-2-ferrocenylethoxide | 113 |
| 4.4.10 Ethyl-3-ferrocenylethenoate | 114 |
| 4.4.11 Ethyl-3-ferrocenylethanoate | 115 |

| | |
|---|------------|
| 4.4.12 3-Ferrocenylpropanol | 115 |
| 4.4.13 Sodium-3-ferrocenylpropoxide | 116 |
| 4.4.14 3-Ferrocenoylpropionic acid | 116 |
| 4.4.15 4-Ferrocenylbutanol | 117 |
| 4.4.16 Sodium-4-ferrocenylbutoxide | 118 |
| 4.5 Synthesis of polyphosphazenes | 118 |
| 4.5.1 Trichloro(trimethylsilyl)phosphoranimine | 118 |
| 4.5.2 Poly(2,2,2-trifluoroethoxy)phosphazene | 119 |
| 4.5.3 Poly((2,2,2-trifluoroethoxy)(ferrocenylmethoxy))phosphazene | 120 |
| 4.5.4 Poly((2,2,2-trifluoroethoxy)(ferrocenylethoxy))phosphazene | 121 |
| 4.5.5 Poly((2,2,2-trifluoroethoxy)(ferrocenylpropoxy))phosphazene | 122 |
| 4.5.6 Poly((2,2,2-trifluoroethoxy)(ferrocenylbutoxy))phosphazene | 123 |
| 4.6 Viscometry | 124 |
| 4.7 Electrochemistry | 124 |
| 4.8 X-ray Photoelectron Spectroscopy | 124 |
| 4.9 Gel Permeation Chromatography | 125 |
| 4.9.1 Shimadzu GPC Manual | 126 |
| 4.10 UV/Vis Kinetics | 134 |
| 4.11 Differential Scanning Calorimetry | 135 |
| 4.12 Cytotoxicity | 135 |
| 4.12.1 Cell Culture | 135 |
| 4.12.2 Cytotoxicity Assay | 135 |
| References | 136 |
| Summary and Future Perspectives | 137 |
| 5.1 Summary | 137 |
| 5.2 Future Perspectives | 141 |
| References | 142 |
| Appendix | i |
| IR Spectra | i |
| Spectrum 1: Ferrocenecarboxaldehyde, 2 | i |
| Spectrum 2: 1-Ferrocenylmethanol, 3 | i |
| Spectrum 3: <i>N,N</i> -Dimethylaminomethylferrocene, 5 | ii |

| | |
|---|------|
| Spectrum 4: <i>N,N,N</i> -Trimethylaminomethylferrocene iodide, 6 | ii |
| Spectrum 5: Ferrocenylacetonitrile, 7 | iii |
| Spectrum 6: 2-Ferrocenylacetic acid, 8 | iii |
| Spectrum 7: 2-Ferrocenylethanol, 9 | iv |
| Spectrum 8: Ethyl-3-ferrocenylethenoate, 11 | iv |
| Spectrum 9: Ethyl-3-ferrocenylethanoate, 12 | v |
| Spectrum 10: 3-Ferrocenylpropanol, 13 | v |
| Spectrum 11: 3-Ferrocenylpropionic acid, 15 | vi |
| Spectrum 12: 4-Ferrocenylbutanol, 16 | vi |
| Spectrum 13: Trichloro(trimethylsilyl)phosphoranimine, 19 | vii |
| Spectrum 14: Poly(dichloro)phosphazene, 20 | vii |
| Spectrum 15: Poly[<i>bis</i> (2,2,2-trifluoroethoxy)phosphazene], 21 | viii |
| Spectrum 16: Poly[<i>tris</i> (2,2,2-trifluoroethoxy)(ferrocenylmethoxy)phosphazene], 22 | viii |
| Spectrum 17: Poly[<i>tris</i> (2,2,2-trifluoroethoxy)(ferrocenylethoxy)phosphazene], 23 | ix |
| Spectrum 18: Poly[<i>tris</i> (2,2,2-trifluoroethoxy)(ferrocenylpropoxy)phosphazene], 24 | ix |
| Spectrum 19: Poly[<i>tris</i> (2,2,2-trifluoroethoxy)(ferrocenylbutoxy)phosphazene], 25 | x |

¹H NMR Spectra

x

| | |
|---|-------|
| Spectrum 20: Ferrocenecarboxaldehyde, 2 | x |
| Spectrum 21: 1-Ferrocenylmethanol, 3 | xi |
| Spectrum 22: <i>N,N</i> -Dimethylaminomethylferrocene, 5 | xi |
| Spectrum 23: Ferrocenylacetonitrile, 7 | xii |
| Spectrum 24: Ferrocenylacetic acid, 8 | xii |
| Spectrum 25: 2-Ferrocenylethanol, 9 | xiii |
| Spectrum 26: Ethyl-3-ferrocenylethenoate, 11 | xiii |
| Spectrum 27: Ethyl-3-ferrocenylethanoate, 12 | xiv |
| Spectrum 28: 3-Ferrocenylpropanol, 13 | xiv |
| Spectrum 29: 3-Ferrocenylpropionic acid, 15 | xv |
| Spectrum 30: 4-Ferrocenylbutanol, 16 | xv |
| Spectrum 31: Trichloro(trimethylsilyl)phosphoranimine, 19 | xvi |
| Spectrum 32: Poly[<i>bis</i> (2,2,2-trifluoroethoxy)phosphazene], 21 | xvi |
| Spectrum 33: Poly[<i>tris</i> (2,2,2-trifluoroethoxy)(ferrocenylmethoxy)phosphazene], 22 | xvii |
| Spectrum 34: Poly[<i>tris</i> (2,2,2-trifluoroethoxy)(ferrocenylethoxy)phosphazene], 23 | xvii |
| Spectrum 35: Poly[<i>tris</i> (2,2,2-trifluoroethoxy)(ferrocenylpropoxy)phosphazene], 24 | xviii |
| Spectrum 36: Poly[<i>tris</i> (2,2,2-trifluoroethoxy)(ferrocenylbutoxy)phosphazene], 25 | xviii |

¹³C NMR Spectra

xix

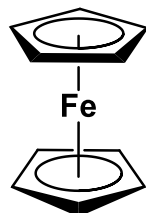
| | |
|---------------------------------------|-----|
| Spectrum 37: 1-Ferrocenylmethanol, 3 | xix |
| Spectrum 38: 2-Ferrocenylethanol, 9 | xix |
| Spectrum 39: 3-Ferrocenylpropanol, 13 | xx |

| | |
|--|---------------|
| Spectrum 40: 4-Ferrocenylbutanol, 16 | xx |
| ³¹P NMR Spectra | xxi |
| Spectrum 41: Trichloro(trimethylsilyl)phosphoranimine, 19 | xxi |
| Spectrum 42: Poly(dichloro)phosphazene, 20 | xxi |
| Spectrum 43: Poly[<i>bis</i> (2,2,2-trifluoroethoxy)phosphazene], 21 | xxii |
| Spectrum 44: Poly[<i>tris</i> (2,2,2-trifluoroethoxy)(ferrocenylmethoxy)phosphazene], 22 | xxii |
| Spectrum 45: Poly[<i>tris</i> (2,2,2-trifluoroethoxy)(ferroncenylethoxy)phosphazene], 23 | xxiii |
| Spectrum 46: Poly[<i>tris</i> (2,2,2-trifluoroethoxy)(ferrocenylpropoxy)phosphazene], 24 | xxiii |
| Spectrum 47: Poly[<i>tris</i> (2,2,2-trifluoroethoxy)(ferrocenylbutoxy)phosphazene], 25 | xxiv |
| ¹⁹F NMR Spectra | xxiv |
| Spectrum 48: Poly[<i>bis</i> (2,2,2-trifluoroethoxy)phosphazene], 21 | xxiv |
| Spectrum 49: Poly[<i>tris</i> (2,2,2-trifluoroethoxy)(ferrocenylmethoxy)phosphazene], 22 | xxv |
| Spectrum 50: Poly[<i>tris</i> (2,2,2-trifluoroethoxy)(ferrocenylethoxy)phosphazene], 23 | xxv |
| Spectrum 51: Poly[<i>tris</i> (2,2,2-trifluoroethoxy)(ferrocenylpropoxy)phosphazene], 24 | xxvi |
| Spectrum 52: Poly[<i>tris</i> (2,2,2-trifluoroethoxy)(ferrocenylbutoxy)phosphazene], 25 | xxvi |
| GPC Chromatograms | xxvii |
| Chromatogram 1: Poly[<i>bis</i> (2,2,2-trifluoroethoxy)phosphazene], 21 | xxvii |
| Chromatogram 2: Poly[<i>tris</i> (2,2,2-trifluoroethoxy)(ferrocenylmethoxy)phosphazene], 22 | xxvii |
| Chromatogram 3: Poly[<i>tris</i> (2,2,2-trifluoroethoxy)(ferrocenylethoxy)phosphazene], 23 | xxviii |
| Chromatogram 4: Poly[<i>tris</i> (2,2,2-trifluoroethoxy)(ferrocenylpropoxy)phosphazene], 24 | xxviii |
| Chromatogram 5: Poly[<i>tris</i> (2,2,2-trifluoroethoxy)(ferrocenylbutoxy)phosphazene], 25 | xxix |
| GPC Calibration Curve | xxx |
| Chromatograms – Polystyrene Standards | xxxi |
| Chromatogram 6: Poly(2,2,2-trifluoroethoxy)(ferrocenylbutoxy)phosphazene, 25 (213 731 daltons) | xxxii |
| Chromatogram 7: Poly(2,2,2-trifluoroethoxy)(ferrocenylbutoxy)phosphazene, 25 (168 475 daltons) | xxxii |
| Chromatogram 8: Poly(2,2,2-trifluoroethoxy)(ferrocenylbutoxy)phosphazene, 25 (126 554 daltons) | xxxii |
| XPS Spectra | xxxiii |
| Poly(dichloro)phosphazene, 20 | xxxiii |
| Poly[<i>bis</i> (2,2,2-trifluoroethoxy)phosphazene], 21 | xxxiv |
| Poly[<i>tris</i> (2,2,2-trifluoroethoxy)(ferrocenylmethoxy)phosphazene], 22 | xxxv |
| Poly[<i>tris</i> (2,2,2-trifluoroethoxy)(ferrocenylethoxy)phosphazene], 23 | xxxvi |
| Poly[<i>tris</i> (2,2,2-trifluoroethoxy)(ferrocenylpropoxy)ferrocene], 24 | xxxvii |
| Poly[<i>tris</i> (2,2,2-trifluoroethoxy)(ferrocenylbutoxy)phosphazene], 25 | xxxviii |
| DSC Calorigrams | xxxix |
| Poly[<i>bis</i> (2,2,2-trifluoroethoxy)phosphazene], 21 | xxxix |
| Poly[<i>tris</i> (2,2,2-trifluoroethoxy)(ferrocenylmethoxy)phosphazene], 22 – Day 1 | xl |
| Poly[<i>tris</i> (2,2,2-trifluoroethoxy)(ferrocenylmethoxy)phosphazene], 22 – Day 2 | xl |

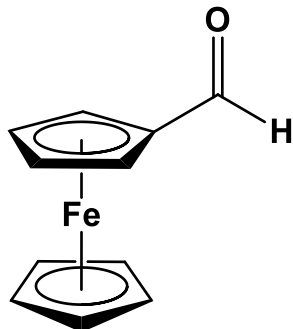
| | |
|--|-------|
| Poly[<i>tris</i> (2,2,2-trifluoroethoxy)(ferrocenylethoxy)phosphazene], 23 – Day 1 | xli |
| Poly[<i>tris</i> (2,2,2-trifluoroethoxy)(ferrocenylethoxy)phosphazene], 23 – Day 2 | xli |
| Poly[<i>tris</i> (2,2,2-trifluoroethoxy)(ferrocenylpropoxy)phosphazene], 24 – Day 1 | xlii |
| Poly[<i>tris</i> (2,2,2-trifluoroethoxy)(ferrocenylpropoxy)phosphazene], 24 – Day 2 | xlii |
| Poly[<i>tris</i> (2,2,2-trifluoroethoxy)(ferrocenylbutoxy)phosphazene], 25 – Day 1 | xliii |
| Poly[<i>tris</i> (2,2,2-trifluoroethoxy)(ferrocenylbutoxy)phosphazene], 25 – Day 2 | xliii |

Declaration

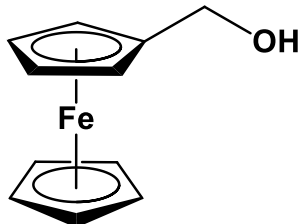
List of Structures



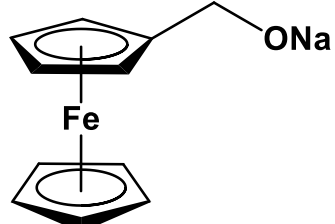
1



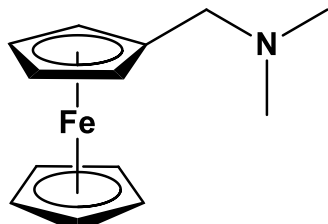
2



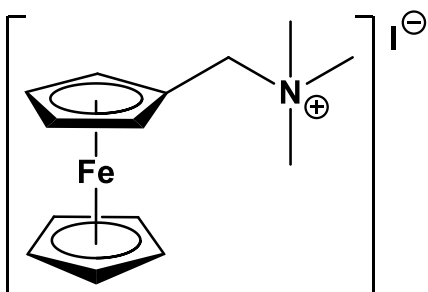
3



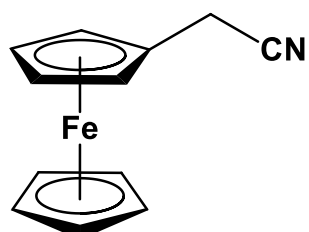
4



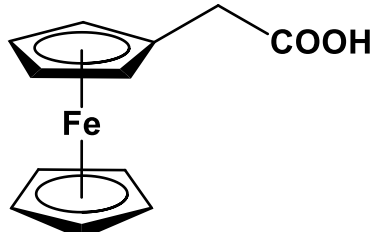
5



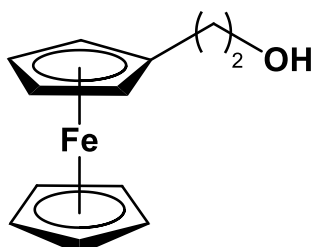
6



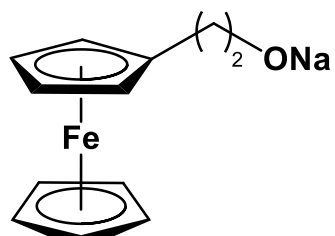
7



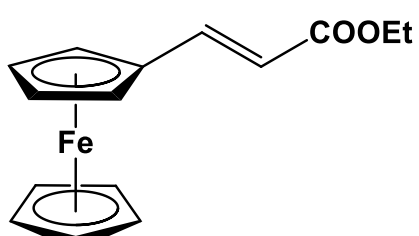
8



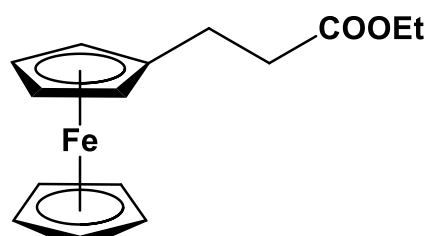
9



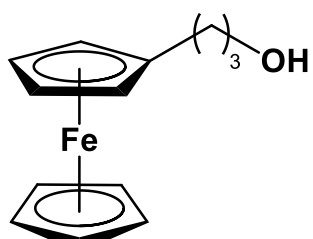
10



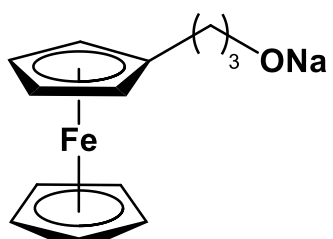
11



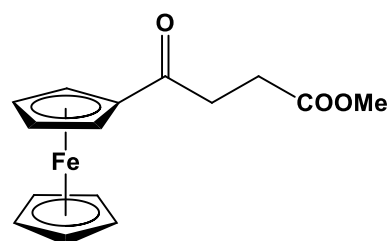
12



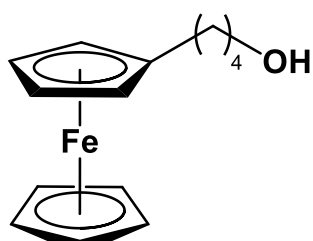
13



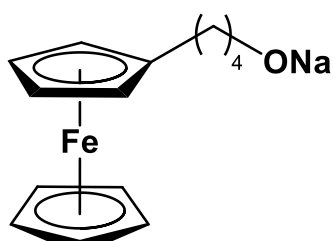
14



15



16



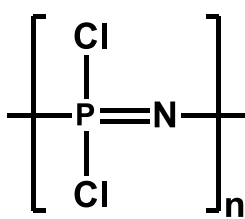
17



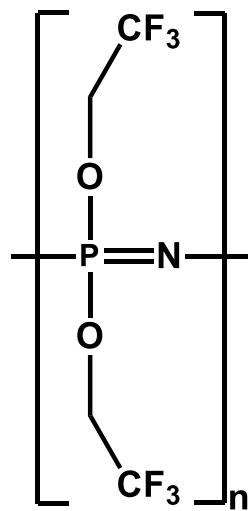
18



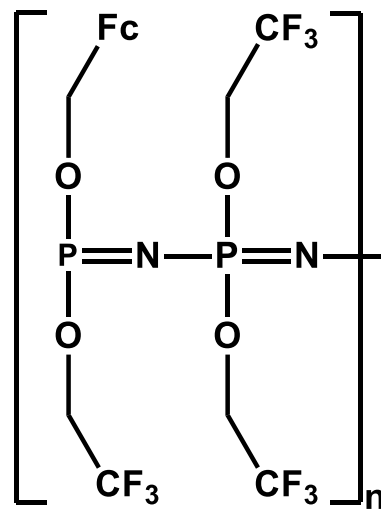
19



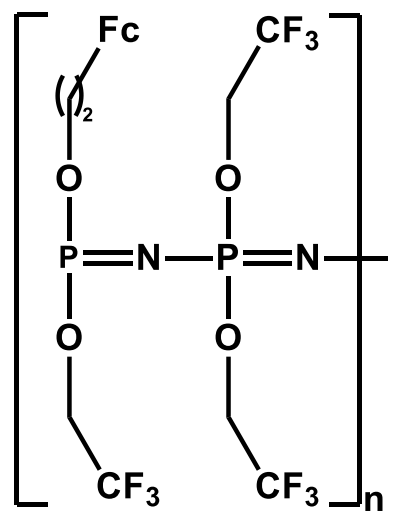
20



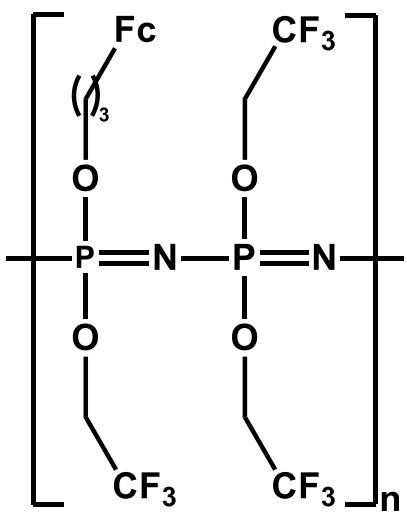
21



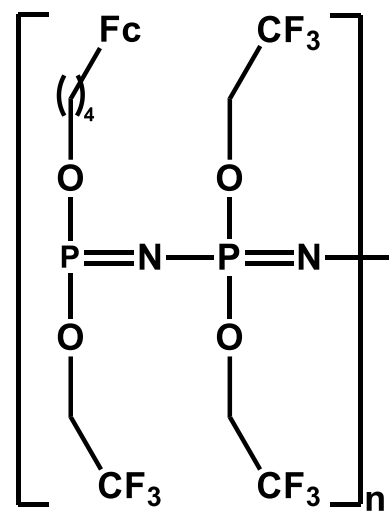
22



23



24



25

List of Abbreviations and Units

| | |
|---------------------|---|
| ΔE_p | separation of forward and reverse peak potentials |
| ^{13}C NMR | carbon nuclear magnetic resonance |
| ^{19}F NMR | fluorine nuclear magnetic resonance |
| ^1H NMR | proton nuclear magnetic resonance |
| ^{31}P NMR | phosphorus nuclear magnetic resonance |
| AR | atomic ratio |
| BE | binding energies |
| ca. | <i>circa</i> (approximately) |
| CV | cyclic voltammetry/cyclic voltammogram |
| DCM | dichloromethane |
| DMAc | <i>N,N</i> -dimethylacetamide |
| DMEM | Dulbecco's Modified Eagle Medium |
| DSC | differential scanning calorimetry |
| E° | formal reduction potential |
| EAT | Ehrlich ascites tumour |
| E_{pa} | peak anodic potential |
| E_{pc} | peak cathodic potential |
| eV | electron volt |
| Fc | ferrocenyl group |
| Fc^* | decamethylferrocene |
| FcH | ferrocene |
| FWHM | full width at half maximum |
| GPC | gel permeation chromatography |
| i_{pa} | peak anodic current |
| i_{pc} | peak cathodic current |
| IR | infra-red |
| LSV | linear sweep voltammetry |
| LVN | intrinsic viscosity |
| m | alkyl chain length |
| M | molar |
| mM | millimolar |
| mmol | millimole |
| mV | millivolts |
| mV/s | millivolts per second |
| PMMA | poly(methylmethacrylate) |

| | |
|--------|----------------------------------|
| SEC | size exclusion chromatography |
| SRB | sulforhodamine B |
| SW | square wave |
| TEA | triethylamine |
| THF | tetrahydrofuran |
| THF-d6 | deuterated tetrahydrofuran |
| UFS | University of the Free State |
| UV | ultraviolet |
| XPS | X-ray photoelectron spectroscopy |

1

Introduction and Aims

1.1 Introduction

Cancer is a group of devastating diseases caused by abnormal cell growth and is the second leading cause of death worldwide.¹ In 2015, the global burden of disease study determined that 90 million people were affected with cancer, of which 8.8 million deaths were cancer related.¹ Despite any individual being at risk of developing cancer, various factors (age, genetics, environmental pollution, infection, tobacco use, etc.) have been found to increase the incidence of diagnosed cancer cases.² Depending on the type and severity of the cancer, a wide variety of existing treatment options range from chemotherapy to surgery.³ Dire need of new and effective treatments have encouraged the establishment of the Federal Drug Administration breakthrough therapy designation, which has boosted oncology research and development since 2012.³

The most prominent properties of cancer to consider upon treatment are cancer cells ability to proliferate as well as becoming resistant to current treatment options. Treatments such as radiation and chemotherapy are non-selective and cause much harm to the healthy cells in the body and are often too hazardous to the patient to effectively combat the cancer cells. Therefore, a large focus in anticancer research is on finding treatment options to selectively eradicate cancer cells. Treatment options which can target the primary tumour, as well as metastatic foci, may increase efficacy and enhance patient survival rate.⁴ Polymeric drug delivery systems are one of several popular research topics in anticancer research as the aim is to produce treatment material which “deliver” the chemotherapeutic agent directly to the cancer site. Utilisation of a biomedically suitable polymer, targeting molecules and chemotherapeutic agents may increase the efficacy of the treatment as well as reduce side effects.⁵

Polyphosphazenes are inorganic polymers, consisting of alternating phosphorus and nitrogen atoms,⁶ in the polymer backbone (Figure 1.1, left). Insight into the properties and modification of soluble inorganic poly(dichloro)phosphazenes started with H.R. Allcock in the 1960s.⁵ Poly(organo)phosphazenes (Figure 1.1, right) have gained attention in research and development due to the formation of diverse skeletal architectures as well as diverse possibilities and combinations of additional functional moieties.⁶

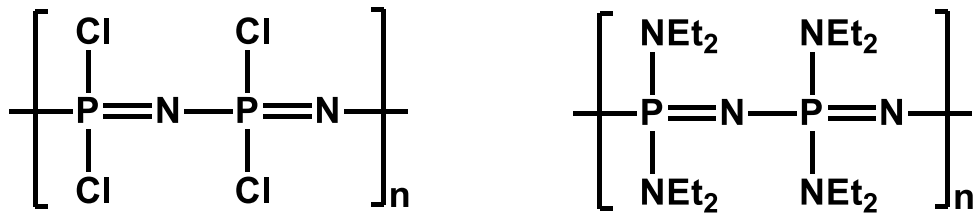


Figure 1.1: Structure of poly(dichlorophosphazene) and poly[bis(diethylamine)phosphazene].

The availability of many different synthetic techniques of poly(organo)phosphazenes have allowed for the preparation of a large range of industrially important phosphazene-based materials such as cross-linked rubbers, elastomers, gels, fibers, films, and hydrogels to name a few.^{5,6} Polyphosphazenes containing multifunctional moieties, such as vitamin substituents, have been developed in literature for use in drug and gene delivery.^{7,8} Polymer-drug conjugates have also been designed and synthesised for use in cancer therapeutics.⁹ Polyphosphazenes in general are biocompatible because the $-(\text{P}=\text{N})_n-$ main chain unit hydrolyses to H_3PO_4 and NH_3 or NH_4OH substances which are not hazardous in living tissue. H_3PO_4 is the acid additive in Coca-Cola, while NH_3 is a chemical made by the bacteria in the intestines and body tissue as proteins are processed. This waste product is excreted from the body by the liver. Biologically active poly(organo)phosphazenes is the main focus for this study.

Functionalisation of the polyphosphazene backbone with water soluble moieties have been used in biomedical applications.^{6,10,11} Moieties such as chemotherapeutic agents as well as cancer targeting agents may be anchored onto the polyphosphazene backbone to prepare a cancer targeting drug delivery system. Further interest in biomedical applications of polyphosphazenes stem from the decomposition of poly(organo)phosphazenes, whereby the resulting medium is a mixture of non-toxic phosphates and ammonia.^{5,12} H. R. Allcock also indicated a controlled release of covalently bonded moieties due to degradation of poly(organo)phosphazenes via hydrolysis.⁶ Poly(organo)phosphazenes were therefore selected as the polymeric backbone carrying chemotherapeutic moieties for the purposes of this study.

From the University of the Free State (UFS) laboratory, ferrocenylalkyl-containing alcohols have been shown to have potential as antineoplastic drugs against HeLa cancer cells.¹³ A relationship between the electrochemistry of ferrocenylalkyl-containing alcohols and chemotherapeutic activity has also been demonstrated in literature.^{13,14} Therefore, these ferrocenylalkyl-containing alcohols

have been selected as the chemotherapeutic agent to be anchored onto a biomedical carrier-polyphosphazene for the purpose of this study.

1.2 Aims

With the information given in the introduction, the following goals were set for this study:

- i. Synthesis and characterisation of a series of antineoplastic ferrocene-containing alcohols of the form $\text{Fc}(\text{CH}_2)_m\text{OH}$, where $m = 1, 2, 3$, and 4 ; $\text{Fc} = \text{Fe}^{\text{II}} [(\eta^5 - \text{C}_5\text{H}_5)(\eta^5 - \text{C}_5\text{H}_4)]$, the ferrocenyl group, Figure 1.2, left.

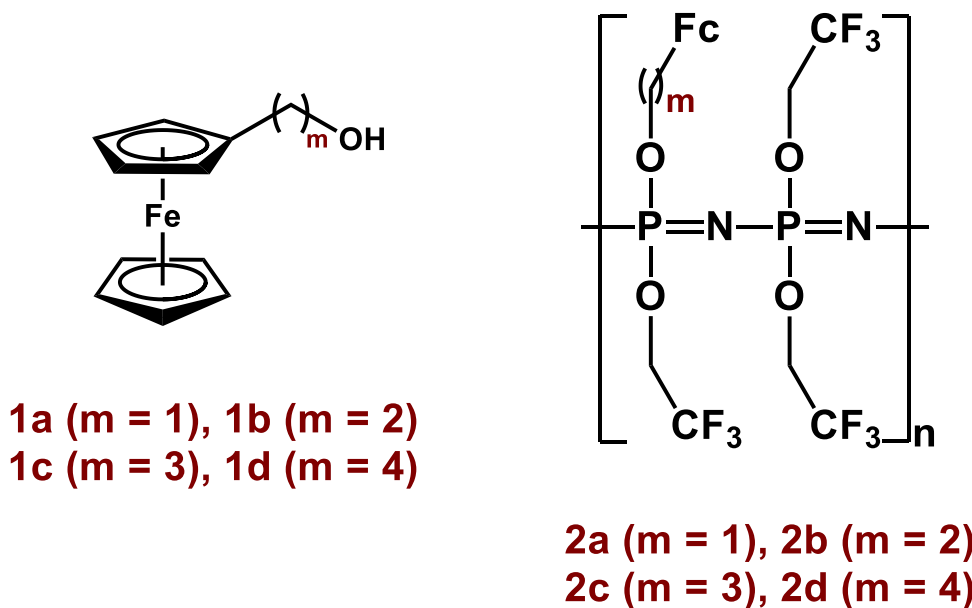


Figure 1.2: Target ferrocenylalcohols and polyphosphazenes for this study.

- ii. Synthesis and characterisation of poly(dichloro)phosphazenes, $-(\text{NPCl}_2)_n-$, where $n > 100$, as a potential drug carrier precursor, Figure 1.1, left.
- iii. Synthesis and characterisation of potential polymeric drug carrier/ferrocene-drug conjugates, by anchoring (i) onto (ii), Figure 1.2, right.
- iv. Molecular weight determinations of synthesised polyphosphazenes described in (iii) above, by viscometry and gel permeation chromatography (GPC).
- v. An electrochemical study of the synthesised ferrocene-containing polyphosphazenes described in (iii) above, to determine redox properties by means of cyclic voltammetry, linear sweep, and square wave electrochemistry.

- vi. An X-ray photoelectron spectroscopic study of the synthesised ferrocene-containing polyphosphazenes described in (iii) above. From this spectroscopic study, elemental compositions could also be found for every polymer.
- vii. Illumination of the hydrolysis kinetics of one example of the synthesised polymers, poly(ferrocenylmethoxy)phosphazene, monitored by UV/vis spectroscopy.
- viii. A thermal analysis study utilising differential scanning calorimetry to highlight the thermal properties of the new ferrocene-containing polyphosphazenes described in (iii).
- ix. Determination of the cytotoxicity of the synthesised poly(ferrocenylalkoxy)phosphazenes against the HeLa cell line and comparison with the cytotoxicity of cisplatin.

References

- 1 *The Lancet*, 2016, **388**, 1659–1724.
- 2 *Global Cancer Facts & Figures*, American Cancer Society, Atlanta, 2nd edn., 2011.
- 3 J. D. Patel, L. Krilov, S. Adams, C. Aghajanian, E. Basch, M. S. Brose, W. L. Carroll, M. de Lima, M. R. Gilbert, M. G. Kris, J. L. Marshall, G. A. Masters, S. J. O'Day, B. Polite, G. K. Schwartz, S. Sharma, I. Thompson, N. J. Vogelzang and B. J. Roth, *J. Clin. Oncol. Off. J. Am. Soc. Clin. Oncol.*, 2014, **32**, 129–160.
- 4 D. Yong Lu and T. R. Lu, *Adv. Tech. Biol. Med.*, DOI:10.4172/2379-1764.1000106.
- 5 S. Rothemund and I. Teasdale, *Chem. Soc. Rev.*, 2016, **45**, 5200–5215.
- 6 H. R. Allcock, *Soft Matter*, 2012, **8**, 7521–7532.
- 7 I. Teasdale, O. Brüggemann, I. Teasdale and O. Brüggemann, *Polymers*, 2013, **5**, 161–187.
- 8 N. L. Morozowich, A. L. Weikel, J. L. Nichol, C. Chen, L. S. Nair, C. T. Laurencin and H. R. Allcock, *Macromolecules*, 2011, **44**, 1355–1364.
- 9 C. Chun, S. M. Lee, C. W. Kim, K.-Y. Hong, S. Y. Kim, H. K. Yang and S.-C. Song, *Biomaterials*, 2009, **30**, 4752–4762.
- 10 H. Allcock, *Phosphorus-Nitrogen Compounds: Cyclic, Linear, and High Polymeric Systems*, Elsevier, 2012.
- 11 A. K. Andrianov, *J. Inorg. Organomet. Polym. Mater.*, 2006, **16**, 397–406.
- 12 H. R. Allcock, *J. Inorg. Organomet. Polym. Mater.*, 2005, **15**, 57–65.
- 13 R. F. Shago, J. C. Swarts, E. Kreft and C. E. J. V. Rensburg, *Anticancer Res.*, 2007, **27**, 3431–3433.
- 14 W. L. Davis, R. F. Shago, E. H. G. Langner and J. C. Swarts, *Polyhedron*, 2005, **24**, 1611–1616.

2.1 Introduction

A literature review of the synthesis and physical methods relevant to this study is presented in this chapter. Chapter 3 contains the results of the author's own research, while chapter 4 contains all experimental procedures by the author.

2.2 Polyphosphazenes

Polyphosphazenes (phosphonitrilic polymers) are inorganic-organic hybrid polymers consisting of a phosphorus and nitrogen backbone.¹ The phosphorus atoms contain side groups, usually of organic nature, which provide added properties to the characteristics of the polymer.^{1,2} Polyphosphazenes also exhibit a wide range of skeletal architectures, e.g., linear, block copolymeric, star, and dendritic polymers (Figure 2.1).^{3,4} Side groups, skeletal architectures, and molecular mass ranges all have an impact on the physical properties of the polyphosphazene polymers (e.g., water solubility, water repellent, flame retardant, stable at high temperatures and resistance to UV radiation).⁵

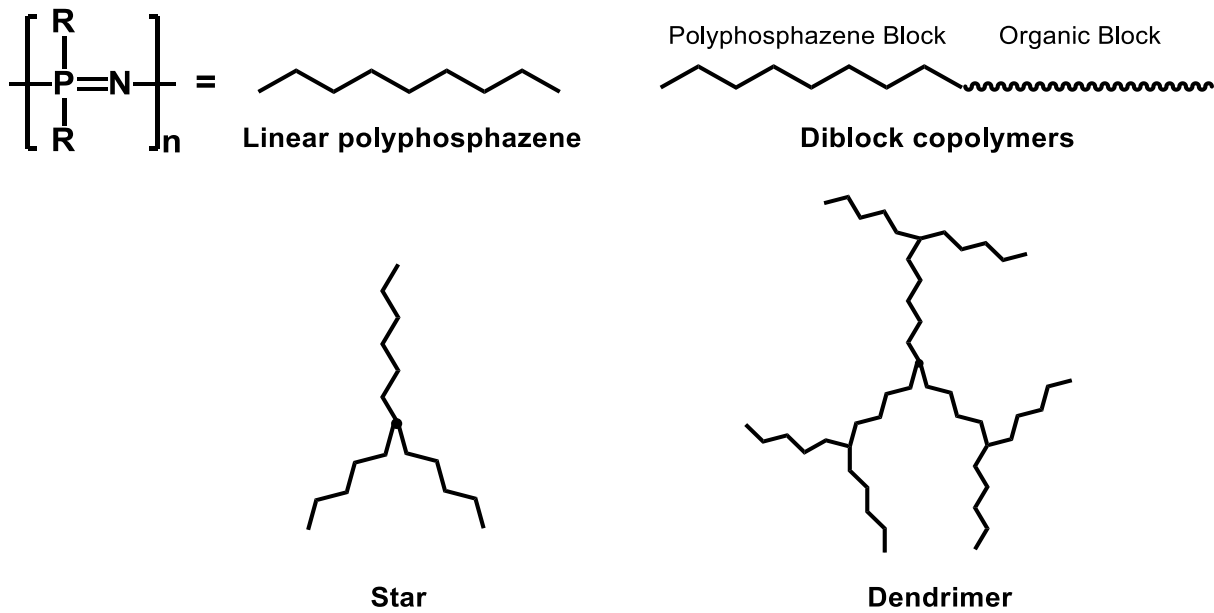


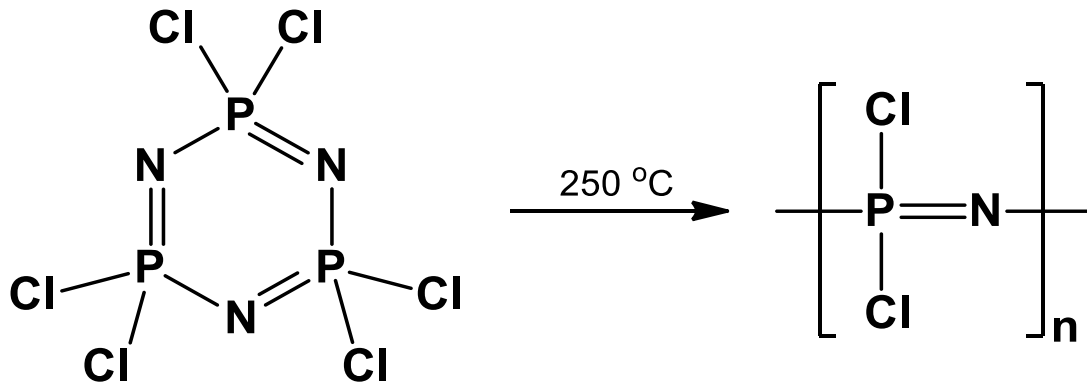
Figure 2.1: Some of the different skeletal architectures of polyphosphazenes, diagram adapted from reference 3.

Poly(dichloro)phosphazenes were first reported in literature by H. N. Stokes as a stable, high molecular mass product with a general formula of $(\text{PNCl}_2)_x$ from a high temperature reaction of cyclic chlorophosphanes.⁶ The stable product was described as an “insoluble rubber” which may have been a cross-linked polyphosphazene polymer.⁷ Presence of impurities (especially H_2O) in the polymerisation of chlorinated cyclophosphazenes caused the product to form insoluble, cross-linked products.⁷ H. Allcock later developed a synthetic method to prepare soluble, linear poly(dichloro)phosphazenes utilising a controlled ring-opening polymerisation of highly pure hexachlorocyclotriphosphazene trimer, in the absence of moisture.^{8,9} Functionalisation of the phosphorus atom with primary and secondary amines were then reported in literature, forming poly(diamino)phosphazenes.¹⁰

Currently, there are two main methods used to synthesise soluble poly(dichloro)phosphazenes, thermal ring-opening polymerisation of highly pure hexachlorocyclotriphosphazene trimer and living cationic polymerisation of phosphoranimine monomer.¹¹

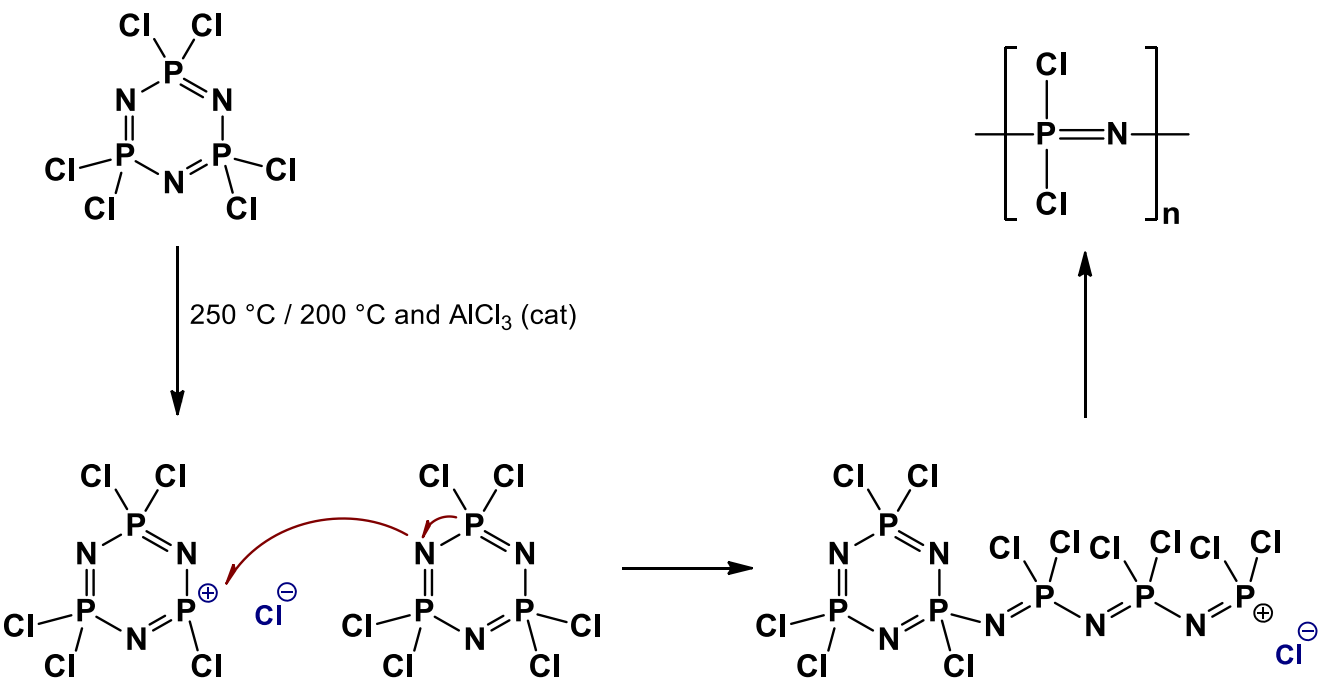
2.2.1 Thermal Ring-opening Polymerisation

Hexachlorocyclotriphosphazene (or phosphonitrilic chloride trimer; a tetramer may also be utilised) monomer is synthesised from phosphorus pentachloride and ammonium chloride and is commercially available.³ Thermal ring-opening polymerisation at $250\text{ }^\circ\text{C}$ produces soluble, high molecular mass polymers; however, with broad polydispersities (Scheme 2.1).⁵



Scheme 2.1: Thermal ring-opening polymerisation of hexachlorocyclotriphosphazene to synthesise poly(dichloro)phosphazene.

The ring-opening polymerisation occurs at 250 °C, due to the high temperature cleavage of the chlorine atoms from hexachlorocyclotriphosphazene.² Temperature control is essential for both fast polymerisation and synthesis of linear (uncross-linked) polyphosphazenes. A temperature of 250 °C is required for cleavage of the chlorine atoms, which initiates the polymerisation reaction (Scheme 2.2).² Below 250 °C, prohibitively slow polymerisation would occur due to fewer Cl atoms being cleaved.² However, higher temperatures cause significant cross-linked (non-linear) polyphosphazenes.² Lewis acid catalysts, e.g., AlCl₃, may be used to catalyse the polymerisation at lower temperatures (200 °C), which may narrow the polydispersity and lower the molecular mass of the polymer that is formed.^{2,5} High molecular masses of greater than 1 000 000 daltons are usually formed with the ring-opening polymerisation method; however, reports in literature for poly(organo)phosphazenes synthesised with this method range between 100 000 and 700 000 daltons.^{12,13} The drawbacks of this method include the high temperature required (250 °C) to initiate polymerisation and the lack of molecular mass control.¹⁴

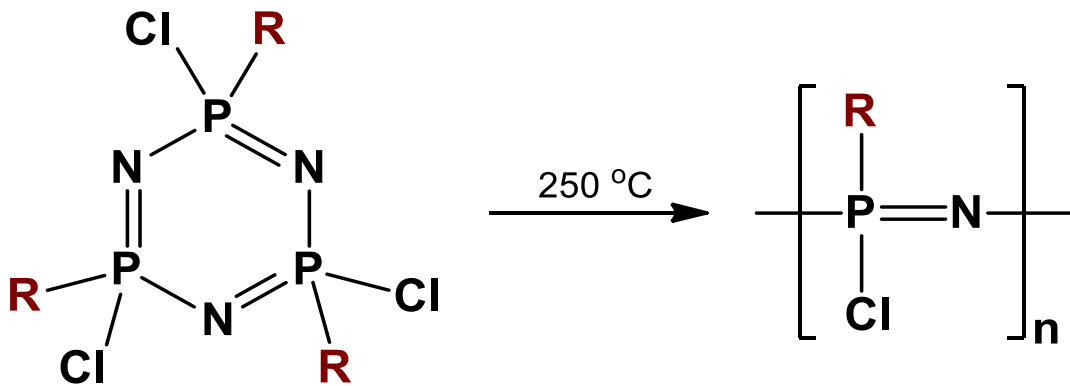


Scheme 2.2: Mechanism for the ring-opening polymerisation of hexachlorocyclotriphosphazene to synthesise poly(dichloro)phosphazene.

When thermal ring-opening polymerisation is utilised, functionalised polyphosphazenes may be synthesised in one of two methods⁵:

1. Polymerisation of hexachlorocyclotriphosphazene to form poly(dichloro)phosphazene and then functionalisation of the chloro groups
2. Functionalisation of the chloro groups on hexachlorocyclotriphosphazene and then polymerisation to form poly(organo)phosphazenes

Method 1, functionalisation of the polymer after polymerisation, is the most popular route in literature, since functionalisation of the highly reactive polar P-Cl bond is easily achieved by oxygen- and nitrogen-containing nucleophiles (See section 2.2.3 below).^{15,16} Method 2, functionalisation of the chloro groups on hexachlorocyclotriphosphazene, have also been noted in literature (Scheme 2.3). However, polymerisation will only occur if (i) the phosphazene trimer contains both substituted organic groups and halogen (in most cases, chlorine) groups, (ii) organic substituents possess minimal steric hindrance effects so as to not inhibit chain propagation and (iii) sufficient ring strain is present from the organic group to promote ring-opening polymerisation.⁹

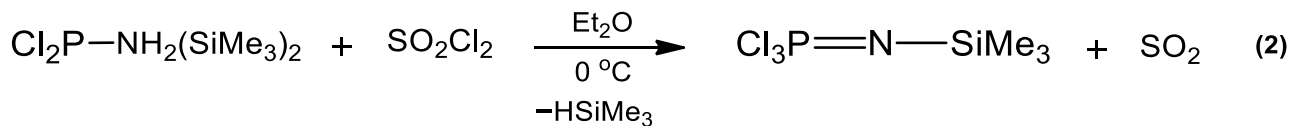


Scheme 2.3: Ring-opening polymerisation of partially substituted hexachlorocyclotriphosphazene to synthesise poly(organo)phosphazenes (R = alkyl, aryl).

Partial halogen replacement of hexachlorocyclotriphosphazene with alkoxy substituents can be achieved by utilising the required stoichiometry and mild reaction conditions.¹⁷ Geminal or nongeminal substitution may occur, which may influence polymerisation due to the cleavage of the chloride bonds being the initiator for ring-opening polymerisation.^{2,17}

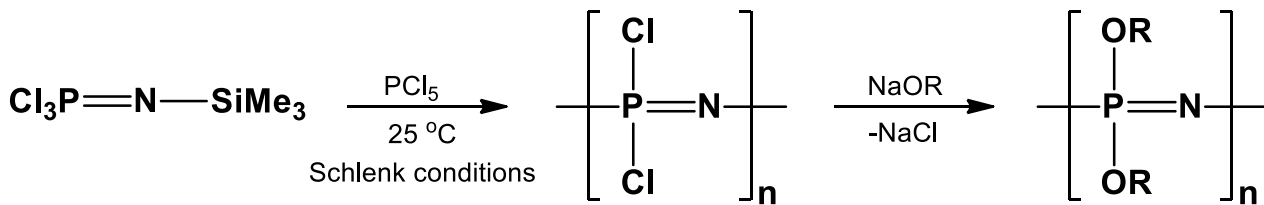
2.2.2 Living Cationic Polymerisation

Manners *et al.* developed a low temperature synthesis of trichloro(trimethylsilyl)phosphoranimine monomer, with yields in excess of 80 %.¹⁸ Phosphorus pentachloride initiates the polymerisation reaction of the phosphoranimine monomer. The synthesis of this monomer utilises phosphorus trichloride as chlorinating agents and sulfonyl chloride in order to dehydrogenate the nitrogen and produce a double bond between the phosphorus and nitrogen atoms (Scheme 2.4).



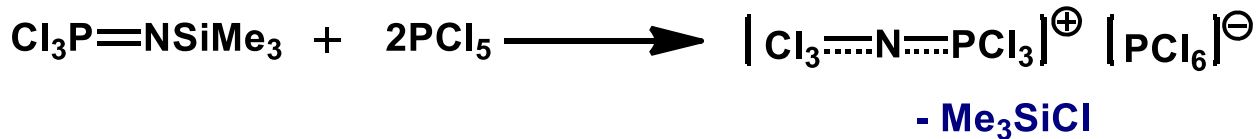
Scheme 2.4: Synthesis of trichloro(trimethylsilyl)phosphoranimine used as a monomer reagent in the synthesis of polyphosphazenes.

The phosphoranimine described in Scheme 2.4 can be used as a monomer in the route to synthesising poly(dichloro)phosphazene (Scheme 2.5).^{14,18} Trichloro(trimethylsilyl)phosphoranimine monomer and phosphorus pentachloride (as initiator) are reacted through a living cationic polymerisation process to produce poly(dichloro)phosphazene polymer. Unlike the ring-opening polymerisation discussed in section 2.2.1 above, which is reacted at 250 °C, the living cationic polymerisation route is performed at room temperature.¹⁴ Control of the molecular mass is achieved by varying the stoichiometric ratio of monomer and initiator.¹⁴ This method also offers narrower polydispersities than the ring-opening polymerisation route.^{2,14,18}



Scheme 2.5: Living cationic polymerisation of trichloro(trimethylsilyl)phosphoranimine monomer with phosphorus pentachloride to synthesise poly(alkoxy)phosphazenes after chlorine displacement with alkoxide.

The living cationic nature of the polymerisation used to synthesise polyphosphazenes is shown in Scheme 2.6. The phosphorus nitrogen salt forms from the reaction of one equivalent of trichloro(trimethylsilyl)phosphoranimine monomer and two equivalents of phosphorus pentachloride; chlorotrimethylsilane is eliminated from the reaction.¹⁴



Formation of phosphorus nitrogen salt and elimination of chlorotrimethylsilane



Additional $\text{Cl}_3\text{P}=\text{NSiMe}_3$ monomer



Additional monomer grows longer cationic phosphorus nitrogen bonds to form the polyphosphazene polymer

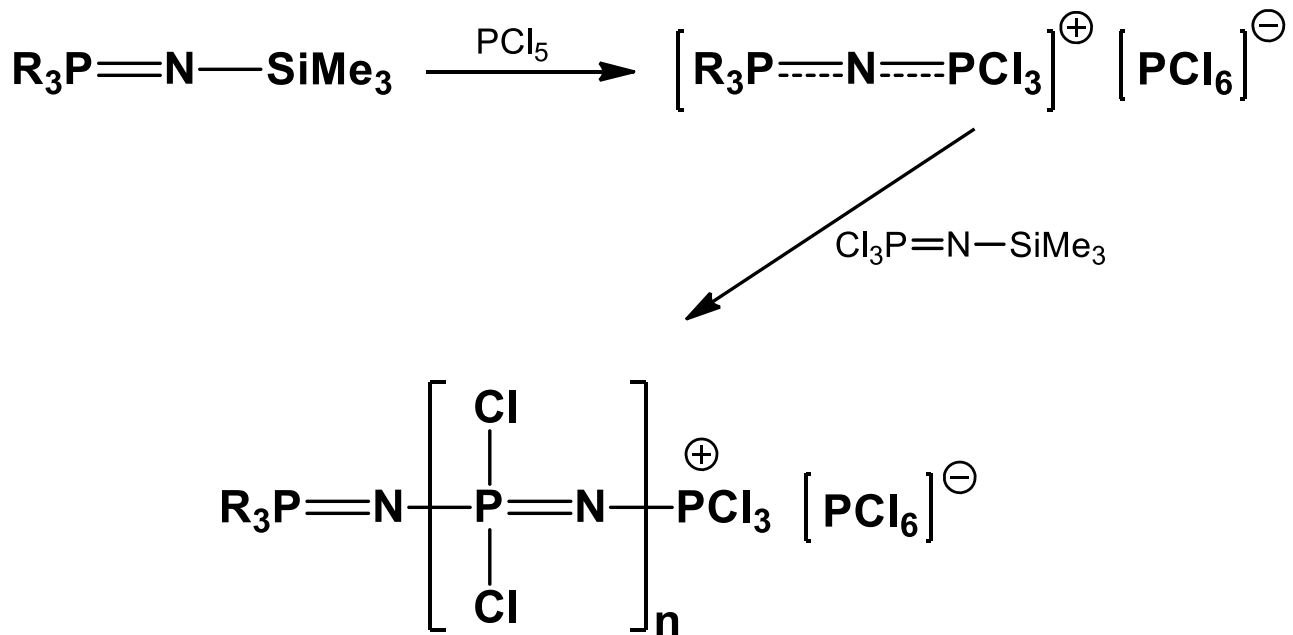


Scheme 2.6: Mechanism for the living cationic polymerisation of polyphosphazenes.¹⁴

The addition of more trichloro(trimethylsilyl)phosphoranimine monomer produces longer phosphorus nitrogen bonds, therefore forming a polyphosphazene polymer.¹⁴ This method affords a high level of control over the molecular mass of the polymer that is grown by adjusting the amount of monomer added to the reaction.¹⁹ Therefore, the monomer to initiator ratio used affects the molecular mass of the polymer. Larger monomer to initiator ratios produce higher molecular mass polyphosphazenes.

Molecular mass of the polyphosphazenes synthesised varies depending on whether bulk or solution phase polymerisation is employed. Bulk phase polymerisation yields molecular masses between 40 000 and 200 000 daltons, with polydispersities of 1.8.¹⁴ However, solution phase polymerisation offers much lower molecular masses, ranging between 7 000 and 14 000 daltons, with polydispersities between 1.04 to 1.2.¹⁴

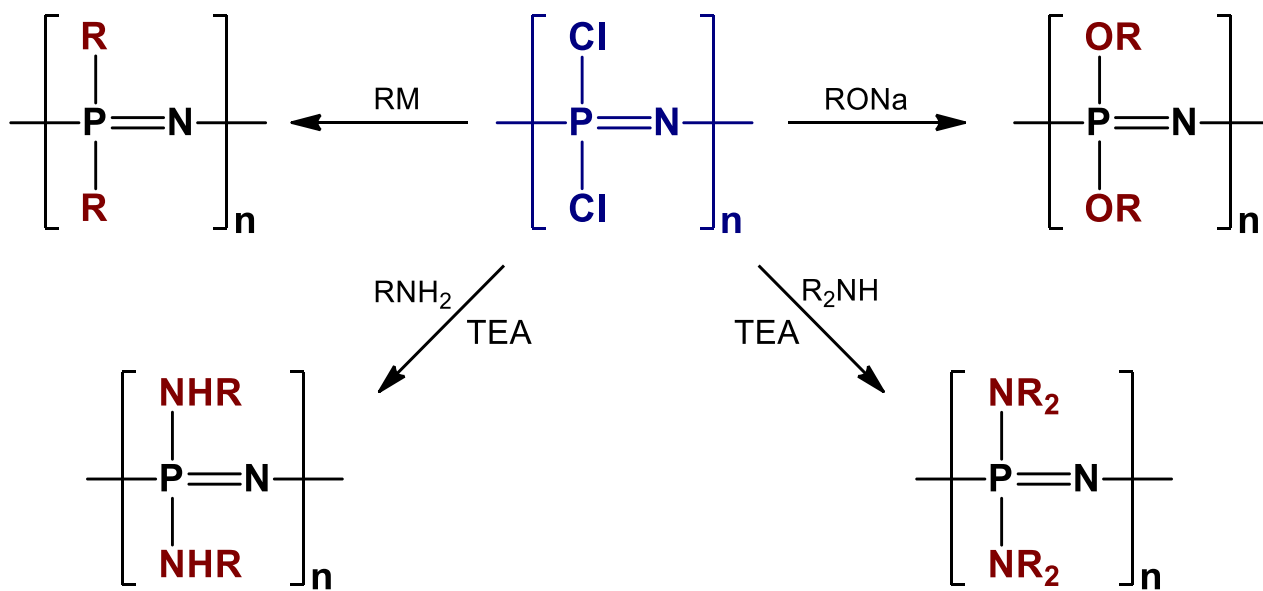
Similar to the ring-opening polymerisation route, functionalised polyphosphazenes can be synthesised in two methods. The first method, functionalisation of poly(dichloro)phosphazene, is discussed in section 2.2.3 below. The second method requires functionalisation of the phosphoranimine monomer (described in Scheme 2.4), which becomes useful in the synthesis of polyphosphazenes with defined chain ends and also in the synthesis of block copolymers.² Synthesis of $\text{R}_3\text{P}=\text{NSiMe}_3$ phosphoranimines allows for chain propagation with monodirectional growth (Scheme 2.7).² Block copolymers may be synthesised by utilising varying stoichiometric ratios of $\text{Cl}_3\text{P}=\text{NSiMe}_3$ and $\text{ClR}_2\text{P}=\text{NSiMe}_3$ monomer units.²



Scheme 2.7: Synthesis of poly(dichloro)phosphazenes with monodirectional chain propagation, utilising alkyl or aryl substituted phosphoranimines (R = alkyl, aryl).²

2.2.3 Functionalisation of poly(dichloro)phosphazenes

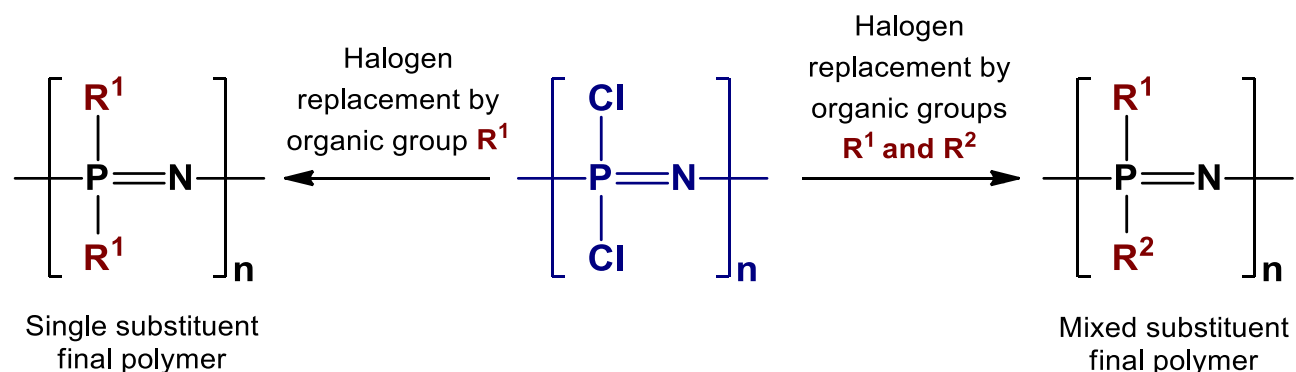
The most prominent approach to functionalising poly(organophosphazene)s in literature is to first synthesise poly(dichloro)phosphazene followed by functionalisation of the chloro groups. This method takes advantage of the high reactivity of the polar phosphorus-chlorine bond, which readily undergoes nucleophilic substitution (Scheme 2.8).¹⁵ However, there is less control of nucleophilic substitution when two or more different organic moieties are utilised and a random distribution of the differing moieties will be present.



Scheme 2.8: Examples of substitution of poly(dichloro)phosphazenes to synthesise poly(organophosphazene)s (R = alkyl, aryl).¹⁵

Scheme 2.8 indicates the anchoring of amines onto polyphosphazene polymers; however, care should be taken in this type of reaction as hydrochloric acid is a by-product. The presence of hydrochloric acid may react with the nitrogen atoms present in the polyphosphazene backbone, resulting in cleavage of the P-N bonds.¹³ Triethylamine (TEA) may be added to the reaction mixture to prevent unwanted breakage of the polymer backbone.¹³

It is possible to functionalise poly(dichloro)phosphazenes to yield single substituent final polymers or mixed substituent final polymers (Scheme 2.9).³



Scheme 2.9: Functionalisation of poly(dichloro)phosphazenes producing single and mixed substituent poly(organo)phosphazenes (R = alkyl, aryl).³

Fluoroalkoxy-substituted polyphosphazenes was one of the first poly(organo)phosphazenes synthesised by H. Allcock, containing trifluoroethoxy side groups.³ This semi-crystalline, high molecular mass polymer, has been found to have fire resistant properties and can be used for hydrophobic films and fibers.^{2,3} Intentional cross-linking of fluoroalkoxy-substituted polyphosphazenes, with two different fluoroalkoxy moieties have been shown to eliminate crystallinity, whereby the product polymer exhibits elastomeric properties.³ Intentional cross-linking of polyphosphazenes are achieved by the use of microcrystallites, formation of covalent cross-links, or by the formation of ionic/coordination cross-links.⁹ Cross-linking of polyphosphazenes (for the purpose of specific material design) may only be achieved after polymerisation has occurred. If cross-linking occurs during the polymerisation process (formation of P-O-P cross-links), complete functionalisation of halogens from the synthesised polyphosphazene becomes almost impossible.⁹ Incomplete halogen replacement results in a polymer which is sensitive to P=N bond cleavage from atmospheric moisture.^{2,9}

Different side groups that are anchored onto the polyphosphazene chains lead to different physical properties. Properties can range from water-solubility, elasticity, fiber and film qualities, biostability, etc. Table 2.1 indicates some of the polymer properties obtained by the anchoring of specific side groups.³

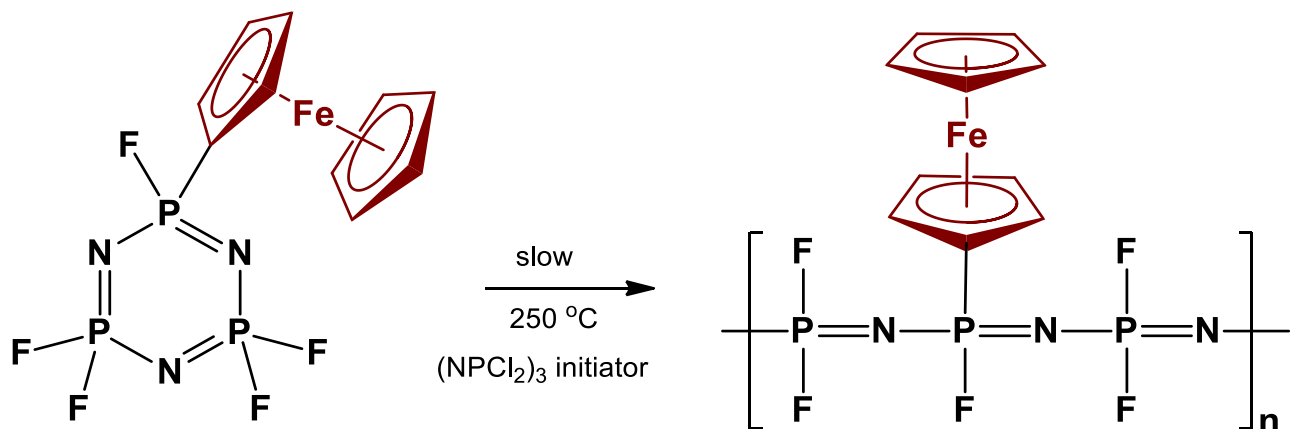
Table 2.1: Side groups which determine the different properties of poly(organo)phosphazenes³

| Water solubility / Hydrogels | Elastomers | Microsphere / Micelles |
|---|--|--|
| NHCH ₃ OCH ₃ OCH ₂ CH ₂ OCH ₂ CH ₂ OCH ₃ OC ₆ H ₄ COONa OC ₆ H ₄ SO ₃ Na Glucosyl, Glyceryl | OCH ₃ , OC ₂ H ₅ , OC ₃ H ₇ , OC ₄ H ₉ OCH ₂ CH ₂ OCH ₃ OCH ₂ CH ₂ OCH ₂ CH ₂ OCH ₃ OCH ₂ CF ₃ / OCH ₂ (CF ₂) _x CF ₂ H OC ₆ H ₅ / OC ₆ H ₄ CH ₃ OCH ₂ CF ₃ / CH ₂ Si(CH ₃) ₃ | OC ₆ H ₄ COOH OC ₆ H ₄ SO ₃ H OC ₆ H ₄ SO ₃ Na / polystyrene OCH ₂ CH ₂ OCH ₂ CH ₃ OCH ₃ OCH ₂ CH ₃ / PEO or PPG |
| Biostability | Bioerosion | Solid Ionic Conductivity |
| OCH ₂ CF ₃ OCH ₂ (CF ₂)CF ₂ H OC ₆ H ₄ R CH ₂ Si(CH ₃) ₃ OCH ₂ CH ₂ OCH ₂ CH ₂ OCH ₃ | NHCH ₂ COOC ₂ H ₅ Imidazolyl Glucosyl Glyceryl OC ₂ H ₅ | OCH ₂ CH ₂ OCH ₂ CH ₂ OCH ₃ OC ₆ H ₅ / OC ₆ H ₄ SO ₃ H OC ₆ H ₅ / OC ₆ H ₄ P(O)(OR) ₂ OH OC ₆ H ₅ / OC ₆ H ₄ S(O ₂)NHS(O ₂)CF ₃ OCH ₂ CH ₂ OCH ₂ CH ₂ OCH ₃ |
| Fibers / Films | Surface Hydrophobicity | Surface Hydrophilicity |
| OCH ₂ CF ₃ OC ₆ H ₅ OC ₆ H ₄ R | OCH ₂ CF ₃ OCH ₂ (CF ₂)CF ₂ H OC ₆ H ₅ CH ₂ Si(CH ₃) ₃ | OCH ₂ CH ₂ OCH ₂ CH ₂ OCH ₃ OC ₆ H ₄ COOH OC ₆ H ₄ SO ₃ Na OC ₆ H ₄ SO ₃ H |

2.2.4 Metallocene-containing polyphosphazenes

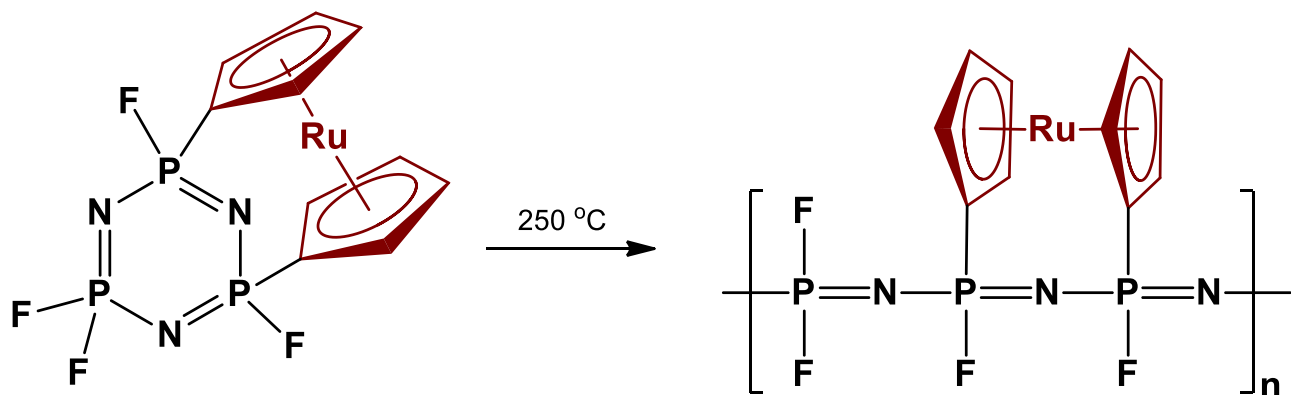
Metallocene-containing polyphosphazenes have been reported in literature by H. R. Allcock, whereby both ferrocene-containing polyphosphazenes and ruthenocene-containing polyphosphazenes were synthesised.¹¹

Hexafluorocyclotriphosphazene cyclic trimers were functionalised with ferrocenyl and ruthenocenyl side groups, linked to the phosphorus atoms as C-P bonds.¹¹ Ring-opening polymerisation method was utilised with these metallocenyl-functionalised phosphazene cyclic trimers; however, hexachlorocyclotriphosphazene trimer was used as an initiator to facilitate the polymerisation process (Scheme 2.10).¹¹ After polymerisation of the ferrocene-functionalised phosphazene trimer, the fluorine side groups were replaced with sodium alkoxides (e.g., sodium trifluoroethoxide) for hydrolytic stability.¹¹



Scheme 2.10: Synthesis of hybrid ferrocene-polyphosphazene polymer utilising the ring-opening polymerisation method.¹¹

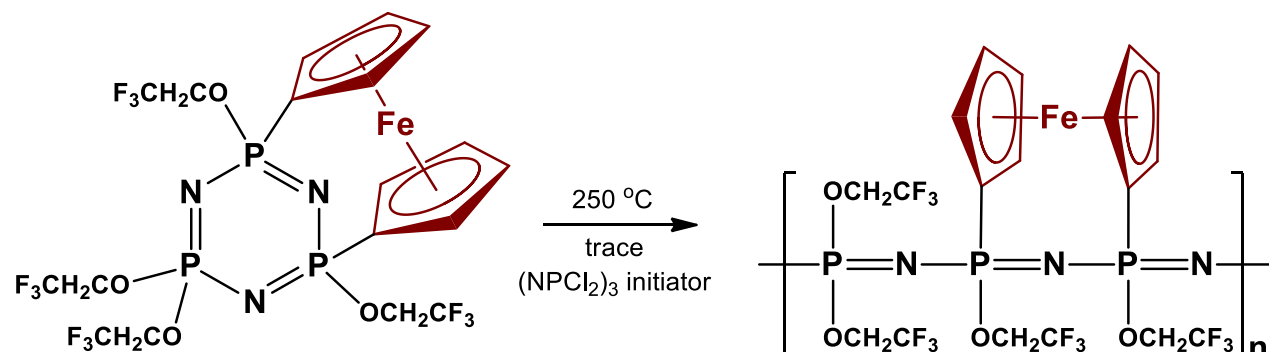
Metallocenes have also been added to two different phosphorus atoms on the phosphazene trimer/tetramer ring. This produces a polyphosphazene polymer with a transannular structure (Scheme 2.11).¹¹ Polymerisation occurs via the thermal ring-opening route at 250 °C.



Scheme 2.11: Ring-opening polymerisation of a ruthenocenyl-substituted cyclophosphazene trimer producing a transannular type ruthenocene-containing polyphosphazene.¹¹

An alternate approach was also used to synthesise hybrid metallocene-phosphazene polymers, whereby a complete organic substituted cyclophosphazene was synthesised (Scheme 2.12).¹¹ In this case, the cyclic phosphazene trimer was substituted with trifluoroethoxy groups and ferrocenyl groups. Polymerisation was then initiated with a trace amount of hexachlorocyclotriphosphazene at 250 °C.¹¹ However, due to the bulky trifluoroethoxy- and ferrocenyl-moieties, polymerisation of this type of trimer is greatly reduced due to steric hindrance. Therefore, polymerisation of “fully-organo-substituted” cyclophosphazene monomers will not produce high molecular mass

polymers.¹¹ This type of reaction should be avoided for highly reactive side groups as it may interfere with the polymerisation process.³

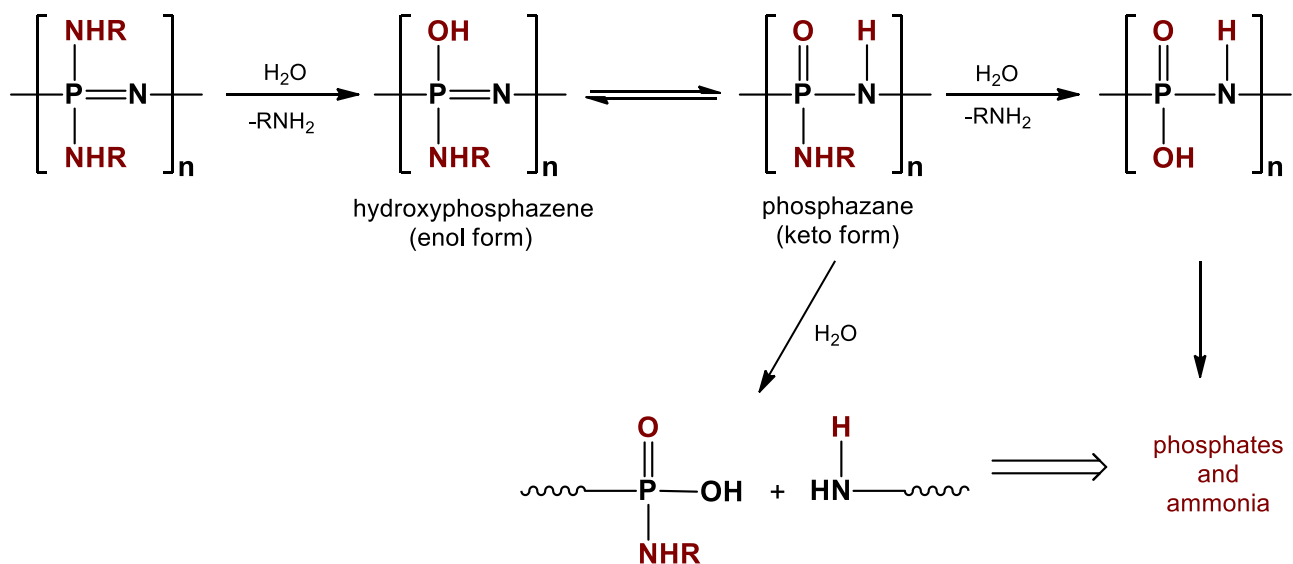


Scheme 2.12: Ring-opening polymerisation of a complete organic substituted cyclophosphazene trimer, containing a ferrocenyl moiety.

2.2.5 Poly(organo)phosphazenes in biomedical applications

Poly(organo)phosphazenes have gained popularity in biomedical applications due to the biodegradability of the polymer.²⁰ Hydrolysis of poly(organo)phosphazenes cleaves the side chains which react with the phosphorus atoms of the polyphosphazene.^{2,21} Degradation of the polyphosphazene via hydrolysis produces a buffer medium of phosphates and ammonia, which is biocompatible.²¹ A mechanism proposed for the hydrolytic degradation of poly(amino)phosphazenes is shown in Scheme 2.13.

Degradation of poly(organo)phosphazenes via hydrolysis greatly depends on the chemistry of the side groups present. Linkage type of the side group, hydrophobicity, hydrophilicity, steric shielding, intermolecular hydrogen bonding as well as cross-linking influences the rate of hydrolysis.²² Poly(organo)phosphazenes with organo groups linked via oxygen atoms are generally more resistant to hydrolysis than groups linked via nitrogen atoms.²² Addition of hydrophobic side groups, such as fluoroalkoxy and aryloxy groups, may enhance polyphosphazene resistance to hydrolysis. The aliphatic components of hydrophobic groups, as well as large bulky side groups, shield the polyphosphazene backbone and therefore reduce the rate of hydrolysis cleavage.²²



Scheme 2.13: Proposed mechanism for the degradation of poly(amino)phosphazenes

(R = alkyl, aryl).^{2,21}

Poly[(amino acid ester)-phosphazenes] have been used in drug delivery and tissue engineering applications due to their ease of degradation via hydrolysis.²¹ However, the presence of bulkier side groups on the polyphosphazene chain will result in a slower rate of hydrolysis. Less bulky, hydrolysis-sensitive side groups will easily undergo hydrolysis at a faster rate than the bulkier side groups.²¹ *In vitro* and *in vivo* applications for different types of L-alanine substituted polyphosphazenes, [ethyl alanato, ((ethyl alanato)(ethylglycinato)), ((ethyl alanato)(*p*-methylphenoxy)), ((ethyl alanato)(*p*-phenylphenoxy)), and ((ethylglycinato)(methylphenoxy)) side groups] exhibited excellent biocompatibility for tissue engineering applications.²¹ The implanted polymers were observed to support bone growth in New Zealand white rabbits with no inflammation being observed. The degradation products of poly[bis(ethyl 4-aminobutro) phosphazene] were tested on Swiss 3T3 and HepG2 cells, of which no proliferation was observed due to the polymer media.²¹ This confirmed the cytotoxicity and biocompatibility of the degradation media of polyphosphazenes for *in vivo* applications.

Poly[di(carboxylatophenoxy)phosphazene], abbreviated as PCPP, have been studied for use as vaccine immunoadjuvants and has been shown to exhibit potent adjuvant activity for certain antigens (e.g., trivalent influenza virus vaccine, hepatitis B surface antigen and tetanus toxoid).²³ PCPP *in vivo* trials, performed for commercial vaccines of influenza strains, showed that the addition of PCPP

enhanced the immune response to influenza antigens at least ten-fold when compared to only the commercial vaccine, as is the definition of an immunoadjuvant.²³

2.3 Ferrocene

Ferrocene was accidentally discovered in 1951 from a Grignard reaction between magnesium bromide and anhydrous iron(III) chloride, in an attempted synthesis of fulvalene.²⁴ The aromatic nature of ferrocene allows functionalisation of the cyclopentadienyl rings via organic type reactions, such as Friedel-Crafts acylation, formylation, sulphonation and amination, to name a few.^{24,25} Synthesis will be focussed on the functionalisation of ferrocenes with alcohol groups, due to the aims of this project (see chapter 1, section 1.2, i).

2.3.1 Biomedical applications

The use of metallocenes in biomedical applications, specifically for anticancer research, is advantageous with their possession of polymorphic properties as well as their structural and reacting flexibility.²⁶ The antineoplastic activity of ferrocene has been extensively studied over the past 25 years.²⁶ Ferrocenyl compounds are highly modifiable and exhibit unique properties, such as redox activity, low toxicity, stability in biological media, penetration of cell membranes due to lipophilicity as well as being commercially available and consisting of various modes of modification.^{25,26}

Unsubstituted ferrocenium salts and substituted ferrocenes have previously been tested in literature for biological activity, including antineoplastic activity, antimalarial activity and treatment of iron deficiency to name a few.^{26–28} Figure 2.2 exhibits a few drugs containing ferrocene, with different biomedical potentials. 1-(Benzotriazolyl)ethylferrocene has been determined to possess antitumor activity, and the ferrocenyl analog of tamoxifen is a hopeful alternative for antiestrogenic effects (for breast cancer treatment). The ferrocenyl analog of chloroquine has shown remarkable antimalarial activity and has reached the first stage of clinical trials. It was determined in literature by Osella *et al.* that the Fe^{II}-ferrocenes did not destroy Ehrlich ascites tumour (EAT) cells during *in vivo* tests.²⁹ However, the Fe^{III}-ferrocenium salts were found to generate hydroxyl radicals which rapidly damaged the DNA of EAT cells.²⁹

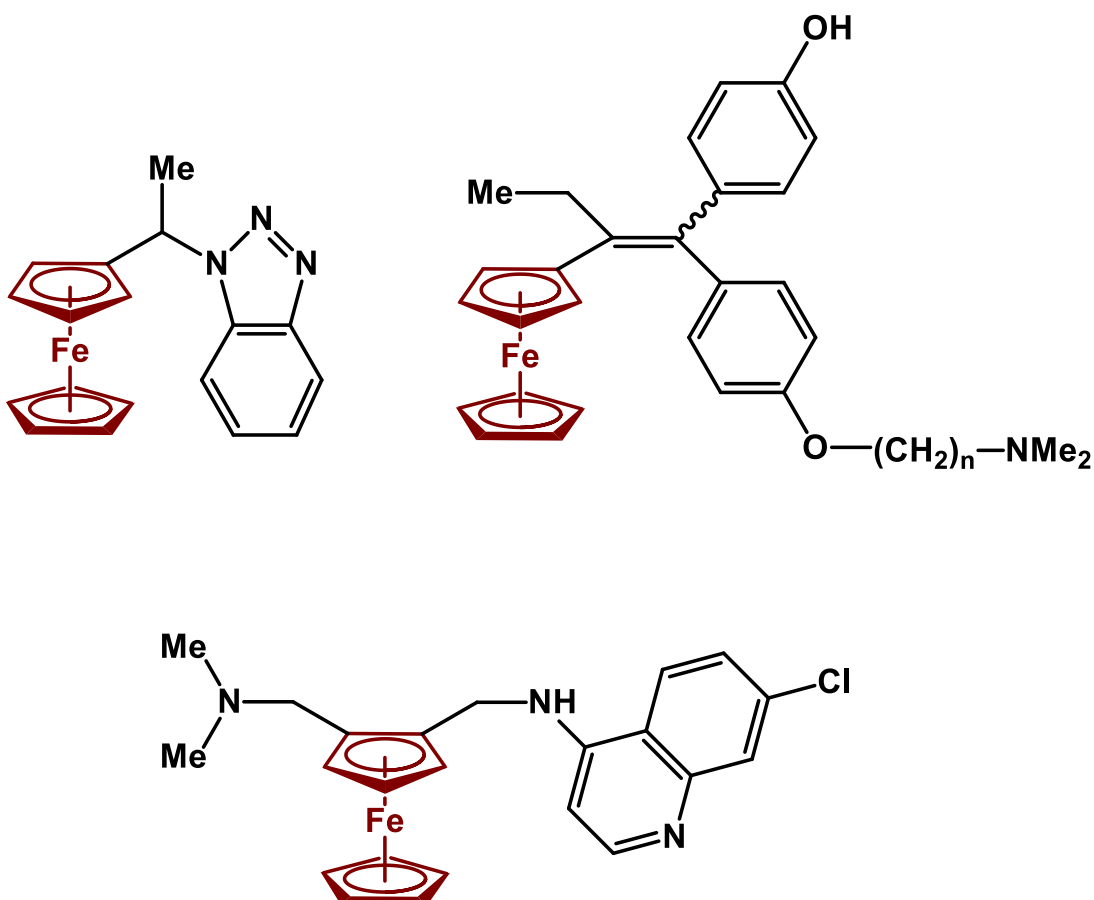


Figure 2.2: Ferrocene-containing drugs which possess antitumor activities,
1-(benzotriazolyl)ethylferrocene (top left), antiestrogen activity,
1-[4-(2-dimethylaminoethoxy)]-1-(phenyl-2-ferrocenyl-but-1-ene) (top right, ferrocenyl analog of tamoxifen) and antimalarial activity, 7-chloro-4{[2-(N,N-dimethylaminomethyl)]-N-methylferrocenylamino}quinoline (bottom, ferrocenyl analog of chloroquine).

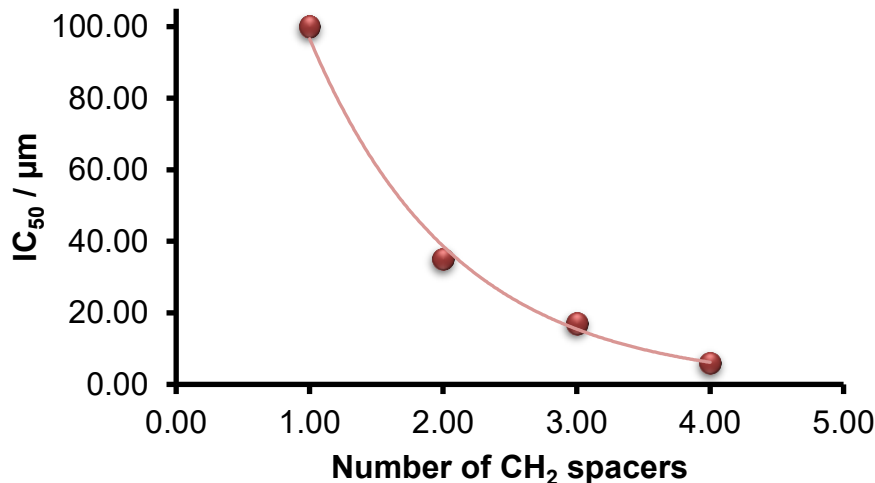


Figure 2.3: Relationship between IC₅₀ values and the number of increasing CH₂ spacers in ferrocene-containing alcohols.³⁰

Antineoplastic activity of ferrocenylalcohols [of the type Fc(CH₂)_nOH] containing different number of methylene spacers were investigated by Swarts *et al.*³⁰ *In vivo* cytotoxic tests against the HeLa cell line determined IC₅₀ (50 % cell growth inhibition) values to decrease as the number of spacers (n) increased, as depicted by Figure 2.3.³⁰

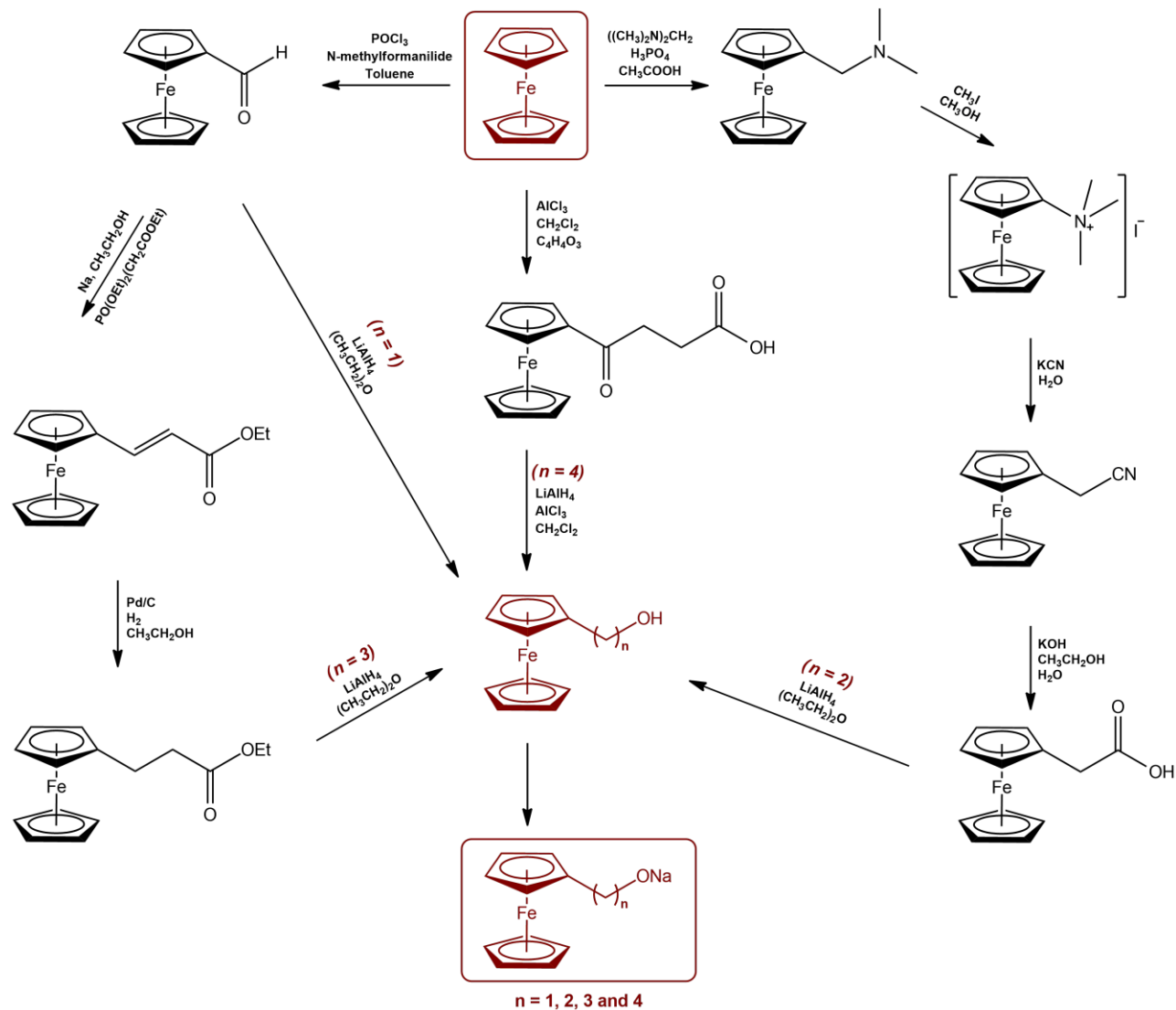
2.3.2 Synthesis of ferrocene-containing alcohols

As per goal (i) of this project, ferrocene-containing alcohols were synthesised before anchorage onto polyphosphazene polymeric supports. Ferrocene is a reactive organometallic compound and easily undergoes electrophilic substitution reactions. Scheme 2.14 shows the synthetic strategies that have previously been used in literature to obtain some ferrocene-containing alcohols.^{31,32} These alcohols have the form Fc(CH₂)_nOH, where n = 1, 2, 3, and 4 and Fc is the ferrocenyl moiety.

Modification of ferrocene to form formylferrocene has previously been achieved utilising the Vilsmeier reaction.³³ Formylferrocene readily undergoes the Wittig reaction, utilising triethyl phosphonoacetate, to yield ethyl-3-ferrocenylethenoate quantitatively.³⁴

Ethyl-3-ferrocenylethanoate is synthesised utilising standard hydrogenation procedure with palladium on carbon and ethyl-3-ferrocenylethenoate.^{32,34} Amination of ferrocene has been achieved in literature by the Mannich reaction, with *N,N,N',N'*-tetramethyldiaminomethane as the aminomethylating agent.³⁵ Iodomethane is used to convert the amine to form

N,N,N-trimethylaminomethylferrocene iodide.³⁶ Synthesis of 2-ferrocenylacetic acid has been achieved by first displacing the trimethylammonium group with potassium cyanide, followed by hydrolysis of 2-ferrocenylacetonitrile.³⁷ Friedel-Crafts acylation was first used to identify the aromatic nature of ferrocene.²⁴ Acylation is preferred over alkylation as the reactions have increased selectivity.²⁴ Methyl-3-ferrocenylpropanoate can be synthesised from the Friedel-Crafts acylation of ferrocene, utilising aluminium trichloride as catalyst and succinic anhydride as the acylating agent.³² All ferrocenylalcohol precursors (carboxylic acids and esters) are converted to their respective ferrocenylalcohols by reduction of the aldehydes, esters or carboxylic acids, utilising lithium aluminium hydride.³² An exception is made for methyl-3-ferrocenylpropanoate, whereby both aluminium trichloride and lithium aluminium hydride is utilised. Addition of aluminium trichloride is important for the removal of the keto carbonyl, thus allowing for the formation of 4-ferrocenylbutanol.³² In preparation for anchorage of ferrocenylalcohols onto the polyphosphazene support, all alcohols have to be converted to its sodium salt derivative. This may be achieved by stirring the alcohol in a solution of sodium hydride in tetrahydrofuran.³⁴



Scheme 2.14: Synthetic strategy for the synthesis of ferrocenylalcohols.

2.4 Viscometry

Viscosity is a measure of resistance to flow of a substance or solution. In polymer chemistry, dilute concentrations (~ 1 % solutions) are used, as polymeric materials cause solutions to become viscous enough to measure change in resistance to flow compared to the pure solvent.³⁸ Viscosity is measured with the aid of a viscometer (Figure 2.4), whereby the efflux time is measured for the dilute polymer solution as well as the pure solvent.

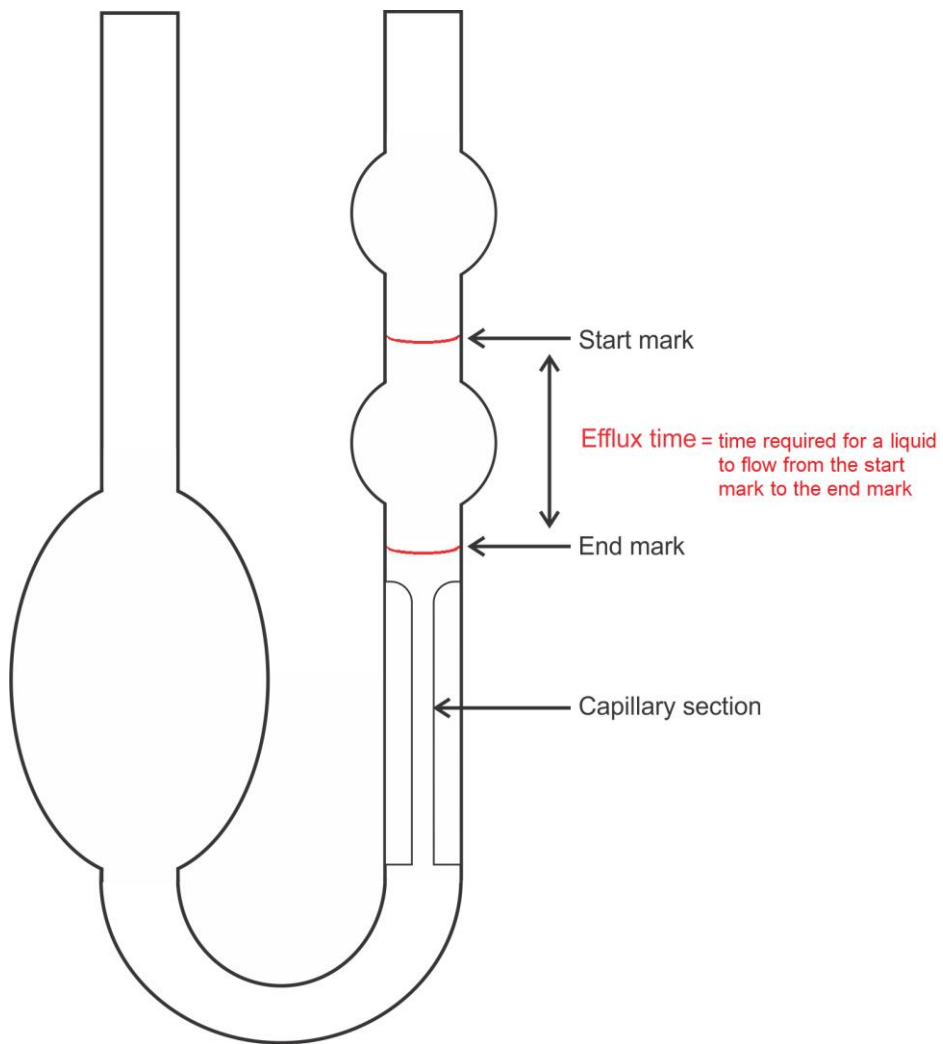


Figure 2.4: Illustration of a viscometer, indicating the flow positions to determine the efflux time and the capillary section, used to determine viscosity.

The efflux time of the pure solvent is denoted as t_0 and the efflux time of the dilute polymer solution is denoted as t .³⁹ The following viscosity parameters can be determined:³⁸

$$\text{Relative viscosity} = \eta_{\text{rel}} = \frac{t}{t_0} \quad \dots \text{equation 1}$$

$$\text{Specific viscosity} = \eta_{\text{sp}} = \eta_r - 1 = \frac{t - t_0}{t_0} \quad \dots \text{equation 2}$$

$$\text{Intrinsic viscosity} = [\eta] = \frac{\eta_{\text{sp}}}{c} \quad \dots \text{equation 3}$$

$$\text{Inherent viscosity} = \eta_{\text{inh}} = \lim_{c \rightarrow 0} \left(\frac{\eta_{\text{sp}}}{c} \right) \quad \dots \text{equation 4}$$

Inherent viscosity, $[\eta]$ at $c = 0$ g/dL, can therefore be determined by a plot of inherent viscosity versus concentration. The value of the y-intercept (i.e., where polymer concentration is zero) is then the inherent viscosity, η_{inh} . Figure 2.5 shows the relationship between concentration and intrinsic viscosity. Note that η_{inh} is also $[\eta]$, the intrinsic viscosity, the concentration of the polymer solution is 0 g/dL.

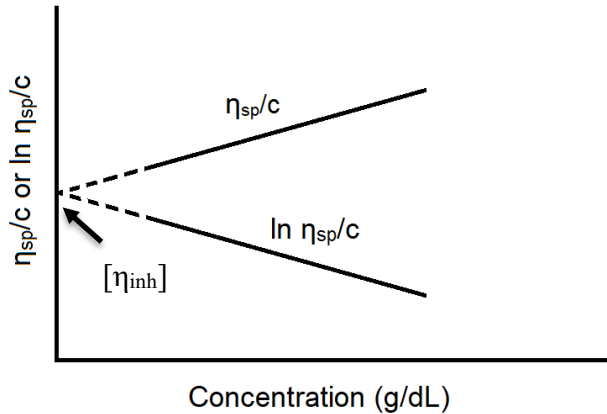


Figure 2.5: Determination of inherent viscosity (y-intercept) from a plot of inherent viscosity versus concentration of polymer.

The molecular mass of a polymer can be related to its inherent viscosity $[\eta] = \lim_{c \rightarrow 0} \left(\frac{\eta_{\text{sp}}}{c} \right)$ or intrinsic viscosity $[\eta] = \left(\frac{\eta_{\text{sp}}}{c} \right)$ at finite c values by utilising the Mark-Houwink equation,^{38,40}

$$[\eta] = KM^a \quad \dots \text{equation 5}$$

or in natural logarithmic form,

$$\ln [\eta] = a \ln M + \ln K \quad \dots \text{equation 6}$$

If the intrinsic viscosity ($\frac{\eta_{sp}}{c}$) are utilised, the concentrations for different samples should be finite, small, and equal. Explanatory note: Intrinsic viscosity $[\eta] = \left(\frac{\eta_{sp}}{c}\right)$, is sometimes also called reduced viscosity.

A plot of $\ln(\text{molecular mass})$ versus $\ln[\eta]$ yields the Mark-Houwink parameters a and K for a specific polymer.^{38,40} Figure 2.6 shows the relationship between $\log(\text{molecular mass})$ and $\log[\eta]$.

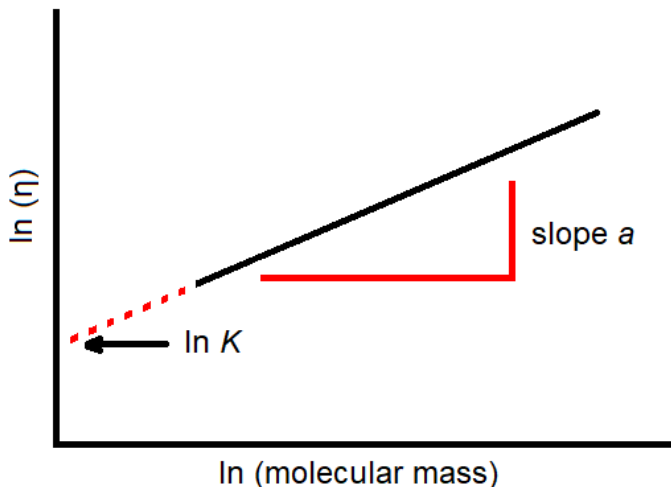


Figure 2.6: Determination of the Mark-Houwink parameters from a plot of the natural log of intrinsic viscosity versus the natural log of the molecular mass of the polymer.

With K and a known, equation 5, the Mark-Houwink equation may be used to calculate the molecular mass of polymer samples.⁴⁰

2.5 Gel Permeation Chromatography

Gel permeation chromatography (GPC), also known as size-exclusion chromatography (SEC), has gained popularity in polymer chemistry as a simple technique to determine molecular mass distribution as well as number- and weight averages in polymers.^{41,42} As opposed to the Mark-Houwink determination of polymer weights, the advantage of GPC allows molecular mass determination without the prior requirement of polymeric parameters specific to a particular type of

polymer. A calibration curve can be determined from standard, commercially available known molecular mass polymer samples, instead of requiring known molecular masses of the same polymer type (as in the Mark-Houwink method).^{40,43} This allows for quick molecular mass determinations, especially for new polymers. Size-exclusion chromatography is also used as a purification technique in biomedical applications for the separation of large biomolecules (such as proteins and peptides).^{44,45} The first separation of biomolecules utilising size-exclusion chromatography were performed by Lindqvist and Storgårds in 1955.⁴⁶ They determined “molecular-sieving” properties of a starch packed column, thereby separating peptides from amino acids.⁴⁶ Since then, different materials have been developed to reduce particle size and improve pore sizes of the column material (enhance chromatographic resolution and speed) as well as in minimising sample interaction (especially sample adsorption onto column material).⁴⁴ Highly cross-linked polymer resins and hybrid organic-inorganic particles are currently used in many GPC/SEC columns, in a variety of pore sizes for different extents of separation.^{44,47}

Figure 2.7 shows the basic principle of GPC, whereby the porosity of the column packing allows for the separation of different sized molecules. During the chromatographic process, larger sized molecules flow through the column with ease since their elution is not inhibited by the packing material. However, the smaller sized molecules enter and travel through the pores of the packing material, thereby eluting from the column at a much slower rate.⁴⁸

The universal calibration concept is utilised in the calculation of molecular mass distribution of polymer samples in GPC.⁴⁸ This means the eluting time of the sample is compared to the eluting profile of polymers with known molecular masses. The intrinsic viscosity-molecular size relationship is used to relate the known Mark-Houwink parameters of a standardised polymer to the unknown polymeric sample being analysed.^{48,49} Therefore, these parameters for the unknown sample are not required for the determination of molecular mass distribution and polydispersity measurements utilising GPC measurements.⁴⁸

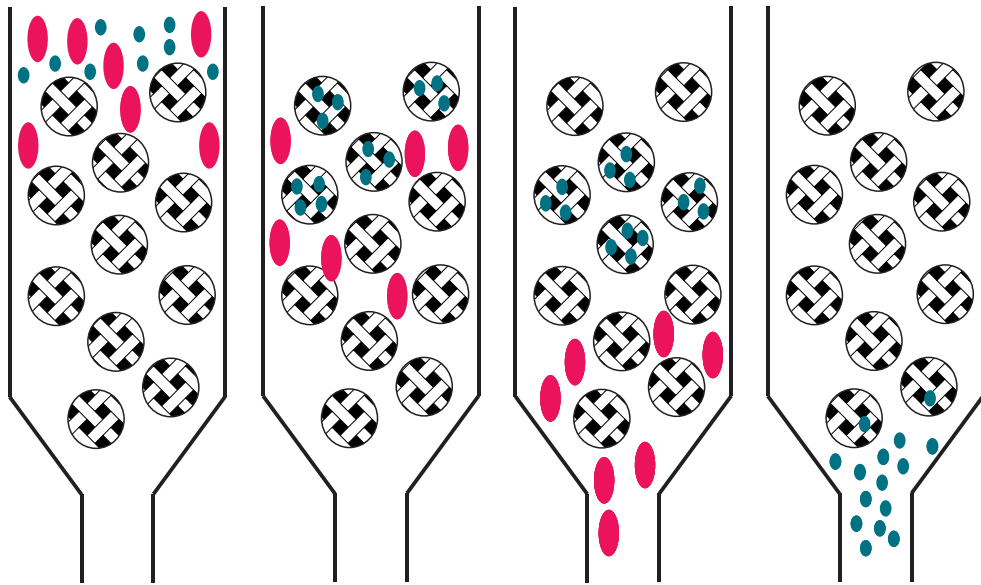


Figure 2.7: Basic principle of gel permeation chromatography, where the sample constituents are separated by interaction with the pores of the column packing. Larger molecules elute quicker as the smaller molecules travel through the pores of the column packing.

2.6 X-Ray Photoelectron Spectroscopy

Since the explanation of the photoelectric effect by Albert Einstein, it has been possible to study core and valence electrons in solid surfaces.^{50,51} One of these surface techniques is X-ray photoelectron spectroscopy (XPS). The first high quality photoelectron spectrum (resulting from X-rays) was determined by Siegbahn and co-workers in Uppsala, Sweden in 1957, as reported by Hollander and Jolly; this resulted in the measurement of binding energy shifts.⁵² The photoemission energy conservation equation is important in being able to quantify the binding energies of electrons (equation 7).⁵⁰

$$KE = hv - BE - \phi \quad \dots \text{equation 7}$$

KE is the kinetic energy of the emitted electron measured by the XPS spectrometer, hv is the photon energy of the X-ray source (h is Planck's constant and v is the photon frequency) and ϕ is the work function of the spectrometer which is determined from calibration of the instrument.

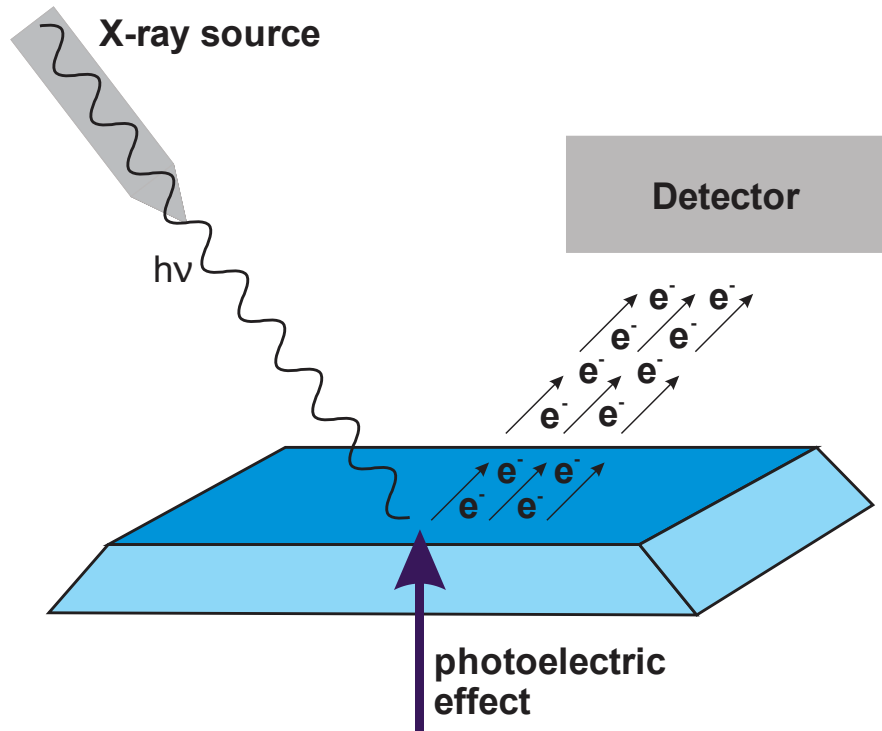


Figure 2.8: Basic principle of X-ray photoelectron spectroscopy (XPS) which utilises the photoelectric effect.

Figure 2.8 indicates the basic principle used in X-ray photoelectron spectroscopy. A high energy X-ray source is required in order to allow ejection of electrons from solid surfaces.⁵³ These electrons then reach the detector, and the kinetic energy of the electrons can be determined. Equation 7 is then utilised to calculate the binding energy of the electrons, which is used to distinguish between elements as well as the oxidation state of the element present in the sample.^{50,51,53}

2.7 Electrochemistry

The electro-analytical techniques that were used in this project will be discussed in this section.

2.7.1 Cyclic Voltammetry

A triangular voltage technique, utilising both forward and reverse scans of voltage changes in a set time (“cycling” back to the starting potential) which results in measurable current flow is known as cyclic voltammetry.^{41,54}

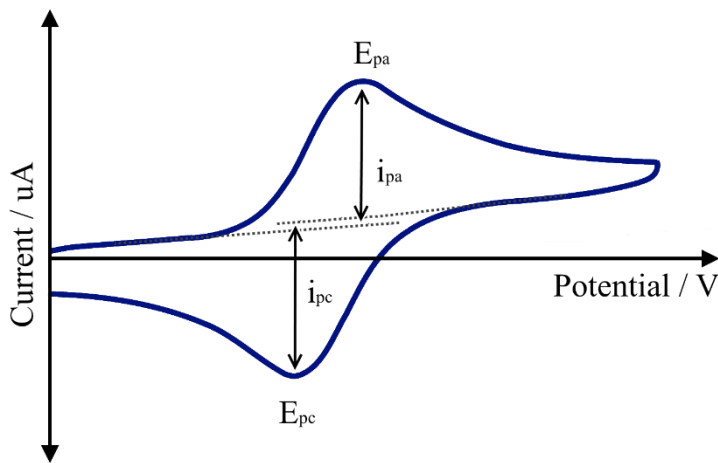


Figure 2.9: A plot of current versus potential to yield a cyclic voltammogram.

A plot of current versus potential (Figure 2.9) results in a cyclic voltammogram from which the following electrochemical parameters may be determined:⁵⁵

$$E^{\circ'} = (E_{pa} + E_{pc})/2 \quad \dots\text{equation 8}$$

$$\Delta E_p = E_{pa} - E_{pc} = 59/n \quad \dots\text{equation 9}$$

$$i_{pc}/i_{pa} = 1 \text{ (denominator is the current from forward scan)} \quad \dots\text{equation 10}$$

$$E = E^{\circ'} + (RT/nF)\ln([\text{oxidation}]/[\text{reduction}]) \quad \dots\text{equation 11}$$

E_{pa} and E_{pc} are the peak anodic and peak cathodic potentials respectively.⁴¹ The formal reduction potential ($E^{\circ'}$, equation 8) is used to calculate as the average of the peak anodic and peak cathodic potentials. Separation of the forward and reverse scans is calculated by ΔE_p (equation 9), whereby the theoretical value of $59/n$ millivolts determines electrochemical reversibility (n being the number

of electrons transferred in the redox process).⁵⁶ Experimentally, cell resistance and over-potentials are always present in the electrochemical system and therefore leads to higher ΔE_p values. Electrochemically reversible systems are therefore, in this thesis, assigned to any process exhibiting ΔE_p values equal to or lower than $90/n$ millivolts.⁵⁴ A quasi-reversible system is also possible, whereby experimental ΔE_p values can range between $90/n$ to $150/n$ millivolts.⁵⁴ Chemical reversibility is assigned when oxidation and reduction are both quantitative (equation 10). For quasi-reversible systems, equation 10 is upheld despite larger values for ΔE_p .⁵⁴ The Nernst equation (equation 11) applies to electrochemically reversible systems and can be used to calculate the relative quantities of oxidative and reductive species of the analyte.⁵⁷

2.7.2 Cyclic voltammetry of ferrocene

Ferrocene exhibits electrochemical and chemical reversibility, forming the ferrocenium ion upon oxidation and reverting back to ferrocene during reduction.⁵⁸ Equations 9 and 10 for electrochemically and chemically reversible systems are obeyed by the redox activity of ferrocene. Due to these findings, ferrocene has become a popular internal standard for cyclic voltammetry experiments in non-aqueous solutions and is referenced at zero millivolts.⁵⁸ Electrochemical experiments such as cyclic voltammetry require an internal standard due to fluctuations in the junction potential between the reference electrode and the solvent. Without a standard like ferrocene, the formal reduction potential calculated would be insignificant, as these fluctuating values cannot be compared to other compounds. For this reason, ferrocene is considered the IUPAC standard in organic media as well. The formal reduction potential of certain compounds may overlap with ferrocene. In these cases, decamethylferrocene is often used as an internal standard.⁵⁹ However, an additional step is required whereby decamethylferrocene is calibrated using ferrocene as an internal standard, utilising the same conditions and solvent as the analyte.⁵⁹

Cyclic voltammetry of ferrocene-containing alcohols of the type $\text{Fc}(\text{CH}_2)_n\text{OH}$, where $n = 1, 2, 3$, and 4 have been studied in literature whereby all alcohols except 1-ferrocenylmethanol exhibit chemical and electrochemical reversibility.^{31,60} Figure 2.10 compares the cyclic voltammograms of ferrocene alongside ferrocenylalcohols with different quantities of methylene groups (utilising acetonitrile as solvent and $0.1\text{M } \text{N}(\text{Bu})_4\text{PF}_6$ as supporting electrolyte). The formal reduction potentials of these ferrocene-containing alcohols were found to shift as the number of methylene groups present in the alcohol increased.^{30,31} Figure 2.11 shows a plot of formal reduction potential

versus the number of methylene groups in the ferrocenylalcohols. The formal reduction potential is observed to decrease as the number of methylene groups on the ferrocenylalcohol increases.²⁹

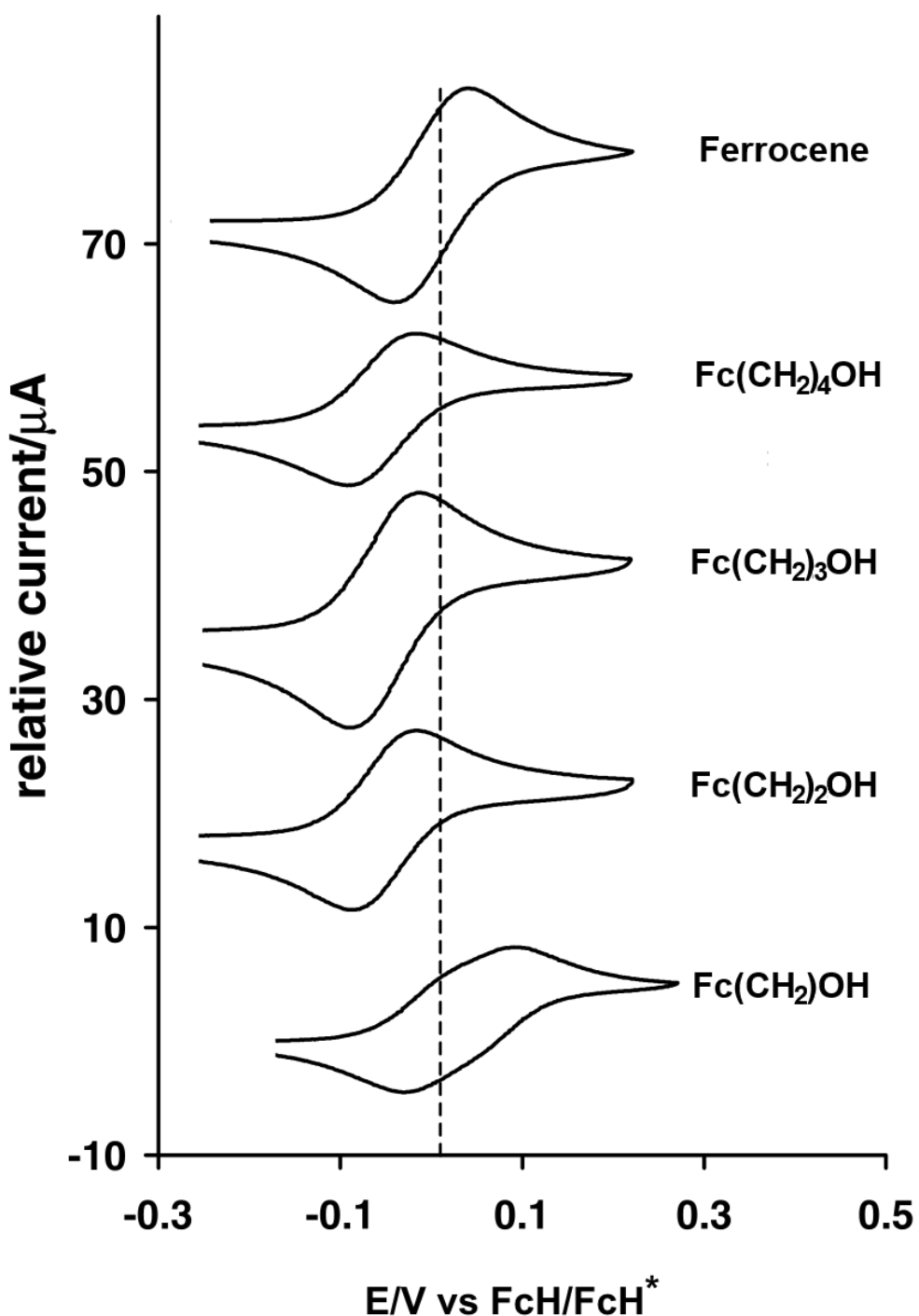


Figure 2.10: Cyclic voltammograms of ferrocene as well as ferrocenylalcohols of the type $\text{Fc}(\text{CH}_2)_m\text{OH}$, where $m = 1, 2, 3$, and 4 .³¹

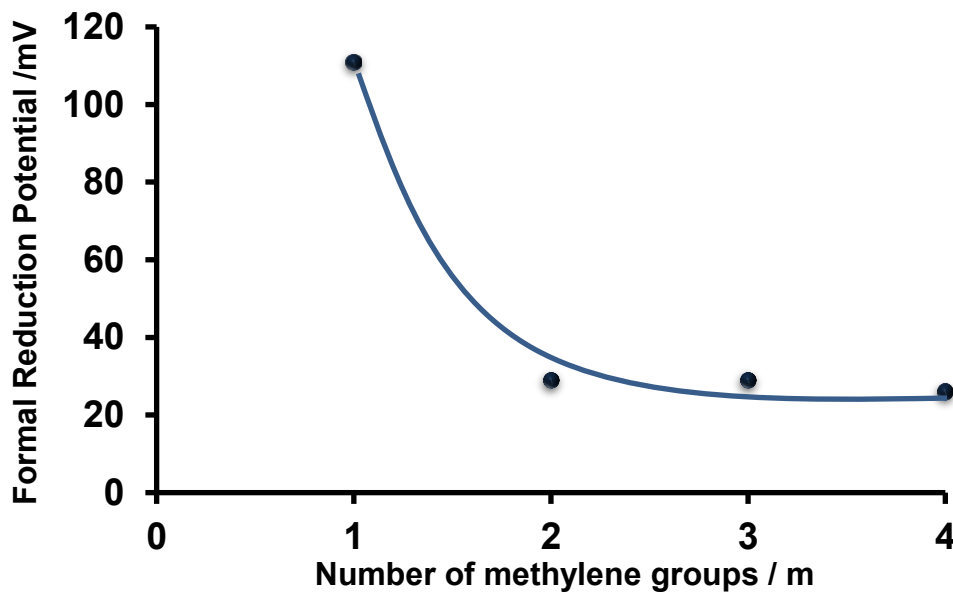


Figure 2.11: Trend of decreasing formal reduction potentials of ferrocenylalcohols as the number of methylene groups increased from one to four.³⁰

As described in section 2.3.1 above, it was determined by Osella *et al.* that Fe^{III}-ferrocenium species were responsible for anticancer activity.³⁰ Swarts *et al.* hypothesised that reducing the redox potential of the Fe^{II} to Fe^{III} couple would increase the antineoplastic activity, since the ferrocenium ion is the active species.³⁰ The formal reduction potential of ferrocenylalcohols [of the type $\text{Fc}(\text{CH}_2)_n\text{OH}$] with increasing methylene spacers (*n*) were observed to decrease as the IC₅₀ values decreased (Table 2.2).³⁰ Therefore, the ease of oxidation in the Fe^{II} to Fe^{III} process resulted in better IC₅₀ values.

Table 2.2: Relationship between number of CH₂ spacers in ferrocenylalcohols, formal reduction potential and IC₅₀ concentration.

| Number of CH ₂ spacers | E° / V | IC ₅₀ / μM |
|-----------------------------------|--------|-----------------------|
| 1 | 0.111 | >100 |
| 2 | 0.029 | 35 |
| 3 | 0.030 | 17 |
| 4 | 0.026 | 5.7 |

This concludes the literature survey of relevant information associated with this study (synthesis of ferrocene-containing alcohols, goal i, chapter 1; synthesis of ferrocenyl derivatised polyphosphazenes, goals ii and iii, chapter 1; molecular weight determinations of all polymeric material, goal iv, chapter 1; an electrochemical study of all redox reactive compounds, goal v, chapter 1; an XPS, kinetic and thermal analysis of all polyphosphazenes, goals vi, vii and viii, chapter 1; and also a cytotoxic study on the polymeric ferrocene-containing derivatives, goal ix, chapter 1. Chapter 3 will discuss the author's own research and chapter 4 will provide all experimental conditions used in this study.

References

- 1 H. R. Allcock, *Sci. Prog.* 1933-, 1980, **66**, 355–369.
- 2 S. Rothemund and I. Teasdale, *Chem. Soc. Rev.*, 2016, **45**, 5200–5215.
- 3 H. R. Allcock, *Soft Matter*, 2012, **8**, 7521–7532.
- 4 Ph. Potin and R. De Jaeger, *Eur. Polym. J.*, 1991, **27**, 341–348.
- 5 R. H. Neilson and P. Wisian-Neilson, *Chem. Rev.*, 1988, **88**, 541–562.
- 6 Stokes, H. N, *Am. Chem. J.*, 1895, **17**, 275–290.
- 7 G. L. Hagnauer, *J. Macromol. Sci. Part - Chem.*, 1981, **16**, 385–408.
- 8 S. Dumitriu and V. I. Popa, *Polymeric Biomaterials: Structure and function*, CRC Press, 2013.
- 9 H. R. Allcock, *Chem. Mater.*, 1994, **6**, 1476–1491.
- 10 H. R. Allcock and R. L. Kugel, *Inorg. Chem.*, 1966, **5**, 1716–1718.
- 11 H. R. Allcock, *J. Inorg. Organomet. Polym. Mater.*, 2005, **15**, 57–65.
- 12 I. Teasdale and O. Brüggemann, *Polymers*, 2013, **5**, 161–187.
- 13 N. L. Morozowich, A. L. Weikel, J. L. Nichol, C. Chen, L. S. Nair, C. T. Laurencin and H. R. Allcock, *Macromolecules*, 2011, **44**, 1355–1364.
- 14 C. H. Honeyman, I. Manners, C. T. Morrissey and H. R. Allcock, *J. Am. Chem. Soc.*, 1995, **117**, 7035–7036.
- 15 J. O. Hollinger, in *An Introduction to Biomaterials*, CRC Press, 2005, pp. 274–290.
- 16 E. Carolina Martínez Ceballos, R. Vera Graziano, G. Martínez Barrera and O. Olea Mejía, Synthesis and Characterization of Polyphosphazenes Modified with Hydroxyethyl Methacrylate and Lactic Acid, <https://www.hindawi.com/journals/ijps/2013/645869/>, (accessed June 4, 2018).
- 17 H. Allcock, in *Phosphorus-Nitrogen Compounds: Cyclic, Linear, and High Polymeric Systems*, Elsevier, 2012, pp. 156–159.
- 18 B. Wang, E. Rivard and I. Manners, *Inorg. Chem.*, 2002, **41**, 1690–1691.
- 19 S. Aoshima and S. Kanaoka, *Chem. Rev.*, 2009, **109**, 5245–5287.
- 20 S. B. Lee, S.-C. Song, J.-I. Jin and Y. S. Sohn, *Polym. J.*, 1999, **31**, 1247–1252.

- 21 M. Deng, S. G. Kumbar, Y. Wan, U. S. Toti, H. R. Allcock and C. T. Laurencin, *Soft Matter*, 2010, **6**, 3119–3132.
- 22 H. R. Allcock and N. L. Morozowich, *Polym. Chem.*, 2012, **3**, 578–590.
- 23 A. K. Andrianov, *J. Inorg. Organomet. Polym. Mater.*, 2006, **16**, 397–406.
- 24 N. J. Long, in *Metallocenes: An Introduction to Sandwiched Complexes*, Wiley-Blackwell, Oxford, 1998, pp. 6–133.
- 25 M. D. Rausch, E. O. Fischer and H. Grubert, *J. Am. Chem. Soc.*, 1960, **82**, 76–82.
- 26 V. N. Babin, Y. A. Belousov, V. I. Borisov, V. V. Gumenyuk, Y. S. Nekrasov, L. A. Ostrovskaya, I. K. Sviridova, N. S. Sergeeva, A. A. Simenel and L. V. Snegur, *Russ. Chem. Bull.*, 2014, **63**, 2405–2422.
- 27 M. T. Johnson, E. Kreft, D. D. N'Da, E. W. Neuse and C. E. J. van Rensburg, *J. Inorg. Organomet. Polym.*, 2003, **13**, 255–267.
- 28 L. V. Snegur, V. N. Babin, A. A. Simenel, Y. S. Nekrasov, L. A. Ostrovskaya and N. S. Sergeeva, *Russ. Chem. Bull.*, 2010, **59**, 2167–2178.
- 29 D. Osella, M. Ferrali, P. Zanello, F. Laschi, M. Fontani, C. Nervi and G. Cavigiolio, *Inorganica Chim. Acta*, 2000, **306**, 42–48.
- 30 R. F. Shago, J. C. Swarts, E. Kreft and C. E. J. V. Rensburg, *Anticancer Res.*, 2007, **27**, 3431–3433.
- 31 W. L. Davis, R. F. Shago, E. H. G. Langner and J. C. Swarts, *Polyhedron*, 2005, **24**, 1611–1616.
- 32 A. I. Vogel, A. R. Tatchell, B. S. Furnis, A. J. Hannaford and P. W. G. Smith, *Vogel's Textbook of Practical Organic Chemistry*, Pearson, Harlow, 5 edition., 1996.
- 33 M. Sato, H. Kono, M. Shiga, I. Motoyama and K. Hata, *Bull. Chem. Soc. Jpn.*, 1968, **41**, 252–252.
- 34 A.-E. Navarro, N. Spinelli, C. Moustrou, C. Chaix, B. Mandrand and H. Brisset, *Nucleic Acids Res.*, 2004, **32**, 5310–5319.
- 35 J. K. Lindsay and C. R. Hauser, *J. Org. Chem.*, 1957, **22**, 355–358.
- 36 G. Grelaud, T. Roisnel, V. Dorcet, M. G. Humphrey, F. Paul and G. Argouarch, *J. Organomet. Chem.*, 2013, **741–742**, 47–58.
- 37 M. Ripert, C. Farre and C. Chaix, *Electrochimica Acta*, 2013, **91**, 82–89.
- 38 C. E. Carraher Jr., in *Introduction to Polymer Chemistry*, CRC Press, 2nd edn., 2010, pp. 73–81.
- 39 Y. Lu, L. An and Z.-G. Wang, *Macromolecules*, 2013, **46**, 5731–5740.
- 40 H. L. Wagner, *J. Phys. Chem. Ref. Data*, 1985, **14**, 1101–1106.
- 41 D. A. Skoog, D. M. West, F. J. Holler and S. R. Crouch, *Fundamentals of Analytical Chemistry*, Brooks Cole, Belmont, CA, 8 edition., 2003.
- 42 H. G. Barth, B. E. Boyes and C. Jackson, *Anal. Chem.*, 1996, **68**, 445–466.
- 43 A. C. OUANO, E. M. BARRALL, A. BROIDO and A. C. JAVIER-SON, in *Polymer Molecular Weight Methods*, AMERICAN CHEMICAL SOCIETY, 1973, vol. 125, pp. 187–193.
- 44 P. Hong, S. Koza and E. S. P. Bouvier, *J. Liq. Chromatogr. Relat. Technol.*, 2012, **35**, 2923–2950.

- 45 D. Otter, in *Encyclopedia of Food Sciences and Nutrition (Second Edition)*, ed. B. Caballero, Academic Press, Oxford, 2003, pp. 4824–4830.
- 46 B. Lindqvist and T. Storgårds, *Nature*, 1955, **175**, 511–512.
- 47 H. D. Burgess, in *Historic Textile and Paper Materials*, American Chemical Society, 1986, vol. 212, pp. 363–376.
- 48 E. P. Otocka, *Acc. Chem. Res.*, 1973, **6**, 348–354.
- 49 J. D. Timpa, *J. Agric. Food Chem.*, 1991, **39**, 270–275.
- 50 C. S. Fadley, *J. Electron Spectrosc. Relat. Phenom.*, 2010, **178–179**, 2–32.
- 51 N. H. Turner, *Anal. Chem.*, 1988, **60**, 377–387.
- 52 (a) Sokolowski, C. Nordling and K. Siegbahn, *Arkiv Fysik*, 1957, **12**, 301.
(b) J. M. Hollander and W. L. Jolly, *Acc. Chem. Res.*, 1970, **3**, 193–200.
- 53 D. Briggs and J. T. Grant, *Surface Analysis by Auger and X-Ray Photoelectron Spectroscopy*, IM Publications, Chichester, 2003.
- 54 H. J. Gericke, N. I. Barnard, E. Erasmus, J. C. Swarts, M. J. Cook and M. A. S. Aquino, *Inorganica Chim. Acta*, 2010, **363**, 2222–2232.
- 55 N. Elgrishi, K. J. Rountree, B. D. McCarthy, E. S. Rountree, T. T. Eisenhart and J. L. Dempsey, *J. Chem. Educ.*, 2018, **95**, 197–206.
- 56 G. A. Mabbott, *J. Chem. Educ.*, 1983, **60**, 697.
- 57 F. J. Vidal-Iglesias, J. Solla-Gullón, A. Rodes, E. Herrero and A. Aldaz, *J. Chem. Educ.*, 2012, **89**, 936–939.
- 58 R. R. Gagne, C. A. Koval and G. C. Lisensky, *Inorg. Chem.*, 1980, **19**, 2854–2855.
- 59 I. Noviandri, K. N. Brown, D. S. Fleming, P. T. Gulyas, P. A. Lay, A. F. Masters and L. Phillips, *J. Phys. Chem. B*, 1999, **103**, 6713–6722.
- 60 N. F. Blom, E. W. Neuse and H. G. Thomas, *Transit. Met. Chem.*, 1987, **12**, 301–306.

This page is intentionally left blank

3

Results and Discussion

3.1 Introduction

The results obtained by the author, with reference to the goals in chapter 1, are presented in this chapter. A series of ferrocene-containing alcohols were synthesised in this study, as shown in Figure 3.1. The series of alcohols that were synthesised are ferrocenylmethanol, **3**, 2-ferrocenyl-ethanol, **9**, 3-ferrocenylpropanol, **13**, and 4-ferrocenylbutanol, **16**. All ferrocenylalcohols were converted to their sodium-ferrocenylalkoxide equivalents (**4**, **10**, **14**, and **17**) as precursors for covalent bonded ferrocene-containing polyphosphazene polymers.

A series of new ferrocene-containing poly(organophosphazene) complexes were then synthesised, which consisted of (Figure 3.1):

- poly(*tris*(2,2,2-trifluoroethoxy)(ferrocenylmethoxy)phosphazene), **22**,
- poly(*tris*(2,2,2-trifluoroethoxy)(ferrocenylethoxy)phosphazene), **23**,
- poly(*tris*(2,2,2-trifluoroethoxy)(ferrocenylpropoxy)phosphazene), **24**,
- poly(*tris*(2,2,2-trifluoroethoxy)(ferrocenylbutoxy)phosphazene), **25**.

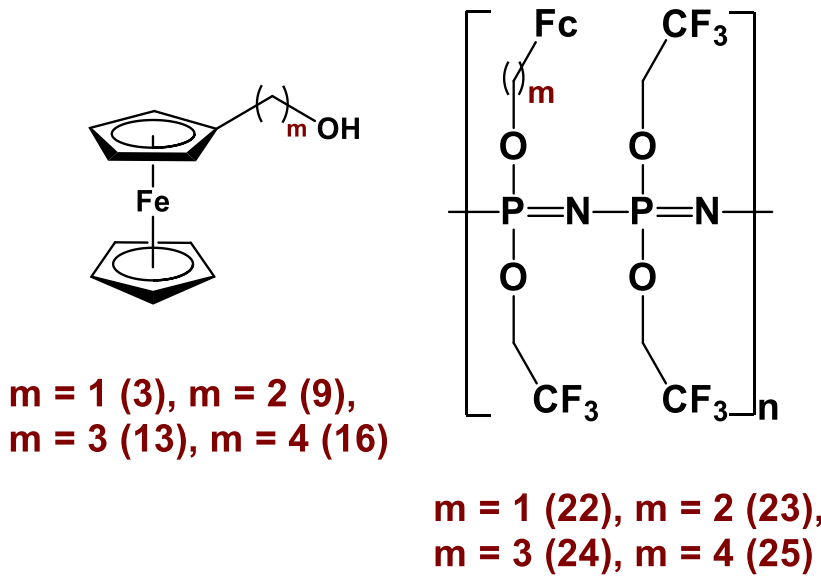


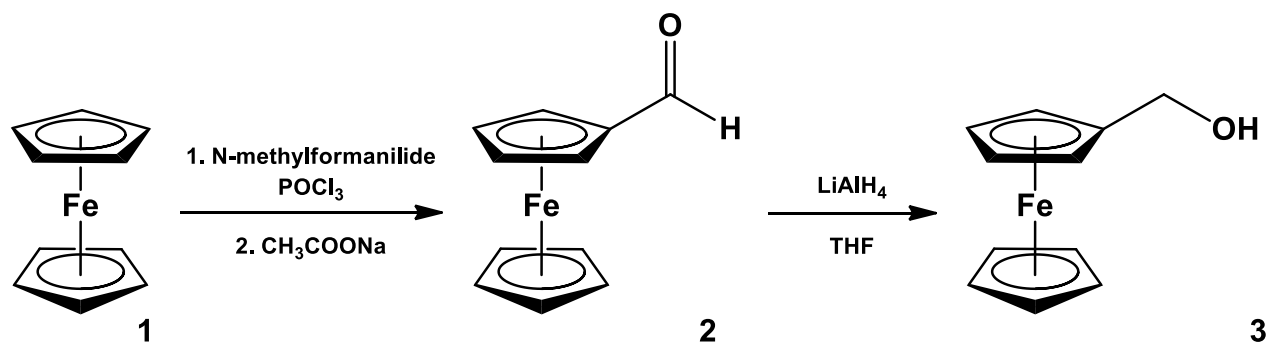
Figure 3.1: Chemical structures of ferrocenylalcohols **3**, **9**, **13**, and **16** as well as poly(*tris*(2,2,2-trifluoroethoxy)(ferrocenylalkoxy)phosphazene) complexes **22**, **23**, **24**, and **25**, synthesised in this study.

Characterisation of the synthesis compounds were achieved utilising proton, phosphorus, and fluorine nuclear magnetic resonance spectroscopy (^1H , ^{31}P and ^{19}F NMR) and infrared spectroscopy (IR). The synthesised ferrocene-containing polyphosphazene complexes were also analysed and characterised by viscometry, GPC, XPS, electrochemistry (cyclic voltammetry, square wave voltammetry and linear sweep voltammetry), UV/vis spectroscopy and differential scanning calorimetry (DSC).

3.2 Synthesis

3.2.1 Ferrocenylmethanol, 3.

Ferrocenylmethanol, **3**, the first alcohol in the series, was synthesised in two steps, according to Scheme 3.1.



Scheme 3.1: Synthesis of ferrocenylmethanol, **3**.

Ferrocenecarboxaldehyde, **2**, was used as a precursor in the synthesis of ferrocenylmethanol, **3**. Ferrocenecarboxaldehyde, **2**, was synthesised using the Vilsmeier formylation method (Scheme 3.1 and section 2.3.2, chapter 2), which utilises phosphorus oxychloride and *N*-methylformanilide. Ferrocenecarboxaldehyde, **2**, was isolated in 83 % yield as a dark red powder after column chromatography with hexane:diethyl ether (1:1) as eluent. Ferrocenylmethanol, **3**, was obtained by the reduction of **2** with lithium aluminium hydride in tetrahydrofuran and was isolated in 98 % yield as an orange powder. Spectroscopically (^1H NMR and ^{13}C NMR) and by elemental analysis complexes **2** and **3** were identical to authentic samples; see Appendix for the NMRs.

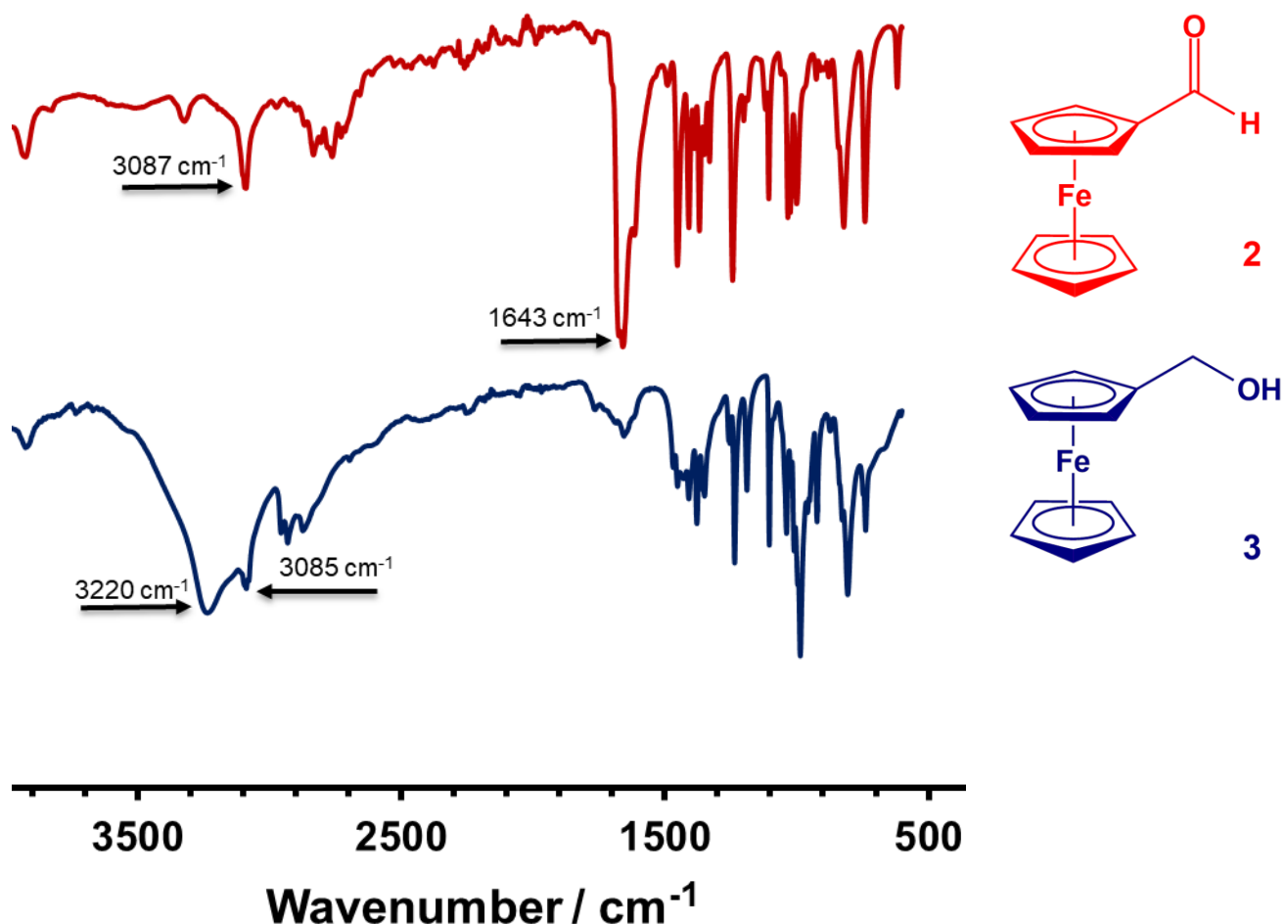
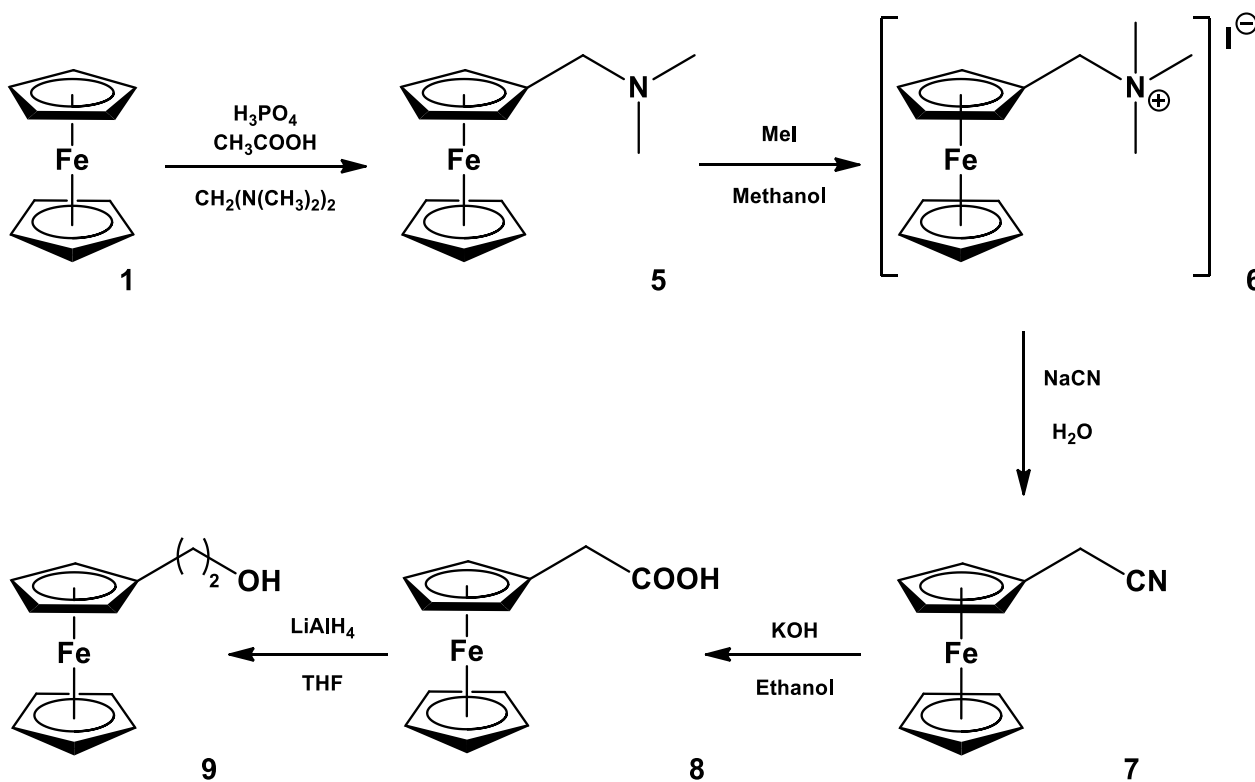


Figure 3.2: Infrared spectra of ferrocenecarboxaldehyde, **2, and ferrocenylmethanol, **3**.**

The IR of **2** and **3** are shown in Figure 3.2. For ferrocenecarboxaldehyde, **2**, the C=O stretching frequency is observed at 1643 cm⁻¹ while the aromatic cyclopentadienyl C-H stretching frequency is at 3087 cm⁻¹. The IR spectrum of ferrocenylmethanol, **3**, exhibit a distinctive, broad O-H stretching vibration between 2500 and 3600 cm⁻¹. The broadness is a characteristic alcohol (O-H) vibration experiencing hydrogen bonding.¹ The absence of the C=O stretching vibration at 1643 cm⁻¹ also confirms the successful reduction of the aldehyde to the alcohol.

3.2.2 2-Ferrocenylethanol, 9.

2-Ferrocenylethanol, **9**, the second alcohol in the series (Figure 3.1) was synthesised in five steps, according to Scheme 3.2.



Scheme 3.2: Synthesis of 2-ferrocenylethanol, 9.

N,N-dimethylaminomethylferrocene, **5**, was synthesised by the Mannich reaction, which utilises acetic acid, phosphoric acid and *bis*(dimethylamino)methane. The amine was isolated in 68 % yield as a yellow oil, boiling between 128 – 130 °C. *N,N,N*-trimethylaminomethylferrocene iodide, **6**, was prepared from iodomethane in methanol solution, which yielded 89 % as a yellow powder. 2-Ferrocenylacetonitrile, **7**, was synthesised by refluxing **6** and sodium cyanide in an aqueous medium, which yielded 76 % as yellow to gold crystals. Ferrocenylacetic acid, **8**, was obtained by the hydrolysis of **7**, with potassium hydroxide and water in an ethanol solution. The product was obtained in 57 % yield as dark golden crystals. 2-Ferrocenylethanol, **9**, was then synthesised by the reduction of **8**, utilising lithium aluminium hydride in tetrahydrofuran. The product was obtained in a 91 % yield as a low melting yellow solid (melting point 32 - 33 °C). The ^1H NMR and elemental analysis of **5** - **9** (see Appendix and Experimental) was in agreement with published values.²

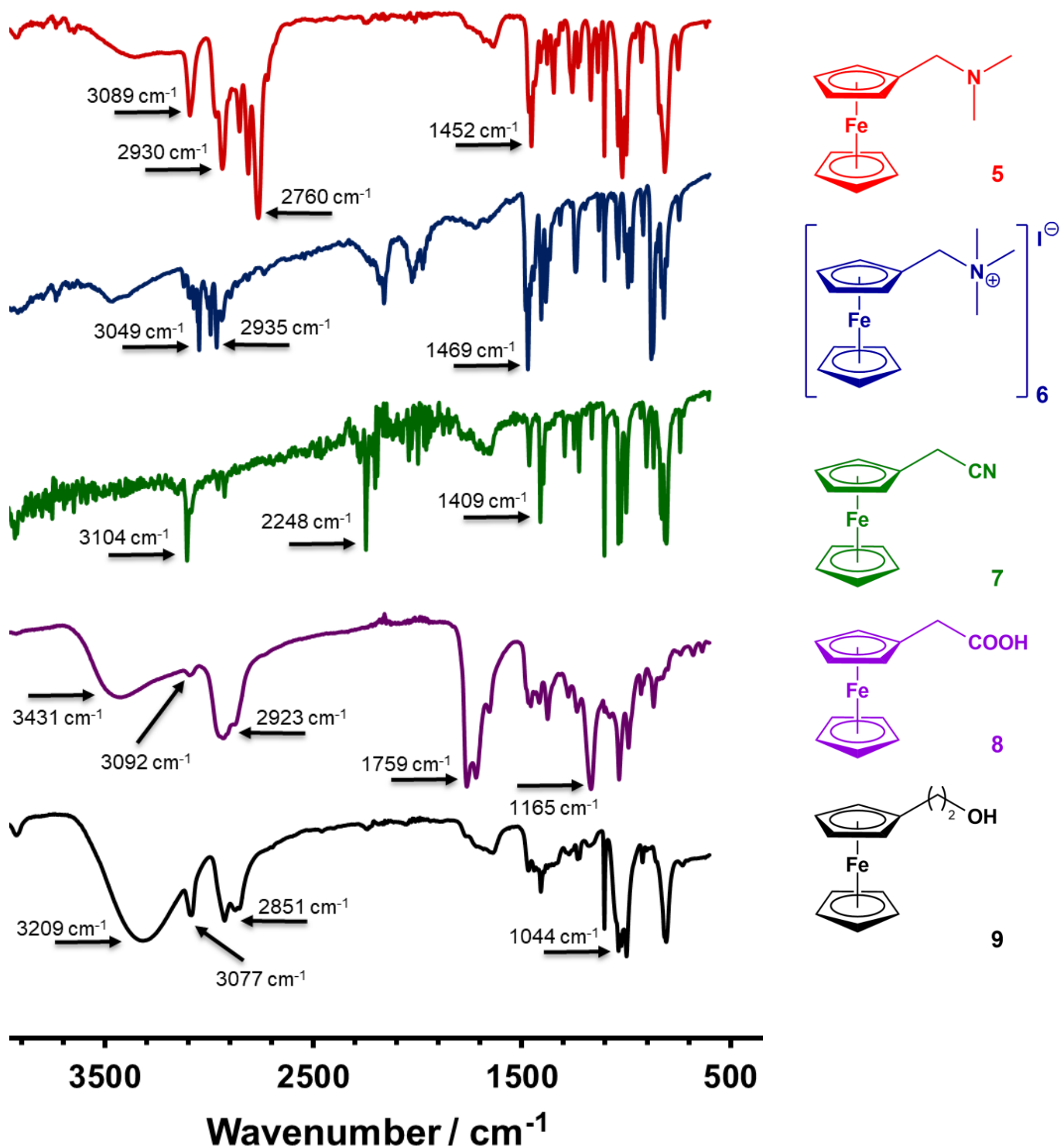


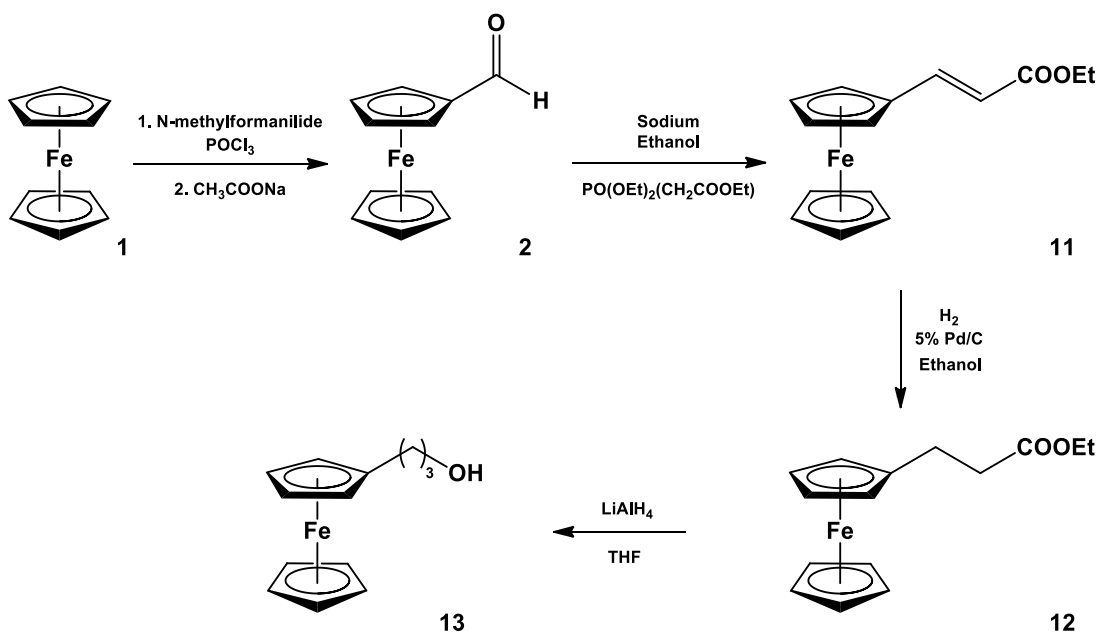
Figure 3.3: Infrared spectra for the series of ferrocenyl derivatives required to synthesise ferrocenylethanol, **9**.

The IR spectra of the series of ferrocenyl derivatives obtained en route to ferrocenylethanol, **9**, are shown in Figure 3.3. The spectrum for *N,N*-dimethylaminomethyl ferrocene, **5**, exhibited the CH₃ bending frequency of 1452 cm⁻¹, the aliphatic C-H stretching frequency between 2760 - 2930 cm⁻¹ and the cyclopentadienyl aromatic C-H stretching vibrations at 3089 cm⁻¹. IR C-H frequencies are observed for *N,N,N*-trimethylaminomethyl ferrocene iodide, **6**, as well as compounds **7** to **9** in the region ± 2850 - 3000 cm⁻¹. The CH₃ bending vibration is observed at 1469 cm⁻¹, the dominant aliphatic C-H vibration at 2935 cm⁻¹ and the aromatic cyclopentadienyl C-H vibration at 3049 cm⁻¹. Additionally, compound **7** showed a nitrile stretching vibration at 2248 cm⁻¹. The vibrations at *ca.* 3400 cm⁻¹ and at 1670 cm⁻¹ is due to moisture. The IR spectrum of ferrocenylacetic acid, **8**, shows a C-O vibration at 1165 cm⁻¹, a C=O stretching vibration at 1759 cm⁻¹ and a broad O-H vibration that is characteristic of carboxylic acids between *ca.* 2400 cm⁻¹ to 3600 cm⁻¹. The C=O carboxylic acid vibrational characteristic disappears in the spectrum for ferrocenylethanol, **9**, but a broad O-H alcohol stretching vibration is observed between 2500 cm⁻¹ and 3600 cm⁻¹, with a maximum frequency at 3209 cm⁻¹. A C-O single bond is observed at 1044 cm⁻¹ and C-H aliphatic stretching vibration at 2851 cm⁻¹.

3.2.3 3-Ferrocenylpropanol, **13**.

3-Ferrocenylpropanol, **13**, the third alcohol in the series (Figure 3.1) was synthesised from the previously prepared ferrocenecarboxaldehyde, **2**, in three steps, according to Scheme 3.3.

Ethyl 3-ferrocenylethenoate, **11**, was prepared from **2** using the Wittig reaction. Sodium metal and ethanol was reacted for the *in situ* formation of sodium ethoxide. Triethylphosphonoacetate was then added to the reaction mixture to form a phosphonium ylide. Ferrocenecarboxaldehyde was then added to form the ester, **11**, in a yield of 78 % as bright orange crystals. Purification by column chromatography using ethyl acetate and *n*-hexane (5:95) as eluent afforded pure **11**. Ethyl 3-ferrocenylethanoate, **12**, was obtained by hydrogenation of **11** over 5 % palladium on carbon as catalyst in an ethanol solution over 24 hours. Complex **12** was obtained in a 98 % yield as an orange/yellow powder. Reduction of **12** with lithium aluminium hydride in tetrahydrofuran gave 100 % of **13**, the desired alcohol, as an orange oil.

**Scheme 3.3: Synthesis of 3-ferrocenylpropanol, 13.**

The ^1H NMR spectra for **2**, **11**, **12** and **13** are presented in Figure 3.4. The proton resonance for the aldehyde proton in **2** is observed at 9.98 ppm due to the electron-withdrawing nature of the carbonyl group of the aldehyde. The resonance frequencies for the cyclopentadienyl protons are observed to shift more upfield as the functional groups present in **2**, **11**, **12** and **13** changed from electron-withdrawing groups to electron-donating groups. The electron-withdrawing effect of the aldehyde group in **2** allows for delocalisation of electrons from the cyclopentadienyl ring to the carbonyl group. This delocalisation allows for a downfield shift of the resonance position of cyclopentadienyl ring protons relative to the resonance frequencies of the unsubstituted cyclopentadienyl ring (Figure 3.4). The ferrocenyl fragments for **2** show resonance frequencies at 4.81 ppm and 4.64 ppm for the protons in the substituted cyclopentadienyl fragment and 4.30 ppm for the unsubstituted cyclopentadienyl fragment (Figure 3.4).

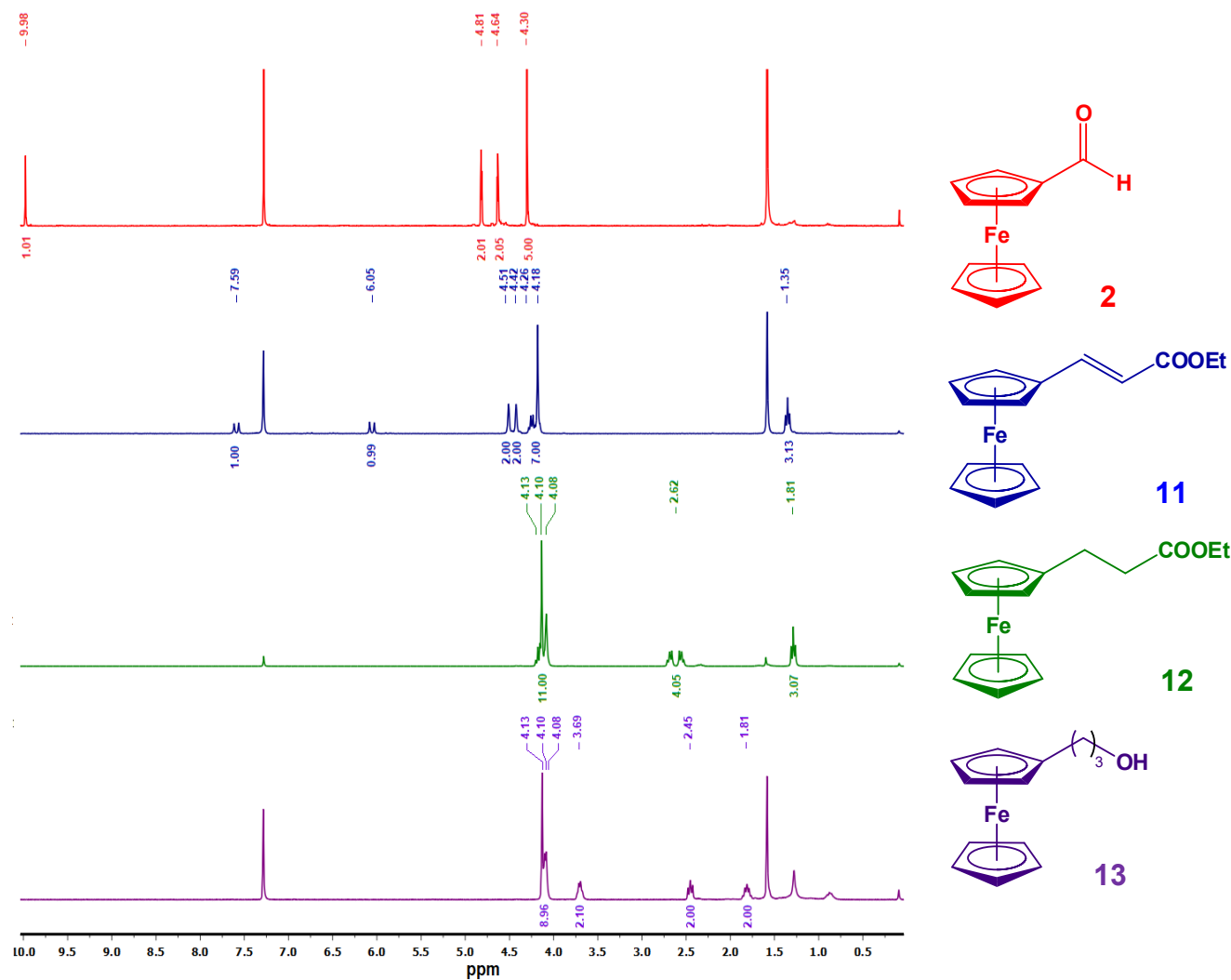


Figure 3.4: ¹H NMR spectra for ferrocenecarboxaldehyde, 2, ethyl 3-ferrocenylethenoate, 11, ethyl 3-ferrocenylethanoate, 12, and ferrocenylpropanol, 13.

Compound **11** also allows for delocalisation of electrons from the carbonyl group to the cyclopentadienyl rings of the ferrocenyl fragment via the alkene bond. This effect is noted relative to the resonance frequency of the protons of the unsubstituted cyclopentadienyl ring. Thus, for **11**, the substituted cyclopentadienyl protons are observed at 4.51 ppm and 4.42 ppm and the unsubstituted cyclopentadienyl protons is observed at 4.18 ppm. The electron-withdrawing effect of the carbonyl group of **11** is not as strong as the electron-withdrawing effect of the aldehyde carbonyl group, therefore the proton resonances of the unsubstituted cyclopentadienyl ring of **11** are not observed as far downfield as that of **2** (in part because it is transmitted over a two carbon bridge to the ferrocenyl group). Reduction of the C=C double bond in **11** to form **12** causes the unsubstituted cyclopentadienyl protons in **12** to shift further upfield because they are now exposed to the electron-donating properties of two adjacent methylene groups. The methylene groups effectively isolate the ferrocenyl group of **12** from its carbonyl group while the double bond in the ethylene group of **11** communicates the electron-withdrawing properties of the carbonyl group to the ferrocenyl group. Therefore, compound **12** exhibits proton resonances for the substituted cyclopentadienyl group at 4.15 ppm and 4.08 ppm and the protons for the unsubstituted cyclopentadienyl group at 4.13 ppm. Reduction of the carbonyl group in **13** to a third methylene group is observed to have little to no effect on the unsubstituted cyclopentadienyl protons and its proton resonances remains at 4.13 ppm (as compared to **12**). However, the electron-donating effect of the larger methylene chain in **13** causes the substituted cyclopentadienyl protons to resonate further upfield at 4.10 ppm and 4.08 ppm (Figure 3.4).

Figure 3.4 also shows resonances for the protons of the unsaturated double bond in **11** and the saturated single bonds in **12**. The electron rich environment of **11** causes the unsaturated aliphatic alkenyl protons to resonate at 7.59 ppm and 6.05 ppm. However, the less electron rich environment of **12** causes the saturated alkyl protons to resonate further upfield at 2.62 ppm. In terms of the ethyl group in the ester functionality of **11** and **12**, the methylene (OCH_2) and the methyl (CH_3) resonance signals are found in the typical position, *ca.* 4.2 ppm and 1.3 ppm, respectively.

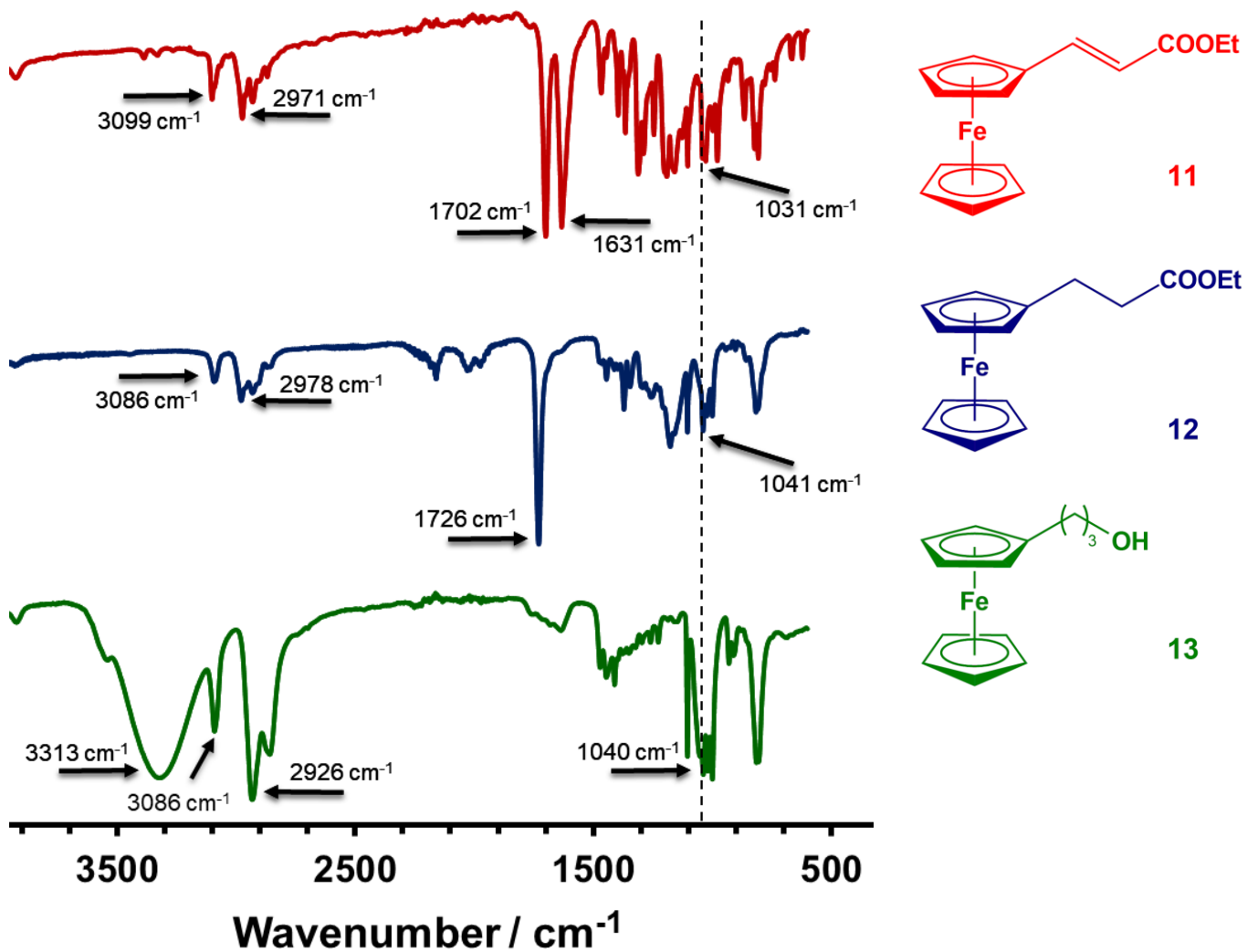


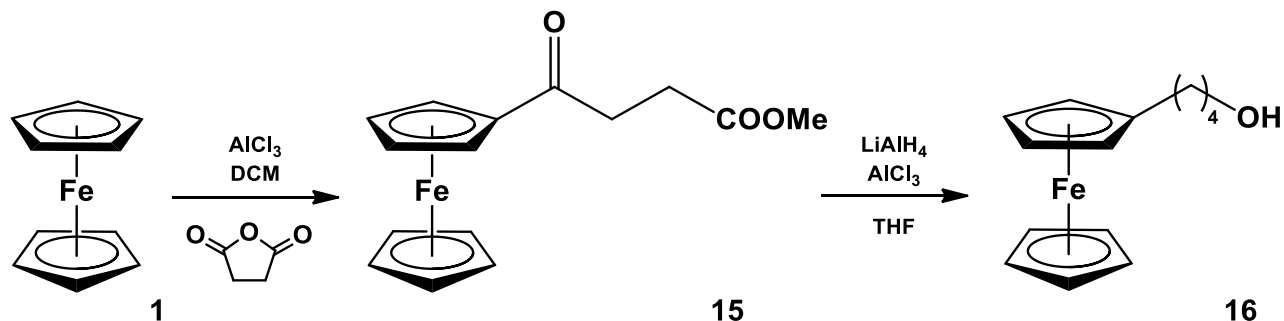
Figure 3.5: Infrared spectra for the series of ferrocenyl derivatives required to synthesise 3-ferrocenylpropanol, **13.**

Figure 3.5 shows the infrared spectra for the ferrocenyl derivatives **11**, **12**, and **13**. Ethyl 3-ferrocenylethenoate, **11**, has a C=C stretching vibration at 1631 cm⁻¹ and a C=O stretching frequency at 1702 cm⁻¹. The aliphatic C-H (2971 cm⁻¹) and aromatic C-H stretching frequencies (3099 cm⁻¹) are also observed for **11**. There is only a C=O stretching band at 1726 cm⁻¹ observed for ethyl 3-ferrocenylethanoate, **12**, since there is no C=C double bond present. The aliphatic C-H (2978 cm⁻¹) and aromatic C-H stretching frequencies (3086 cm⁻¹) are also observed for **12**. 3-Ferrocenylpropanol, **13**, shows a broad alcohol band between 2500 cm⁻¹ and 3600 cm⁻¹, with a vibrational maximum at 3313 cm⁻¹. The C-O single bond for **11**, **12** and **13** is in all these cases

observed at $\sim 1040\text{ cm}^{-1}$. The C-H aliphatic stretching frequency for **13** is at 2926 cm^{-1} and the C-H aromatic stretching frequency at 3086 cm^{-1} .

3.2.4 4-Ferrocenylbutanol, **16**.

4-Ferrocenylbutanol, **16**, the last alcohol in the envisaged series (Figure 3.1) was synthesised in two steps, as shown in Scheme 3.4.



Scheme 3.4: Synthesis of 4-ferrocenylbutanol, **16.**

Friedel-Crafts acylation of ferrocene, **1**, utilising succinic anhydride and aluminium chloride in dichloromethane, produced 3-ferrocenylpropionic acid, **15**, in 48 % yield as a light brown powder. Reduction of **15**, utilising aluminium chloride and lithium aluminium hydride in tetrahydrofuran solution, gave **16** as an orange oil, with a yield of 87 %.

The ^1H NMR spectra of **15** and **16** were in agreement with those of published procedures (see Appendix) and elemental analysis (see Chapter 4) were as expected.²

The IR spectra of 3-ferrocenylpropionic acid, **15**, and 4-ferrocenylbutanol, **16**, are shown in Figure 3.6. The two carbonyl groups for **15** vibrates at 1654 cm^{-1} (keto C=O) and 1711 cm^{-1} (carboxylic acid C=O). The cyclopentadienyl aromatic C-H vibration for **15** are observed at 3108 cm^{-1} . The broad peak for the O-H bond of the carboxylic acid is observed between 2591 cm^{-1} and 3108 cm^{-1} . The IR spectrum of ferrocenylbutanol, **16**, indicates the broad O-H alcohol vibrational band between 3050 cm^{-1} and 3550 cm^{-1} , with a maximum at 3314 cm^{-1} , as well as the C-H aliphatic (2934 cm^{-1}) and C-H aromatic (3094 cm^{-1}) stretching frequencies. The C-O stretching vibrations for **15** and **16** are observed at 1078 cm^{-1} and 1055 cm^{-1} respectively.

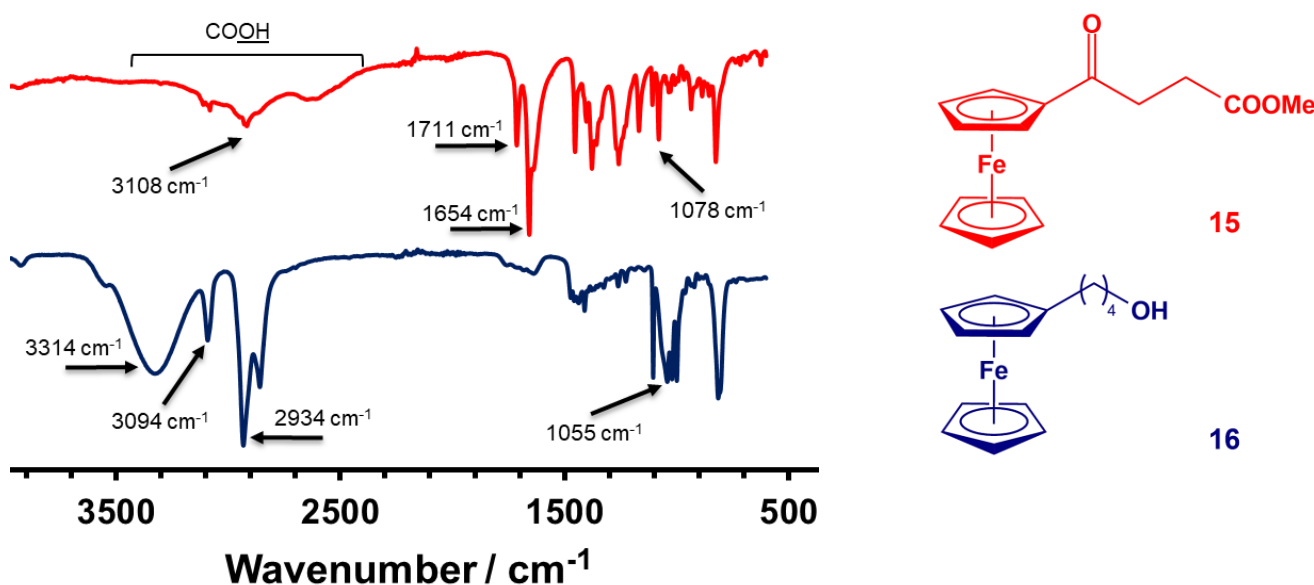
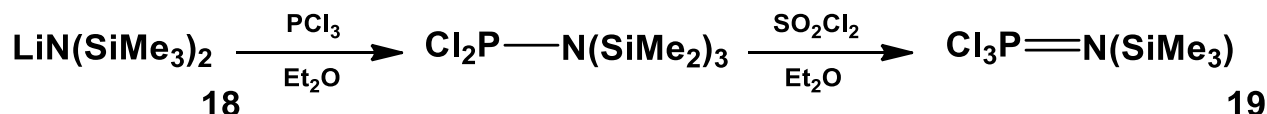


Figure 3.6: Infrared spectra of 3-ferrocenoylpropionic acid, 15, and 4-ferrocenylbutanol, 16.

3.2.5 Trichloro(trimethylsilyl)phosphoranimine, 19.

Trichloro(trimethylsilyl)phosphoranimine, **19**, serves as a suitable monomer for the synthesis of polyphosphazenes and was synthesised in two *in situ* steps from lithium bis(trimethylsilyl)amide, **18**, phosphorus trichloride and sulfuryl chloride (Scheme 3.5).



Scheme 3.5: Synthesis of trichloro(trimethylsilyl)phosphoranimine monomer, 19.

Lithium bis(trimethylsilyl)amide, **18**, was reacted with phosphorus trichloride to form $\text{Cl}_2\text{P}-\text{N}(\text{SiMe}_3)_2$ *in situ* together with the elimination of lithium chloride. Addition of sulfonyl chloride as chlorinating agent produces **19**, with sulphur dioxide and chlorotrimethylsilane as byproducts. Distillation of the crude product yielded **19** as a clear liquid in 66 % yield.

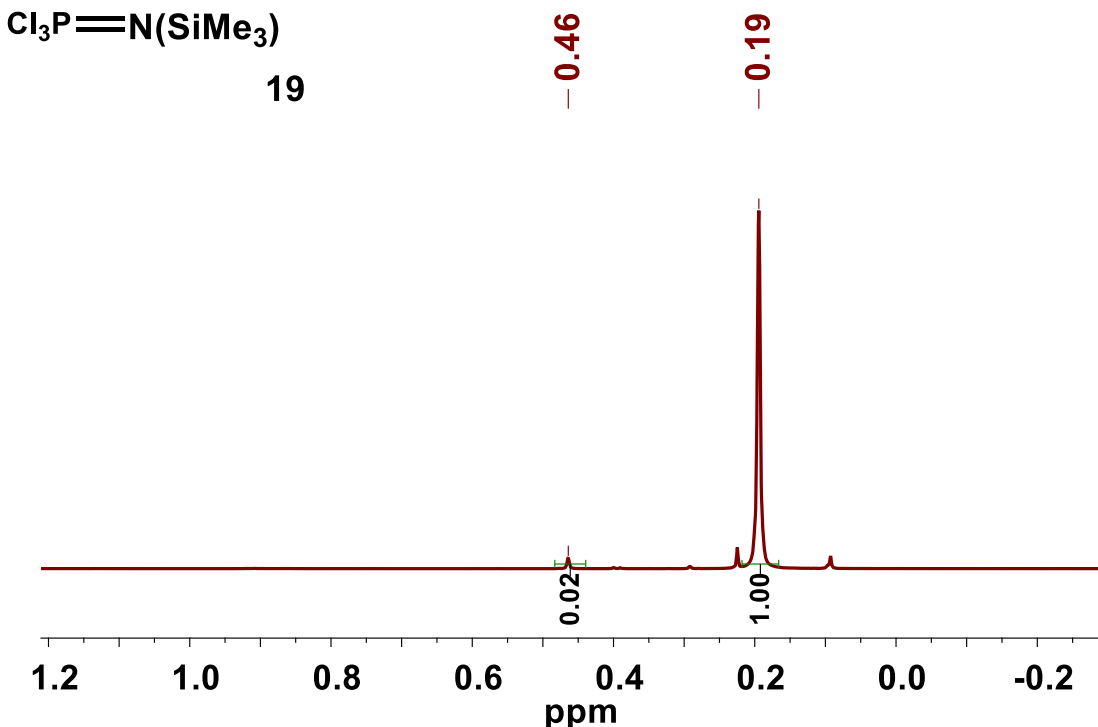


Figure 3.7: ¹H NMR spectrum of trichloro(trimethylsilyl)phosphoranimine monomer, **19**.

The ¹H and ³¹P NMR spectra for trichloro(trimethylsilyl)phosphoranimine, **19**, are shown in Figure 3.7 and Figure 3.8 respectively. In the ¹H spectrum, the peak at 0.19 ppm is the signal for the three CH₃ groups of the trimethylsilyl fragment of **19**. The ¹H NMR also indicates 2 % of chlorotrimethylsilane impurity at 0.46 ppm. The majority of this impurity was removed via vacuum distillation of **19**; however, a trace amount remained and was observed in the proton NMR.

It is interesting to observe the influence of a Si-atom on the resonance position of the methyl groups in the SiMe₃ fragments of **19**. If the Si atom was replaced with a C-atom, the Me groups of -CMe₃ would be expected to resonate at *ca.* 0.8 ppm. For **19**, the three Me groups resonated at 0.19 ppm, almost where the ¹H NMR standard of SiMe₄ resonates: 0.00 ppm. The ¹H NMR resonance position of compound **19** shifted downfield from 0.00 ppm due to the electron-withdrawing properties of the P(V) fragment Cl₃P=N- relative to the SiMe₃ fragment.

The ³¹P NMR of **19** shows a peak at -50 ppm. This peak represents the phosphorus atom of the monomer, **19**. Both the proton and phosphorus data is consistent with literature.³

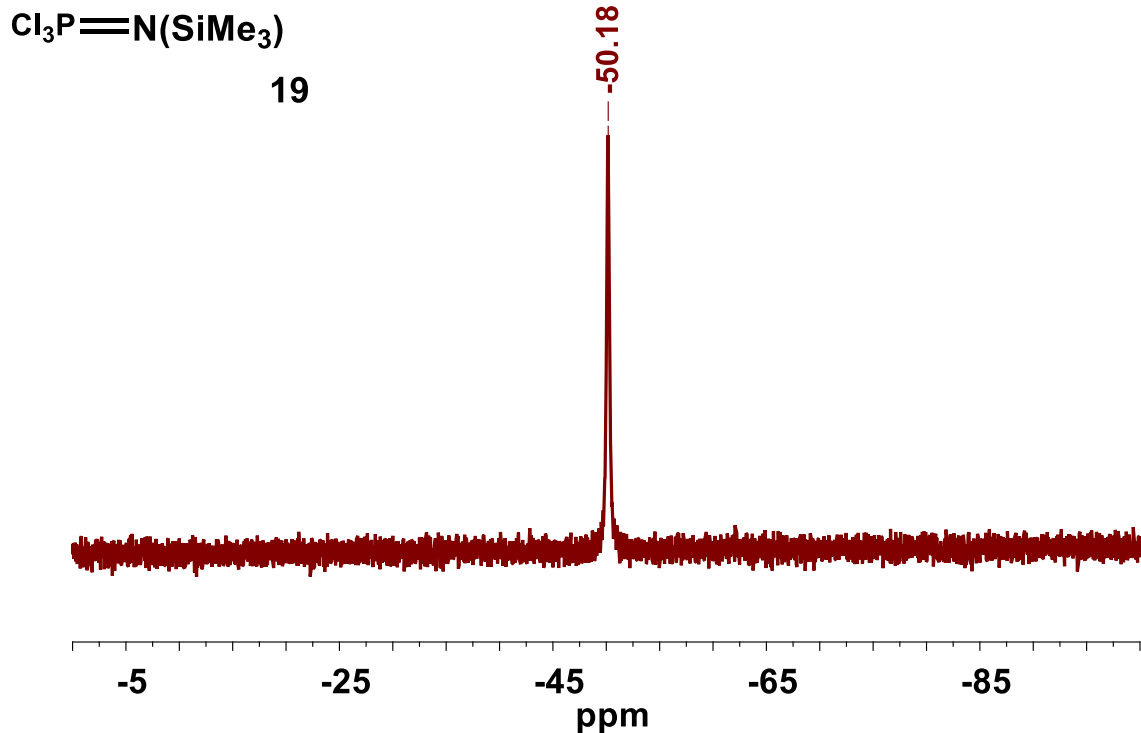
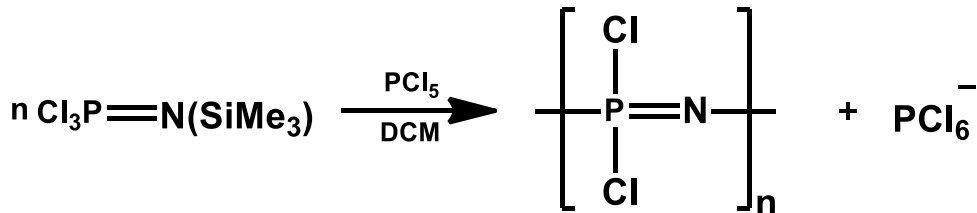


Figure 3.8: ^{31}P NMR of trichloro(trimethylsilyl)phosphoranimine monomer, **19**.

3.2.6 Poly(dichlorophosphazene), **20**.

Poly(dichlorophosphazene), **20**, was synthesised in one step from trichloro(trimethylsilyl)phosphoranimine monomer, **19**, by using phosphorus pentachloride as initiator in dichloromethane (Scheme 3.6).



Scheme 3.6: Synthesis of poly(dichloro)phosphazene, **20**.

A sample of very reactive and therefore unstable poly(dichlorophosphazene), **20**, was isolated for characterisation. Once samples were taken for characterisation, the chloride side groups of the highly reactive poly(dichlorophosphazene), **20**, were immediately replaced with less-reactive-than Cl side groups rendering the polymer stable enough to store (as discussed in the following Section 3.2.7).

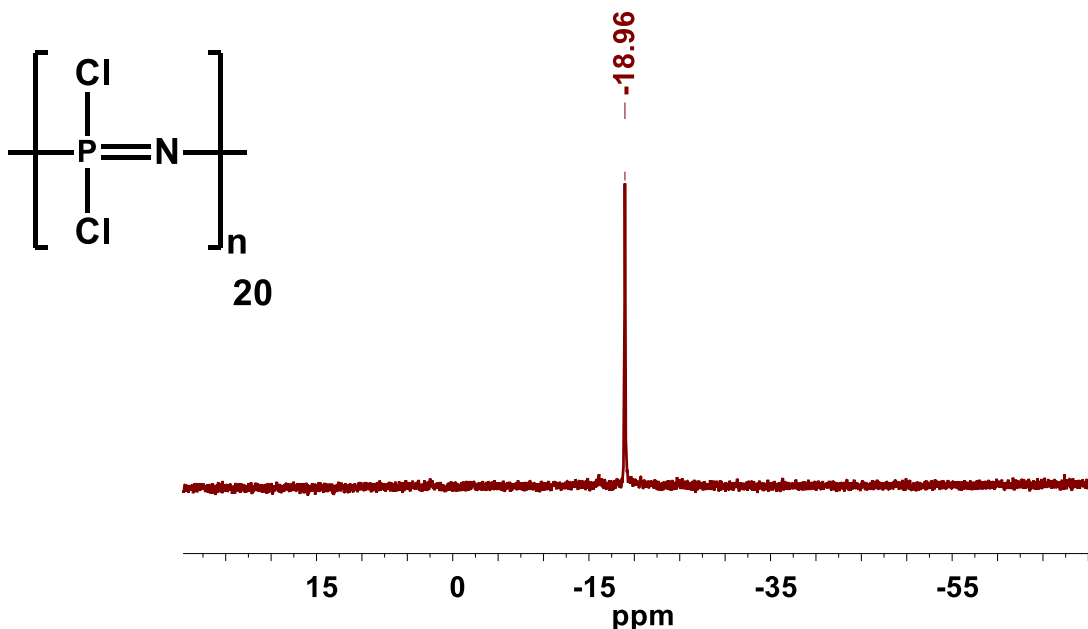


Figure 3.9: ^{31}P NMR of poly(dichlorophosphazene), **20**.

^{31}P NMR of poly(dichlorophosphazene), **20**, is presented in Figure 3.9 (since **20** has no hydrogen atoms, a ^1H NMR cannot be provided). The phosphorus signal in **20** is observed at -19 ppm; these resonances are consistent with literature.⁴

IR spectra for trichloro(trimethylsilyl)phosphoranimine, **19**, and poly(dichlorophosphazene), **20**, are shown in Figure 3.10. These spectra are very similar to each other due to the similar functional groups detected by IR spectroscopy on both **19** and **20**. The P-Cl bond vibration for both **19** and **20** are observed at 731 cm^{-1} . A slight shift in the dominant stretching frequency of the P=N double bond is observed from 1191 cm^{-1} for **19** to 1223 cm^{-1} for **20**. As expected, sharper (better resolved) signals (731 cm^{-1} as well as 1191 cm^{-1}) are also observed for the monomer, **19**, compared to the IR spectrum of the polymer, **20**, because repeating units for **20** are not exposed to a uniform environment while a P=N functionality in monomer **19** is exposed to the same chemical environment for all monomer molecules in the analysed sample.

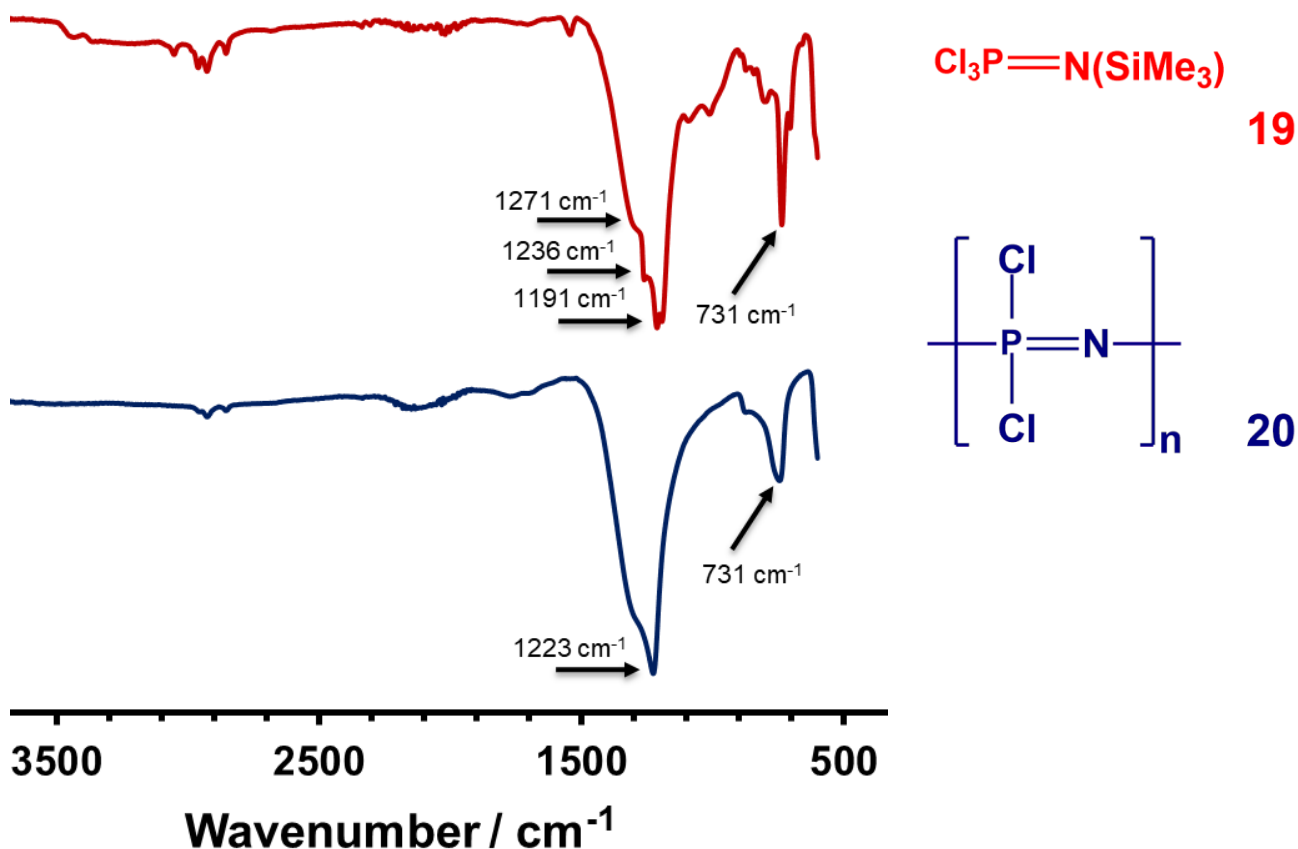


Figure 3.10: Infrared spectra of trichloro(trimethylsilyl)phosphoranimine, **19**, and poly(dichlorophosphazene), **20**.

The molecular weight and properties of polymer **20** is controlled by the initiator to monomer ratio. Additionally, the cationic polymerisation method (see Scheme 2.6 in chapter 2, page 10) used is considered a living polymerisation process. This means that once the polymer is synthesised in a pure enough environment, if additional monomer is added to this reaction, the polymer chain will continue to grow, increasing the molecular weight of the polymer. Typical for living polymers, the number average molecular mass, \overline{M}_n , may be estimated from monomer / initiator ratios as follows:

$$\overline{M}_n = \left(\frac{n_{\text{monomer}}}{n_{\text{initiator}}} \times M_{r,\text{monomer}} \right) + M_{r,\text{endgroups}}$$

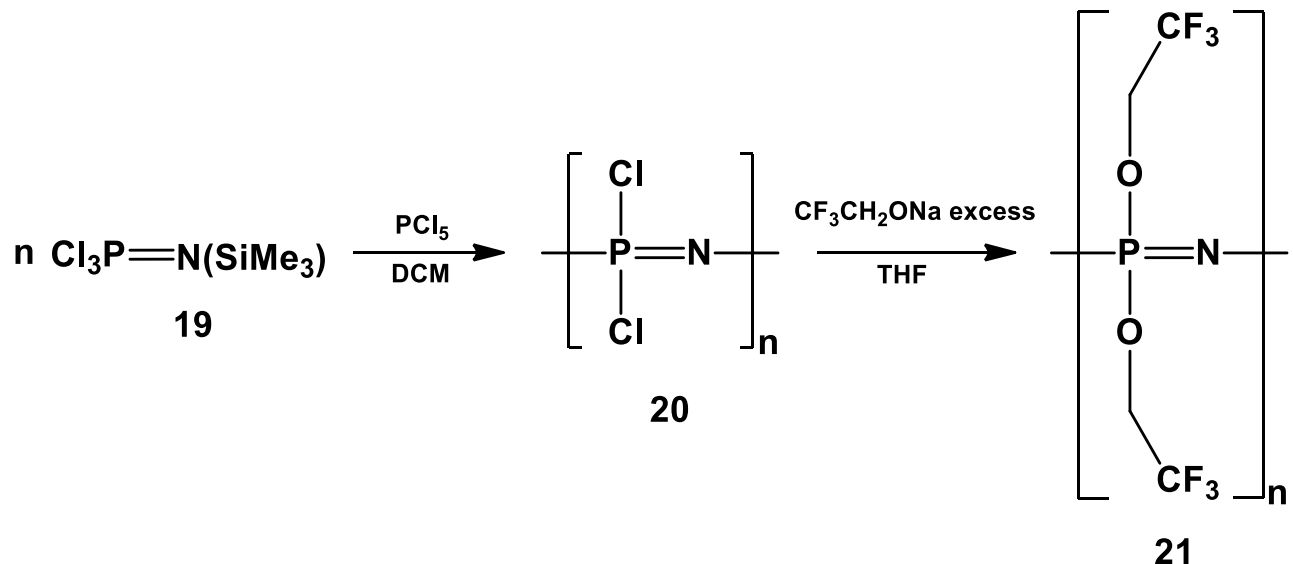
Typically, when 10 moles of **19** is reacted with 1 mole of PCl5,

$$\overline{M}_n = \left(\frac{10}{1} \times 115.9 \text{ g/mol} \right) + 243.7 \text{ g/mol} = 1402 \text{ g/mol}$$

If the ratio was 25:1, the \overline{M}_n would be 3141 g/mol. It was eventually decided to focus on a monomer/initiator ratio as $\text{Cl}_3\text{P}=\text{NSiMe}_3 : \text{PCl}_5 = 25:1$ for this study, but due to the instability of **20**, no molecular mass determinations were performed. Molecular masses were confirmed by GPC as well as viscosity measurements for follow-up polymers **21** to **25** and will be discussed in Sections 3.3 and 3.4 of this chapter. Based on an extrapolation of the results for compounds **21** to **25**, it is probable that the molecular mass of **20** was as expected for a 25:1 monomer/initiator ratio.

3.2.7 Poly[bis(2,2,2-trifluoroethoxy)phosphazene], **21**.

Poly[bis(2,2,2-trifluoroethoxy)phosphazene], **21**, was synthesised according to Scheme 3.7, by reacting poly(dichlorophosphazene), **20**, with an excess of sodium trifluoroethoxide.



Scheme 3.7: Synthesis of poly[bis(2,2,2-trifluoroethoxy)phosphazene], **21.**

The ratio between the initiator and monomer used in the synthesis of poly(dichlorophosphazene), **20**, determined the molecular weight and the properties of the final polymer.

First attempts at making **21** were utilised with a molar ratio of initiator (PCl_5) to monomer, **19**, of 1:10. A low monomer concentration of 0.05 mM was used. The product isolated was an insoluble, white, rubbery material which could not be characterised by ^{31}P NMR and ^1H NMR Spectroscopy (Figure 3.11, left). For this ratio, theoretically, $\overline{M}_n \approx 2674$ g/mol. Fractionation by partial precipitation allowed in later experiments to obtain higher molecular mass fractions. A higher

monomer concentration of 0.5 mM was then used and an initiator to monomer molar ratio of 1:25. This yielded 21.4 % of a soluble white powder after workup which could be characterised by ^{31}P and ^1H NMR spectroscopy (Figure 3.11, right, and Figure 3.12). The obtained spectra is consistent with what one would expect (by comparison with literature) of **21**.⁴



Figure 3.11: Poly[*bis*(2,2,2-trifluoroethoxy)phosphazenes], **21, as an insoluble rubber (left) and as a soluble white powder (right).**

Figure 3.12 shows the ^{31}P NMR spectrum of poly[*bis*(2,2,2-trifluoroethoxy)phosphazenes], **21**. The phosphorus resonance for the $\text{P}-\text{O}-\text{CH}_2\text{CF}_3$ fragment is observed at -7.85 ppm. The absence of other ^{31}P NMR signals emphasised the purity of the polymer. The monomer phosphorus atom resonates at -50.18 ppm, while insoluble impurities were removed in the workup step.⁴

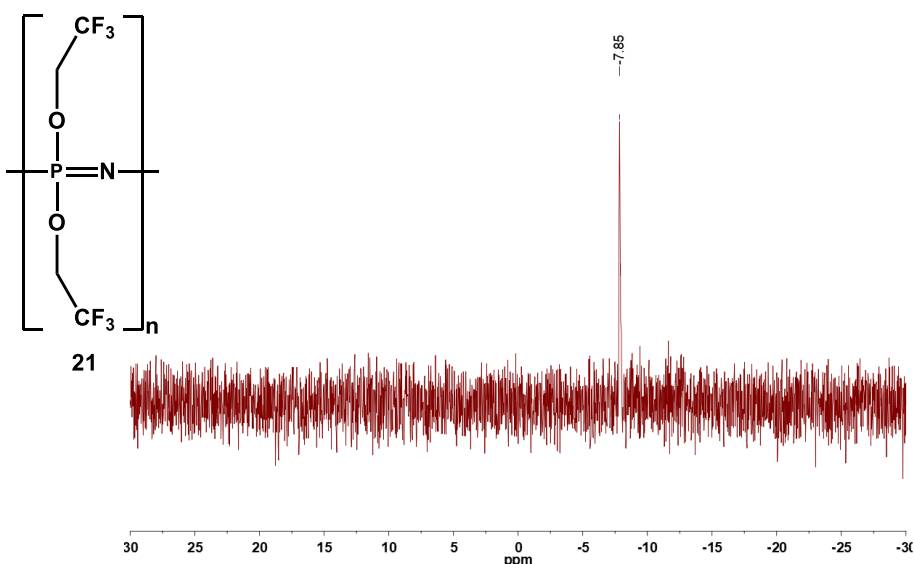
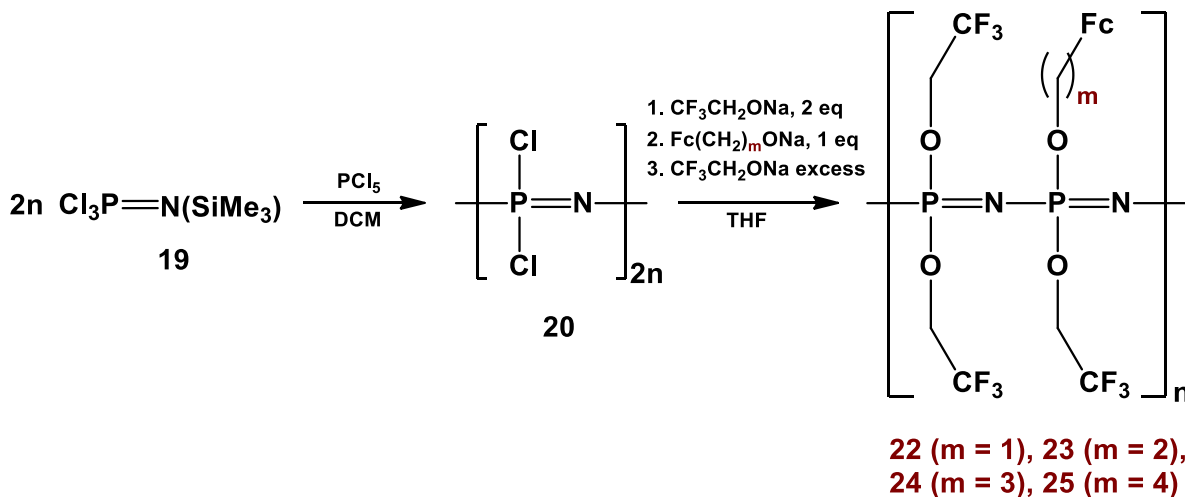


Figure 3.12: ^{31}P NMR spectra of poly[bis(2,2,2-trifluoroethoxy)phosphazene], **21**.

3.2.8 Poly[*tris*(2,2,2-trifluoroethoxy)(ferrocenylalkoxy)phosphazene] complexes

Poly[*tris*(2,2,2-trifluoroethoxy)(ferrocenylalkoxy)phosphazene] complexes (**22**, **23**, **24** and **25**) were synthesised according to Scheme 3.8. Alkyl chain lengths, m, on the ferrocenylalkoxy groups were 1, 2, 3, and 4 for compounds **22**, **23**, **24**, and **25** respectively.



Scheme 3.8: Synthesis of poly[tris(2,2,2-trifluoroethoxy)(ferrocenylalkoxy)phosphazene] complexes, 22, 23, 24, and 25, where $m = 1, 2, 3$, and 4 . It should be noted that the indicated structures of 22 -25 are idealised, giving an overall statistical average stoichiometry. However, in practise, the ferrocenylalkoxy group will be found in a random distribution pattern over the entire main chain.

Compounds 22, 23, 24, and 25 were all synthesised with the initiator to monomer ratio of 1:25, as shown in Scheme 3.8, which all produced soluble polymeric material. The mean \overline{M}_n is expected to be 15074 g/mol for 22, 15425 g/mol for 23, 15775 g/mol for 24 and 16125 g/mol for 25. For the addition of the ferrocenylalkoxide salt, substitution of 25 % of the side chains of the polymer was the target. Once poly(dichlorophosphazene) was synthesised and dissolved in tetrahydrofuran, 50 mol% of sodium trifluoroethoxide (dissolved in THF) was immediately added to the polymer solution and allowed to react for 24 hours. To allow for the substitution to favour a random distribution, the solution was stirred vigorously and the dissolved sodium trifluoroethoxide added dropwise. The appropriate mass of ferrocenylalkoxide sodium salt (i.e., 1 eq) (e.g., sodium ferrocenylmethoxide for compound 22) was dissolved in dry THF and added dropwise to the reaction mixture and again stirred for 24 hours. To complete the substitution of the remaining chlorine atoms, an excess of roughly 80 mol % of sodium trifluoroethoxide was added to the reaction mixture. The sequence of this procedure was previously reported in literature, for polymers bearing phenyleneoxy side chains, and was adapted for the synthesis of poly[tris(2,2,2-trifluoroethoxy)(ferrocenylalkoxy)phosphazene] complexes.⁵

Table 3.1: Yields for the synthesis of 22, 23, 24 and 25, poly[*tris*(2,2,2-trifluoroethoxy)(ferrocenylalkoxy)phosphazene] complexes

| Compound | Yield after fractional precipitation / % |
|-------------------|--|
| 22 (m = 1) | 11.6 |
| 23 (m = 2) | 13.5 |
| 24 (m = 3) | 12.2 |
| 25 (m = 4) | 10.3 |

Table 3.1 summarises the yields of the polyphosphazene obtained for poly[*tris*(2,2,2-trifluoroethoxy)(ferrocenylalkoxy)-polyphosphazene] compounds, **22**, **23**, **24**, and **25**. Compared to the yield of poly[*bis*(2,2,2-trifluoroethoxy)phosphazene], **21** (21.4 % yield), the yields of the polyphosphazene polymers containing ferrocenylalkoxy groups are about 50 % lower, with an average yield of 12 %. The bulky electron-donating ferrocenylalkoxy group may contribute to solubility of the polymeric chain during precipitation, thereby causing smaller oligomeric material from precipitating; therefore, the smaller (better soluble) fractions may be washed away during workup of the reaction mixture. The workup involved separation of the precipitated polymer by centrifugation. Smaller oligomeric molecules and broken polymeric segments which are soluble in the distillate and not able to separate during centrifugation would have been washed away. This is due to the effect of molecular mass on the solubility of the polymer, as generally, an increase in molecular mass is observed to decrease the polymers solubility.⁶

In terms of ¹H NMR, all compounds **21 – 25** showed the expected resonances, (see Appendix and Chapter 4). Figure 3.13 shows the ¹H NMR spectrum of 4-ferrocenylbutanol, **16**, stacked on the ¹H NMR spectrum of poly[*tris*(2,2,2-trifluoroethoxy)(ferrocenylbutoxy)phosphazene], **25**. The overlapping resonances of 3 × CF₃CH₂-O and O-CH₂CH₂CH₂CH₂Fc are found in the region 5.5 ppm - 4.2 ppm. The resonances of these protons is found in a relatively broad band due to the multitude of possible environments for each proton upon coiling of the polymeric main chain. The resonance for O-CH₂CH₂CH₂CH₂Fc is found at 3.6 ppm for 4-ferrocenylbutanol, **16**, and at 3.4 ppm for compound **25**. The O-CH₂CH₂CH₂CH₂Fc resonance in **16** and **25** appear at 2.38 ppm and 2.3 ppm, respectively, while the resonance for the remaining 4 protons in O-CH₂CH₂CH₂CH₂Fc fragments of **16** and **25** appear at 1.61 ppm and 1.28 ppm, respectively. The polymer resonances (**25**) were consistently broader than the resonances of **16**; the resonances of **25** shifted upfield

compared to that of **16** because of the different polymer solvent (THF-d8) used and the deshielding of the protons by the size of the polymeric main chain.

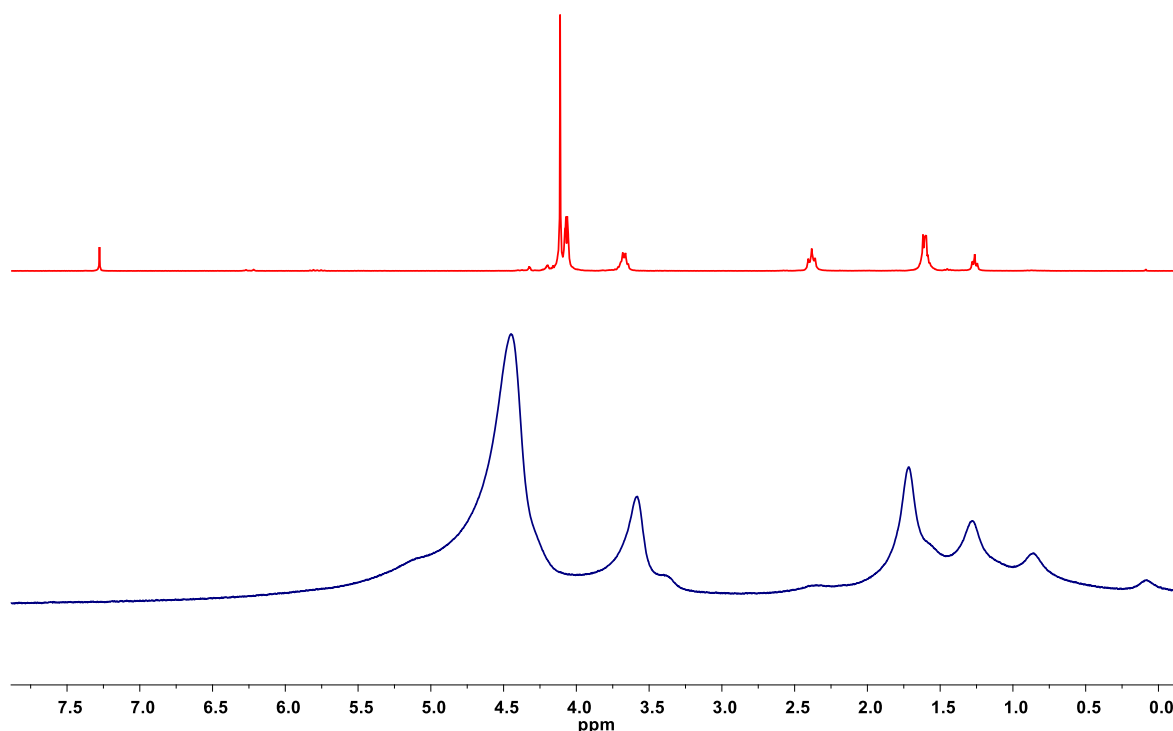


Figure 3.13: ¹H NMR Spectra of 4-ferrocenylbutanol, **16** (above), and poly[tris(2,2,2-trifluoroethoxy)(ferrocenylbutoxy)phosphazene], **25** (below).

Figure 3.14 shows the infrared spectra of poly[bis(2,2,2-trifluoroethoxy)phosphazene], **21**, as well as poly[tris(2,2,2-trifluoroethoxy)(ferrocenylalkoxy)phosphazene] complexes where the alkoxy chain length, **m**, is 1 (**22**), 2 (**23**), 3 (**24**), and 4 (**25**). Similar bonding vibrations are observed for all the substituted poly(organophosphazenes) that were synthesised. The P=N vibration is observed at approximately 1260 cm⁻¹ for compounds **21**, **22**, **23**, **24**, and **25**. Bonding vibration of the P-O-C stretching is observed between 1154 – 839 cm⁻¹ for compounds **21**, **22**, **23**, **24**, and **25**.⁷ The stretching frequency for the C-F bond of trifluoro derivatives are reported in literature between 937 – 1102 cm⁻¹ and also between 1117 – 1210 cm⁻¹.⁸ These stretching frequencies are; however, not clearly observed and are most likely overlapped by the P=N and P-O-C stretching vibrations. Part of the P=N stretch is observed at 1260 cm⁻¹. From the infrared spectra alone, it is easy to distinguish unsubstituted poly(dichlorophosphazene) with the P-Cl stretch, from substituted poly(organophosphazene) with the P-O-C stretch.

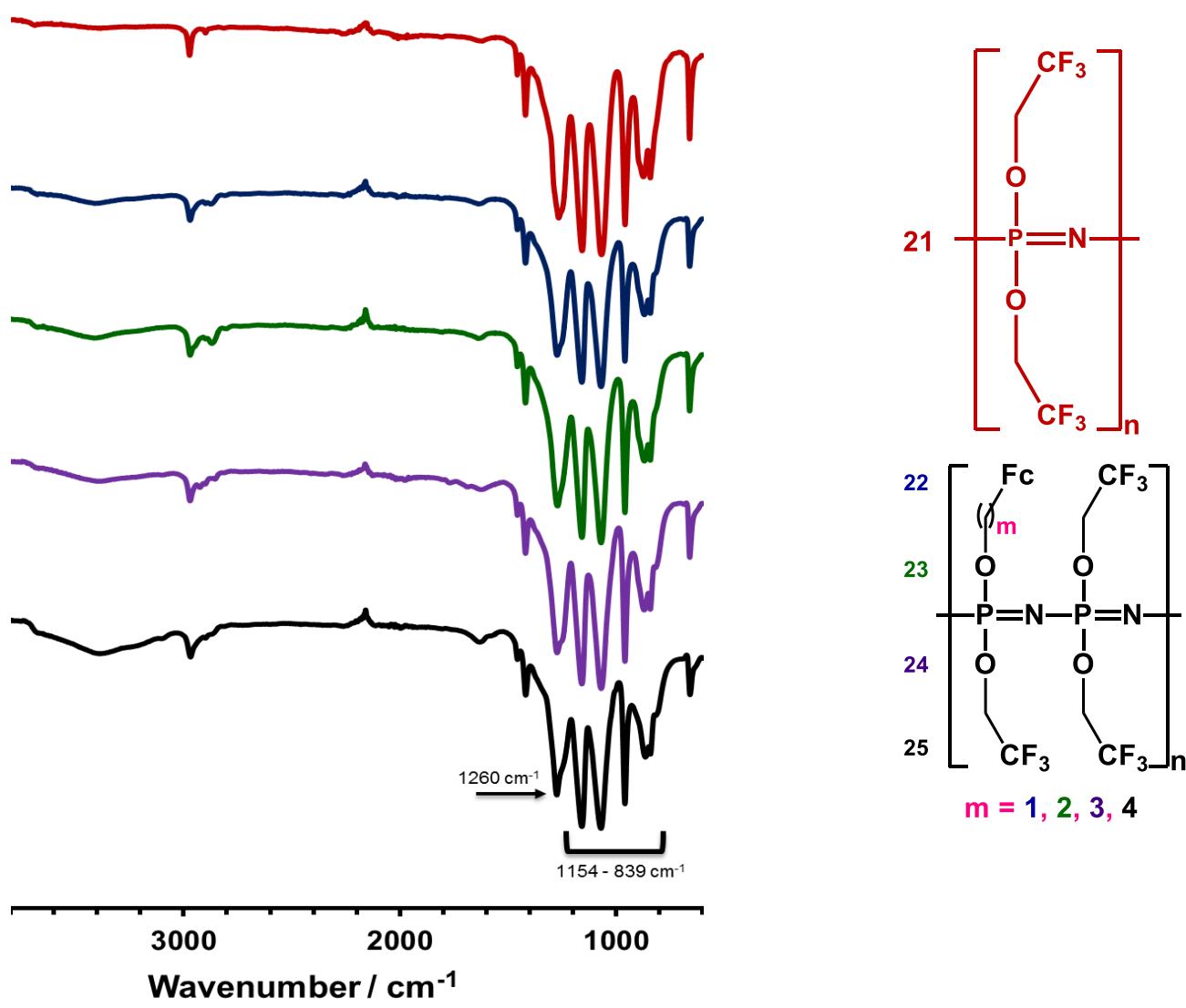


Figure 3.14: Infrared spectra of poly[bis(2,2,2-trifluoroethoxy)phosphazene], 21, and poly[tris(2,2,2-trifluoroethoxy)(ferrocenylalkoxy)phosphazene] compounds, 22, 23, 24, and 25.

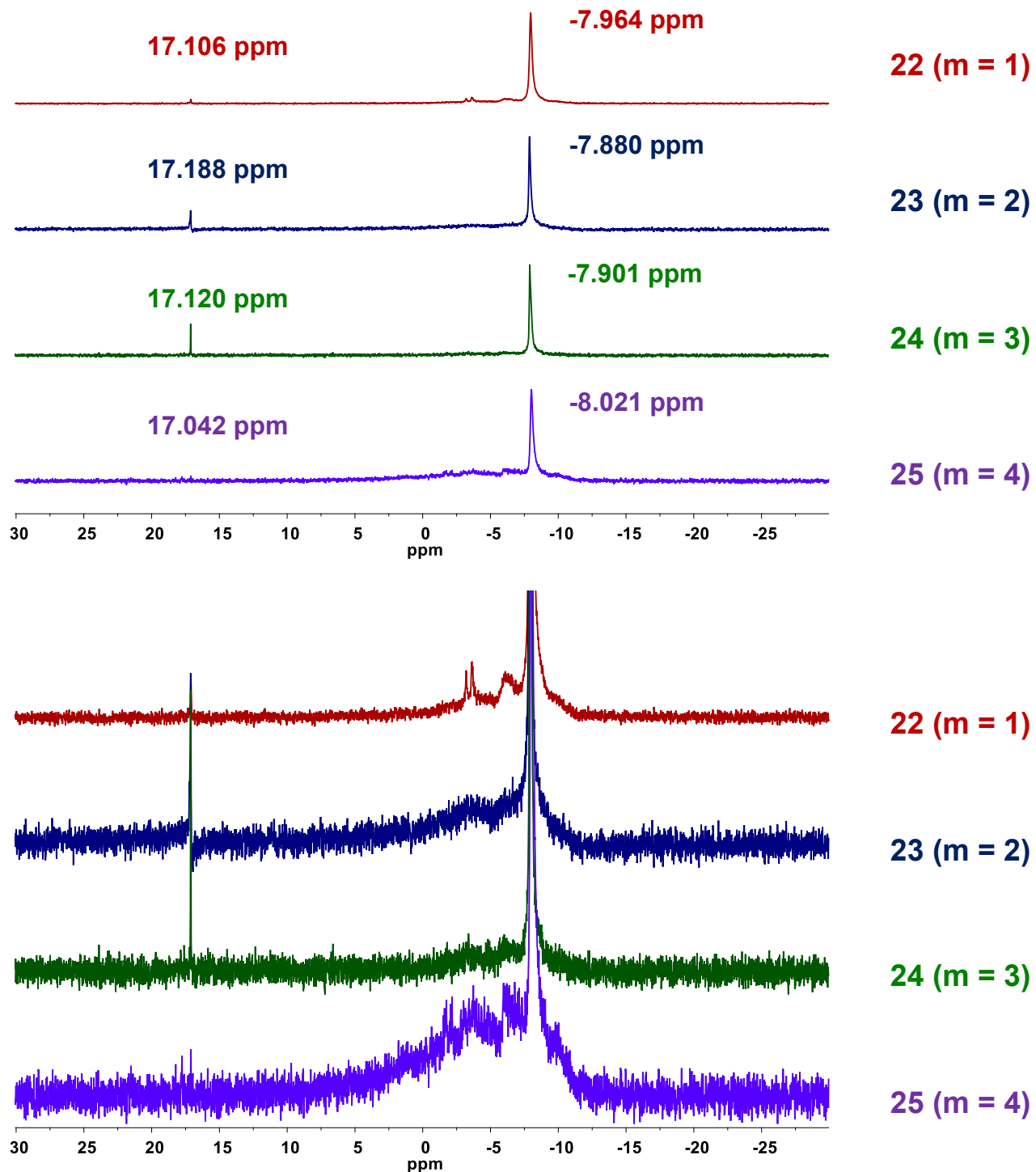


Figure 3.15: ^{31}P NMR of poly[tris(2,2,2-trifluoroethoxy)(ferrocenylalkoxy)phosphazene] compounds where alkoxy chain length $m = 1, 2, 3$ and 4 (22 – 25).

The ^{31}P NMR spectra of poly[*tris*(2,2,2-trifluoroethoxy)(ferrocenylalkoxy)phosphazenes] compounds **22** ($m = 1$), **23** ($m = 2$), **24** ($m = 3$), and **25** ($m = 4$) are shown in Figure 3.15. The amplitude of the spectra are enlarged at the bottom of Figure 3.15 so that the broad peaks due to polymeric properties can be observed clearly. The phosphorus signal for the P-O-CH₂-CF₃ environment for **22**, **23**, **24**, and **25** are consistent with phosphorus signal for **21** between -7.88 ppm to -8.02 ppm (Figure 3.12 and Figure 3.15). Broad bands are observed for **22**, **23**, **24**, and **25** due to multiple combinations of phosphorus environments due to the polymeric nature of the synthesised polyphosphazenes (caused by different chemical environments from the multitude of folding patterns of the polymer chains). These linear polymeric ferrocenylalkoxy-containing polyphosphazenes are able to coil and entangle, providing multiple environments and interactions with the phosphorus atoms on the polymeric backbone. Therefore, broad peaks are observed in the ^{31}P NMR shown in Figure 3.15. The absence of ^{31}P NMR resonances at -50 ppm and -19 ppm, or elsewhere in the spectra, strongly implies the absence of any other functionalised polyphosphazene entities.

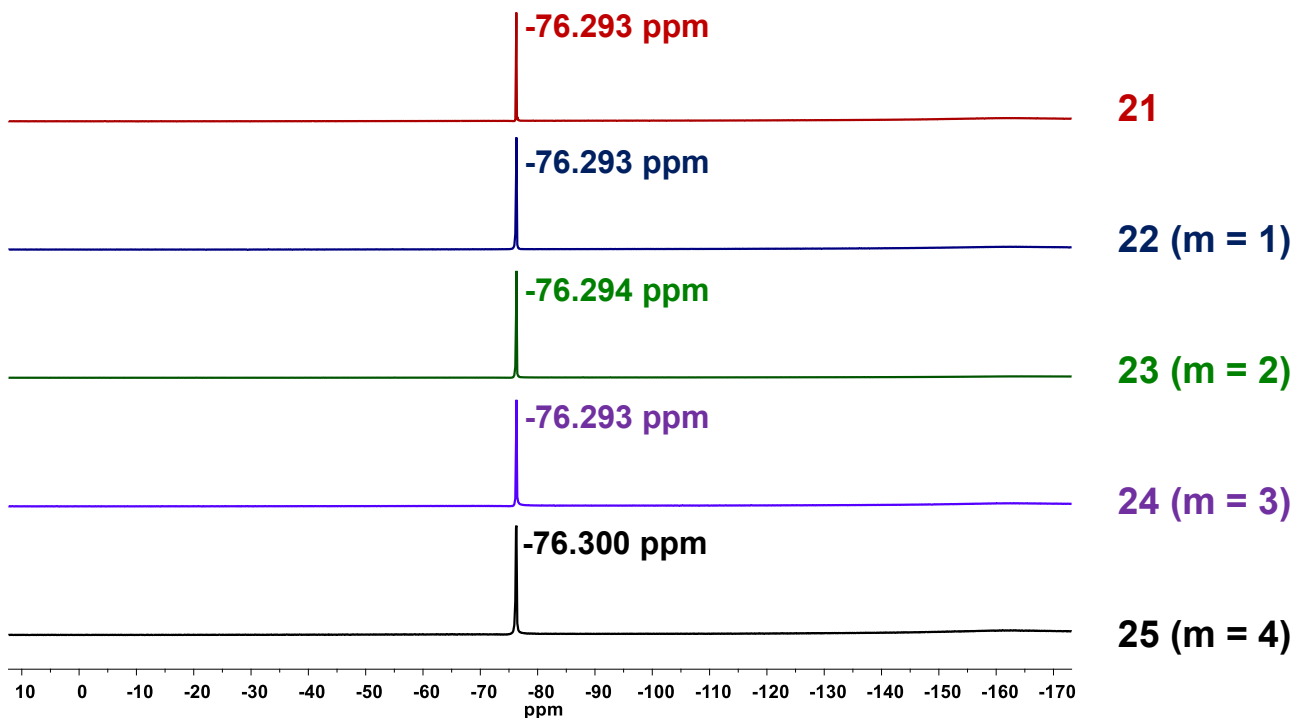


Figure 3.16: ^{19}F NMR of poly[*bis*(2,2,2-trifluoroethoxy)phosphazene], **21**, and poly[*tris*(2,2,2-trifluoroethoxy)(ferrocenylalkoxy)phosphazene] compounds **22** - **25**.

Figure 3.16 shows the ^{19}F NMR spectra for poly[*bis*(2,2,2-trifluoroethoxy)phosphazenes], **21** and poly[*tris*(2,2,2-trifluoroethoxy)(ferrocenylalkoxy)phosphazenes] compounds, **22**, **23**, **24**, and **25**. The fluorine signal for the 2,2,2-trifluoroethoxy groups are observed at -76.3 ppm. The position of the ^{19}F NMR resonances in **22 – 25** is found in a much smaller range (-76.29 ppm to -76.30 ppm) than the ^{31}P NMR resonances of **22 – 25** (-8.02 ppm to -7.88 ppm) because the P=N functionality is in the main polymer chain, whereas the CF₃ functionality is an endgroup right at the end of the O-CH₂CF₃ side chains. It is therefore much more capable of free rotation and motion than the P=N groups in the main polymer chain.

3.3 Gel Permeation Chromatography

GPC measurements in *N,N*-dimethylacetamide were performed to determine the molecular masses compared against poly(methylmethacrylate) (PMMA) of the synthesised poly[*bis*(2,2,2-trifluoroethoxy)phosphazene], **21**, as well as poly[*tris*(2,2,2-trifluoroethoxy)(ferrocenylalkoxy)-phosphazene] complexes, **22 – 25**. The results are summarised in Table 3.2.

Table 3.2: Number average molecular masses of poly(organophosphazene) complexes, **21 – 25 referenced against PMMA standards, utilising gel permeation chromatography. [PMMA = poly(methylmethacrylate); molecular masses are number average molecular masses, \overline{M}_n]**

| # | Name | Theoretically calculated $\overline{M}_n/\text{g mol}^{-1}\text{a}$ | GPC Determined $\overline{M}_n/\text{g mol}^{-1}$ |
|------------------|--|--|--|
| 21 | Poly[<i>bis</i> (2,2,2-trifluoroethoxy)phosphazene] | 6284.39 | 6307 |
| 22, m = 1 | Poly[<i>tris</i> (2,2,2-trifluoroethoxy)(ferrocenylmethoxy)phosphazene] | 14858.25 | 3410 |
| 23, m = 2 | Poly[<i>tris</i> (2,2,2-trifluoroethoxy)(ferrocenylethoxy)phosphazene] | 15208.25 | 3876 |
| 24, m = 3 | Poly[<i>tris</i> (2,2,2-trifluoroethoxy)(ferrocenylpropoxy)phosphazene] | 15558.25 | 7421 |
| 25, m = 4 | Poly[<i>tris</i> (2,2,2-trifluoroethoxy)(ferrocenylbutoxy)phosphazene] | 15901.25 | 3310 |

^a Calculated with formula $\overline{M}_n = \left(\frac{n_{\text{monomer}}}{n_{\text{initiator}}} \times M_{r,\text{monomer}} \right) + M_{r,\text{endgroups}}$ (see Section 3.2.6, p 51)

The GPC-determined molecular mass of a year old sample of **21**, which did not contain any ferrocenyl groups, was observed to be 6307 g mol⁻¹, which is almost identical to the expected theoretical molecular mass. GPC \overline{M}_n values of a year old samples of ferrocene-containing polyphosphazenes **22 – 25** deviated between *ca.* 50 (**24**) – 80 % (**25**) from the theoretical. This demonstrates the higher lability that the ferrocenyl group introduces into main chain stability. It was

expected that \overline{M}_n (GPC) should be larger than \overline{M}_n (theoretical) because during workup, the polymeric product was isolated by fractional precipitation, filtration and drying. Aged samples had to be used because, at the time of synthesis, access to a GPC instrument was not available.

Once a GPC instrument became available in the department, additional polymers of **25** were freshly synthesised and immediately subjected to GPC mass determinations. Molecular mass results of these polymers labelled **25a**, **25b**, and **25c** are provided in Table 3.3. The monomer:initiator ratios used were 100:1, 50:1, and 33:1 respectively. Table 3.3 clearly shows, by determining the molecular mass of freshly prepared samples, fractional precipitation of the crude product and further workup resulted in polymers (as expected) of much higher than theoretically predicted \overline{M}_n . This is consistent with the conclusion above, that the polymer main chain of **22 – 25** slowly hydrolyses over time, resulting in smaller molecular mass polymers. This conclusion was tested by an initial hydrolysis kinetic study; results of this kinetic study is presented in Section 3.7.

Table 3.3: Number average molecular mass, \overline{M}_n , of synthesised poly[*tris*(2,2,2-trifluoroethoxy)(ferrocenylbutoxy)phosphazene] complexes **25** as well as **25a – 25c** with varied quantities of initiator (PCl₅), utilising gel permeation chromatography, GPC, referenced against polystyrene or poly(methylmethacrylate) (for **25**) mass standards.

| # | Monomer:Initiator ratio | Theoretically calculated $\overline{M}_n/\text{g mol}^{-1}$ | GPC Determined $\overline{M}_n/\text{g mol}^{-1}$ |
|------------|-------------------------|---|---|
| 25a | 100:1 | 63000.25 | 213 731 |
| 25b | 50:1 | 31608.25 | 168 475 |
| 25c | 33:1 | 20932.25 | 126 554 |
| 25 | 25:1 | 15901.25 | 3 310 |

^a See Table 3.2 for the equation used in these calculations

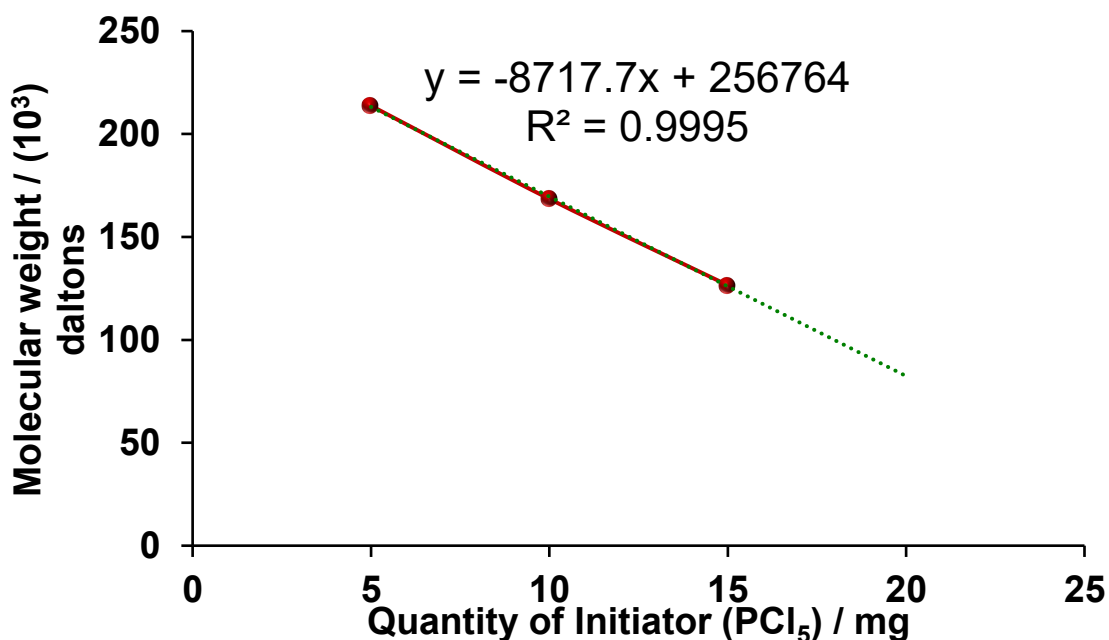


Figure 3.17: Trend between molecular weight versus quantity of initiator used for poly[tris(2,2,2-trifluoroethoxy)(ferrocenylbutoxy)phosphazene], 25, measured against polystyrene standards, showing the living cationic polymerisation nature of the synthesis.

Using the trend in Figure 3.17, it can be determined that the original molecular weight of **25** which was first synthesised would have been approximately 82410 g/mol.

Until the execution of this research study, the chemistry department did not have access to a GPC polymer molecular mass determination system. A new instrument from Shimadzu was purchased during the course of this study and part of the author's PhD was to initiate the use of this instrument and develop procedures for GPC mass determinations. The experimental chapter (chapter 4) has a full experimental procedure for utilising this instrument. The author also wishes to acknowledge Prof du Prez's laboratory at the University of Ghent and his staff, especially Bernhard De Meyer (Laboratory Manager, Department of Organic and Macromolecular Chemistry), for giving valuable guidance on how to use GPC systems.

3.4 Viscometry

Although GPC is accurate in determining molecular masses of polymers, it is a time consuming process. Frequently, easy to obtain viscometry measurements are used instead to determine polymer molecular masses.^{9,10} Provided the intrinsic viscosity, $[\eta]$, at a specific concentration as well as the

Mark-Houwink constants “a” and “K” are known, the viscosity average molecular mass may be determined from the Mark-Houwink equation below,

$$[\eta] = KM^a$$

In this study, specific viscosities of **21 - 25** were first determined at 30 °C at different concentrations in acetonitrile utilising the formula,

$$\eta_{sp} = \frac{t - t_0}{t_0}$$

Table 3.4 shows the specific viscosities, η_{sp} , of the synthesised poly(organophosphazene) complexes. These were obtained by measuring the time, t_0 , of pure solvent flowing between the marks of a viscosity meter as well as measuring the time, t , of different diluted solutions of known concentrations of polyphosphazene complexes passing between these marks.

The specific viscosity at a concentration of *ca.* 0.11 g/dL is observed to decrease about fifteen fold for **21** (polyphosphazene with only trifluoroethoxy group attached as side chains) and **22, 23, 24, 25** (polyphosphazene with both trifluoroethoxy and ferrocenylalkoxy groups attached as side chains).

Table 3.4 Specific viscosity, η_{sp} , data of poly[*bis*(2,2,2-trifluoroethoxy)phosphazene], **21, and poly[*tris*(2,2,2-trifluoroethoxy)(ferrocylalkoxy)phosphazene] complexes **22 – 25** where alkoxy chain length $m = 1, 2, 3$ and 4 . Polymer concentration = 0.11 g/dL acetonitrile**

| Compound | Average Time (t) / s | Specific Viscosity / η_{sp} |
|---------------------|-------------------------|-------------------------------------|
| Acetonitrile | 28.80 | |
| 21 | 35.50 | 0.2326 |
| 22, m = 1 | 29.26 | 0.0160 |
| 23, m = 2 | 29.22 | 0.0146 |
| 24, m = 3 | 29.18 | 0.0132 |
| 25, m = 4 | 29.04 | 0.0083 |

Specific viscosities at different concentrations of polymer **24** are shown in Table 3.5.

Table 3.5: Specific viscosities, η_{sp} , of 24 at the indicated concentrations as well as η_{sp} / C

| Concentration of 24 [mM] | 0.5 | 1.8 | 4 | 6 | 10 |
|--|--------|--------|--------|--------|--------|
| Concentration of 24, C (g/100mL) | 0.0307 | 0.1105 | 0.2456 | 0.3684 | 0.6140 |
| Specific Viscosity of 24 (η_{sp}) | 0.0132 | 0.0222 | 0.0264 | 0.0313 | 0.0396 |
| [η] = η_{sp}/C (dL/g) | 0.4300 | 0.2009 | 0.1075 | 0.0850 | 0.0645 |

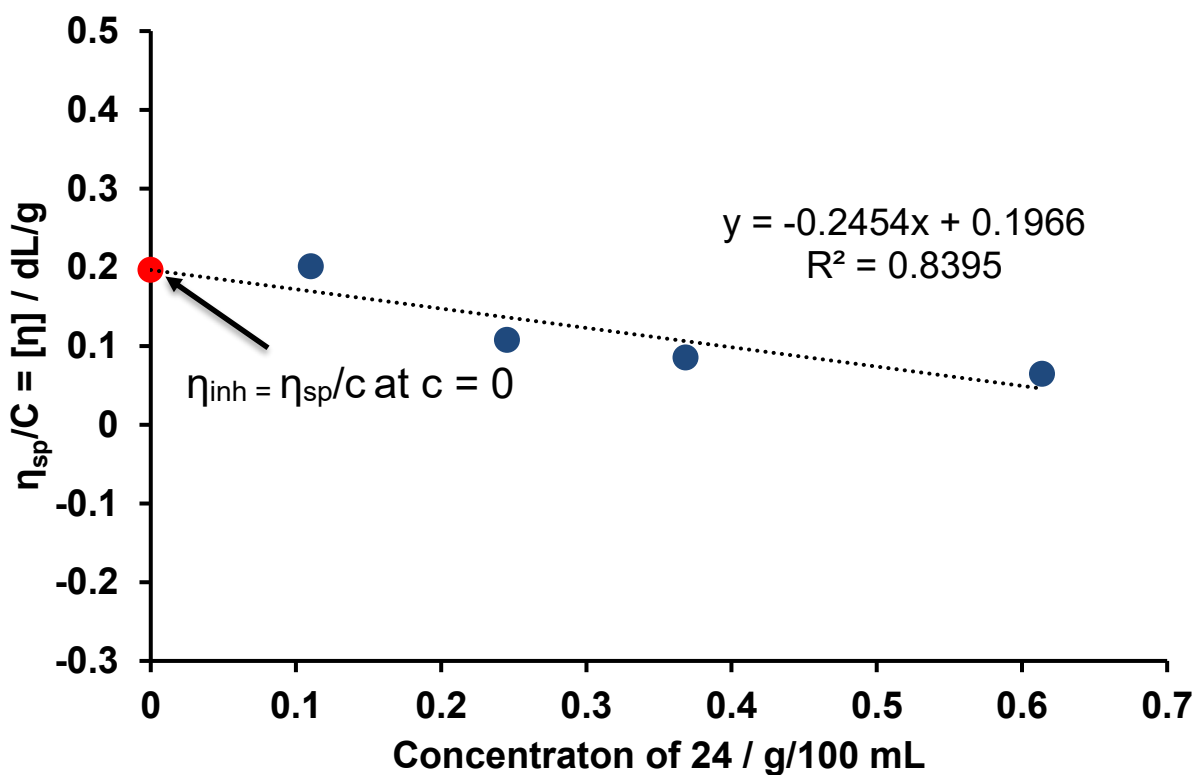
**Figure 3.18: Plot of intrinsic viscosity, η_{sp}/C , versus concentration of poly[tris(2,2,2-trifluoroethoxy)(ferrocenylpropoxy)phosphazene], 24.**

Figure 3.18 shows the plot of the ratio $\eta_{sp}/C = [\eta]$ versus differing concentrations of **24**. The y-intercept is the inherent viscosity, η_{inh} , of the polymer at zero concentration. In this case, the inherent viscosity for poly[tris(2,2,2-trifluoroethoxy)(ferrocenylpropoxy)phosphazene], **24** is 0.1966 dL/g.

It is well known that intrinsic viscosities ($[\eta] = \eta_{sp}/C$) of polymers with very similar structures are identical or almost identical.¹¹ Inherent viscosities ($\eta_{inh} = [\eta]$ at $C = 0$ or η_{sp}/C at $C = 0$) for **22 – 25**

were determined here and found to vary between 0.189 – 0.203 dL/g. In this research work we accepted $[\eta] = 0.195$ dL/g for all polymers.

With $[\eta] = \left(\frac{\eta_{sp}}{c}\right)$ values at $c = 0$ or at $c = 0.11$ g/dL available, it became possible to determine the Mark-Houwink constants to allow determination of viscosity average molecular masses of **22 – 25**. The concentrations of different molecular mass samples were in all cases 0.11 g/100 mL acetonitrile.

The natural logarithmic form of the Mark-Houwink equation $[m] = Km^a$, is:

$$\ln [\eta] = a \ln M + \ln K$$

The plot of $\ln [\eta]$ versus $\ln M$ will result in a slope of a and y-intercept $\ln K$. Different molecular mass polymers for **25** were synthesised (see Section 3.3); accurate molecular masses were determined by GPC. Figure 3.19 shows this plot for data presented in Table 3.6.

Table 3.6: Specific viscosity values, η_{sp} , values at ca. 0.11 g/dL and molecular masses (g/mol) utilised to determine the Mark-Houwink constants of polymer 25.

| | | | | |
|---|----------|---------|---------|---------|
| Molecular mass (M) / gmol⁻¹ | 3310 | 126554 | 168475 | 213731 |
| C / g.dL⁻¹ | 0.113 | 0.117 | 0.116 | 0.114 |
| η_{sp} | 0.0083 | 0.2156 | 0.2632 | 0.3080 |
| $[\eta] = \left(\frac{\eta_{sp}}{c}\right)^a$ | 0.07375 | 1.84295 | 2.26892 | 2.70163 |
| $\ln [\eta] = \ln \left(\frac{\eta_{sp}}{c}\right)^a$ | -2.60712 | 0.61137 | 0.81930 | 0.99386 |
| $\ln (M)$ | 8.1047 | 11.7484 | 12.0345 | 12.2725 |

^a Concentration (C) will always be in g.dL⁻¹ for these calculations.

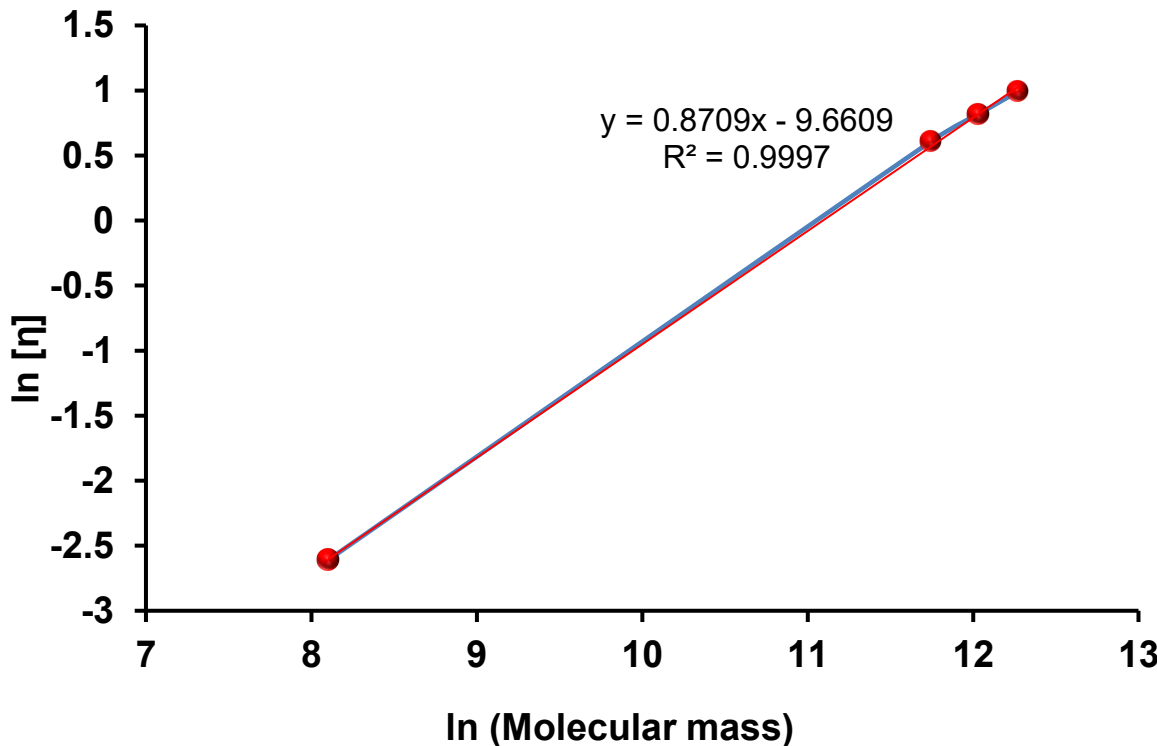


Figure 3.19: Plot of \ln (Molecular Mass) versus $\ln [\eta]$ to determine the Mark-Houwink parameters of poly[*tris*(2,2,2-trifluoroethoxy)(ferrocenylbutoxy)phosphazene], 25.

Mark-Houwink parameters for **25** that was determined from Figure 3.19 are presented in Table 3.7.

Table 3.7: Mark-Houwink parameters of poly[*tris*(2,2,2-trifluoroethoxy)(ferrocenylbutoxy)phosphazenes], 25, determined in acetonitrile at 30 °C.

| Mark-Houwink parameters | Compound 25 |
|-------------------------|-------------|
| a | 0.87 |
| K (dL/g) | 0.0000634 |

Finally, the derived Mark-Houwink equation applicable to **25**, $[\eta] = \left(\frac{\eta_{sp}}{c}\right) = KM^a = 6.34 \times 10^{-5} M^{0.87}$ at $c = 0.11$ g/dL were cross-checked by calculating the viscosity average molecular masses of **22**, **23** and **24** utilising the formula applicable to **25** and comparing them with the GPC determined molecular masses. Results are summarised in Table 3.8. Although the GPC and viscosity masses were not exactly equal, deviations were at most a factor of 2.2 times larger than expected. The deviations were 122 % (only 2.2 times) for **22** ($m = 1$), 73 % for **23** ($m = 2$), and -22 % for **24** ($m = 3$). It is clear the closer the structure of the polymers were to that of **25** ($m = 4$), the more accurate the

average viscosity molecular mass was. Results from this study therefore agree with published reports that intrinsic viscosities for polymers with very similar structures are almost identical^{9,11} because the Mark-Houwink equation for polymer **25** gave molecular masses for **22 – 24** deviating at most 2.2 times than the GPC determined molecular masses.

Table 3.8: Applicability of the derived Mark-Houwink equation to polymers 22 - 24

| Compound | C / g.dL ⁻¹ | GPC Determined \bar{M}_n / g mol ⁻¹ | Viscosity Determined \bar{M}_n / g mol ⁻¹ | Deviation ^a (%) |
|------------------|------------------------|--|--|----------------------------|
| 22, m = 1 | 0.106 | 3410 | 7648 | +122 |
| 23, m = 2 | 0.108 | 3876 | 6702 | +73 |
| 24, m = 3 | 0.111 | 7421 | 5784 | -22 |

^aCalculated with formula $deviation = \left(\frac{\text{Viscosity determined } \bar{M}_n - \text{GPC determined } \bar{M}_n}{\text{GPC determined } \bar{M}_n} \right) \times 100$

3.5 X-ray Photoelectron Spectroscopy

X-ray Photoelectron Spectroscopy (XPS) measurements were made for the unsubstituted poly(dichlorophosphazene), **20**, as well as the poly[*tris*(2,2,2-trifluoroethoxy)(ferrocenylalkoxy)-phosphazene] complexes, **21**, **22**, **23**, **24**, and **25**. From these measurements, the binding energies of each atom could be established, the empirical formula (i.e., elemental stoichiometry) could be estimated and differences in atomic environments of the polymer main chain fractions (or substituent types) could be highlighted.

3.5.1 Poly(dichlorophosphazene), **20**.

The XPS spectra for phosphorous, nitrogen and chlorine were recorded for poly(dichlorophosphazene), **20**. Because poly(dichlorophosphazene), **20**, is unstable in air, samples were transferred from a glovebox to an inert, gas-filled vessel for transport to the XPS spectrometer. The photoelectron lines obtained for phosphorus, nitrogen, and chlorine are presented in Figure 3.20.

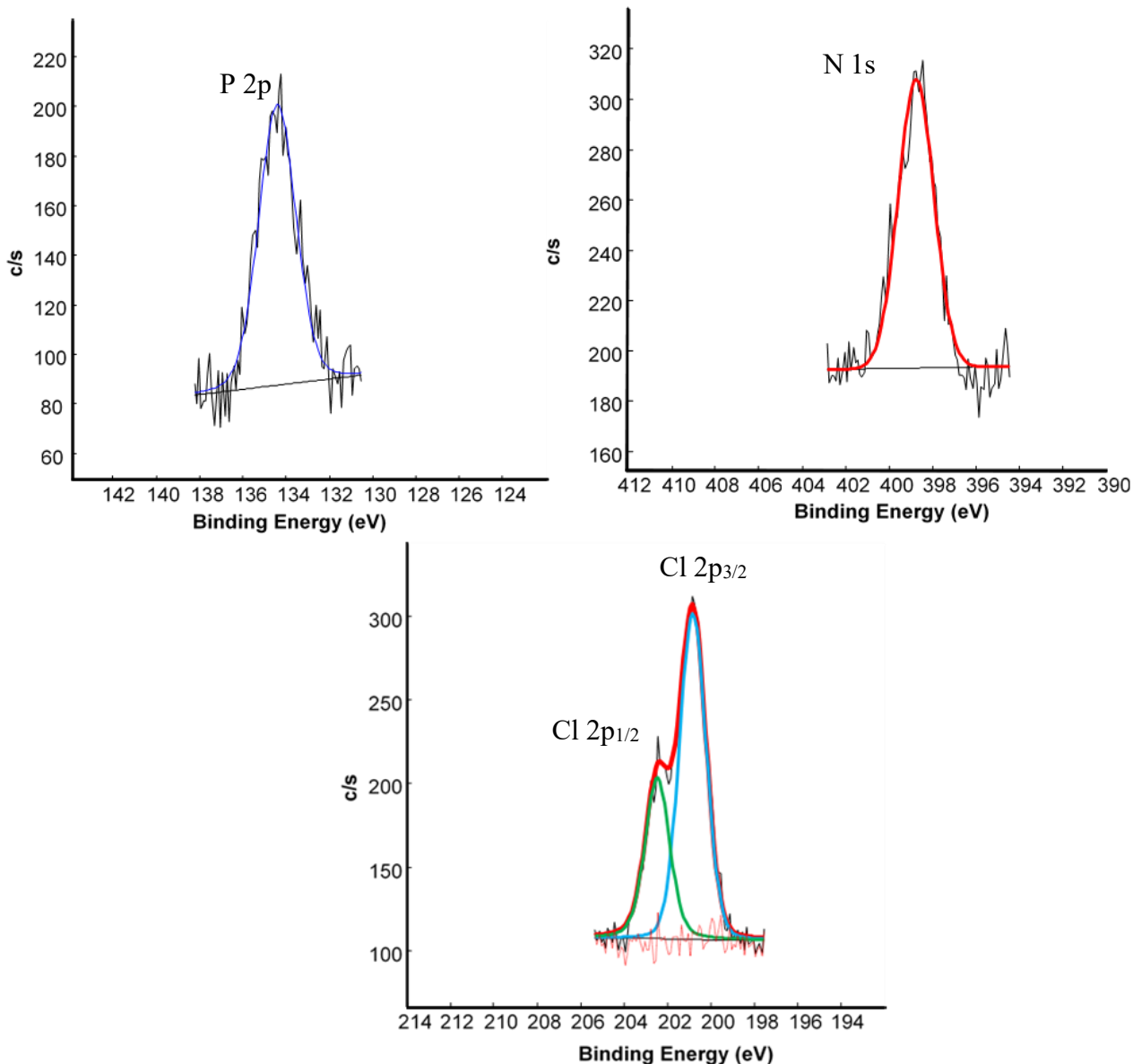


Figure 3.20: Photoelectron lines for phosphorous (top left), nitrogen (top right) and chlorine (bottom), in poly(dichlorophosphazene), 20, using Gaussian-Lorentz fits. The P 2p photoelectron line of phosphorus consists of two components, P 2p_{1/2} and P 2p_{3/2}, but unlike for Cl, cannot be resolved.

Phosphorus (P 2p) has two photoelectron lines, one for P 2p_{1/2} and another for P 2p_{3/2}. However, for **20** these two peaks were not resolved and only one apparent photoelectron line is observed. It is noted in literature¹² that these two lines sometimes do overlap with each other to the extent that it becomes difficult to resolve them. Chlorine also has two photoelectron lines, Cl 2p_{1/2} and Cl 2p_{3/2}, but they could be resolved into two separate photoelectron lines. Nitrogen only has one photo-

electron line, N 1s. Binding energies (BEs) of these elements were as expected and is reported in Table 3.9, as is atomic ratios as well as full width at half maximums (FWHM).¹²

Table 3.9: Ratio of phosphorus, nitrogen, and chlorine in poly(dichlorophosphazene), 20, determined by XPS surface measurement.

| Element | Phosphorus 2p | Nitrogen 1s | Chlorine 2p _{1/2} ; 2p _{3/2} |
|------------------------|---------------|-------------|--|
| Binding energy (eV) | 134.4 | 398.7 | 202.5 ; 200.8 |
| Atom percentage (%) | 35.7 | 34.6 | 29.7 |
| Atomic ratio | 1.03 | 1.00 | 0.86 |
| FWHM ^a (eV) | 2.02 | 1.93 | 1.33 ; 1.44 |

^a FWHM = full width at half maximum

Atomic ratios in the formula P_xN_yCl_z should theoretically be 1:1:2 for the empirical formula P₁N₁Cl₂ for **20**. Experimentally, these atomic ratios were determined from the XPS-measured atomic percentages in Table 3.9 and it resulted in the empirical formula P_{1.03}N_{1.00}Cl_{0.86}.

The chlorine quantity is much lower than the theoretical value (P:Cl should be 1:2). It is reported in literature that poly(dichloro)phosphazene degrade and lose chlorine atoms upon X-ray irradiation of the sample.¹³ The combined effect of radiation instability as well as chemical instability of the P-Cl bond towards, for example, trace amounts of oxygen, O₂, and water, H₂O, may explain the low chlorine content observed. However, the successful synthesis of **21** from **20** showed that **20** was still intact at the time of synthesis of **21**, but did not survive the isolation, transportation to the XPS and irradiation condition to obtain the correct Cl content.

3.5.2 Poly[bis(2,2,2-trifluoroethoxy)phosphazene], **21**.

Figure 3.21 presents the X-ray photoelectron lines for fluorine, phosphorus, oxygen, nitrogen, and carbon in poly[bis(2,2,2-trifluoroethoxy)phosphazene], **21**. The BEs and atomic ratios (ARs) of the elements and full width at half maximum values (FWHM) are summarised in Table 3.10.

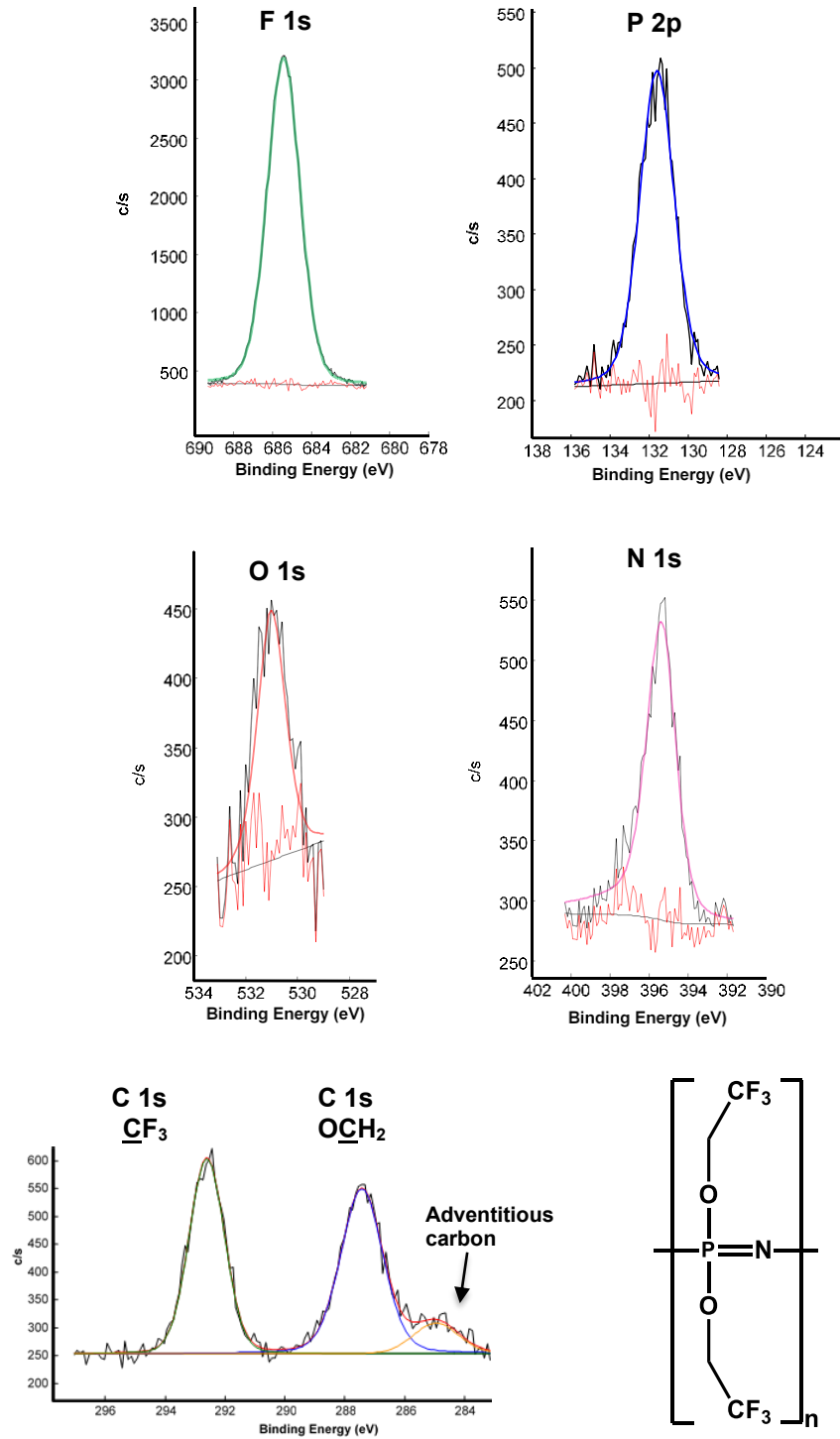


Figure 3.21: Photoelectron lines for fluorine (top left), phosphorus (top right), oxygen (bottom left), and nitrogen (bottom right), in poly[bis(2,2,2-trifluoroethoxy)phosphazene], 21.

Table 3.10 Binding energies, atomic percentages, atom ratios and FWHM of phosphorus, nitrogen, oxygen, fluorine and carbon in poly[bis(2,2,2-trifluoroethoxy)phosphazene], 21, determined by XPS surface measurement.

| Element | P 2p _{1/2} ; 2p _{3/2} | N 1s | O 1s | F 1s | C 1s for CF ₃ ; OCH ₂ ; C _{adventitious} |
|------------------------|--|--------|--------|--------|--|
| BE (eV) | 134.84 ; 134.00 | 398.08 | 533.62 | 688.07 | 292.61 ; 287.44 ; 284.96 |
| Atom % | 7.4 | 7.7 | 13.5 | 41.6 | 29.7 |
| Atomic ratio | 1.00 | 1.04 | 1.82 | 5.62 | 4.01 |
| FWHM ^a (eV) | 1.87 ; 1.87 | 2.05 | 1.86 | 2.00 | 1.61 ; 1.61 ; 1.61 |

^a FWHM = full width at half maximum

^b not included in the stoichiometry of 21

In contrast to what was observed for **20**, for **21**, two phosphorus peaks, 2p_{1/2} at 134.84 eV and 2p_{3/2} at 134.00 eV could be fitted into the photoelectron line. Binding energies differed by 0.8 eV and the FWHM values were 1.87 eV for each photoelectron line. This is noticeably smaller than the FWHM value for **20** of 2.02 eV (Table 3.9). Binding energies for phosphorus as well as nitrogen were very close to each other for these two complexes. The oxygen photoelectron line was observed at 533.62 eV and the fluorine photoelectron line at 688.07 eV. The carbon photoelectron line was very informative. The photoelectron line of the carbon atom with three fluorine atoms bonded to it was observed at 292.61 eV, whereas the photoelectron line of the carbon atom bonded to an oxygen atom was observed at 287.44 eV. This clearly indicates that the carbon atom with the three fluorine atoms bound to it associates much stronger with its bonding electrons than the OCH₂ carbon. This is consistent with atomic electronegativity of fluorine (4.0) being larger than the atomic electronegativity of oxygen (3.5). The binding energy of the adventitious carbon is the smallest because it is not associated with any powerful electron-withdrawing atoms bonded to it.

The atomic percentages observed for **21** resulted in an empirical formula of P_{1.00}N_{1.04}O_{1.82}F_{5.62}C_{4.01} which corresponds very well with the theoretical empirical formula of P₁N₁O₂F₆C₄.

The FWHM values of phosphorus in **21** (1.87) was slightly smaller than that of **20** (2.02), which is consistent with **20** not having resolved phosphorus photoelectron lines. The difference in the nitrogen FWHM of **21** (2.05) compared to the corresponding value of **20** (1.93) is not so large that it is considered at this stage as meaningful (however, see next paragraph), although it is known that polymerisation of monomers often cause peak broadening in, for example, ¹H NMR resonances.

3.5.3 Poly[*tris*(2,2,2-trifluoroethoxy)(ferrocenylalkoxy)phosphazene] complexes 22 - 25

The BEs of phosphorus, nitrogen, oxygen, fluorine, iron and carbon, atom percentages, ARs and FWHM values for **22 – 25** are summarized in Table 3.11, while Figure 3.22 gives representative examples of the photoelectron line of every atom (P, N, O, F, Fe and C) found in complexes **22 – 25**. For all four complexes, **22 – 25**, the P 2p_{1/2} and P 2p_{3/2} could be fitted with binding energy differences = $\Delta\text{BE} = \text{BE}_{2\text{p}_{1/2}} - \text{BE}_{2\text{p}_{3/2}} = 0.84$ eV. All phosphorus 2p photoelectron line maximums were found in the region 133.73 – 135.46 eV. Figure 3.22 shows the phosphorus photoelectron line for **25** as a representative example. The nitrogen 1s photoelectron line maximum for these complexes were found between 398.20 eV and 399.06 eV; Figure 3.22 shows the N 1s photoelectron line for **24** as a representative example.

Two different environments border the oxygen atoms in complexes **22 – 25**. Each complex has four oxygen atoms in the monomeric unit $-[(\text{F}_3\text{C}-\text{CH}_2-\text{O}^{\text{A}})_2\text{P}=\text{N}-\text{P}(\text{O}^{\text{A}}-\text{CH}_2-\text{CF}_3)(\text{O}^{\text{B}}-(\text{CH}_2)_m-\text{Fc})=\text{N}]-$. Three of these oxygen atoms are found in the $\text{F}_3\text{C}-\text{CH}_2-\text{O}^{\text{A}}-$ unit and one oxygen atom in the $-\text{O}^{\text{B}}-(\text{CH}_2)_m-\text{Fc}$ unit. XPS spectroscopy could differentiate between the environments of these two oxygen atom types. The O^{A} oxygen atom in the three $\text{F}_3\text{C}-\text{CH}_2-\text{O}^{\text{A}}-$ fragments are found at *ca.* 533.57 - 534.66 eV peak maximum, while O^{B} peak maximum of the single $-\text{O}^{\text{B}}-(\text{CH}_2)_m-\text{Fc}$ fragment was found in the region 531.33 – 532.14 eV respectively. The resolution between these two photoelectron lines is *ca.* 2.4 eV. The experimentally determined $\text{O}^{\text{A}}:\text{O}^{\text{B}}$ ratios were 2.7:1.0 (for **22**), 3.1:1.0 (for **23**), 2.7:1.0 (for **24**), and 2.5:1.0 (for **25**) and compared very well to the theoretical ratio of 3:1. The difference in binding energies is due to the difference in group electronegativities of fluorine (3.01 for $\text{F}_3\text{C}-\text{CH}_2-\text{O}^{\text{A}}-$ and 1.87 for $-\text{O}^{\text{B}}-(\text{CH}_2)_m-\text{Fc}$, the ferrocenyl group).¹⁴ The O 1s photoelectron line for **24** is shown in Figure 3.22.

The fluorine 1s photoelectron line maximum were found at 688.22 – 689.10 eV for complexes **22 – 25** (Table 3.11); Figure 3.22 shows this photoelectron line for **23** as a representative example.

Three C 1s photoelectron lines were observed for all four complexes **22 - 25**. The lowest energy line is that of aliphatic and aromatic carbon atoms overlapping with adventitious carbons in the sample at 284.89 eV, see Figure 3.22 for **22**. Bordering this adventitious carbon photoelectron line is the photoelectron line associated with carbon atoms bonded to oxygen atoms at 287.44 – 288.33 eV (Table 3.10). Each monomeric unit in **22 – 25** has four such carbon atoms and correspond to $-\text{O}-\text{CH}_2-$ moieties in each polymer.

Table 3.11: Binding energies, atomic percentages, atom ratios and FWHM of phosphorus, nitrogen, oxygen, fluorine, iron and carbon in poly[*tris*(2,2,2-trifluoroethoxy)(ferrocenylalkoxy)phosphazene] complexes , 22 – 25, determined by XPS surface measurements.

| | P 2p | N 1s | O 1s | F 1s | Fe ^{II} 2p (shake-up) | Fe ^{III} 2p (shake-up) | C 1s ^a |
|--|--|--------|--|--------|--|--|--|
| Polymer 22, [(F ₃ C-CH ₂ -O ^A) ₂ P=N-P(O ^A -CH ₂ -CF ₃)(O ^B -(CH ₂) _m -Fc)=N], m = 1 ; theoretical empirical formula = P ₂ N ₂ O ₄ F ₉ C ₁₇ H ₁₇ Fe | | | | | | | |
| BE (eV) | 2p _{1/2} : 135.46 2p _{3/2} : 134.62 | 399.06 | F ₃ C-CH ₂ O ^A : 534.66 Fc-(CH ₂) _m O ^B : 532.14 | 689.10 | 2p _{1/2} : 720.04 (725.59) 2p _{3/2} : 707.34 (712.62) | 2p _{1/2} : 721.25 (735.19) 2p _{3/2} : 708.55 (716.91) | CF ₃ : 293.63 ^a OCH ₂ : 288.33 |
| Atom % | 7.8 | 8.2 | O ^A :O ^B = 2.7:1 Total O % = 16.4 | 20.3 | Relative Fe ^{II} = 55.5 % ; Relative Fe ^{III} = 44.5 % Total Fe % = 2.8 % | | CF ₃ :OCH ₂ = 3.0:3.7 Total C % = 34.5 |
| Atom ratio | 2.0 | 2.1 | 4.2 | 7.8 | 0.7 | | 9.4 |
| FWHM | 1.87 ; 1.87 | 2.34 | 1.76 | 2.07 | 4.29 (4.29) | 4.29 (4.29) | 1.52 |
| Polymer 23, [(F ₃ C-CH ₂ -O ^A) ₂ P=N-P(O ^A -CH ₂ -CF ₃)(O ^B -(CH ₂) _m -Fc)=N], m = 2 ; theoretical empirical formula = P ₂ N ₂ O ₄ F ₉ C ₁₈ H ₁₉ Fe | | | | | | | |
| BE (eV) | 2p _{1/2} : 134.57 2p _{3/2} : 133.73 | 398.20 | F ₃ C-CH ₂ O ^A : 533.57 Fc-(CH ₂) _m O ^B : 531.33 | 688.22 | 2p _{1/2} : 718.41 (724.14) 2p _{3/2} : 707.48 (711.95) | 2p _{1/2} : 720.23 (735.33) 2p _{3/2} : 710.50 (715.41) | CF ₃ : 292.88 ^a OCH ₂ : 287.44 |
| Atom % | 9.1 | 8.9 | O ^A :O ^B = 3.1:1.0 Total O % = 15.1 | 41.6 | Relative Fe ^{II} = 61.2 % ; Relative Fe ^{III} = 38.8 % Total Fe % = 2.7 | | CF ₃ :OCH ₂ = 3.0:3.7 Total C % = 22.6 |
| Atom ratio | 2.0 | 2.0 | 3.4 | 9.3 | 0.6 | | 5.6 |
| FWHM^b | 1.87 ; 1.87 | 2.34 | 1.76 | 2.07 | 3.64 (3.64) | 3.64 (3.64) | 1.52 |

^a Adventitious carbon at 284.89 eV for 22 – 25

^b FWHM = full width at half maximum

Table 3.11 (continued): Binding energies, atomic percentages, atom ratios and FWHM of phosphorus, nitrogen, oxygen, fluorine, iron and carbon in poly[*tris*(2,2,2-trifluoroethoxy)(ferrocenylalkoxy)phosphazene] complexes , 22 – 25, determined by XPS surface measurements.

| | P 2p | N 1s | O 1s | F 1s | Fe ^{II} 2p (shake-up) | Fe ^{III} 2p (shake-up) | C 1s ^a |
|--|--|--------|--|--------|--|--|--|
| Polymer 24, [(F ₃ C-CH ₂ -O ^A) ₂ P=N-P(O ^A -CH ₂ -CF ₃)(O ^B -(CH ₂) _m -Fc)=N], m = 3 ; theoretical empirical formula = P ₂ N ₂ O ₄ F ₉ C ₁₉ H ₂₁ Fe | | | | | | | |
| BE (eV) | 2p _{1/2} : 134.80 2p _{3/2} : 133.96 | 398.35 | F ₃ C-CH ₂ O ^A : 533.71 Fc-(CH ₂) _m O ^B : 531.46 | 688.40 | 2p _{1/2} : 718.23 (721.25) 2p _{3/2} : 707.53 (712.46) | 2p _{1/2} : 719.72 (736.06) 2p _{3/2} : 708.74 (715.84) | CF ₃ : 292.87 ^a OCH ₂ : 287.59 |
| Atom % | 8.2 | 8.4 | O ^A :O ^B = 2.7:1.0 Total O % = 15.3 | 37.8 | Relative Fe ^{II} = 66.7 % ; Relative Fe ^{III} = 33.3 % Total Fe % = 2.8 | | CF ₃ :OCH ₂ = 3.0:3.8 Total C % = 27.5 |
| Atom ratio | 2.0 | 2.1 | 3.7 | 9.0 | 0.7 | | 6.7 |
| FWHM | 1.87 ; 1.87 | 2.46 | 1.69 | 2.06 | 3.98 (3.98) | 3.98 (3.98) | 1.53 |
| Polymer 25, [(F ₃ C-CH ₂ -O ^A) ₂ P=N-P(O ^A -CH ₂ -CF ₃)(O ^B -(CH ₂) _m -Fc)=N], m = 4 ; theoretical empirical formula = P ₂ N ₂ O ₄ F ₉ C ₂₀ H ₂₃ Fe | | | | | | | |
| BE (eV) | 2p _{1/2} : 134.80 2p _{3/2} : 133.96 | 398.35 | F ₃ C-CH ₂ O ^A : 533.71 Fc-(CH ₂) _m O ^B : 531.46 | 688.40 | 2p _{1/2} : 717.95 (724.14) 2p _{3/2} : 707.91 (711.84) | 2p _{1/2} : 720.55 (736.10) 2p _{3/2} : 710.50 (715.05) | CF ₃ : 292.88 ^a OCH ₂ : 287.44 |
| Atom % | 11.1 | 11.5 | O ^A :O ^B = 2.5:1 Total O % = 12.5 | 40.9 | Relative Fe ^{II} = 59.3 % ; Relative Fe ^{III} = 40.7 % Total Fe % = 2.6 | | CF ₃ :OCH ₂ = 3.0:4.0 Total C % = 21.4 |
| Atom ratio | 2.0 | 2.1 | 2.3 | 7.4 | 0.5 | | 3.9 |
| FWHM^b | 1.98 ; 1.98 | 2.73 | 1.63 | 2.25 | 3.64 (3.64) | 3.64 (3.64) | 1.82 |

^a Adventitious carbon at 284.89 eV for 22 - 25

^b FWHM = Full width at half maximum

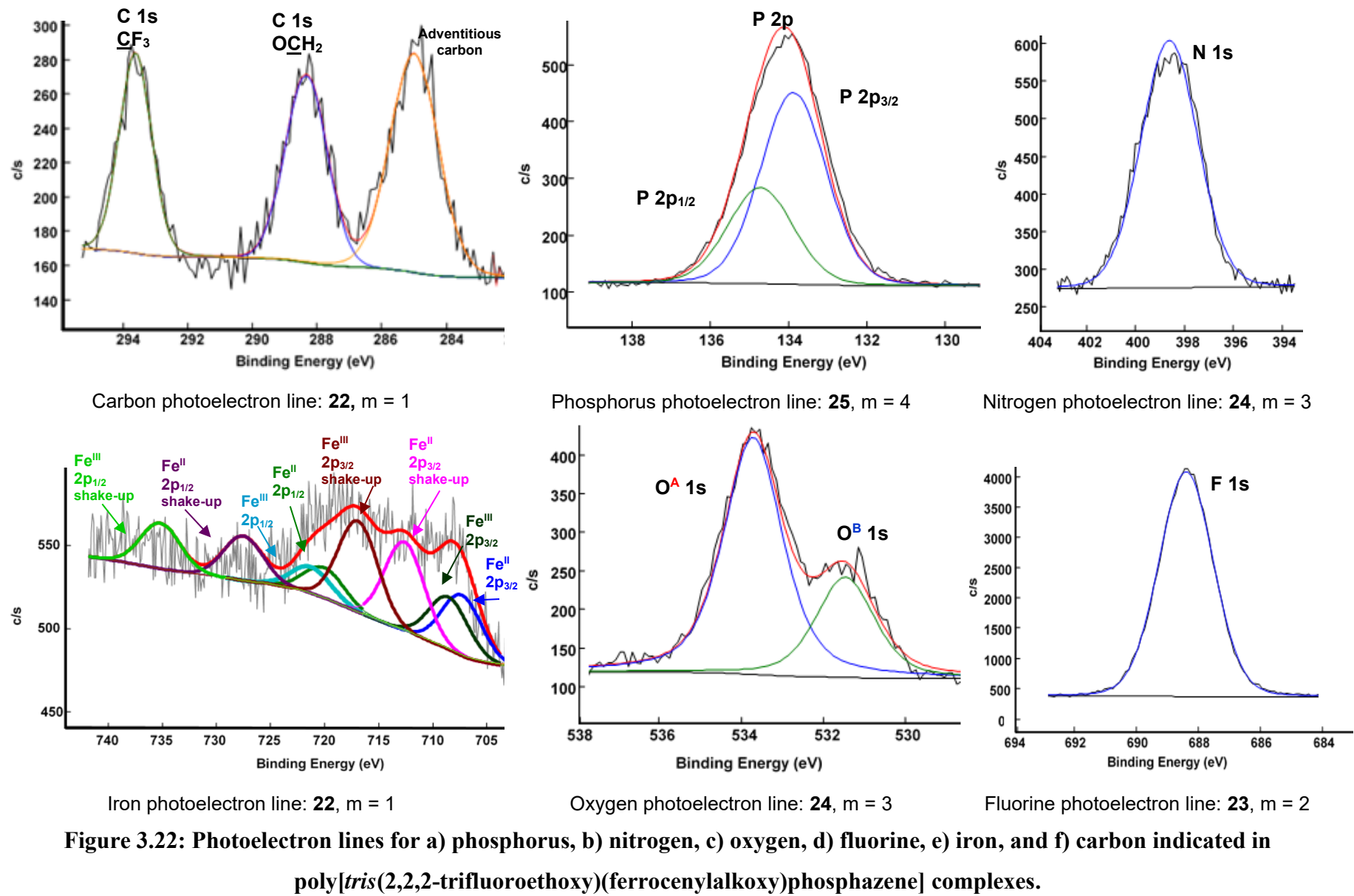


Figure 3.22: Photoelectron lines for a) phosphorus, b) nitrogen, c) oxygen, d) fluorine, e) iron, and f) carbon indicated in poly[tris(2,2,2-trifluoroethoxy)(ferrocenylalkoxy)phosphazene] complexes.

The $-\text{CF}_3$ carbon atom of the three $-\text{OCH}_2\text{-CF}_3$ moieties in each monomeric unit of **22 – 25** exhibited a photoelectron line maximum in the region 292.87 – 293.63 eV. This photoelectron line was resolved from the photoelectron line associated with the $-\text{O-CH}_2-$ moiety by *ca.* 5.28 – 5.44 eV. The theoretical ratio between these two different types of carbon atoms should be $\text{CF}_3:\text{OCH}_2 = 3:4$. Experimentally, XPS measurements found this ratio to be 3.0:3.7 for both **22** and **23**, 3.0:3.8 for **24** and 3.0:4.0 for **25**.

The iron photoelectron lines were very weak and very complex. Other researchers also observed complex Fe XPS spectra and demonstrated that the longer the irradiation times are, the more complex Fe XPS spectra are obtained.¹⁵ Theoretically there should only be one Fe^{II} atom in the repeating unit of each polymer and this iron atom is associated with the ferrocenyl group in the overall structure. However, the Fe^{II} center of the ferrocenyl groups are very labile with respect to oxidation to Fe^{III} under X-ray irradiation, and even more so in the presence of oxygen atoms. Although free oxygen is not present during XPS measurements, every repeating unit in every polymeric structure has four oxygen atoms associated with it. Under XPS conditions, the ferrocenyl group bearing an Fe^{II} atom is easily oxidised to Fe^{III} forming amongst others the ferrocenium cation,^{16,17} $\alpha\text{-Fe}_2\text{O}_3$ (haematite) and $\gamma\text{-Fe}_2\text{O}_3$ (maghaemite). Should trace amounts of moisture be present on the sample surface, the latter two Fe^{III} species can decompose into $\alpha\text{-Fe}^{\text{III}}\text{OOH}$ (goethite) and $\gamma\text{-Fe}^{\text{III}}\text{OOH}$ (lepidocrocite). A representative Fe 2p photoelectron line of **22** is shown in Figure 3.22. Ferrocenyl $\text{Fe}^{\text{II}}\text{ 2p}_{1/2}$ and $\text{Fe}^{\text{II}}\text{ 2p}_{3/2}$ photoelectron lines at 720.04 and 707.34 eV respectively as well as their shake-up peaks at 725.59 and 712.62 eV is clearly identified.^{18,19} However, broad $\text{Fe}^{\text{III}}\text{ 2p}$ photoelectron lines due to the high spin nature of Fe^{III} are also visible. The presence of $\text{Fe}^{\text{III}}\text{ 2p}_{3/2}$ photoelectron lines at 708.55 eV is associated with haematite, $\alpha\text{-Fe}_2\text{O}_3$, while the $\text{Fe}^{\text{III}}\text{ 2p}_{1/2}$ shake-up peak at 735.19 eV is associated with lepidocrocite, $\gamma\text{-FeOOH}$.²⁰ Other Fe^{III} decomposition products may also be present in the XPS spectra of **22 – 25**; however, due to poor resolution and overall weak intensity of the combined $\text{Fe}^{\text{II/III}}\text{ 2p}$ photoelectron lines, further assignments could not be made with certainty. This unknown broth of decomposed Fe^{III} products is consistent with $\text{Fe 2p}_{1/2} - \text{Fe 2p}_{3/2}$ photoelectron line separations deviating from the normally accepted *ca.* 13.6 eV.¹²

From the atom ratios given in Table 3.11, the XPS determined empirical formulas were as follows (hydrogen cannot be determined by XPS and is shown as H_x.):

- a. For **22**, m = 1: (P₂N₂O₄F₉C₁₇H₁₇Fe)_{theoretical}, (P_{2.0}N_{2.1}O_{4.2}F_{7.8}C_{9.4}H_xFe_{0.7})_{XPS}
- b. For **23**, m = 2: (P₂N₂O₄F₉C₁₈H₁₉Fe)_{theoretical}, (P_{2.0}N_{2.0}O_{3.4}F_{9.3}C_{5.6}H_xFe_{0.6})_{XPS}
- c. For **24**, m = 3: (P₂N₂O₄F₉C₁₉H₂₁Fe)_{theoretical}, (P_{2.0}N_{2.1}O_{3.7}F_{9.0}C_{6.7}H_xFe_{0.7})_{XPS}
- d. For **25**, m = 4: (P₂N₂O₄F₉C₂₀H₂₃Fe)_{theoretical}, (P_{2.0}N_{2.1}O_{2.3}F_{7.4}C_{3.9}H_xFe_{0.5})_{XPS}

Excluding carbon, these formulas corresponded very well with the theoretically predicted formula. The consistently low carbon content is considered the result of ferrocenyl group (Fe^{II}C₁₀H₉) decomposition liberating iron oxide, Fe₂O₃, and volatile carbon moieties upon irradiation during an XPS experiment. Upon oxidation of ferrocene to the ferrocenium cation, the latter invariably decomposes to liberate free, gaseous cyclopentadiene as discussed by Kumpan and co-workers.²¹

The author mentioned in Section 3.5.2 that peak broadening in for example ¹H NMR spectroscopy, happen when moving from small molecules (monomers) to polymers. In XPS, peak broadening would result in an increase of FWHM values. An increase in FWHM values with enhanced complexity of polymer structure would be most observable in the XPS FWHM values of the main chain atoms, phosphorus and nitrogen. Enhanced flexibility of the side chains, coupled with ferrocenyl decomposition prohibits comparison of the other atoms FWHM values. For nitrogen, in moving from **20**, poly(dichlorophosphazene), to **21**, poly[*bis*(2,2,2-trifluoroethoxy)phosphazene], to ultimately **25**, poly[*tris*(2,2,2-trifluoroethoxy)(ferrocenylbutoxy)phosphazene] with m = 4, resulted in FWHM values increasing from 1.93 to 2.05 to 2.73 eV. For phosphorus, FWHM values for the experimentally observed resultant photoelectron line increased from 2.02 eV for **20** to 2.36 eV for **25**. Figure 3.23 shows how FWHM for these atoms increased in moving from **22 – 25** where m increased from 1 – 4.

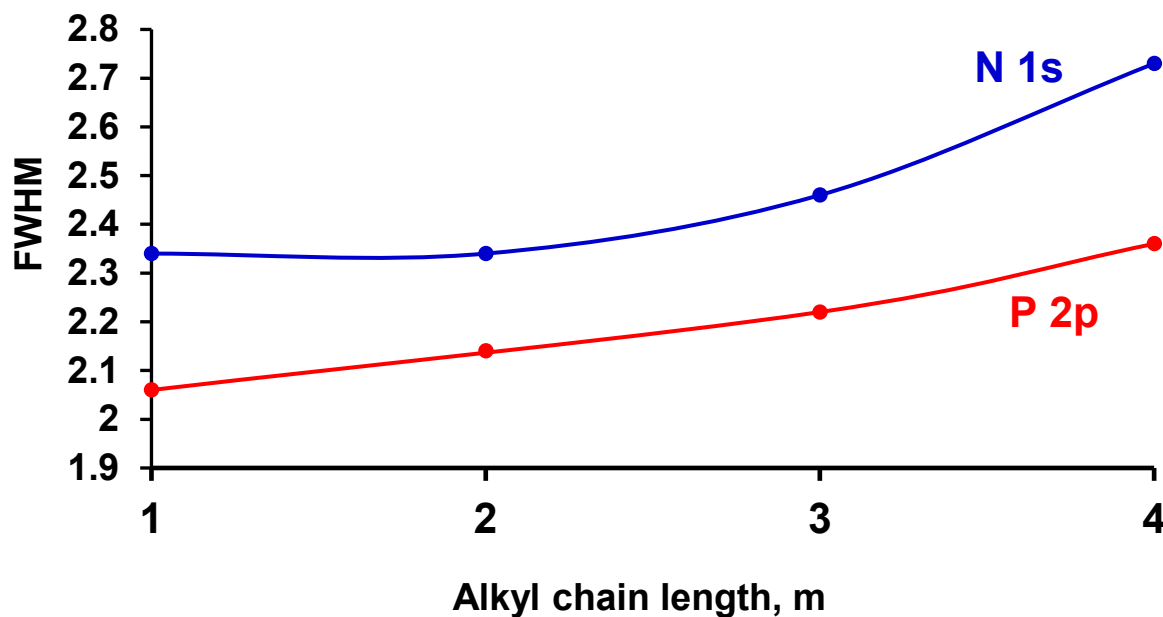


Figure 3.23: Plot of full width at half maximum (FWHM) for N 1s and the overall resultant P 2p photoelectron lines versus alkyl chain length, m, in ferrocenylalkoxy-containing polyphosphazenes, **22 ($m = 1$), **23** ($m = 2$), **24** ($m = 3$), and **25** ($m = 4$).**

This observation is consistent with the shorter, more rigid, ferrocenylmethoxy groups in **22** being less able to rotate than the ferrocenylbutoxy group of **25**. This would mean polymer **25** would be prone to more structural fluctuations and bigger differences in the chemical environments of the polymer main chain and manifests in the largest FWHM values for **25** ($m = 4$).

It is concluded that XPS, just as ^1H NMR spectroscopy, is also sensitive to increased structural complexity and it manifests in an increased FWHM value.

3.6 Cyclic Voltammetry

Cyclic voltammetry measurements in acetonitrile in the presence of 0.1M $[N(^nBu_4)][PF_6]$ and 0.25 mM decamethylferrocene, Fc^* , as internal standard were conducted on poly[*tris*(2,2,2-trifluoroethoxy)(ferrocenealkoxy)phosphazene] complexes **22 – 25** (2 mM). This was done in order to determine the effect that the alkyl chain lengths, $m = 1, 2, 3$, and 4, has on the electrochemistry of these complexes.

All potentials were experimentally referenced against a silver wire in the presence of decamethylferrocene as internal standard. Under these experimental conditions the Fc^*/Fc^{*+} couple has a formal reduction potential (E°) of -515 mV vs FcH/FcH^+ in acetonitrile. Peak anodic potentials (E_{pa}), peak cathodic potentials (E_{pc}) both corrected to be versus FcH/FcH^+ , peak anodic currents (i_{pa}), peak cathodic currents (i_{pc}), formal reduction potentials (E°) and the ratio i_{pc}/i_{pa} for compounds **22 – 25** are summarised in Table 3.12 and selected cyclic voltammograms are shown in Figures 3.24 and 3.25.

At slow scan rates (100 mV/s) $\Delta E = E_{pa} - E_{pc}$ for **22** was 97.0 mV; while for **23 – 25** it was less than 88 mV (Table 3.12). Theoretically electrochemical reversibility of a one electron process should be 59 mV²² although experimentally any value less than 90 mV is often regarded to indicate electrochemical reversibility. It is concluded that **23 – 25** exhibits electrochemical reversibility, while **22** exhibits quasi-electrochemical reversibility. Electrochemical quasi-reversibility of **22** is ascribed to the short alkoxy chain length, $O-CH_2-$, separating the ferrocenyl group from the polyphosphazene main chain. This short connecting chain pulls the ferrocenyl group close to main chain proximity resulting in a large steric hindrance between ferrocenyl group and electrode surface. This prohibits the ferrocenyl group to effectively approach the electrode surface for fast electron transfer and results in a large ΔE value. As the length of this connecting unit increased from $m = 1$ to $m = 4$, i.e., $O-(CH_2)_4-$, ΔE decreased to 73 mV at 100 mV/s scan rate which is consistent with expectation if steric hindrance as described for **22** is valid.

Table 3.12: Cyclic voltammetric data (potentials versus $\text{Fc}^*/\text{Fc}^{*+}$) at a glassy carbon electrode of 2 mmol dm^{-3} solutions of poly(2,2,2-trifluoroethoxy)(ferrocenylalkoxy)phosphazenes in acetonitrile containing $0.1 \text{ mol dm}^{-3} [\text{N}(\text{nBu}_4)]\text{PF}_6$ as supporting electrolyte. Fc = ferrocenyl.

| Compound | Scan rate | E_{pa} / mV | E_{pc} / mV | $i_{pa} / \mu\text{A}$ | $i_{pc} / \mu\text{A}$ | E° / mV | $\Delta E / \text{mV}$ | i_{pc}/i_{pa} |
|----------------|-----------|----------------------|----------------------|------------------------|------------------------|-----------------------|------------------------|-----------------|
| , 22 | 100 | 72,0 | -25,0 | 2,52 | 0,72 | 23,5 | 97,0 | 0,288 |
| | 200 | 74,5 | -26,5 | 4,99 | 1,29 | 24,0 | 101,0 | 0,258 |
| | 300 | 77,0 | -28,0 | 6,66 | 1,59 | 24,5 | 105,0 | 0,239 |
| | 400 | 79,0 | -29,0 | 8,74 | 1,98 | 25,0 | 108,0 | 0,227 |
| | 500 | 81,0 | -30,0 | 10,27 | 2,20 | 25,5 | 111,0 | 0,214 |
| | 2000 | 96,0 | -24,0 | 37,87 | 5,84 | 36,0 | 120,0 | 0,154 |
| Average | | | | | | 26,4 | | 0,230 |
| , 23 | 100 | 17,0 | -66,0 | 2,22 | 0,64 | -24,5 | 83,0 | 0,287 |
| | 200 | 22,5 | -62,0 | 3,40 | 1,05 | -21,5 | 84,5 | 0,309 |
| | 300 | 27,0 | -66,0 | 3,82 | 1,34 | -19,5 | 93,0 | 0,350 |
| | 400 | 32,0 | -65,0 | 5,39 | 1,32 | -17,0 | 97,0 | 0,245 |
| | 500 | 34,0 | -67,0 | 6,48 | 1,59 | -16,5 | 101,0 | 0,245 |
| | 2000 | 63,0 | -66,0 | 19,04 | 1,46 | -1,5 | 129,0 | 0,077 |
| Average | | | | | | -16,8 | | 0,252 |
| , 24 | 100 | -10,5 | -80,5 | 2,88 | 1,95 | -45,5 | 70,0 | 0,676 |
| | 200 | -7,0 | -77,0 | 4,76 | 3,11 | -42,0 | 70,0 | 0,652 |
| | 300 | -8,5 | -73,0 | 6,16 | 3,59 | -41,0 | 64,5 | 0,584 |
| | 400 | -4,0 | -77,0 | 7,56 | 4,31 | -40,5 | 73,0 | 0,570 |
| | 500 | -1,5 | -71,0 | 9,26 | 5,17 | -36,5 | 70,0 | 0,559 |
| | 2000 | 10,0 | -78,0 | 27,03 | 11,41 | -34,0 | 88,0 | 0,422 |
| Average | | | | | | -39,9 | | 0,577 |
| , 25 | 100 | -15,0 | -85,0 | 5,39 | 4,53 | -50,0 | 70,0 | 0,839 |
| | 200 | -12,0 | -88,0 | 7,00 | 5,64 | -50,0 | 76,0 | 0,805 |
| | 300 | -14,0 | -85,0 | 9,88 | 7,31 | -49,5 | 79,0 | 0,739 |
| | 400 | -8,0 | -89,0 | 11,22 | 8,13 | -48,5 | 81,0 | 0,725 |
| | 500 | -8,0 | -86,5 | 13,94 | 9,06 | -47,5 | 81,0 | 0,650 |
| | 2000 | -4,0 | -82,0 | 38,43 | 15,81 | -43,0 | 78,0 | 0,411 |
| Average | | | | | | -48,3 | | 0,694 |

Chemical reversibility is characterised by current ratios of $i_{pc}/i_{pa} = 1$. In Table 3.12 it can be seen that i_{pc}/i_{pa} systematically increased from 0.288 for **22** to 0.839 for **25** at 100 mV/s/. This implies the oxidised ferrocenium species undergoes substantial decomposition before reduction can take place during the reverse cathodic sweep. This is consistent with the ferrocenium ion being reduced by the free electrons of the four oxygen atoms in the monomeric unit of polymers **22 – 25**. The further away the ferrocenyl group was from the oxygen atoms, i.e., as m increased from 1 to 4, the more difficult it becomes for the free electron pair on the oxygen atom to reduce the ferrocenium cation simply because the contact distance becomes larger.

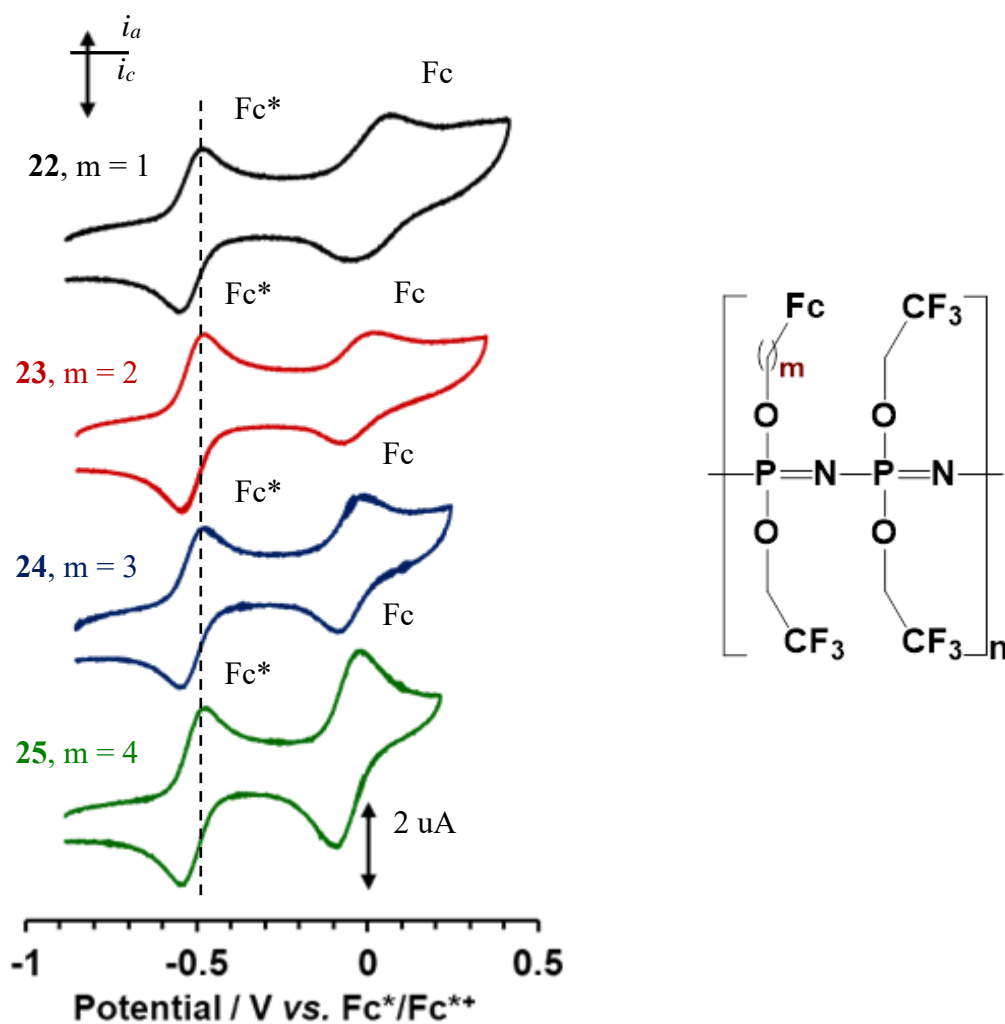


Figure 3.24: Cyclic voltammograms of poly[*tris*(2,2,2-trifluoroethoxy)(ferrocenylalkoxy)phosphazene] complexes 22 - 25, with alkyl chain length, m = 1 - 4 at 100 mV/s scan rate.
Fc* = internal marker, decamethylferrocene, and Fc = polymer bound ferrocenyl group.

It is concluded that none of the complexes **22 – 25** exhibited true chemical reversibility but the longer the connecting unit between the ferrocenyl group and oxygen atom becomes, the closer chemical reversible behaviour was approached.

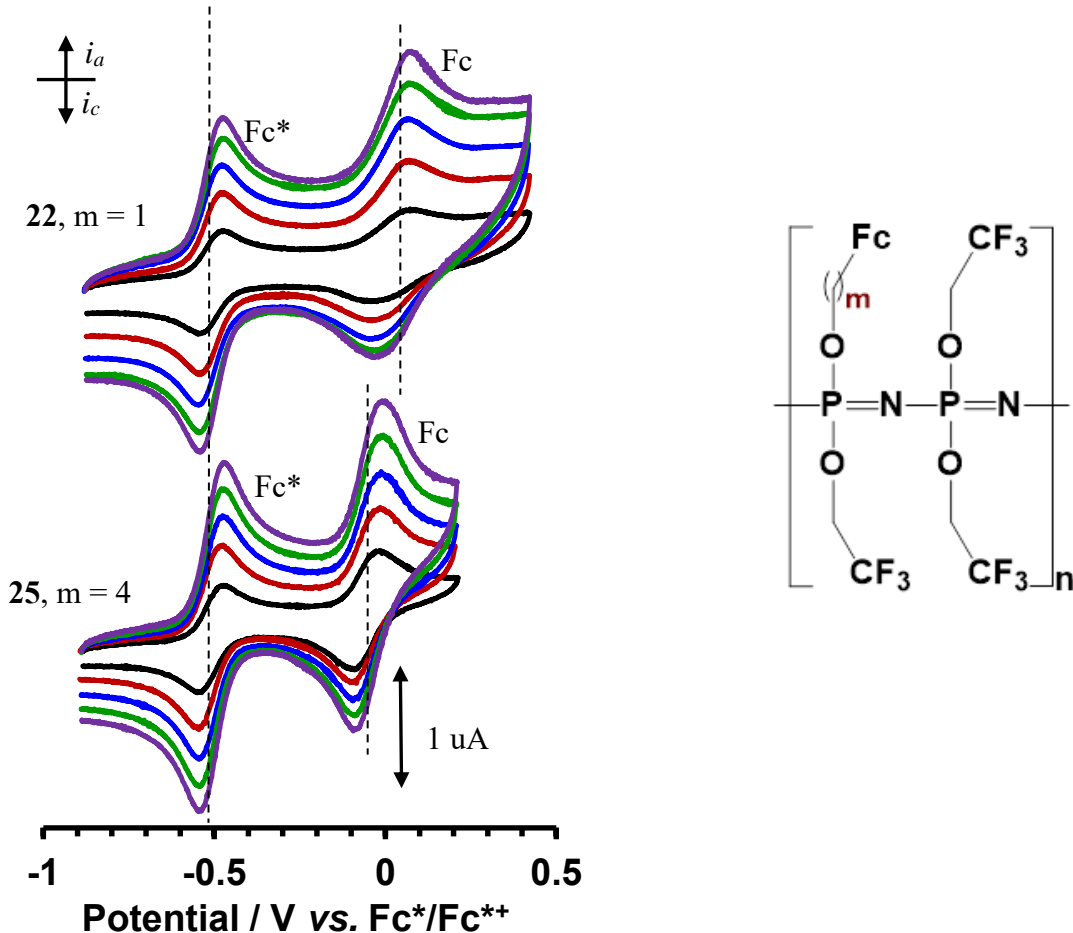


Figure 3.25: Cyclic voltammograms of poly(2,2,2-trifluoroethoxy)(ferrocenylmethoxy) phosphazene, **22, (above) and poly(2,2,2-trifluoroethoxy)(ferrocenylbutoxy)phosphazene, **25**, (below) at 100, 200, 300, 400, and 500 mV/s scan rates. Fc^* = internal marker, decamethylferrocene, and Fc = polymer bound ferrocenyl group.**

Since polymers **22 – 25** either exhibited electrochemical reversibility or came very close in doing so at slow scan rates, formal reduction potentials for the ferrocenyl groups may be estimated by the formula $E^{\circ'} = \frac{1}{2} (E_{pa} + E_{pc})$. As shown in Table 3.12, $-51.5 < E^{\circ'} > 23.5$ mV and $E^{\circ'}$ becomes smaller as m increases from 1 to 4. This reflects two properties of the side chain separating the ferrocenyl group from the oxygen atom. Firstly, the electron-withdrawing properties of the oxygen atom as indicated by its atomic electronegativity of 3.5 is more effectively shielded from the

electron-donating ferrocenyl group ($\chi_{\text{Fc}} = 1.87$; χ = group electronegativity). This resulted in E° decreasing (i.e., easier to oxidise) as m increases. Secondly, alkyl groups are known electron donors. The electron-donating power of alkyl groups changes in the order (strongest) butyl > propyl > ethyl > methyl (weakest). This implies that the ferrocenyl groups of polymer **25** are under the influence of a stronger electron-donating group, the $(-\text{CH}_2)_4$ group, than the ferrocenyl group of polymer **22**, with a methylene spacer adjacent to the ferrocenyl group. This is also consistent with the ferrocenyl group of **25** being easier to oxidise than the ferrocenyl group of **22** as shown by the decreasing values of E° . Figure 3.26 shows graphically the relationship between E° and m . It is evident from this graph that E° will reach an asymptotic limit approximately at $m = 5$ and the potential close to -55 mV versus FcH/FcH^+ .

It is instructive to note that a separate electrochemical study on the parent ferrocene-containing alcohols, $\text{Fc}-(\text{CH}_2)_m-\text{OH}$ and $m = 1, 2, 3$, and 4 , exhibited the same trend as shown in Figure 3.26 (see Figure 2.10 in chapter 2).²

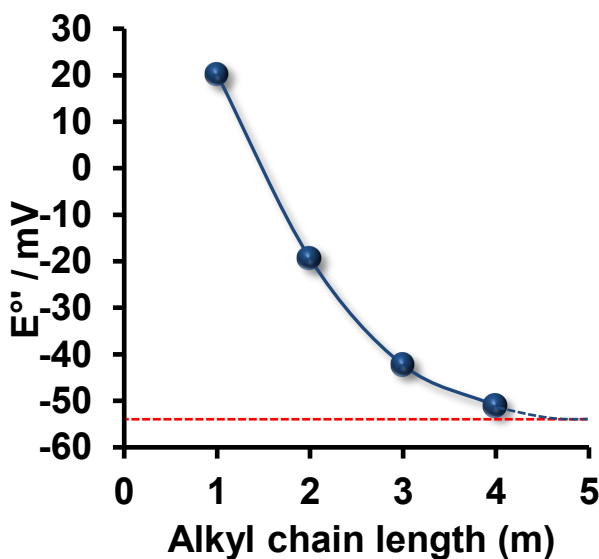
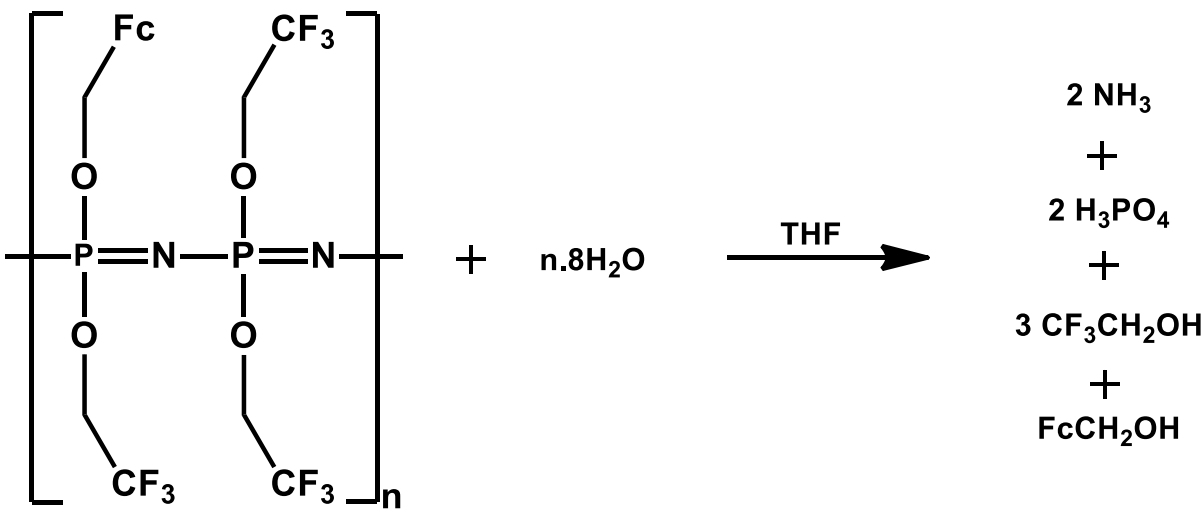


Figure 3.26: Relationship between the formal reduction potential, E° of poly[*tris*(2,2,2-trifluoroethoxy)(ferrocenylalkoxy)phosphazene] complexes, **22 - 25**, and alkyl chain length of alkoxy groups (m).

3.7 Kinetics of hydrolysis

Hydrolysis kinetics of poly[*tris*(2,2,2-trifluoroethoxy)(ferrocenylmethoxy)phosphazene], **22**, was investigated as a representative example of **22 – 25** by monitoring the formation of phosphoric acid in tetrahydrofuran/water mixtures as solvent at 325 nm using UV/vis spectroscopy. Different concentrations of water as co-solvent and hydrolysing reagent was used to determine the effect on the rate of polymer hydrolysis. The stoichiometric hydrolysis reaction is shown Scheme 3.9.



Scheme 3.9: Exhaustive hydrolysis of poly[*tris*(2,2,2-trifluoroethoxy)(ferrocenylmethoxy)phosphazene], polymer **22.**

It is emphasised that the kinetic results presented here does not constitute a full kinetic study that includes pH control by buffers. Such a study falls completely outside the boundaries of the research performed and presented in this thesis. It is envisaged that a comprehensive follow-up PhD study may address this. The aim of the present study was merely to determine whether polymer hydrolysis is possible at pH = *ca.* 7 and if more than one hydrolysis step is identifiable.

Rothenmund and Teasdale discussed the hydrolysis of polyphosphazenes with amine side chains, see Section 2.2.5 (chapter 2). In essence they reported first the hydrolysis of the two amine side chains which takes place in two consecutive steps, whereafter the polymer main chain decomposes into phosphates and ammonia. It was attempted to identify the corresponding steps for **22** and to develop a feel for the timescales involved in water/THF mixed solvents. THF was required to dissolve **22** and the water was required for the hydrolysis. Pseudo-first-order reaction conditions were used,

ensuring that the concentration of water was in excess of 3894-fold (**Reaction 1**), 7788-fold (**Reaction 2**), and 15579-fold (**Reaction 3**) compared to the concentration of **22** as shown in Table 3.13. The concentration of the polymer reactant is presented utilising the repeating unit concentration containing one ferrocenyl group, (see Scheme 3.9 for the repeating unit).

Table 3.13: Concentrations used for the kinetics of hydrolysis of poly[*tris*(2,2,2-trifluoroethoxy)(ferrocenylmethoxy)phosphazene], **22.**

| | [H ₂ O] / mol dm ⁻³ | [22] / mmol dm ⁻³ | Excess H ₂ O |
|-------------------|---|------------------------------|-------------------------|
| Reaction 1 | 13.89 | 2.377 | 3894-fold |
| Reaction 2 | 18.51 | 2.377 | 7788-fold |
| Reaction 3 | 27.78 | 1.783 | 15579-fold |

Figure 3.27 exhibits the absorbance changes during hydrolysis for **22**, between 1 and 100 hours and 300 to 600 nm wavelengths. Significant hydrolysis could be observed spectrophotometrically between 315 nm and 340 nm, therefore 325 nm was used to follow the reaction.

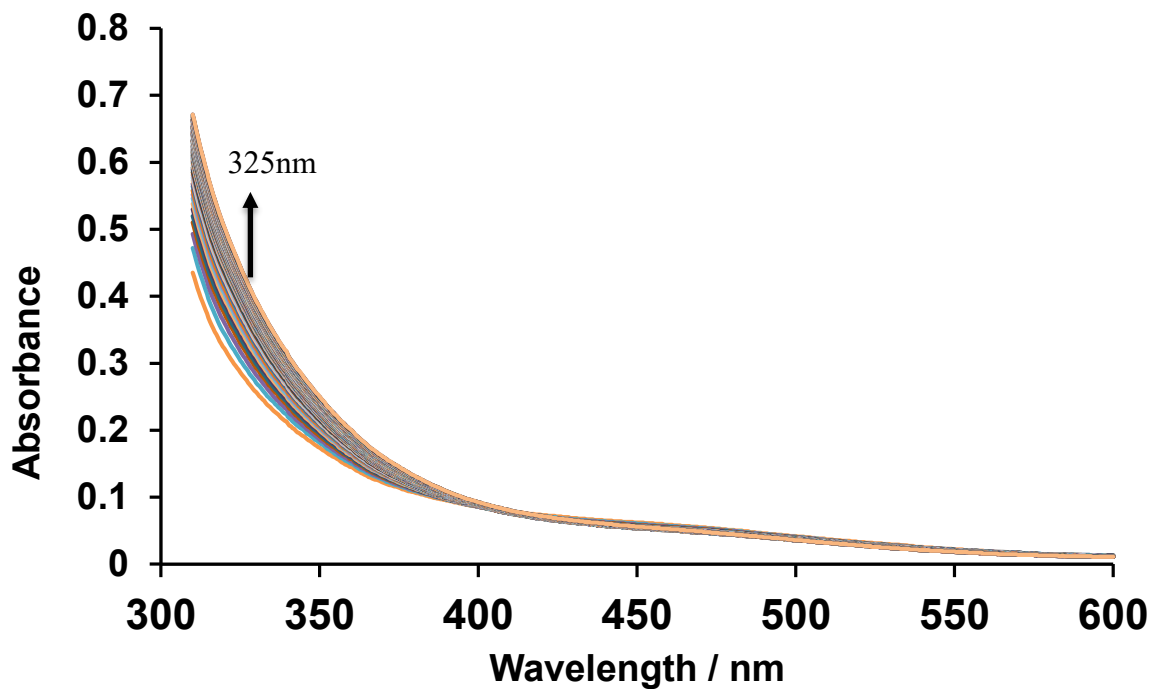


Figure 3.27 Time-dependent UV absorbance spectra (between 300 – 600 nm) for the hydrolysis of poly[*tris*(2,2,2-trifluoroethoxy)(ferrocenylmethoxy)phosphazene], **22, between 1 and 100 hours.**

The reaction with the lowest concentration of water used, was monitored at 325 nm for 100 hours. However, hydrolysis was extremely slow and the data could not kinetically be interpreted. Despite the concentration of polymer to water ratio being 1:3894 (**Reaction 1**), the bulkiness and coiling of the polymer chains did not allow for the hydrolysis process to be fast enough to obtain reliable kinetic results. Therefore, higher concentrations of water was used to determine whether the hydrolysis of the polymer could be sped up in order to be followed kinetically.

Figure 3.28 shows the time-based UV absorbance changes of **22**, at $\lambda = 325$ nm. A polymer to water concentration of 1:7788 (**Reaction 2**) allowed for fast enough hydrolysis to interpret results kinetically. The first 10 hours of the reaction (see insert Figure 3.28) shows spectroscopic changes that is consistent with the initial but simultaneous hydrolysis of the three trifluoroethoxy groups (the first overall kinetic step) followed by hydrolysis of the ferrocenylmethoxy group in second overall kinetic step. This means trifluoroethoxy hydrolysis and ferrocenylmethoxy hydrolysis followed each other in two consecutive steps. Trifluoroethanol was mostly liberated during the first 3 hours and ferrocenylmethanol was liberated mostly until *ca.* 7 hours of reaction time. In the process the hydrophobic polymer **22** converted to a phosphazene baring hydroxyl side chains. The flat line between $t = 10$ and $t = \text{ca. } 25$ hours is consistent with this new hydrophilic polymer recoiling thereby changing polymer morphology (folding pattern) to assume a coiled shape that are more compatible and more stable in the aqueous environment.²³ The main portion of Figure 3.28 shows a time trace of main chain hydrolysis between 25 and 100 hours to produce phosphoric acid and ammonia.

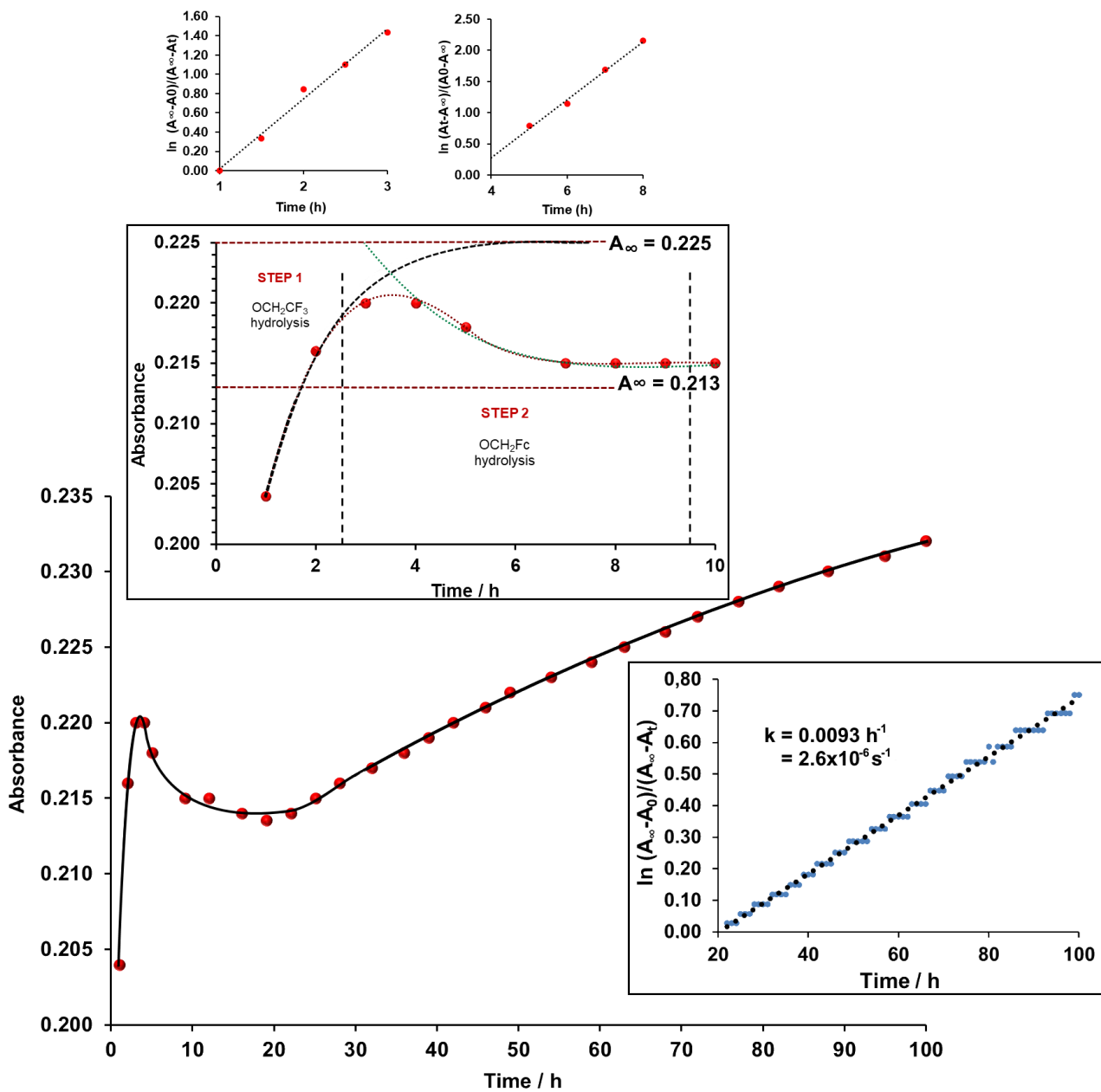


Figure 3.28: Absorbance versus time (in hours) for the hydrolysis of the polyphosphazene backbone, where $[\text{H}_2\text{O}] = 18.51 \text{ M}$ and $[22] = 2.377 \times 10^{-3} \text{ M}$, (Reaction 2) at 325 nm.

The order of both steps of side chain hydrolysis under pseudo order conditions (water is in 3894 fold excess) was 1 for both side chain types, OCH_2CF_3 and OCH_2Fc , because a linear relationship between $\ln(\text{absorbance})$ and time exists (see linear line inserts in Figure 3.28, top). Trifluoroethanol was liberated almost twice as fast as ferrocenylmethanol. Half-lives of these two processes were approximately $(\ln 2)/k = (\ln 2)/0.0121 = 57 \text{ min}$ and $(\ln 2)/k = (\ln 2)/0.00774 = 90 \text{ min}$ respectively.

Main chain decomposition was also first order for the same reason but much slower. The half-life of main chain hydrolysis was *ca.* 74 hours. Pseudo first order and second order rate constants using time units of seconds are summarised in Table 3.14.

Table 3.14: Rate constants (k_{obs} and k_2) calculated for the hydrolysis of 22 (for Reaction 2 and 3), using different concentrations of water (18.51 M and 27.78 M).

| $[H_2O]$ / mol dm $^{-3}$ | k_{obs} / s $^{-1}$ | | | k_2 / dm 3 mol $^{-1}$ s $^{-1}$ | | |
|---------------------------|-----------------------|-----------------------|----------------------|---------------------------------------|-----------------------|-----------------------|
| | Step 1 | Step 2 | Step 3 | Step 1 | Step 2 | Step 3 |
| 18.51 | 2.01×10^{-4} | 1.29×10^{-4} | 2.6×10^{-6} | 1.09×10^{-5} | 7.00×10^{-6} | 1.38×10^{-7} |
| 27.78 | | | | 2.92×10^{-5} | | |

Figure 3.29 shows the time-based reaction trace for **22** at $\lambda = 325$ nm with solvent composition THF:H₂O 1:27.78 implying the water excess over polymer is 15580 fold, Reaction 3. Such a large excess of water allowed for complete main chain hydrolysis after 30 hours. The time scale for side chain hydrolysis and refolding of the resulting hydroxyl-containing hydrophilic polymer main chain was so short that it could not be investigated with any degree of accuracy.

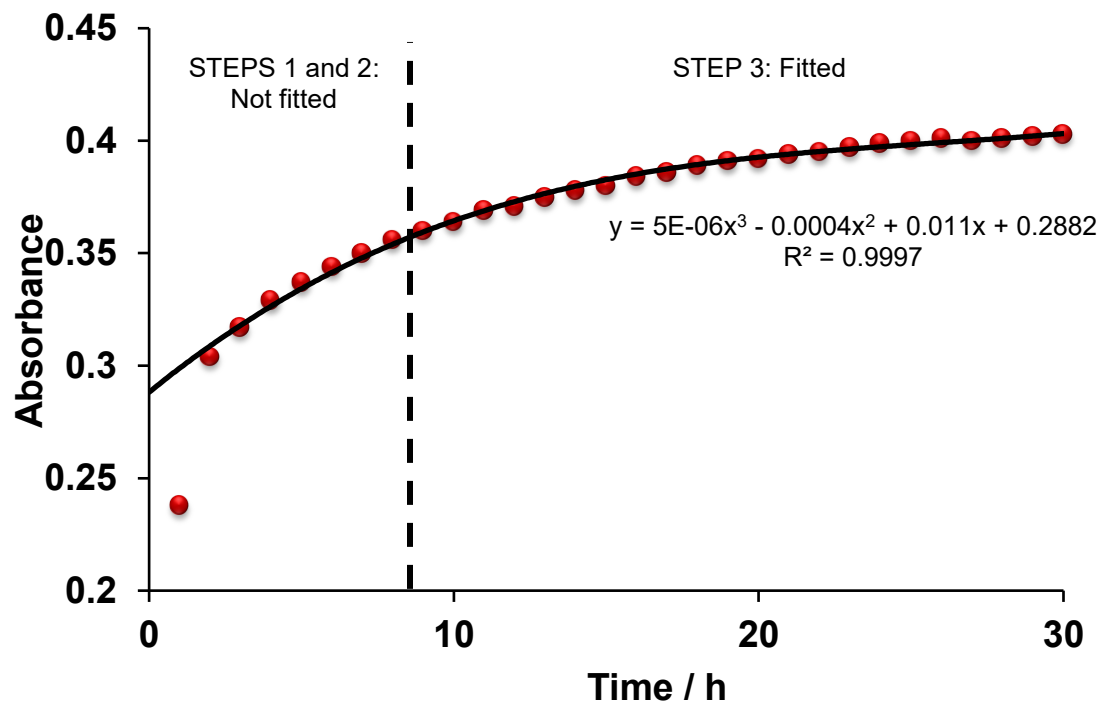


Figure 3.29: Absorbance versus time (in hours) for the hydrolysis of 22 at 325 nm, Reaction 3.

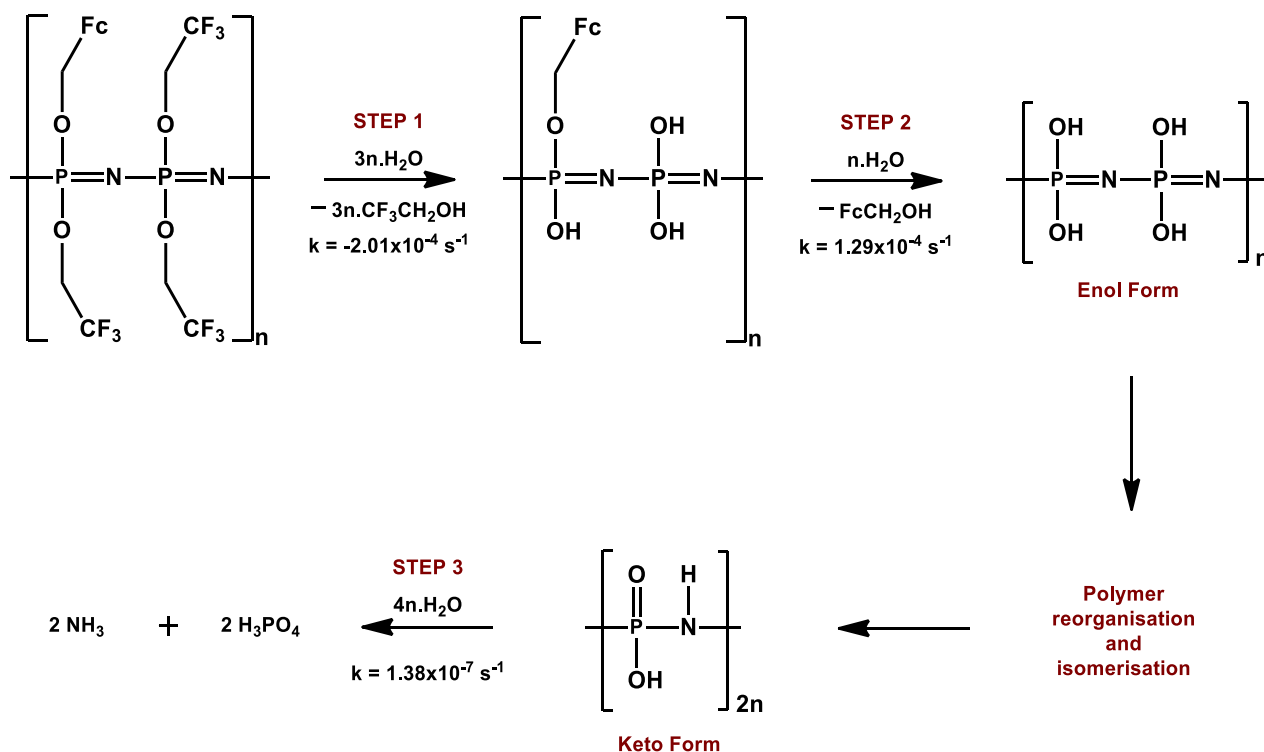
$[H_2O] = 27.77$ M and $[22] = 1.783 \times 10^{-3}$ M.

The second order rate constant for main chain hydrolysis under these conditions was $1.05 \times 10^{-6} \text{ dm}^3 \text{ mol}^{-1} \text{ s}^{-1}$. Surprisingly it was observed that the rate constant for reaction 2, $k_2 = 1.38 \times 10^{-7} \text{ dm}^3 \text{ mol}^{-1} \text{ s}^{-1}$ and reaction 3, $k_2 = 1.05 \times 10^{-6} \text{ dm}^3 \text{ mol}^{-1} \text{ s}^{-1}$ were not the same; it differed by more than one order of magnitude. This is ascribed to the lack of use of buffers in these trial experiments to keep the pH constant. The pH of the reaction mixture is expected to change more quickly in reaction 3 than in reaction 2 during the course of the reaction because the 6 protons that is liberated during hydrolysis accumulates much faster in a more aqueous rich environment (Reaction 3) than an aqueous poor environment (Reaction 2). It is clear that hydrolysis is very sensitive to pH and buffers should be used in the detailed follow-up kinetic study. At this stage it can be concluded that the present series of ferrocene-containing polyphosphazenes will have much potential as anticancer drug carriers because the present results indicate that hydrolysis is slow at high pH and accelerates substantially at low pH. Since the pH inside cancer cells vary between 5 and 6 it follows that the present polyphosphazene-ferrocene drug would be relatively stable while circulating in the blood (pH 7.35 to 7.45) but set the ferrocene-containing drug quickly free when internalised into cancer cells.²⁴

The above described results indicated a first-order dependence on polymer concentration but no clear evidence could be found for the order with respect to water because the k_2 values (Table 3.13) were not constant. Upon assigning an order of x to the water dependence of hydrolysis the rate law of hydrolysis may with the present knowledge be written as:

$$\text{hydrolysis rate} = k_{\text{obs}}[\text{polyphosphazene}] \text{ with } k_{\text{obs}} = k_x [\text{H}_2\text{O}]^x$$

The mechanism of hydrolysis for **22** can with the above results be postulated as shown in Scheme 3.10.



Scheme 3.10: Postulated mechanism of hydrolysis of poly[tris(2,2,2-trifluoroethoxy)ferrocenylmethoxy]phosphazene, 22.

3.8 Differential Scanning Calorimetry (DSC)

The thermal properties of the synthesised poly[*bis*(2,2,2-trifluoroethoxy)phosphazene], 21, and poly[*tris*(2,2,2-trifluoroethoxy)(ferrocenylalkoxy)phosphazene] complexes, 22, 23, 24, and 25, were investigated utilising DSC. An experimental sequence of heating followed by cooling cycles was developed to determine if the polymer exhibited any thermal events (e.g., melting or other phase transitions). The heating/cooling profile developed is shown in Figure 3.30.

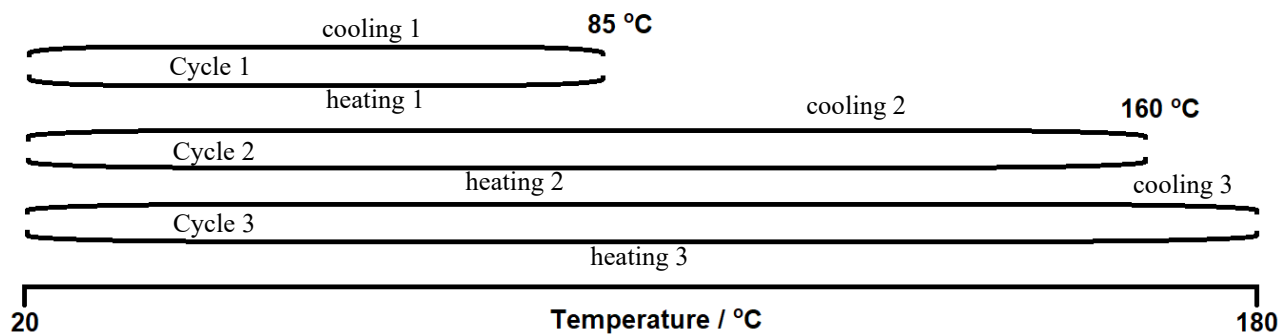


Figure 3.30: Temperature profiles developed to determine the thermal properties of polyphosphazenes 21 – 25.

Figure 3.31 shows the DSC thermogram for poly[*bis*(2,2,2-trifluoroethoxy)phosphazene], **21**. The melting point is observed on the first heating cycle at the onset temperature of 68.46 °C and crystallisation of the super-cooled liquid during the first cooling cycle at the onset temperature of 52.83 °C. During cycle 2, the melting was observed at the onset melting temperature lowered to 65.89 °C and the onset crystallisation temperature to 49.76 °C. However, for cycle 3 the onset melting temperature was 58.25 °C and onset crystallisation temperature was 48.54 °C. Utilising the melting temperatures for each cycle the onset melting temperature systematically lowered with each successive cycle. In addition the temperature range in which melting occurred (= endset temperature – onset temperature) increased from 4.12 °C for cycle 1 to 6.01 °C for cycle 2 to 9.55 °C for cycle 3. This is indicative of thermal cracking of the polymer main chain to smaller molecular mass fragments and an increased molecular mass size distribution in the sample as it is exposed to higher and higher temperatures.

Polymer **21** is known to have a glass transition temperature of 203 K (-70 °C); but unfortunately, the instrumentation at our disposal cannot operate below -50 °C and hence we could not observe it.^{25,26} However, utilising the approximation equation $T_g = 2/3 T_{melt}$, T_g for **21** may be calculated as approximately 220 K for cycle 1. This is close to the literature value of 203 K. It should be noted that T_{melt} and T_g varies with molecular mass. It is concluded that the molecular mass of **21** used here (6307 g/mol, see Table 3.2) is different from the (unknown) molecular mass of the sample giving the published T_g value of 203 K.

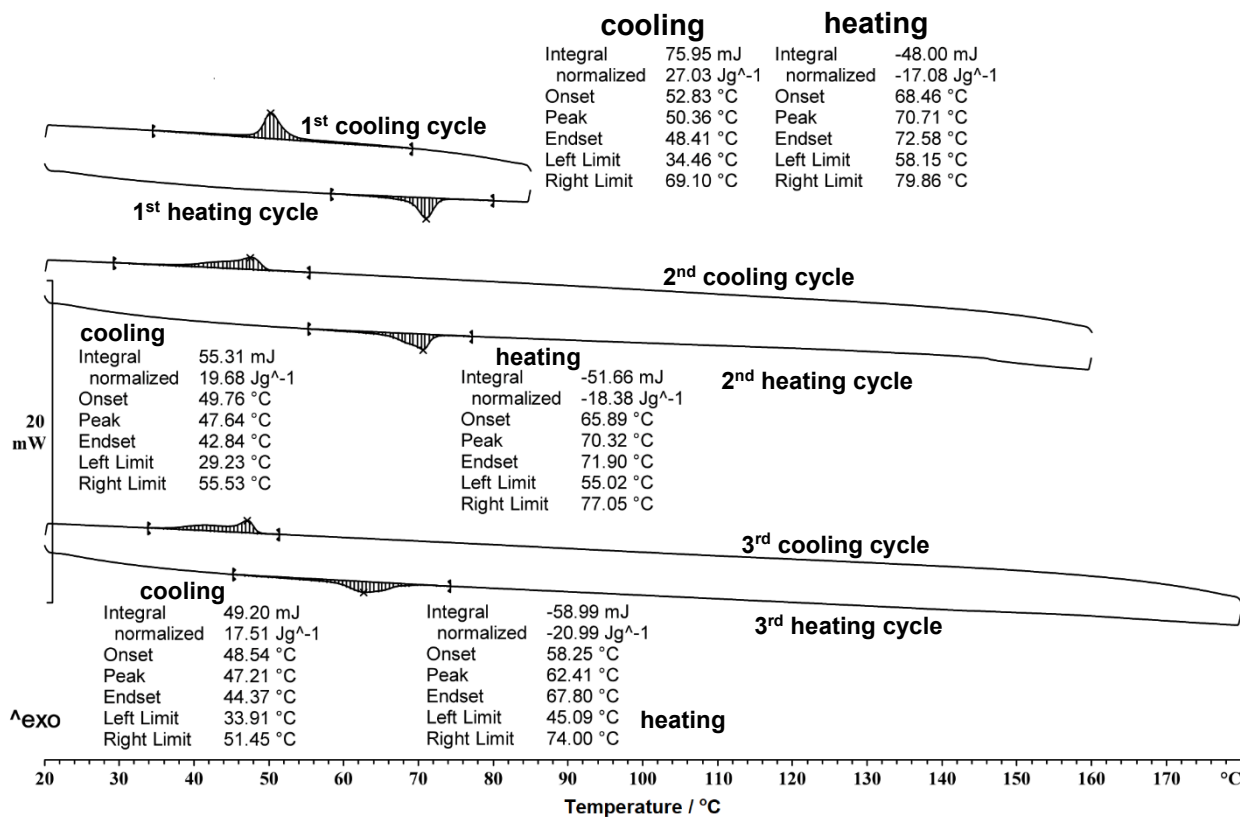


Figure 3.31: DSC thermogram of poly[bis(2,2,2-trifluoroethoxy)phosphazene], 21.

The thermal profiles of newly synthesised poly(2,2,2-trifluoroethoxy)(ferrocenylalkoxy) phosphazenes, **22**, **23**, **24** and **25** were somewhat different. The first heating cycle showed a melting point, see Figure 3.32 utilising **22** as a representative example, but in every forthcoming heating and cooling cycle **22 – 25** appeared to be thermally silent. It meant either **22 – 25** are thermoset polymers rather than thermoplastic polymers (as **21**), or relaxation times of **22 – 25** are much longer than for **21** (Figure 3.32). The melting temperatures determined by these initial DSC experiments for **22 – 25** are summarised in Table 3.15.

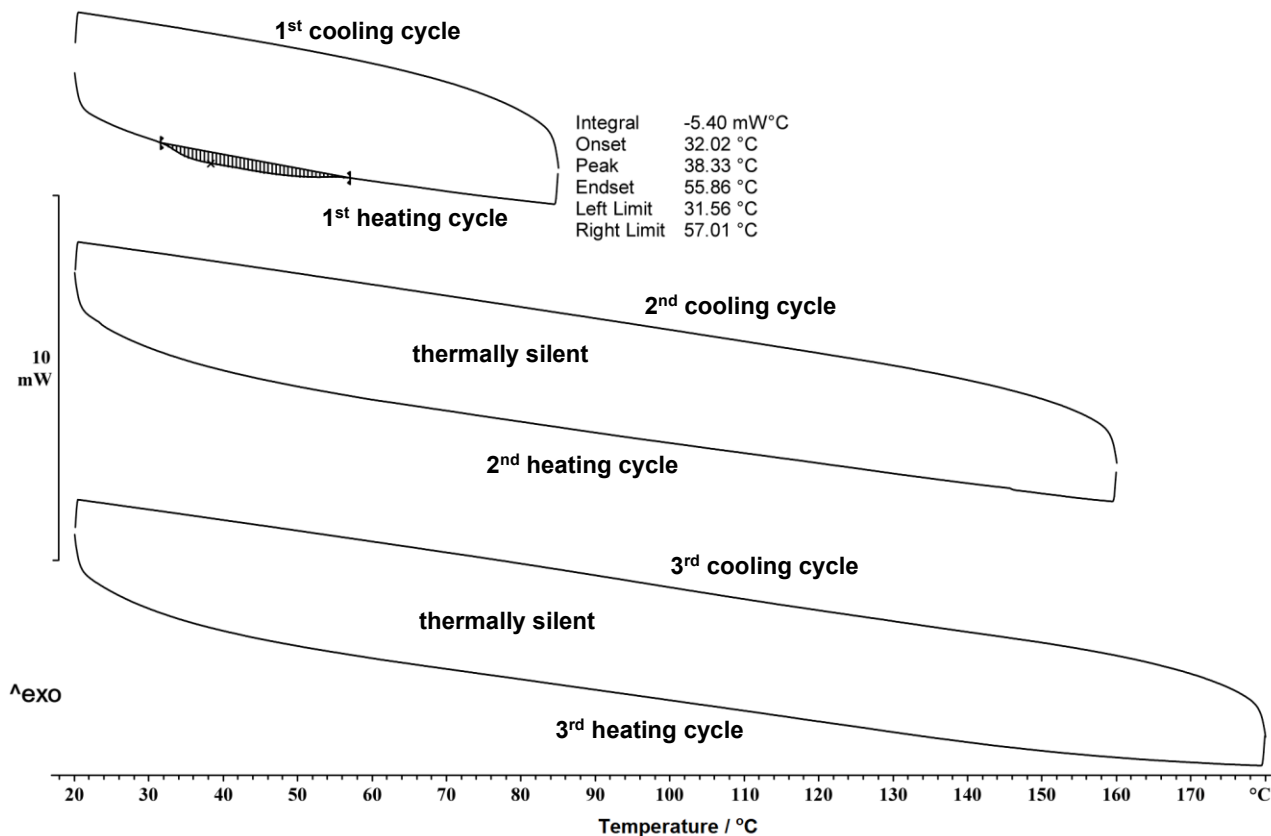


Figure 3.32: DSC thermogram of poly[tris(2,2,2-trifluoroethoxy)(ferrocenylmethoxy)phosphazene], 22.

Table 3.15: Initial experimental melting point temperatures for synthesised compounds 22, 23, 24 and 25, poly[tris(2,2,2-trifluoroethoxy)(ferrocenylalkoxy)phosphazenes]

| Compound | Temperature / °C |
|-----------|------------------|
| 22 | 38.3 |
| 23 | 42.4 |
| 24 | 70.1 |
| 25 | 38.7 |

To determine whether **22 – 25** are thermosets or thermoplastics, DSC experiments were repeated following the heating and cooling sequences shown in Figure 3.30, the sample was then left to stand for 24 hours. A second sequence of heating and cooling was then performed between -35 °C and 80 °C to determine if thermal activity were regained. Figure 3.33 presents the second set of thermograms for all four synthesised poly[bis(2,2,2-trifluoroethoxy)(ferrocenylalkoxy)]

phosphazenes, **22 – 25**, 24 hours after the first set of thermograms were obtained, utilising the same sample (Table 3.16).

Table 3.16: Melting point temperatures for synthesised compounds **22, **23**, **24** and **25**, poly[*tris*(2,2,2-trifluoroethoxy)(ferrocenylalkoxy)phosphazenes]**

| Compound | Temperature / °C |
|-----------|------------------|
| 22 | 42.52 |
| 23 | 43.68 |
| 24 | 63.07 |
| 25 | 44.59 |

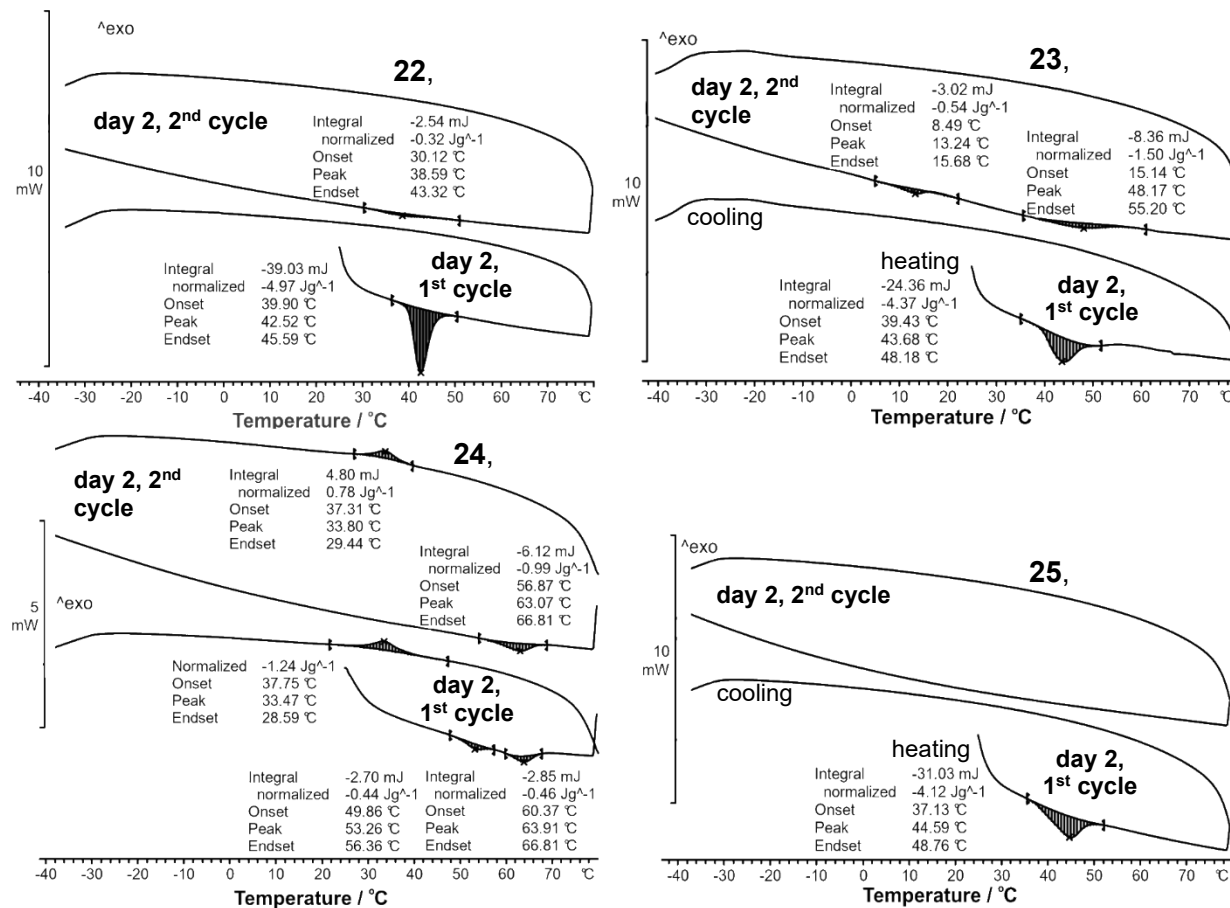


Figure 3.33: DSC thermograms (day 2) of all synthesised poly[*tris*(2,2,2-trifluoroethoxy)(ferrocenylalkoxy)phosphazenes] **22 (top left), **23** (top right), **24** (bottom left) and **25** (bottom right).**

From these thermograms, the melting points for each polymer was redetermined. Thermal activity for all four polymers were regained cycle 1 on day 2. Polymer **22** exhibited a melting onset temperature of 42.52 °C during heating cycle 1. However, no crystallisation was still observed during cooling cycle 1 day 2. Only a small amount of polymer was observed to melt during heating cycle 2 at $T_{\text{onset}} = 38.59$ °C. Polymer **23** was observed to melt at 43.68 °C during heating cycle 1. As was observed for **22**, no crystallisation was observed during cooling cycle 1 for **23**. The second heating cycle of **23** on day 2 showed two thermal events. The first at 8.49 °C is assigned to a solid state relaxation enthalpy and the second with $T_{\text{peak}} = 48.1$ °C represents the maximum energy flow during the melting process.

Polymer **24** (Figure 3.33) exhibited two different phase changes during heating cycle 1, one at 53.26 °C and the other at 63.91 °C. The thermal event at 53.26 °C is assigned to a solid state relaxation event while the 63.92 °C transition onset represents the start of a melting process. During cooling cycle 1, supercooled polymer **24** crystallised at 33.47 °C. Melting was observed for polymer **24** during heating cycle 2 at 63.07 °C followed by crystallisation of the supercooled polymer during cooling cycle 2 at 33.80 °C. Polymer **24** was the only poly[*tris*(2,2,2-trifluoroethoxy)(ferrocenylalkoxy)phosphazene] in the series **22 - 25** which exhibited observable crystallisation on a cooling cycle. Polymer **25** melted at 44.59 °C during cycle 1 of day 2 and exhibited no other thermal properties. From the thermograms presented in Figure 3.34 for polymers **22 - 25** utilising **23** as an example, it was concluded that polymers **22 - 25** all exhibited, as expected, reversible thermoplastic properties. Phase transition kinetics was simply very slow to observe them if an inadequate amount of time had elapsed between heating and cooling cycles.

A second set of experiments were performed to confirm reproducibility of results. This is demonstrated for **23** in Figure 3.34. The same sample in two consecutive experiments on different days gave similar peaks although the energies involved became less during the second day of experiments. As described for **21**, (Figure 3.31) this is also consistent with thermal cracking to smaller molecular masses for these polymers.

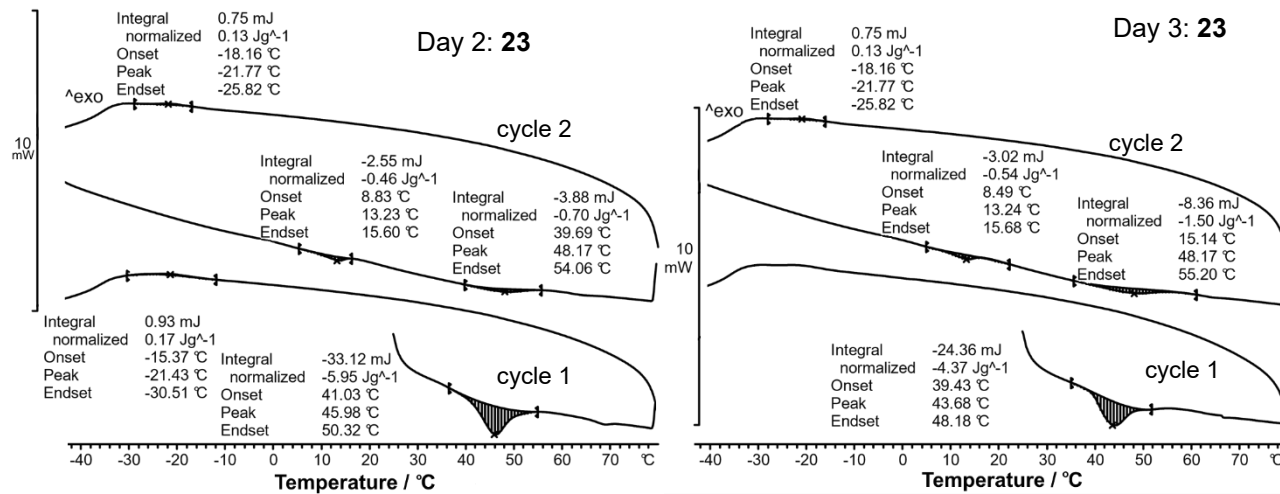


Figure 3.34: DSC thermograms of poly[tris(2,2,2-trifluoroethoxy)(ferrocenylethoxy) phosphazene], 23, on day 2 (left) and day 3 (right).

In a final experiment, two different molecular mass samples were subjected to DSC experiments to establish the influence molecular mass has on the thermal profile of these polymers. Figure 3.35 presents the thermograms of **25**, poly[tris(2,2,2-trifluoroethoxy)(ferrocenylbutoxy)phosphazene] at two different molecular weights, $\overline{M}_n = 126\,554$ (**25c**) and $168\,475$ (**25b**).

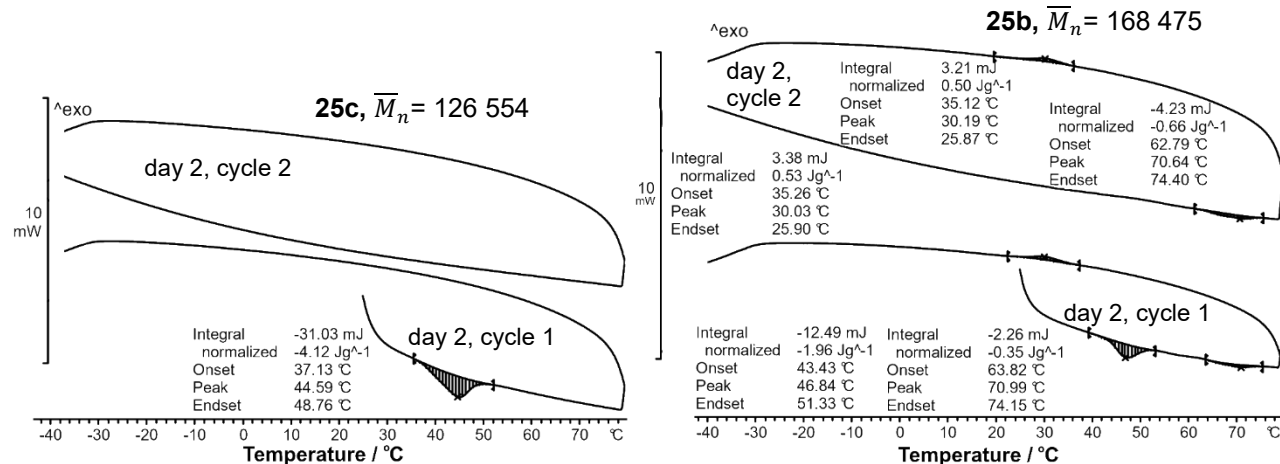


Figure 3.35: DSC thermograms of poly[tris(2,2,2-trifluoroethoxy)(ferrocenylbutoxy) phosphazene], 25, on day 2, with different molecular weights, GPC determined $\overline{M}_n = 126\,554$ (left, **25c) and $168\,475$ (right, **25b**).**

Two different melting points were observed in that the higher molecular weight sample ($\overline{M}_n = 168\,475$, **25b**) exhibited melting onset during heating cycle 1 at 43.43 and 63.82 °C, while the single

melting onset of the lower molecular weight ($\overline{M}_n = 126\,554$, **25c**) sample was 37.13 °C. It is clear that higher molecular mass polymers have higher onset melting temperatures than the lower molecular mass polymers, here 37.13 °C for **25c** versus 43.43 and 63.83 °C for **25b**. The two melting temperatures observed for **25b** is consistent with phase separation between higher and lower molecular mass fractions during DSC experiments on day 1.

3.9 Cytotoxicity

The author would like to acknowledge the Physical Chemistry BioLab for assistance in performing the cytotoxicity tests on polymers **22 - 25** and the reference compound cisplatin as this was the first time such experiments were done in our laboratory with new equipment. All cytotoxicity measurements were performed on the HeLa cervical cancer cell line.

Table 3.17 presents the half maximal inhibitory concentration (IC_{50}) for the synthesised polymers **22 - 25** as well as for cisplatin (reference chemotherapeutic drug). This measurement quantitatively indicates the concentration of compound necessary to inhibit *in vitro* cell growth by 50% (i.e., measure of potency of the compound; the IC_{50} concentration is inversely proportional to the potency of the compound).

Table 3.17: Half maximal inhibitory concentration (IC_{50}) measurements for all synthesised poly[*bis*(2,2,2-trifluoroethoxy)(ferrocenylalkoxy)phosphazenes], **22 - 25, and cisplatin (reference) against HeLa cells. Values in brackets are for the free alcohols, $Fc(CH_2)_mOH$.**

| Polymer | IC_{50} (μM) | | |
|-------------------|----------------------------------|---------------|-------------------------|
| | Test 1 | Test 2 | Average |
| 22 (m = 1) | 18.53 | 17.95 | 18.24 (> 100) |
| 23 (m = 2) | 42.07 | 38.23 | 40.15 (35) |
| 24 (m = 3) | 76.87 | 58.83 | 67.85 (17) |
| 25 (m = 4) | 62.58 | 55.59 | 59.09 (5.5) |
| Cisplatin | 1.26 | 1.16 | 1.21 |

The reference drug, cisplatin, was observed to exhibit an IC_{50} concentration of 1.21 μM under our conditions. Poly[*tris*(2,2,2-trifluoroethoxy)(ferrocenylalkoxy)phosphazenes], **22 - 25**, exhibited

anticancer activity against the HeLa cell line. However, IC₅₀ concentrations for **22 – 25** were 15 – 56 times larger than that of cisplatin.

Figure 3.36 represents the percentage of HeLa cell growth when treated with **22 – 25** or versus that observed for a control (i.e., no drug added) with all other conditions remaining the same. These figures are also known as dose-response curves. The dose-response curve for cisplatin indicates that the maximal efficacy of cisplatin occurred at 100 µM. This is, however, not a useful concentration *in vivo*, as 50% of test animals die due to drug toxicity at 47 µM per kg mass of test animals.²⁷

Table 3.17 also presents the IC₅₀ concentrations of the free equivalent ferrocenylalcohols previously determined in literature; ferrocenylbutanol exhibited the highest potency of 5.7 µM and ferrocenylmethanol exhibited the lowest potency of > 100 µM.²⁸ The trend between IC₅₀ values and **m** for the polymers were however, opposite in direction (see Figure 3.37). Shago *et al* also showed IC₅₀ values of free alcohols, Fc(CH₂)_nOH decrease with the decreasing formal reduction potential of the ferrocenyl group, Figure 3.38.^{2,28} This trend is also reversed for the polymers **22 – 25**, see Figure 3.38.

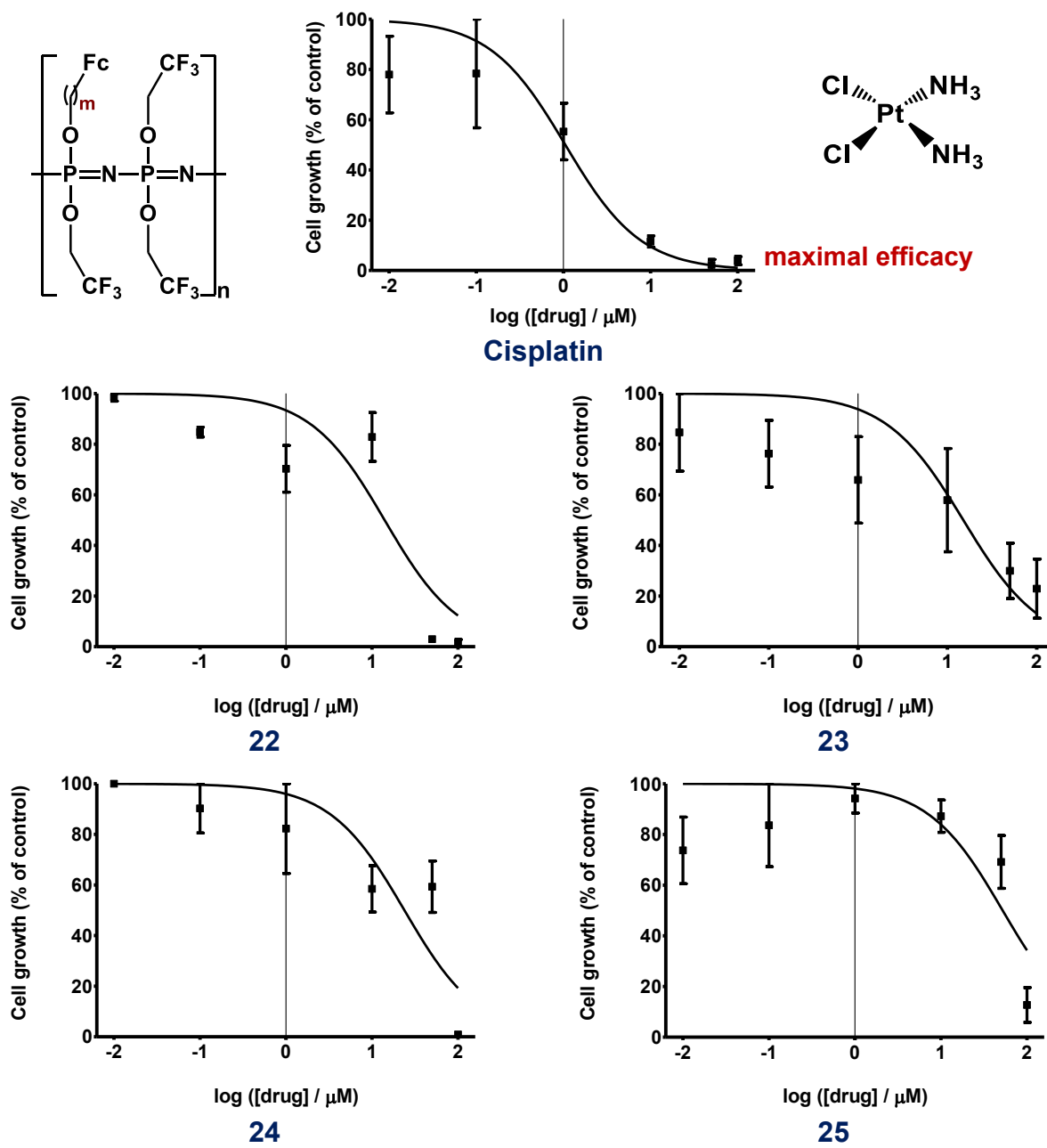


Figure 3.36: Dose response for cisplatin (reference) and poly[tris(2,2,2-trifluoroethoxy)(ferrocenylalkoxy)phosphazenes] 22 – 25.

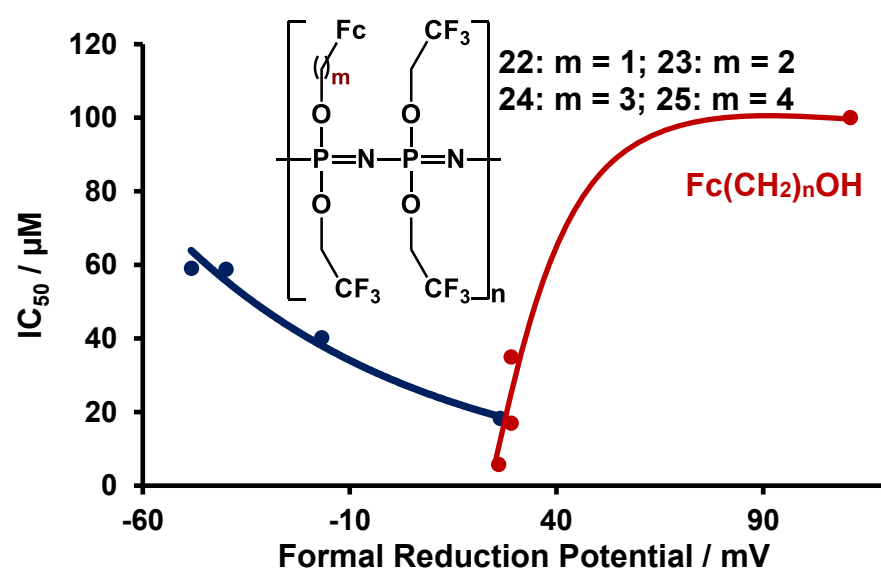
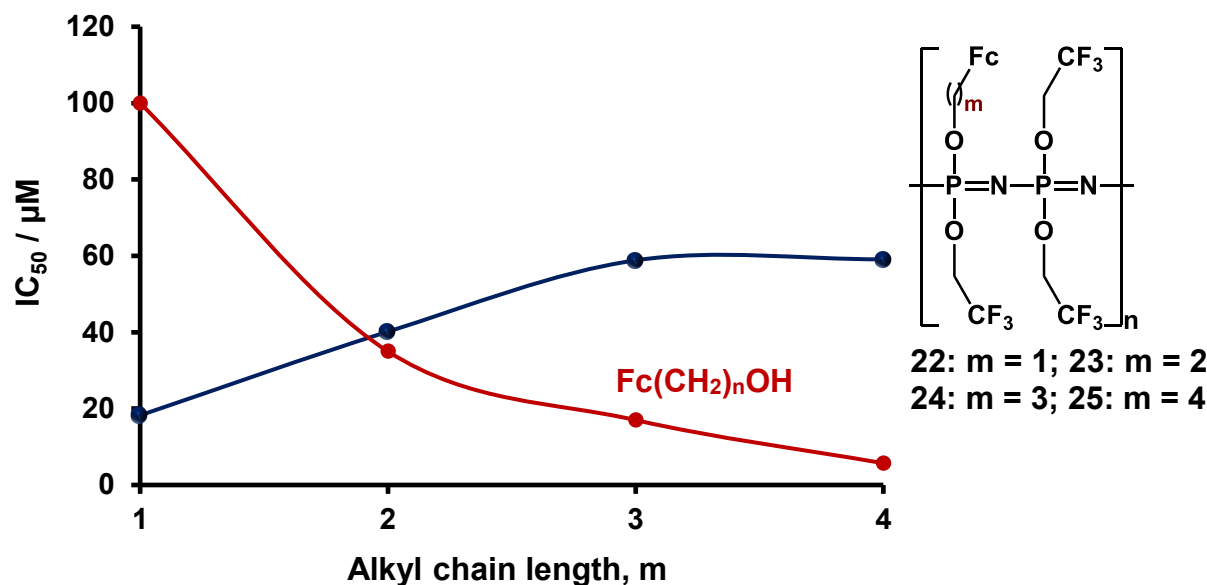


Figure 3.38: Relationship between IC_{50} values and formal reduction potential of polymers at 100 mV/s scan rate 22 – 25 (blue) as well as the free ferrocenylalcohols, $Fc(CH_2)_nOH$ (red).

The main purpose for covalent bonding of the ferrocenylalcohols with proven anticancer ability to the polyphosphazene polymer was to create a drug/drug-delivery conjugate, with the ferrocenylalcohols being the active drug. It was expected that the cytotoxic results obtained for **22 – 25** should follow the same trends as the published results for the free ferrocenylalcohols. Differences observed are firstly that the IC₅₀ values obtained for **23 – 25** were higher than those of the free ferrocenylalcohols, while the IC₅₀ of **22** are better than for free Fc(CH₂)OH, see Table 3.17. Secondly, IC₅₀ values of the polymeric systems **22 – 25** increased asymptotically for increasing values of **m**, but for the free alcohols, Fc(CH₂)_nOH, it decreased asymptotically with increasing values of **m**, Figure 3.37. Thirdly, the relationship between E°' and IC₅₀ for the free alcohols exhibited a direct proportionality but an inverse proportionality for the polymers. Interpreting these results, the first important observation is that polyphosphazenes were successful in acting as drug delivery system because in the cytotoxicity tests, cytotoxicity was observed. If the drug was not released from the carrier polyphosphazene polymer, no cytotoxicity would be observed at all for **22 – 25**.

To explain the direct IC₅₀ – **m** trend though for the polymers compared to the inverse IC₅₀ – **m** trend for the free ferrocenylalcohols, is more difficult. The increased IC₅₀ values of compounds **23 – 25** may be attributed to the structure, folding pattern and the hydrolysis kinetic rates of the polymer-drug conjugate. Polymers are known to fold and coil into itself when in solution, especially when compatibility with the solvent is low. Comparing the structure of **22** bearing hydrophilic Fc(CH₂)O- side chains with the structure of **25** having hydrophobic Fc(CH₂CH₂CH₂CH₂)O- side chains, it is evident that folding patterns of these two polymers in aqueous solutions would differ. Polymer **25** would fold in such a way as to bury the Fc(CH₂CH₂CH₂CH₂)O- hydrophobic chains in hydrophobic pockets in the interior of the coiled polymer backbone, while such pockets would be much less evident for **22** with its hydrophilic Fc(CH₂)O- side chains. This argument would lead to the ferrocenylalkoxy moieties becoming more and more trapped inside the hydrophobic pockets of the folded polymer as the alkoxy chain length increases from **m** = 1 to **m** = 4. This would imply hydrolysis of the ferrocenylalkoxy drug from the polymer becomes more difficult with increasing **m**. Therefore, less drug would be released in a specific timescale with increasing values of **m** and a higher apparent IC₅₀ value would be obtained for complexes with increasing values of **m**. The slower release (equivalent of drug activation) also explains the lower IC₅₀ to E°' proportionality observed for **22 – 25**. Further research is required to elaborate on this explanation.

This then concludes the discussion of the research performed by the author. Experimental details for all experiments performed by the author may be found in Chapter 4, while Chapter 5 will provide a short summary as well as future perspectives.

References

- 1 J. Clayden, N. Greeves, S. Warren and P. Wothers, *Organic Chemistry*, Oxford University Press, Oxford ; New York, 1 edition., 2000.
- 2 W. L. Davis, R. F. Shago, E. H. G. Langner and J. C. Swarts, *Polyhedron*, 2005, **24**, 1611–1616.
- 3 B. Wang, E. Rivard and I. Manners, *Inorg. Chem.*, 2002, **41**, 1690–1691.
- 4 C. H. Honeyman, I. Manners, C. T. Morrissey and H. R. Allcock, *J. Am. Chem. Soc.*, 1995, **117**, 7035–7036.
- 5 T. Modzelewski, N. M. Wonderling and H. R. Allcock, *Macromolecules*, 2015, **48**, 4882–4890.
- 6 E. P. Otocka, *Acc. Chem. Res.*, 1973, **6**, 348–354.
- 7 G. Socrates, *Infrared and Raman Characteristic Group Frequencies: Tables and Charts*, Wiley, Chichester, 3 edition., 2004.
- 8 J. H. Simons, in *Fluorine Chemistry, Volume 2*, Academic Press, 2012, p. 157.
- 9 A. A. Berlin, *Polym. Sci. USSR*, 1966, **8**, 1465–1472.
- 10 H. L. Wagner, *J. Phys. Chem. Ref. Data*, 1985, **14**, 1101–1106.
- 11 C. E. Carraher Jr., in *Introduction to Polymer Chemistry*, CRC Press, 2nd edn., 2010, pp. 73–81.
- 12 F. Moulder, W. F. Stickle and K. D. Bomben, in *Handbook of X-ray Photoelectron Spectroscopy*, ULVAC-PHI, Inc, Enzo, Chigasaki, Japan, 1995, pp. 45, 57, 143.
- 13 D. Briggs and J. T. Grant, *Surface Analysis by Auger and X-Ray Photoelectron Spectroscopy*, IM Publications, Chichester, 2003.
- 14 W. (Ina) du Plessis, J. J. Erasmus, G. J. Lamprecht, J. Conradie, T. S. Cameron, M. A. Aquino and J. C. Swarts, *Can. J. Chem.*, 1999, **77**, 378–386.
- 15 Y. Yokota, Y. Mino, Y. Kanai, T. Utsunomiya, A. Imanishi and K. Fukui, *J. Phys. Chem. C*, 2015, **119**, 18467–18480.
- 16 D. O. Cowan, J. Park, M. Barber and P. Swift, *J. Chem. Soc. Chem. Commun.*, 1971, **22**, 1444–1446.
- 17 G. Riveros, S. Meneses, S. Escobar, C. Garín and B. Chornik, *J. Chil. Chem. Soc.*, 2010, **55**, 61–66.
- 18 A. B. Fischer, M. S. Wrighton, M. Umana and R. W. Murray, *J. Am. Chem. Soc.*, 1979, **101**, 3442–3446.
- 19 S. Chernyy, Z. Wang, J. J. K. Kirkensgaard, A. Bakke, K. Mortensen, S. Ndoni and K. Almdal, *J. Polym. Sci. Part Polym. Chem.*, 2017, **55**, 495–503.
- 20 A. P. Grosvenor, B. A. Kobe, M. C. Biesinger and N. S. McIntyre, *Surf. Interface Anal.*, 2004, **36**, 1564–1574.
- 21 N. Kumpan, T. Poonsawat, L. Chaicharoenwimolkul, S. Pornsuwan and E. Somsook, *RSC Adv.*, 2017, **7**, 5759–5763.

- 22 H. J. Gericke, N. I. Barnard, E. Erasmus, J. C. Swarts, M. J. Cook and M. A. S. Aquino, *Inorganica Chim. Acta*, 2010, **363**, 2222–2232.
- 23 S. Rothemund and I. Teasdale, *Chem. Soc. Rev.*, 2016, **45**, 5200–5215.
- 24 I. F. Tannock and D. Rotin, *Cancer Res.*, 1989, **49**, 4373–4384.
- 25 J. Brandrup and E. H. Immergut, Eds., in *Polymer Handbook, 3rd Edition*, Wiley-Interscience, New York, 3rd edition., 1989, p. VI/249.
- 26 R. L. Miller and L. E. Nielsen, *J. Polym. Sci.*, 1960, **44**, 391–395.
- 27 Wolpert-DeFillipps, *Cancer Treat. Rep.*, 1979, **63**, 1453–1458.
- 28 R. F. Shago, J. C. Swarts, E. Kreft and C. E. J. V. Rensburg, *Anticancer Res.*, 2007, **27**, 3431–3433.

This page is intentionally left blank

4.1 Introduction

The materials, equipment, experimental procedures and techniques that were used in this study are presented in this chapter.

4.2 Materials

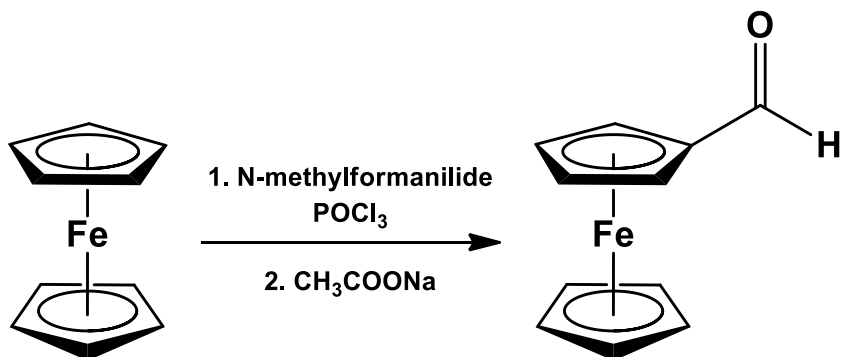
Solid and liquid reagents (Aldrich and Merck) were used without further purification unless otherwise stated. Organic solvents used in this study were dried and distilled according to published methods.¹ Kieselgel 60 (Merck, grain size 0.040 – 0.063 mm) was used to perform column chromatography. Filtration and vacuum evaporation were conducted using a water aspirator, or a pump with liquid nitrogen trap in case of air and/or moisture sensitive compounds. Melting points (m.p.) were measured using the Olympus BX51 microscope equipped with a Linkham THMS 600 heating/cooling stage and the values are uncorrected.

4.3 Spectroscopic Measurements

¹H NMR spectra were measured at 298 K on a Bruker Avance DPX 300 NMR spectrometer. A few specified ¹H NMR, all ¹³C NMR, ³¹P NMR and ¹⁹F NMR spectra were measured using a Bruker Avance II 600 NMR spectrometer. Probe for ¹³C and ¹H = 5 mm DUAL 13C-1H/D probe with z-gradients. Probe for ³¹P and ¹H = 5 mm TBI 1H/31P/D-BB probe with z-gradients (¹H frequency = 600.28 MHz; ¹³C frequency = 150.95 MHz; ³¹P NMR frequency = 242.99 MHz; ¹⁹F NMR frequency = 564.83 MHz). Chemical shifts are reported relative to SiMe₄ (TMS) at 0.00 ppm relative to TMS, the ¹H NMR peak. The ¹H NMR peak for deuterated chloroform (CDCl₃) is at 7.27 ppm and the peak for trace amounts of water in CDCl₃ is at 1.60 ppm. The ¹H NMR peaks for deuterated tetrahydrofuran (THF-d₈) are at 1.73 ppm and 3.58 ppm and deuterated water (D₂O) has a peak at 4.65 ppm in this solvent. IR measurements were taken using a Nicolet iS50 ATR Fourier Transform spectrometer.

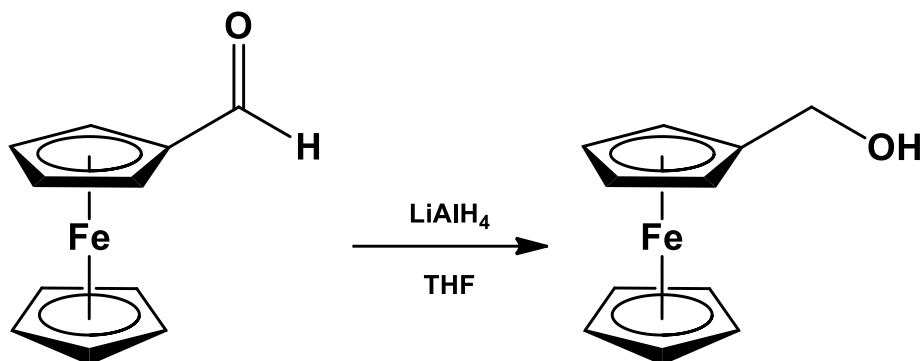
4.4 Synthesis of ferrocene derivatives

4.4.1 Ferrocene carboxaldehyde



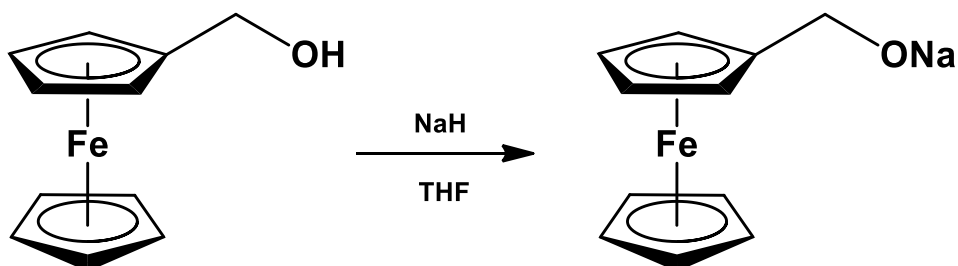
A solution of N-methylformanilide (9.73 g, 0.072 mmol, 2.6 eq) and POCl_3 (6.9 g, 0.045 mmol, 1.6 eq) was stirred vigorously under argon atmosphere. Ferrocene (5 g, 0.027 mmol) was added slowly over twenty minutes. The mixture was allowed to stir for one hour at room temperature and then at 65°C for two hours. Once cooled to 0°C , sodium acetate (15 g in 125 cm^3) was added slowly and allowed to stir overnight at room temperature. Diethyl ether ($3 \times 100 \text{ cm}^3$) was used to extract the mixture. The combined ether extracts were washed with equal quantities of 1M HCl, water, saturated sodium carbonate and lastly with a saturated solution of sodium chloride. The organic phase was dried over MgSO_4 and the solvent removed using rotary evaporation. Column chromatography was used to purify the product with eluent hexane:ether 1:1 which yielded red/brown crystals. Yield 4.75 g (83 %). Melting point = $191 - 121^\circ\text{C}$. IR: $\nu/\text{cm}^{-1} = 1643 (\text{C=O})$, **Spectrum 1.** $^1\text{H NMR}$ (300 MHz, CDCl_3)/ppm = 4.30 (s, 5H, C_5H_5), 4.64 (t, 2H, 0.5 x C_5H_4), 4.81 (t, 2H, 0.5 x C_5H_4) 9.98 (s, 1H, CHO), **Spectrum 20.**

4.4.2 1-Ferrocenylmethanol



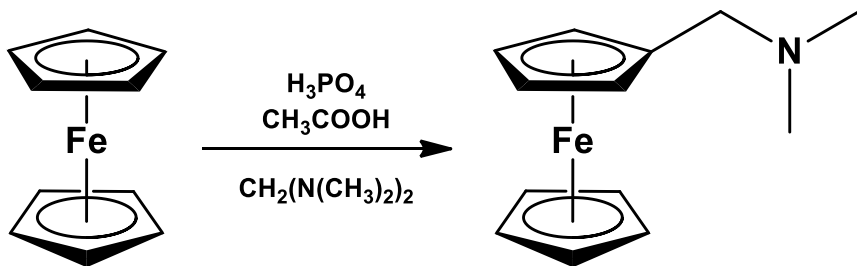
In a three neck round bottom flask fitted with gas inlet tap and condenser, argon was used to purge the system for ten minutes. LiAlH₄(1 g, 28 mmol, 2.8 eq) was added to the dry flask. A solution of ferrocene carboxaldehyde (2.091 g, 9.815 mmol) in 50 cm³ THF was added dropwise. The reaction mixture was refluxed for thirty minutes and then cooled to room temperature. Distilled water was added and the product was extracted with diethyl ether (3 x 50 cm³). The combined ether extracts were dried over MgSO₄ and the solvent removed using rotary evaporation. Yield 2.084 g (98 %). Melting point = 56 – 60 °C. IR: ν/cm^{-1} = 985 (C-O), 3240 (O-H broad), **Spectrum 2**. ¹H NMR (300 MHz, CDCl₃)/ppm = 4.22 (s, 5H, C₅H₅), 4.28 (t, 2H, 0.5 x C₅H₄), 4.34 (t, 2H, 0.5 x C₅H₄), 2.20 (s, 2H, CH₂), **Spectrum 21**. ¹³C NMR (600 MHz; CDCl₃)/ppm = 88.47 (C₅H₅), 69.17 (CH₂OH), 68.29 (C₅H₄), 67.88 (C₅H₄), 60.78 (C_{ipso}; C₅H₄), **Spectrum 37**.

4.4.3 Sodium-1-ferrocenylmethoxide



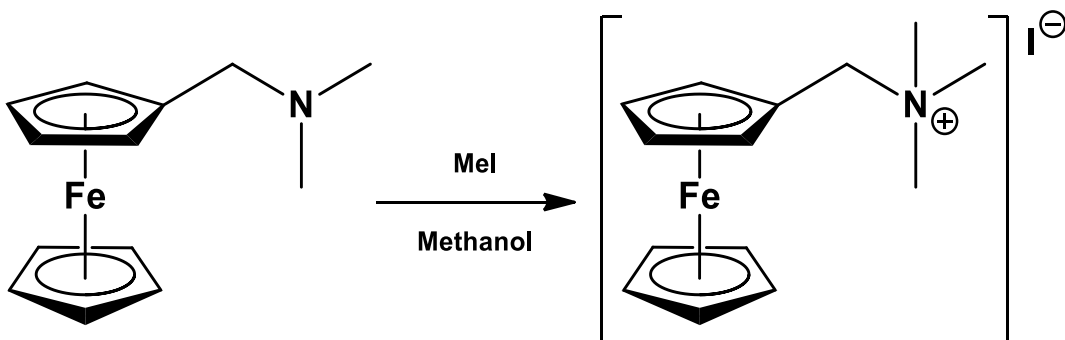
Sodium hydride (68 mg, 2.779 mmol, 1 eq) was weighed into a two neck round bottom flask fitted with gas inlet tap, under inert conditions. The flask was placed in an ice bath and 10 cm³ dry THF was added slowly. 1-Ferrocenylmethanol (606 mg, 2.779 mmol) was dissolved in 10 cm³ dry THF and this solution was slowly added to the sodium hydride. The reaction mixture was allowed to stir overnight at room temperature. The solution was filtered the next day by cannula. The solvent was removed under reduced pressure and the product was stored in a glovebox.

4.4.4 N,N-Dimethylaminomethylferrocene



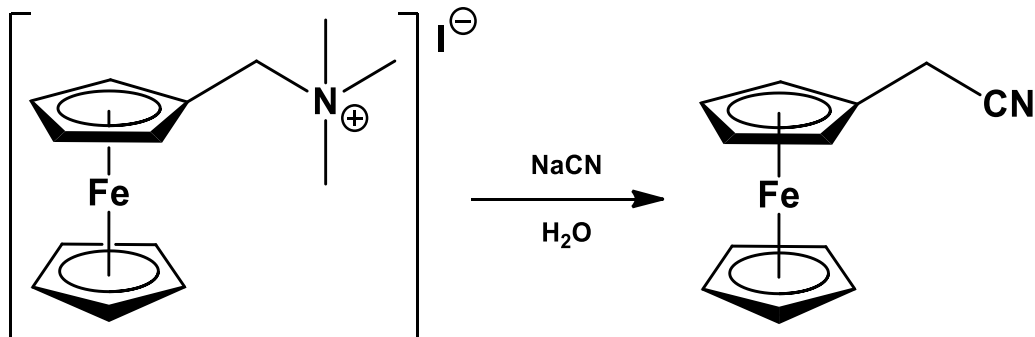
A solution of phosphoric acid (9 cm³, 160 mmol, 1.7 eq) and glacial acetic acid (160 cm³) was flushed with argon, then cooled in an ice bath, and bis(dimethylamino)methane (21 cm³, 91.4 mmol, 1 eq) was added dropwise with stirring. Ferrocene (17 g, 91.2 mmol) was added and the mixture refluxed overnight. The solution was allowed to cool, diluted with 100 cm³ of cold distilled water and unreacted ferrocene extracted from the acidic medium with diethyl ether (3 x 80 cm³). The acidic aqueous solution was then treated with ice and with 2M NaOH until alkaline, and further extracted with diethyl ether (3 x 80 cm³). The ether extracts were dried over anhydrous MgSO₄ and solvent removed by rotary evaporation, yielding 68 % (15.354 g) as a yellow oil. IR: ν/cm^{-1} = 1452 (CH₃), 2760 – 2932 (C-H aliphatic), 3089 (C-H aromatic), **Spectrum 3**. ¹H NMR (300 MHz, CDCl₃)/ppm = 4.12 (m, 7H, C₅H₅ + 0.5 C₅H₄), 4.18 (t, 2H, 0.5 C₅H₄), 3.29 (s, 2H, CH₂), **Spectrum 22**.

4.4.5 *N,N,N*-trimethylaminomethylferrocene iodide



N,N-dimethylaminomethylferrocene (15 g, 61.47 mmol) was dissolved in methanol (40 cm³) and iodomethane (4 cm³, 64.2 mmol, 1 eq) was slowly added. The reaction mixture was refluxed for one hour. After cooling to room temperature, diethyl ether (60 cm³) was added slowly. The crude product, separated as a fine yellow powder, was filtered to yield 88.9 % (20.98 g). Melting point = decomposed at 189 – 194 °C. IR: ν/cm^{-1} = 1469 (CH₃), 2935 – 3003 (C-H aliphatic), 3049 – 3092 (C-H aromatic), **Spectrum 4**.

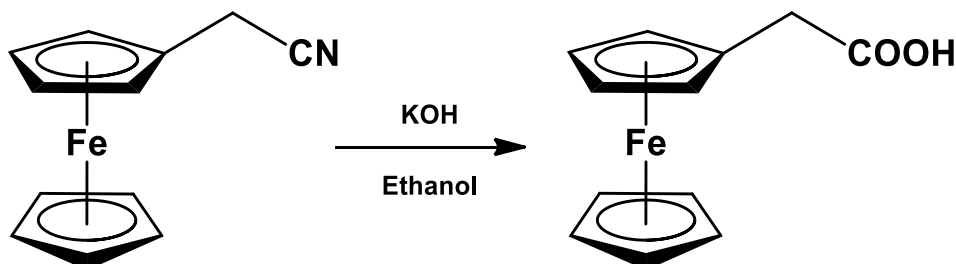
4.4.6 Ferroceneacetonitrile



A solution of *N,N,N*-trimethylaminomethylferrocene iodide (19.830 g, 51.38 mmol) and NaCN (15.2 g, 310 mmol, 6 eq) was refluxed in H₂O (100 cm³) for three hours. The dark brown solution was allowed to cool to room temperature and H₂O (50 cm³) was added. The reaction mixture was extracted with dichloromethane (3 x 80 cm³). The combined organic extracts were washed with water, dried over MgSO₄ and the solvent removed by rotary evaporation. Yield = 8.846 g (76.2 %).

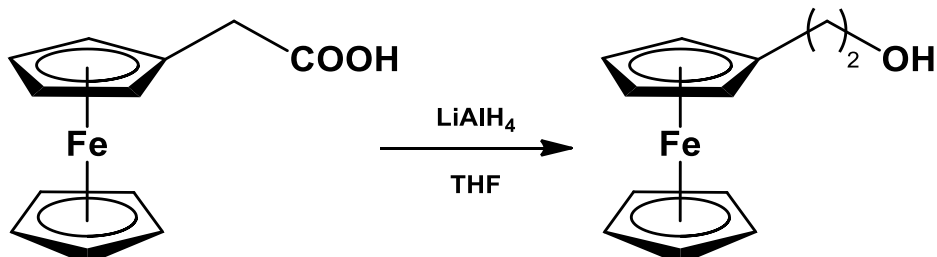
Melting point = 81 – 85 °C. IR: ν/cm^{-1} = 2248 (C≡N), **Spectrum 5**. ^1H NMR (300 MHz, CDCl_3)/ppm = 4.92 (s, 1H, -CH₂CN), 4.58 (t, 2H, 0.5 x C₅H₄), 4.36 (t, 2H, 0.5 x C₅H₄), 4.32 (s, 5H, C₅H₅), **Spectrum 23**.

4.4.7 Ferroceneacetic acid



Potassium hydroxide (5 g, 85 mmol, 9 eq) in distilled water (50 cm³) was added to a solution of 2-ferrocenylacetonitrile (2.048 g, 9.06 mmol) in absolute ethanol (20 cm³). The reaction mixture was refluxed for 3 hours until evolution of ammonia ceased. The ethanol was removed under reduced pressure. The residual suspension was dissolved in water (50 cm³) and extracted with diethyl ether. The aqueous layer was acidified with 2M HCl and left in an ice bath until golden crystals formed. The crystals were filtered, washed with small amounts of cold distilled water and air dried. Yield = 1.26 g (57 %). Melting point = 148 - 151 °C. IR: ν/cm^{-1} = 1165 (C-O), 1759 (C=O), 2923 (C-H aromatic), 3431 (O-H broad, acid), **Spectrum 6**. ^1H NMR (300 MHz, CDCl_3)/ppm = 4.14 - 4.23 (m, 9H, C₅H₅ + C₅H₄), 3.43 (s, 2H, CH₂), **Spectrum 24**.

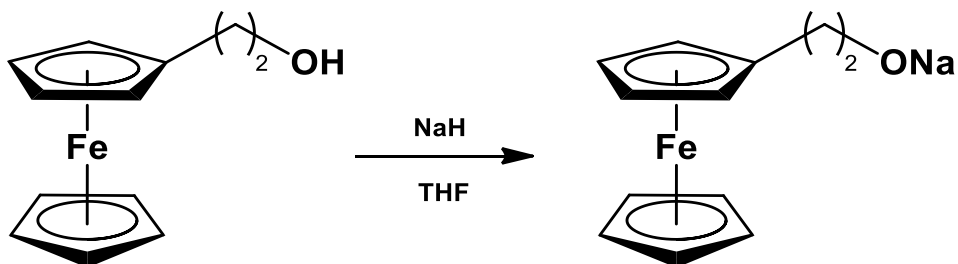
4.4.8 2-Ferrocenylethanol



In a three neck round bottom flask fitted with gas inlet tap and condenser, argon was used to purge the system for ten minutes. LiAlH₄ (190 mg, 4.92 mmol, 2.6 eq) was added to the dry flask. A solution of 2-ferrocenylethanoic acid (448 mg, 1.83 mmol) in 50 cm³ THF was added dropwise. The reaction mixture was refluxed for one hour then cooled to room temperature. Distilled water was added and the product was extracted with diethyl ether (3 x 50 cm³). The combined ether extracts

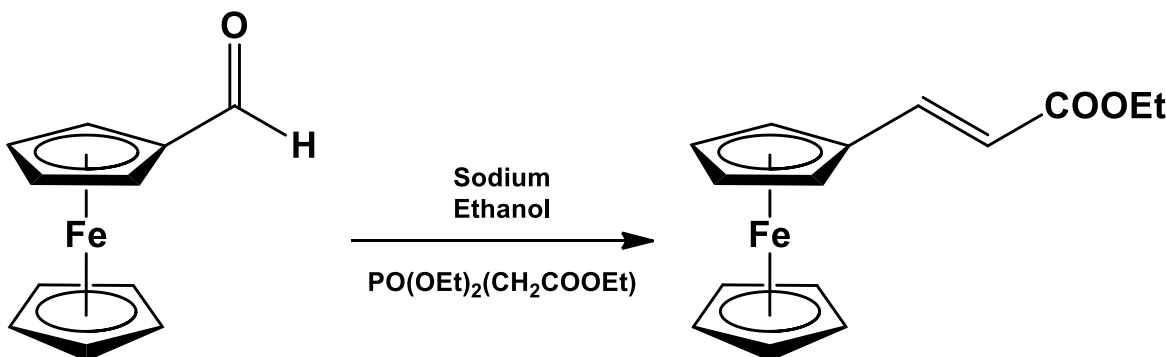
were dried over MgSO₄ and the solvent removed using rotary evaporation. Yield 481 mg (91 %) as an orange oil. IR: ν/cm^{-1} = 999 – 1035 (C-O), 2851 – 2919 (C-H aliphatic), 3220 (O-H broad), **Spectrum 7.** ¹H NMR (300 MHz, CDCl₃)/ppm = 4.26 (s, 5H, C₅H₅), 4.84 (t, 2H, 0.5 C₅H₄), 4.55 (t, 2H, 0.5 C₅H₄), 3.11 (t, 2H, CH₂), 2.77 (t, 2H, CH₂), **Spectrum 25.** ¹³C NMR (600 MHz; CDCl₃)/ppm = 84.82 (C₅H₅), 68.60 (-CH₂OH), 67.88 (C₅H₄), 67.66 (C₅H₄), 63.49 (C_{ipso}; C₅H₄), 32.83 (-CH₂CH₂OH), **Spectrum 38.**

4.4.9 Sodium-2-ferrocenylethoxide



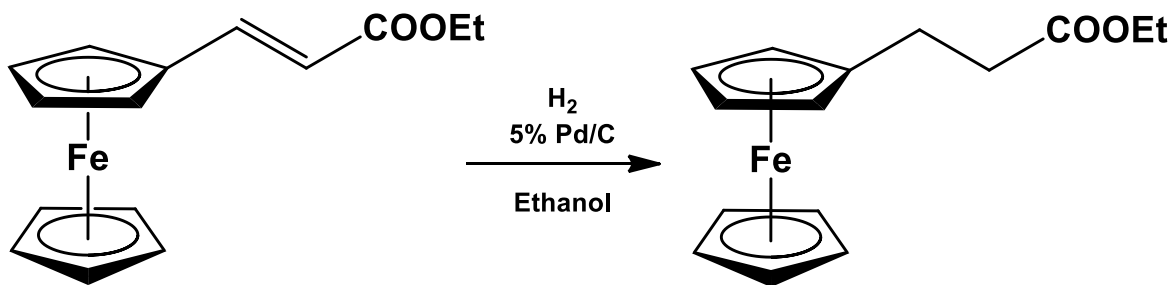
Sodium hydride (40 mg, 1.6 mmol, 1 eq) was weighed into a two neck round bottom flask fitted with gas inlet tap under inert conditions. The flask was placed in an ice bath and 10 cm³ dry THF was added slowly. 2-Ferrocenylethanol (481 mg, 1.67 mmol) was dissolved in 10 cm³ dry THF and this solution was slowly added to the sodium hydride. The reaction mixture was allowed to stir overnight at room temperature. The solution was filtered the next day by cannula. The solvent was removed under reduced pressure and the flask was immediately transferred into the glovebox for storage.

4.4.10 Ethyl-3-ferrocenylethenoate



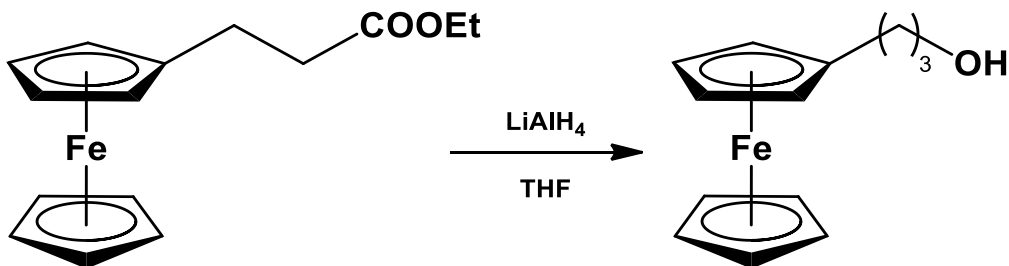
In a two-neck round bottom flask fitted with gas inlet tap and rubber septum, argon was used to purge the system for ten minutes. Sodium (0.11 g, 6.67 mmol, 1.2 eq) was added, along with 46 cm³ of absolute ethanol and the flask was cooled to 0 °C. Ferrocenecarboxaldehyde (1.112 g, 5.20 mmol) was dissolved in 20 cm³ of absolute ethanol and this solution was added dropwise to the reaction flask. Triethylphosphonoacetate (1 cm³, 0.93 g, 4.67 mmol, 0.9 eq) was added dropwise. The reaction was allowed to stir for one hour at room temperature. The solvent was removed under reduced pressure and the product was purified with column chromatography using eluent ethyl acetate:n-hexane 5:95. Yield 1.16 g (78 %). Melting point = 66 – 69 °C. IR: ν/cm^{-1} = 1631 (C=C), 1702 (C=O), 2871 – 2971 (C-H aliphatic), 3099 (C-H aromatic), **Spectrum 8**. ¹H NMR (300 MHz, CDCl₃)/ppm = 7.59 (d, 1H, C=H), 6.05 (d, 1H, C=H), 4.51 (t, 2H, 0.5 C₅H₄), 4.42 (t, 2H, 0.5 C₅H₄), 4.18 (m, 7H, C₅H₄ + CH₂), 1.35 (t, 3H, CH₃), **Spectrum 26**.

4.4.11 Ethyl-3-ferrocenylethanoate



Ethyl-3-ferrocenylethanoate (500 mg, 1.76 mmol) was dissolved in 50 cm³ absolute ethanol. Palladium on carbon (5 %, 0.05 g) was added to the reaction flask and the atmosphere was saturated with hydrogen gas. The reaction was left to stir for 24 hours, filtered over celite and the solvent removed by rotary evaporation. Yield 136 mg (98 %). Melting point = 30 – 31 °C. IR: ν/cm^{-1} = 1726 (C=O), 2852 – 2978 (C-H aliphatic), 3086 (C-H aromatic), **Spectrum 9**. ¹H NMR (300 MHz, CDCl₃)/ppm = 4.13 (m, 11H, C₅H₄ + C₅H₄ + CH₂), 2.62 (m, 4H, CH₂CH₂), 1.29 (t, 3H, CH₃), **Spectrum 27**.

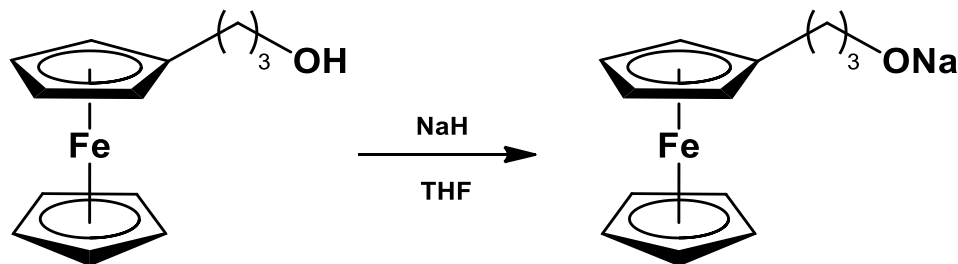
4.4.12 3-Ferrocenylpropanol



In a three neck round bottom flask fitted with gas inlet tap and condenser, argon was used to purge the system for ten minutes. LiAlH₄(188 mg, 4.92 mmol, 3 eq) was added to the dry flask. A solution of 3-ferrocenylethanoate (400 mg, 1.64 mmol) in 50 cm³ THF was added dropwise. The reaction mixture was refluxed for one hour then cooled to room temperature. Distilled water was added and the product was extracted with diethyl ether (3 x 50 cm³). The combined ether extracts were dried over MgSO₄ and the solvent removed using rotary evaporation. Yield 4.01 mg (100 %) as an orange oil. IR: ν/cm^{-1} = 2855 – 2926 (C-H aliphatic), 3087 (C-H aromatic), 3313 (O-H broad),

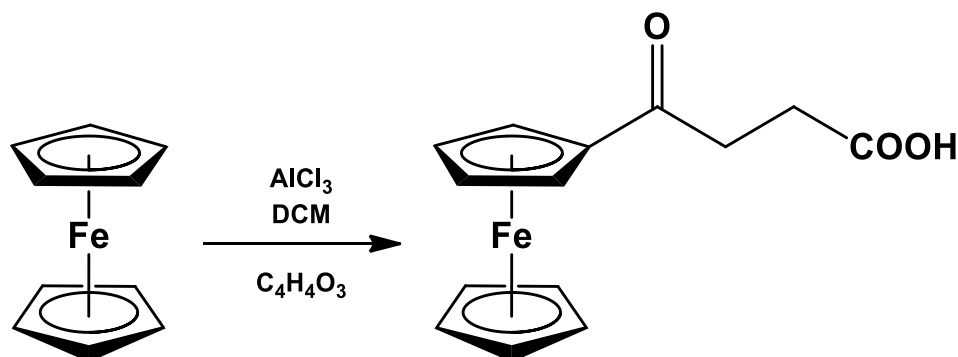
Spectrum 10. ^1H NMR (300 MHz, CDCl_3)/ppm = 4.10 (m, 9H, $\text{C}_5\text{H}_5 + \text{C}_5\text{H}_4$), 3.69 (t, 2H, CH_2), 2.45 (t, 2H, CH_2), 1.81 (t, 2H, CH_2), **Spectrum 28.** ^{13}C NMR (600 MHz; CDCl_3)/ppm = 88.97 (C_5H_5), 68.94 ($-\text{CH}_2\text{CH}_2\text{CH}_2\text{OH}$), 68.48 (C_5H_4), 67.63 (C_5H_4), 63.07 (C_{ipso} ; C_5H_4), 34.39 ($-\text{CH}_2\text{CH}_2\text{CH}_2\text{OH}$) 26.25 ($\text{CH}_2\text{CH}_2\text{CH}_2\text{OH}$), **Spectrum 39.**

4.4.13 Sodium-3-ferrocenylpropoxide



Sodium hydride (39.41 mg, 1.643 mmol, 1 eq) was weighed into a two neck round bottom flask fitted with gas inlet tap, under inert conditions. The flask was placed in an ice bath and 10 cm³ dry THF was added slowly. 3-Ferrocenylpropanol (401 mg, 1.643 mmol) was dissolved in 10 cm³ dry THF and this solution was slowly added to the sodium hydride. The reaction mixture was allowed to stir overnight at room temperature. The solution was filtered the next day by cannula. The solvent was removed under reduced pressure and the product stored in a glovebox.

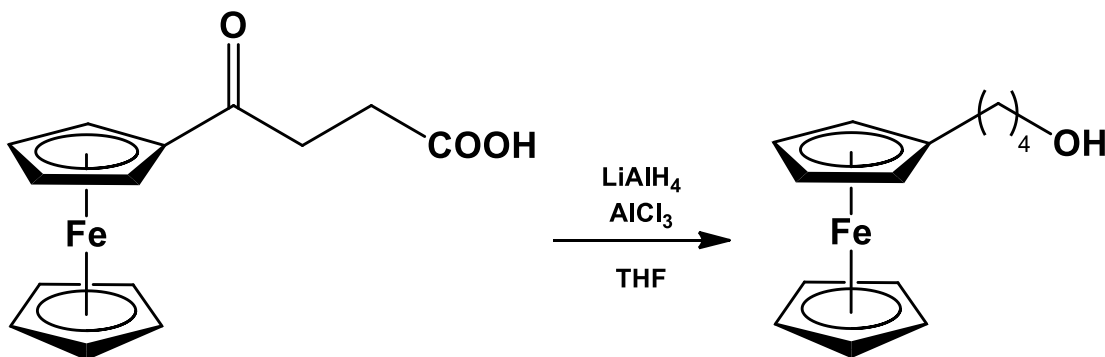
4.4.14 3-Ferrocenoylpropionic acid



In a three neck round bottom flask fitted with gas inlet and outlet taps, rubber septum and bubbler, argon was used to purge the system for ten minutes. A solution of succinic anhydride (2.9 g, 27 mmol, 1 eq) in dichloromethane was added slowly to a mixture of ferrocene (5.125 g, 27 mmol)

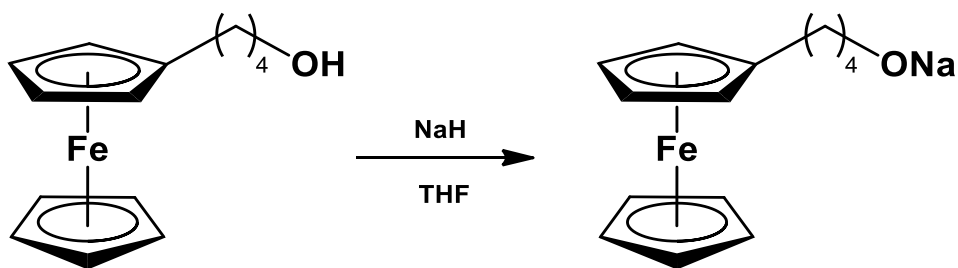
and AlCl_3 (7.8 g, 56 mmol, 2.1 eq) in dichloromethane. Total dichloromethane volume was 250 cm^3 . The reaction mixture was allowed to stir overnight at room temperature. Ice was added to the mixture and allowed to stir for 15 minutes. The aqueous layer was extracted with dichloromethane to remove unreacted ferrocene. The aqueous layer was then neutralised with 0.5 M NaOH solution and slowly acidified with 1M HCl. The product slowly crystallised as light brown crystals. Yield = 3.8 g (48.3 %). Melting point = $161 - 164^\circ\text{C}$. IR: $\nu/\text{cm}^{-1} = 1654$ (C=O keto), 1171 (C=O acid), 2591 – 3108 (O-H broad), **Spectrum 11**. ^1H NMR (300 MHz, CDCl_3)/ppm = 4.84 (t, 2H, 0.5 C_5H_4), 4.55 (t, 2H, 0.5 C_5H_4), 4.26 (s, 5H, C_5H_5), 3.11 (t, 2H, CH_2), 2.77 (t, 2H, CH_2), **Spectrum 29**.

4.4.15 4-Ferrocenylbutanol



In a three neck round bottom flask fitted with gas inlet tap and condenser; argon was used to purge the system. LiAlH_4 (850 mg, 22.5 mmol, 3 eq) was added to THF (50 cm^3). AlCl_3 (2.2 g, 16.5 mmol, 2.2 eq) in THF (50 cm^3) was also added. 3-Ferrocenoylpropionic (2.15 g, 7.519 mmol) dissolved in THF (20 cm^3) was added to the flask and allowed to stir for 30 minutes at room temperature. This was followed by reflux for three hours. The solution was cooled and filtered over celite. Ice was added to the mixture and extracted with diethyl ether. The combined organic phases were dried over MgSO_4 and solvent removed by rotary evaporation. Yield = 1.678 g (86.5 %) as an orange oil. IR: $\nu/\text{cm}^{-1} = 2862 - 2934$ (C-H aliphatic), 3094 (C-H aromatic), 3314 (O-H broad), **Spectrum 12**. ^1H NMR (300 MHz, CDCl_3)/ppm = 4.07 (m, 9H, $\text{C}_5\text{H}_5 + \text{C}_5\text{H}_4$), 3.68 (t, 2H, CH_2), 2.38 (t, 2H, CH_2), 1.61 (t, 2H, CH_2), **Spectrum 30**. ^{13}C NMR (600 MHz; CDCl_3)/ppm = 89.03 (C_5H_5), 68.50 (C_5H_4), 68.09 (C_5H_4), 67.12 ($-\text{CH}_2\text{CH}_2\text{OH}$), 62.96 (C_{ipso} ; C_5H_4), 33.67 ($-\text{CH}_2\text{CH}_2\text{OH}$) 29.41 ($-\text{CH}_2\text{CH}_2\text{CH}_2\text{CH}_2\text{OH}$) 27.29 ($-\text{CH}_2\text{CH}_2\text{CH}_2\text{CH}_2\text{OH}$), **Spectrum 40**.

4.4.16 Sodium-4-ferrocenylbutoxide



Sodium hydride (92 mg, 3.8 mmol, 1 eq) was weighed into a two neck round bottom flask fitted with gas inlet tap, under inert conditions. The flask was placed in an ice bath and 10 cm³ dry THF was added slowly. 4-Ferrocenylbutanol (600 mg, 3.8 mmol) was dissolved in 10 cm³ dry THF and this solution was slowly added to the sodium hydride. The reaction mixture was allowed to stir overnight at room temperature. The solution was filtered the next day by cannula. The solvent was removed under reduced pressure and the product was stored in a glovebox.

4.5 Synthesis of polyphosphazenes

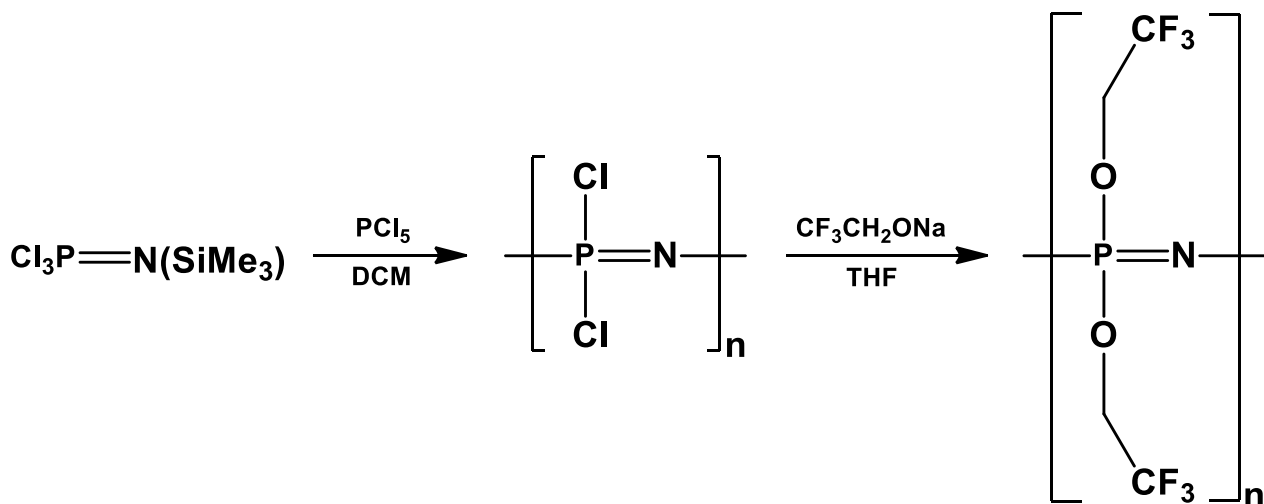
4.5.1 Trichloro(trimethylsilyl)phosphoranimine



$\text{LiN(SiMe}_3)_2$ (16.23 g, 97 mmol) was weighed in a glovebox. The flask was cooled to -78 °C using an isopropanol/liquid nitrogen bath. Diethyl ether (250 cm³) was transferred to the flask and allowed to cool. Freshly distilled PCl_3 (7.6 cm³, 88 mmol, 0.9 eq) was added dropwise and the mixture allowed to stir at -78 °C for 15 minutes. Freshly distilled SO_2Cl_2 (7 cm³, 88 mmol, 0.9 eq) was added dropwise and allowed to stir for a further 15 minutes at -78 °C. Stirring was then stopped and the precipitate formed was allowed to settle at the bottom of the flask. The reaction mixture was then filtered into a clean flask under inert conditions, using a cannula. The diethyl ether was removed under vacuum until a volume of about 50 cm³. This remaining liquid was transferred into a smaller flask and kept frozen in a liquid nitrogen bath. The product was distilled under a strong vacuum, while allowing the sample to slowly warm up to room temperature. Yield 12.86 g (65.4 %) as a clear liquid. IR: $\nu/\text{cm}^{-1} = 731$ (P-Cl), 1191 (P=N), **Spectrum 13**. $^1\text{H NMR}$ (300 MHz, CDCl_3)/ppm =

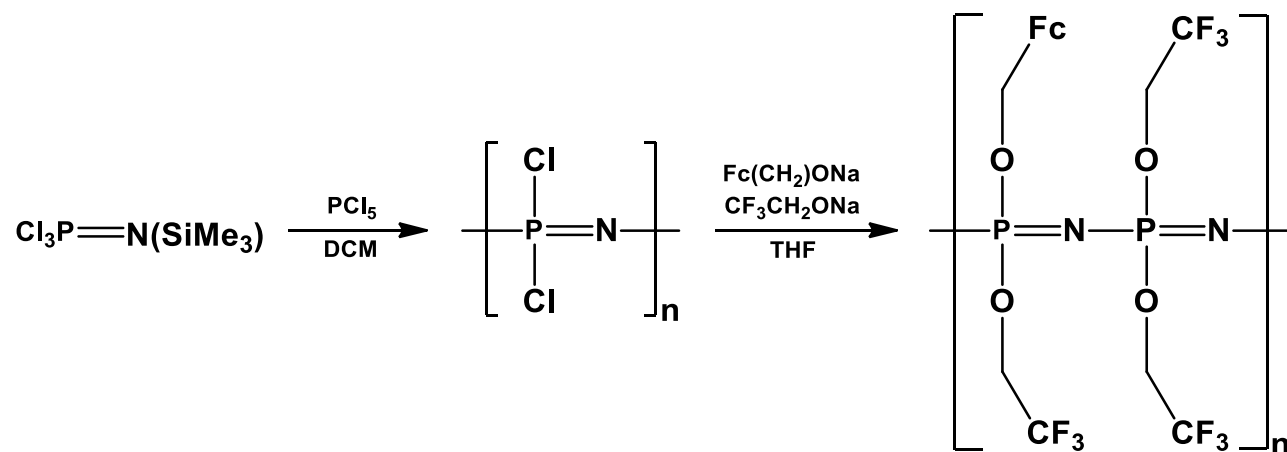
0.19 (s, H, SiMe₃), **Spectrum 31.** ³¹P NMR (600 MHz, CDCl₃)/ppm = -50.18 (s, P, P=N), **Spectrum 41.**

4.5.2 Poly(2,2,2-trifluoroethoxy)phosphazene



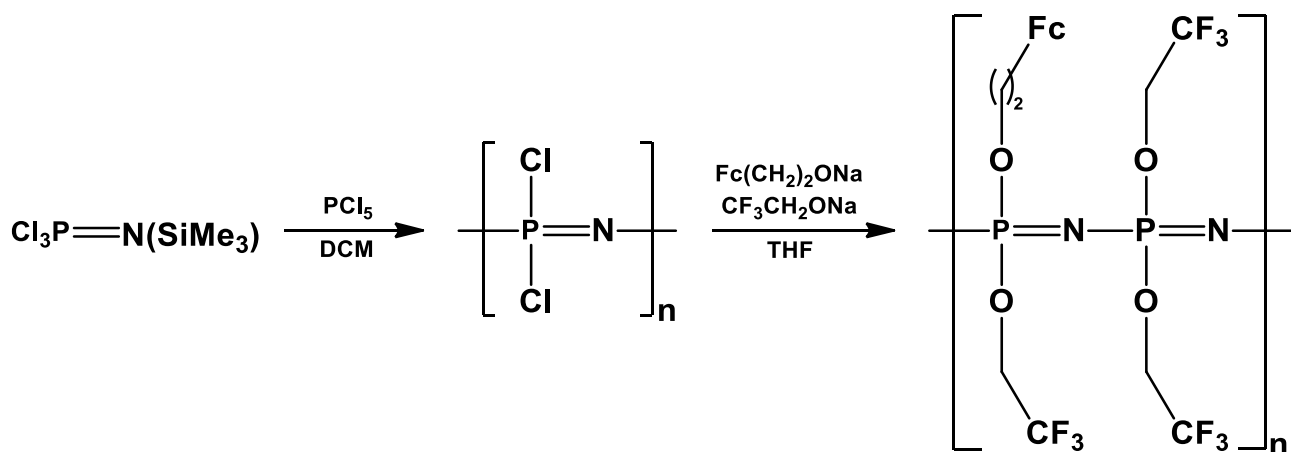
Cl₃P=NSiMe₃ (1 g, 4.453 mmol) was dissolved in dry DCM (4 cm³) in a glovebox. A solution of PCl₅ (35 mg, 0.17 mmol, 0.038 eq) in DCM (4 cm³) was added quickly to the phosphoranimine solution and allowed to stir vigorously. The solvent was removed under vacuum. The residue consisting of unstable poly(dichlorophosphazene) product was then immediately dissolved in THF (4 cm³). Sodium trifluoroethoxide (1.7 g, 14 mmol, 3.2 eq) was dissolved in dry THF (8 cm³) and added dropwise to the reaction mixture. The reaction was allowed to stir at room temperature for two hours. Water was added to the reaction mixture and the product was centrifuged (8000 rpm for 30 minutes) to obtain a white solid (230 mg). IR: $\nu/\text{cm}^{-1} = 731$ (P-O-C sym), 1223 (P-O-C asym), **Spectrum 14**; 839 (P-O-C sym), 958 – 1154 (P-O-C asym), 1260 (C-O), **Spectrum 15**. ¹H NMR (600 MHz, THF-d₈)/ppm = 4.46 (m, H, CH₂), **Spectrum 32**. ³¹P NMR (600 MHz, THF-d₈)/ppm = -18.96 (s, P, PNCl₂), **Spectrum 42**; -7.85 (s, P, P-OCH₂CF₃), **Spectrum 43**. ¹⁹F NMR (600 MHz, THF-d₈)/ppm = -76.28 ppm (m, F, P-O-CF₃), **Spectrum 48**.

4.5.3 Poly((2,2,2-trifluoroethoxy)(ferrocenylmethoxy))phosphazene



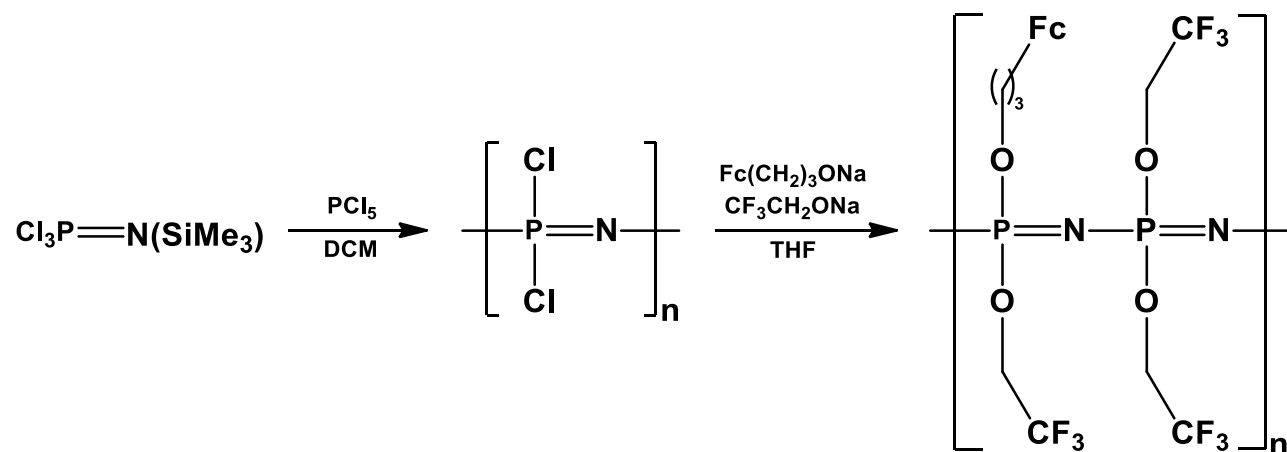
$\text{Cl}_3\text{P}=\text{NSiMe}_3$ (500 mg, 2.217 mmol) was dissolved in DCM (2 cm^3) in a glovebox. A solution of PCl_5 (30 mg, 0.15 mmol, 0.06 eq) in dry DCM (2 cm^3) was added quickly to the phosphoranimine solution and allowed to stir vigorously for three hours. The solvent was removed under vacuum. The residue consisting of poly(dichlorophosphazene) product was then dissolved in dry THF (2 cm^3). Sodium trifluoroethoxide (180 mg, 1.48 mmol, 0.66 eq) was dissolved in dry THF (2 cm^3) and added dropwise to the reaction mixture and allowed to stir at room temperature for 24 hours. Sodium-1-ferrocenylmethoxide (185 mg, 0.8 mmol, 0.36 eq) dissolved in dry THF (4 cm^3) added dropwise to the reaction mixture and allowed to stir at room temperature for 24 hours. Sodium trifluoroethoxide (1 g, 8.2 mmol, 3.6 eq) in THF (2 cm^3) added to the reaction mixture and allowed to stir for a further 24 hours. The precipitated product was washed with water ($4 \times 50 \text{ cm}^3$), followed by washing with *n*-hexane ($4 \times 50 \text{ cm}^3$), using a centrifuge (8000 rpm for 30 minutes). Yield = 309 mg. IR: $\nu/\text{cm}^{-1} = 839$ (P-O-C sym), 956 – 1154 (P-O-C asym), 1260 (C-O), **Spectrum 16**. $^1\text{H NMR}$ (600 MHz, THF-d_8)/ppm = 4.45 (m, H, CH_2), **Spectrum 33**. $^{31}\text{P NMR}$ (600 MHz, THF-d_8)/ppm = -7.96 (s, P, $\text{P-OCH}_2\text{CF}_3$), -3.59 (m, P, $\text{P-OCH}_2\text{CF}_3 + \text{P-OCH}_2\text{Fc}$), 17.11 (s, P, $\text{P-OCH}_2\text{Fc}$), **Spectrum 44**. $^{19}\text{F NMR}$ (600 MHz, THF-d_8)/ppm = -76.29 (s, F, CF_3), **Spectrum 49**. It should be noted that the indicated structures of **22 - 25** are idealised, giving an overall statistical average stoichiometry. However, in practise, the ferrocenylalkoxy group will be found in a random distribution pattern over the entire main chain.

4.5.4 Poly((2,2,2-trifluoroethoxy)(ferrocenylethoxy))phosphazene



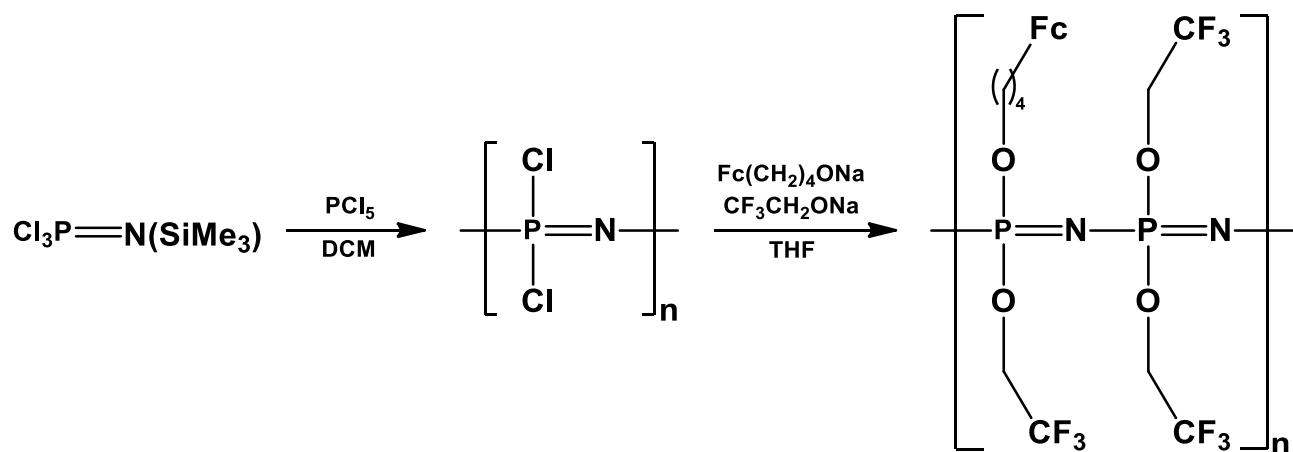
$\text{Cl}_3\text{P}=\text{NSiMe}_3$ (500 mg, 2.217 mmol) was dissolved in dry DCM (2 cm^3) in a glovebox. A solution of PCl_5 (19 mg, 0.1 mmol, 0.05 eq) in dry DCM (2 cm^3) was added quickly to the phosphoranimine solution and allowed to stir vigorously for three hours. The solvent was removed under vacuum. The residue poly(dichlorophosphazene), was dissolved in dry THF (2 cm^3). Sodium trifluoroethoxide (300 mg, 2.46 mmol, 1.1 eq) was dissolved in dry THF (2 cm^3) and added dropwise to the reaction mixture and allowed to stir at room temperature for 24 hours. Sodium-2-ferrocenylethoxide (300 mg, 1.1 mmol, 0.5 eq) dissolved in dry THF (4 cm^3) added dropwise to the reaction mixture and allowed to stir at room temperature for 24 hours. Sodium trifluoroethoxide (1 g, 8.2 mmol, 3.6 eq) in THF (2 cm^3) added to the reaction mixture and allowed to stir for a further 24 hours. The precipitated product was washed with water ($4 \times 50 \text{ cm}^3$), followed by washing with *n*-hexane ($4 \times 50 \text{ cm}^3$), using a centrifuge (8000 rpm for 30 minutes). Yield = 369 mg. IR: $\nu/\text{cm}^{-1} = 839$ (P-O-C sym), $839 - 1154$ (P-O-C asym), 1260 (C-O), **Spectrum 17**. ^1H NMR (600 MHz, THF-d₈)/ppm = 4.13 (m, H, CH₂), **Spectrum 34**. ^{31}P NMR (600 MHz, THF-d₈)/ppm = -7.88 (m, P, P-OCH₂CF₃ + P-OCH₂CH₂Fc), 17.12 (s, P, P-OCH₂CH₂Fc), **Spectrum 45**. ^{19}F NMR (600 MHz, THF-d₈)/ppm = -76.29 (s, F, CF₃), **Spectrum 50**. It should be noted that the indicated structures of **22 - 25** are idealised, giving an overall statistical average stoichiometry. However, in practise, the ferrocenylalkoxy group will be found in a random distribution pattern over the entire main chain.

4.5.5 Poly((2,2,2-trifluoroethoxy)(ferrocenylpropoxy))phosphazene



$\text{Cl}_3\text{P}=\text{NSiMe}_3$ (500 mg, 2.217 mmol) was dissolved in dry DCM (2 cm^3) in a glovebox. A solution of PCl_5 (19 mg, 0.1 mmol, 0.05 eq) in dry DCM (2 cm^3) was added quickly to the phosphoranimine solution and allowed to stir vigorously for three hours. The solvent was removed under vacuum. The solid remains, poly(dichlorophosphazene) product was then dissolved in dry THF (2 cm^3). Sodium trifluoroethoxide (300 mg, 2.46 mmol, 1.1 eq) was dissolved in dry THF (2 cm^3) and added dropwise to the reaction mixture and allowed to stir at room temperature for 24 hours. Sodium-3-ferrocenylpropoxide (300 mg, 1.1 mmol, 0.5 eq) dissolved in dry THF (4 cm^3) added dropwise to the reaction mixture and allowed to stir at room temperature for 24 hours. Sodium trifluoroethoxide (1 g, 8.2 mmol, 3.7 eq) in dry THF (2 cm^3) added to the reaction mixture and allowed to stir for a further 24 hours. The precipitated product was washed with water ($4 \times 50 \text{ cm}^3$), followed by washing with *n*-hexane ($4 \times 50 \text{ cm}^3$), using a centrifuge (8000 rpm for 30 minutes). Yield = 340 mg. IR: $\nu/\text{cm}^{-1} = 839$ (P-O-C sym), $839 - 1154$ (P-O-C asym), 1260 (C-O), **Spectrum 18.** $^1\text{H NMR}$ (600 MHz, THF-d_8)/ppm = 4.42 (m, H, CH_2), **Spectrum 35.** $^{31}\text{P NMR}$ (600 MHz, THF-d_8)/ppm = -7.90 (m, P, $\text{P-OCH}_2\text{CF}_3 + \text{P-OCH}_2\text{CH}_2\text{Fc}$), 17.12 (s, P, $\text{P-OCH}_2\text{CH}_2\text{Fc}$), **Spectrum 46.** $^{19}\text{F NMR}$ (600 MHz, THF-d_8)/ppm = -76.28 (s, F, CF_3), **Spectrum 51.** It should be noted that the indicated structures of **22 - 25** are idealised, giving an overall statistical average stoichiometry. However, in practise, the ferrocenylalkoxy group will be found in a random distribution pattern over the entire main chain.

4.5.6 Poly((2,2,2-trifluoroethoxy)(ferrocenylbutoxy))phosphazene



$\text{Cl}_3\text{P}=\text{NSiMe}_3$ (530 mg, 2.36 mmol) was dissolved in dry DCM (2 cm^3) in a glovebox. A solution of PCl_5 (29 mg, 0.14 mmol, 0.06 eq) in dry DCM (2 cm^3) was added quickly to the phosphoranimine solution and allowed to stir vigorously for three hours. The solvent was removed under vacuum. The residue, poly(dichlorophosphazene) product was then dissolved in dry THF (2 cm^3). Sodium trifluoroethoxide (200 mg, 1.64 mmol, 0.68 eq) was dissolved in dry THF (2 cm^3) and added dropwise to the reaction mixture and allowed to stir at room temperature for 24 hours. Sodium-4-ferrocenylbutoxide (340 mg, 1.2 mmol, 0.5 eq) dissolved in dry THF (4 cm^3) added dropwise to the reaction mixture and allowed to stir at room temperature for 24 hours. Sodium trifluoroethoxide (1 g, 8.2 mmol, 3.4 eq) in dry THF (2 cm^3) added to the reaction mixture and allowed to stir for a further 24 hours. The precipitated product was washed with water ($4 \times 50 \text{ cm}^3$), followed by washing with *n*-hexane ($4 \times 50 \text{ cm}^3$), using a centrifuge (8000 rpm for 30 minutes). Yield = 296 mg. IR: ν/cm^{-1} = 839 (P-O-C sym), 839 – 1154 (P-O-C asym), 1260 (C-O), **Spectrum 19.** ^1H NMR (600 MHz, THF-d₈)/ppm = 4.23 (m, H, CH₂), **Spectrum 36.** ^{31}P NMR (600 MHz, THF-d₈)/ppm = -8.02 (P, P-OCH₂CF₃), -3.82 (m, P, P-OCH₂CF₃ + P-OCH₂CH₂Fc), 17.37 (s, P, P-OCH₂CH₂Fc), **Spectrum 47.** ^{19}F NMR (600 MHz, THF-d₈)/ppm = -76.23 (s, F, CF₃), **Spectrum 52.** It should be noted that the indicated structures of **22 - 25** are idealised, giving an overall statistical average stoichiometry. However, in practise, the ferrocenylalkoxy group will be found in a random distribution pattern over the entire main chain.

4.6 Viscometry

Viscosity measurements of the synthesised polyphosphazenes were performed using a KPG Cannon-Fenkse (App Nr: 95405) viscometer from Schott Geräte in acetonitrile at 30 °C. Specific viscosity was calculated according to the following formula,

$$\eta_{sp} = \frac{t - t_0}{t_0}$$

where t_0 is the time taken for pure solvent and t is the time for the polymer solution. The specific viscosity for different molecular mass samples was measured between 0.2326 - 0.0083 dL/g at polymer concentrations of 1.76 mM = 0.11 g/100 mL in acetonitrile as solvent.

4.7 Electrochemistry

Cyclic voltammetry (CV), linear-sweep voltammetry (LSV) and square wave voltammetry (SW) were performed using a Princeton Applied Research PARSTAT 2273. Voltammographs were recorded using Powersuite (version 2.58). A platinum wire was used as an auxiliary electrode and a silver wire as reference electrode. A glassy carbon electrode was used as the working electrode, with surface area 3.14 mm². The working electrode was polished on a Buhler polishing mat, utilising 1 micron and followed by ¼ micron diamond paste.

4.8 X-ray Photoelectron Spectroscopy

X-ray Photoelectron Spectroscopy (XPS) was performed on all synthesised polyphosphazene samples. XPS data were recorded on a PHI 5000 Versaprobe system with monochromatic AlK X-ray source. Spectra were obtained using the aluminium anode (Al K α = 1486.6 eV) operating at 50 μ m, 12.5 W and 15 kV energy. The survey scans were recorded at constant pass energy of 187.85 eV and region scans at constant pass energy of 29.35 eV with the analyzer resolution \leq 0.5 eV. The background pressure was 2 x 10⁻⁸ mbar. The XPS data were analyzed utilizing Multipak version 8.2c computer software² using Gaussian–Lorentz fits (the Gaussian/Lorentz ratios were always > 95%).

4.9 Gel Permeation Chromatography

Gel permeation chromatography (GPC) was performed on all synthesised polyphosphazene samples utilising the following equipment and parameters:

- Hardware: Shimadzu LC-20AD UFC Liquid Chromatograph pump
Shimadzu DGU-20A Degassing Unit
Shimadzu RID-10A Refractive Index Detector
Shimadzu CTO-2-A Prominence Column Oven
Shimadzu CBM-20A Communication Bus Module
- Software: Shimadzu LC-Solution
- Solvent: *N,N*-dimethylacetamide
- Calibration: Polystyrene (results are relative to polystyrene)
- Method: Oven at 40 °C; RID detector at 35 °C; Solvent flow at 1 mL/min; Runtime at 30 min.

GPC is a new analytical technique in the Physical Chemistry research group and therefore the author received training for GPC operation at Prof du Prez's laboratory at Gent University, Polymer Chemistry Research Group, Belgium. As part of the PhD study of the author, a manual for operation of the GPC was compiled and is provided in this section (section 4.9.1) of the Experimental Chapter of this thesis.

The samples were first analysed at the Polymer Chemistry Research group, Gent University. The instrument details in Gent and experimental parameters were as follow:

- Hardware: Waters 1525 Binary HPLC pump
Waters 2414 RI Detector
Merck Hitachi column oven L-7300
Waters 717 Plus Autosampler
- Software: Empower
- Solvent: *N,N*-dimethylacetamide
- Calibration: Polymethylmethacrylate (PMMA) standards (results are relative to PMMA)
- Method: Oven at 40 °C; RI-detector at 35 °C; Solvent flow at 1 mL/min; Runtime at 55 min.

The same samples were analysed in Bloemfontein on the Shimadzu at the UFS lab (hardware described at the top of this page). Results were mutually consistent.

4.9.1 Shimadzu GPC Manual

On start-up, gradually increase solvent flow by 0.1 mL/min increments until 1 mL/min is reached. Check the pressure with the maximum pressure allocated by the supplier. The pressure must be stable, if not, it indicates that the pump may not be working properly.

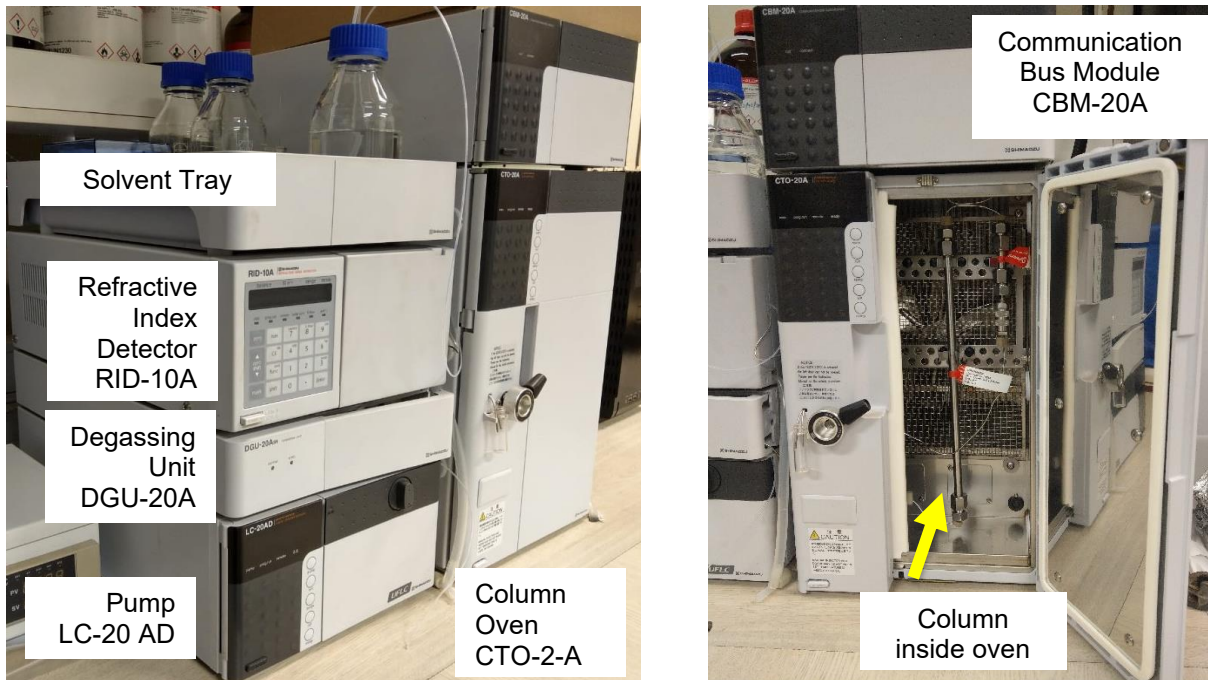


Figure 4.1: Shimadzu GPC Instrumentation at the Physical Chemistry Lab, UFS.

Starting up the instrument

Switch on all units (CBM unit last) before you start the LC-Solution Software (otherwise it will not recognise the instrument and will not turn online). Ensure that the solvent bottle is full and that there are no air bubbles throughout the solvent line. Purge the line if bubbles are present. Switch on the instrument in the LC-Solution software (oven + pump **ON** in toolbar) and wait a few minutes until the instrument is ready (this is to allow the oven to reach the required temperature). Press the function button on the detector until **CELL** appears and ensure that the values are roughly 4000 for both the reference and sample side of the detector (these values need to be balanced for good data). If these values are incorrect, balancing of the detector is required.



Figure 4.2: Communication Bus Module (left) allows the GPC unit to communicate with the LC-Solution Software (right).

| Item | Value | Units |
|---------------------------------|--------|--------|
| Pump A. Flow | 0.1000 | mL/min |
| Pump A. Pressure | 24 | psi |
| Pump A Pressure Limits(Maximum) | 1422 | psi |
| Cell Temp. | 30.2 | C |
| Oven Temperature | 35.0 | C |
| Room Temperature | 19.6 | C |
| Maximum Temperature | 85 | C |

Figure 4.3: Equipment parameters shown on the right column of the LC-Solution software, where you can monitor the parameters to ensure that the GPC is running correctly.

Balancing the detector

Switch on **RID R.Flow** in the LC-Solution software to ensure the reference side of the detector is flushed. Wait until the baseline stabilises. Then, proceed to switch back to the sample side of the detector by clicking **Balance RID**. Repeat this process until both values on the detector labelled **CELL** is roughly 4000.



Figure 4.4: Photo of the refractive index detector (left) and balanced reference and sample cells indicated by the detector (right).

Purging

Ensure that the LC compartment is switched on. Turn the pump off. Open the purge valve in front of the LC compartment by turning it counterclockwise at a 45 degree angle. Press the purge button and allow the line to properly purge (either with a different solvent or to remove air bubbles). Press the purge button again to switch it off and close the valve.



Figure 4.5: Photo of the LC-20AD pump with purge valve indicated by the red arrow.

Creating a Method (Data Acquisition)

If you make a new calibration curve, you need to create a new method.

File > New Method File > Simple Settings (Tab) > LC Stop Time (run time) example 45 min.

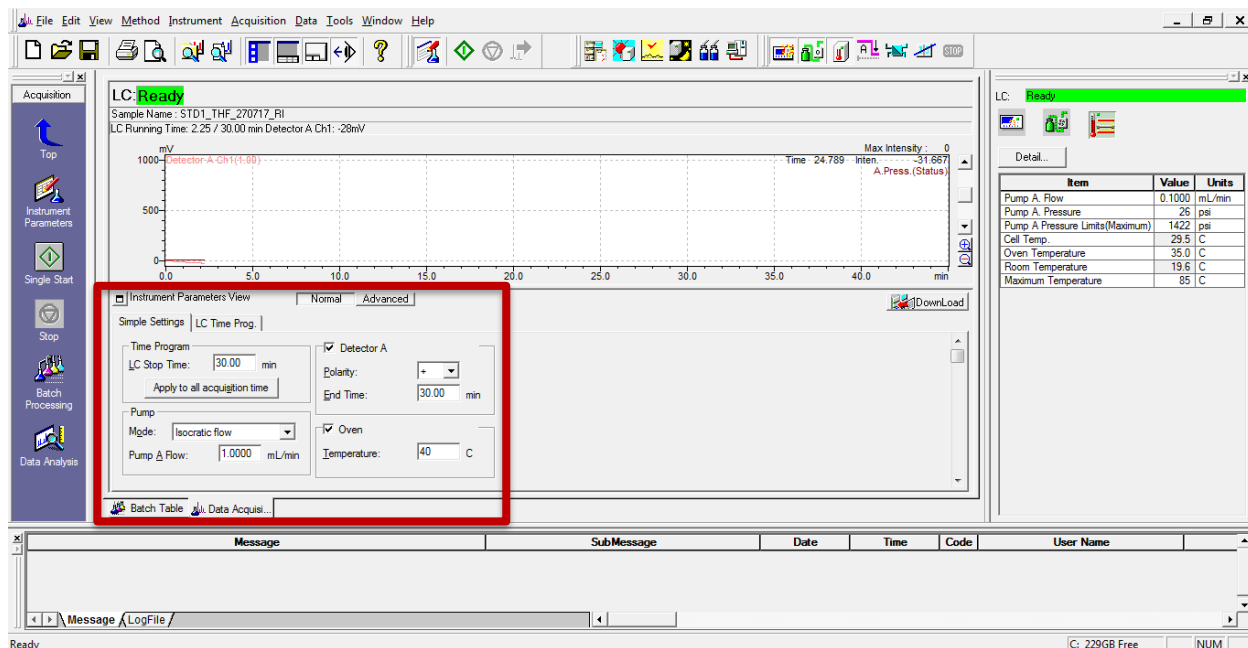


Figure 4.6: Screenshot of LC-Solution software for creating a method file, whereby sample settings (described below) should be entered into the area indicated by the red box.

Mode: Isocratic (one solvent, one flow)

Pump flow: 1 mL/min

Detector: Polarity (can be positive or negative depending on the polymer. If you run a polymer sample and the peak is negative, flip the polarity and run the sample gain to make it positive.)

End time (run time): example 30 min

Temperature: (Needs to be suitable for the solvent being used. Example, for tetrahydrofuran, you would use 35 °C maximum [no higher temperature]; acetonitrile should also be used at 35 °C). The temperature is used to lower the viscosity of the solvent and eases the pressure through the entire system. File > Save Method File (Give appropriate name example PS_THF_270617_RI.lcm, PS: polystyrene; THF:solvent; date; RI:Refractive Index).

Saves in Lab Solutions > Data in C Drive.

Batch type: Manually enter samples in one list, if an automated system is present all the samples will be analysed once the runs are initialised; however, we do not have an automated system. In the absence of an automated system, the batch type method can still be used to enter all the samples required for analysis, but after each analysis, the next sample will have to be manually injected into the system.

File > New Batch File > New

Sample type: Standard sample input. Use the initial calibration curve method and then for a sample choose unknown.

Analysis type: Usually used in liquid chromatography. Leave both checked.

Choose the new method file you just created. Don't worry about level.

Injection volume: Enter the same injection volume as the injection loop (Usually 20 – 100 µL, 100 µL is usually for higher concentration, therefore higher peak).

Making a calibration

On the computer, choose: GPC Postrun > Window GPC Calibration > Open Method (new method previously created without calibration data) > Data File List > Add > Select Calibration Files (this is after you run the calibration samples through GPC).

You only need the peak maximum of every peak.

You want to remove the baseline that the software makes. View (top right) > Right Click > Manual Integration Bar > Reject Peaks > Draw a line between the area you want to remove.

Insert Peak > Draw baseline for each peak > Add to calibration curve > Edit tab (top right) > Pick up (bottom right) > All Peaks > Add > Table on right (you need to insert the molecular weight values for the standard solutions).

Method > Data Analysis Parameters > GPC calculation tab (check the GPC calibration option is “Linear” for mixed pore size column and “3rd order” for same pore size column. At UFS, we use a same pore size column so we choose 3rd order calibration curve). Check: Use pump flow 1 mL/min (default setting).

Integration > Advanced > Max Slices (choose the maximum number example 5000) for the slices, the more the better, as it increases the accuracy.

Apply > OK.

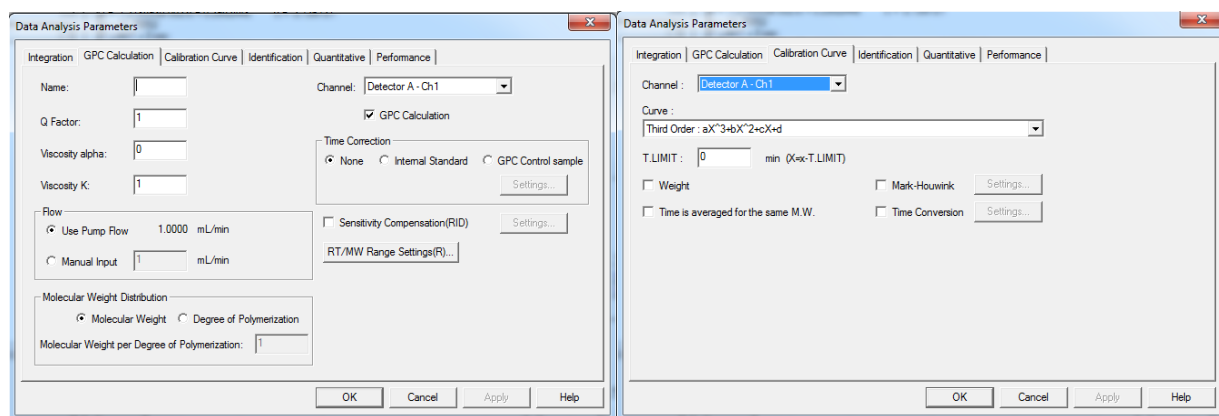


Figure 4.7: Data Analysis Parameters settings required to set up a calibration curve on the LC-solution software

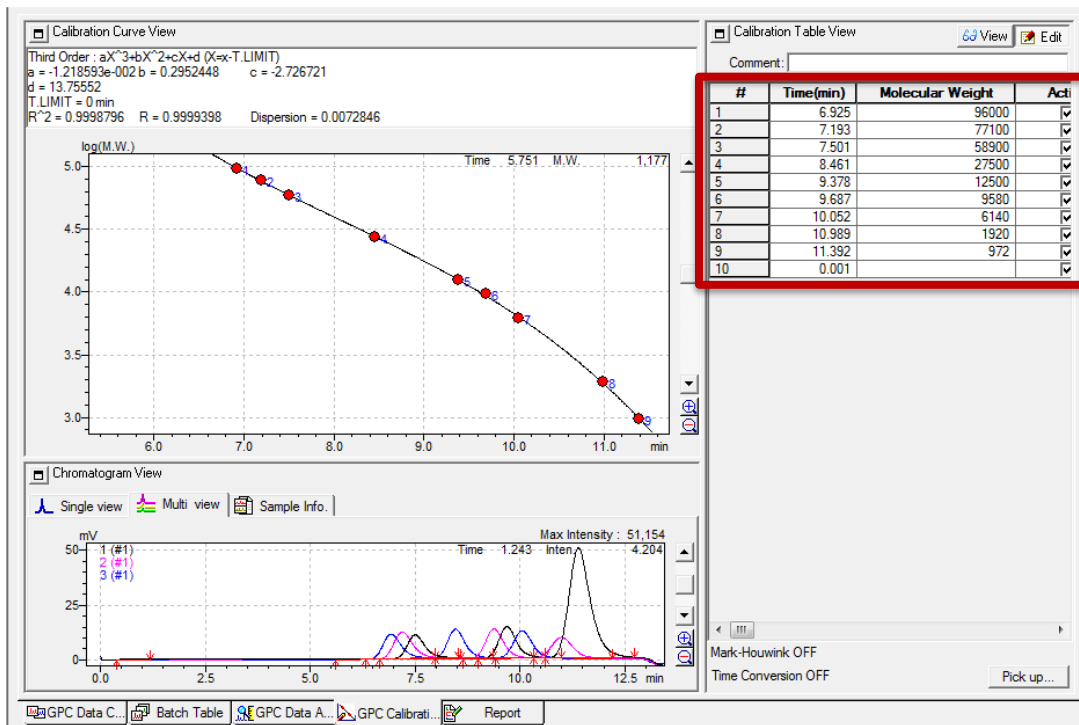


Figure 4.8: GPC calibration curve, whereby the red box indicates the area where the molecular mass standards should be entered for calibration parameters.

Once the calibration curve is created, the molecular masses of the standards used (in this case polystyrene standards) can be entered into the right column of the software to (see Figure 4.6). There is sometimes a negative peak in the chromatogram (this is usually a system peak due to using a different solvent or sometimes air in the system).

Save Method File.

Sample

Data tab > Select data file in list.

If any software workup: Right click > Manual Integration Bar > Remove peaks. Then proceed to insert peaks for the sample (work up the data manually).

View > Slice data > Average Molecular Weight tab

Slice data tab: You can export the data to draw your own chromatogram on excel.

PSS: German company that specialises in polymer characterisation.

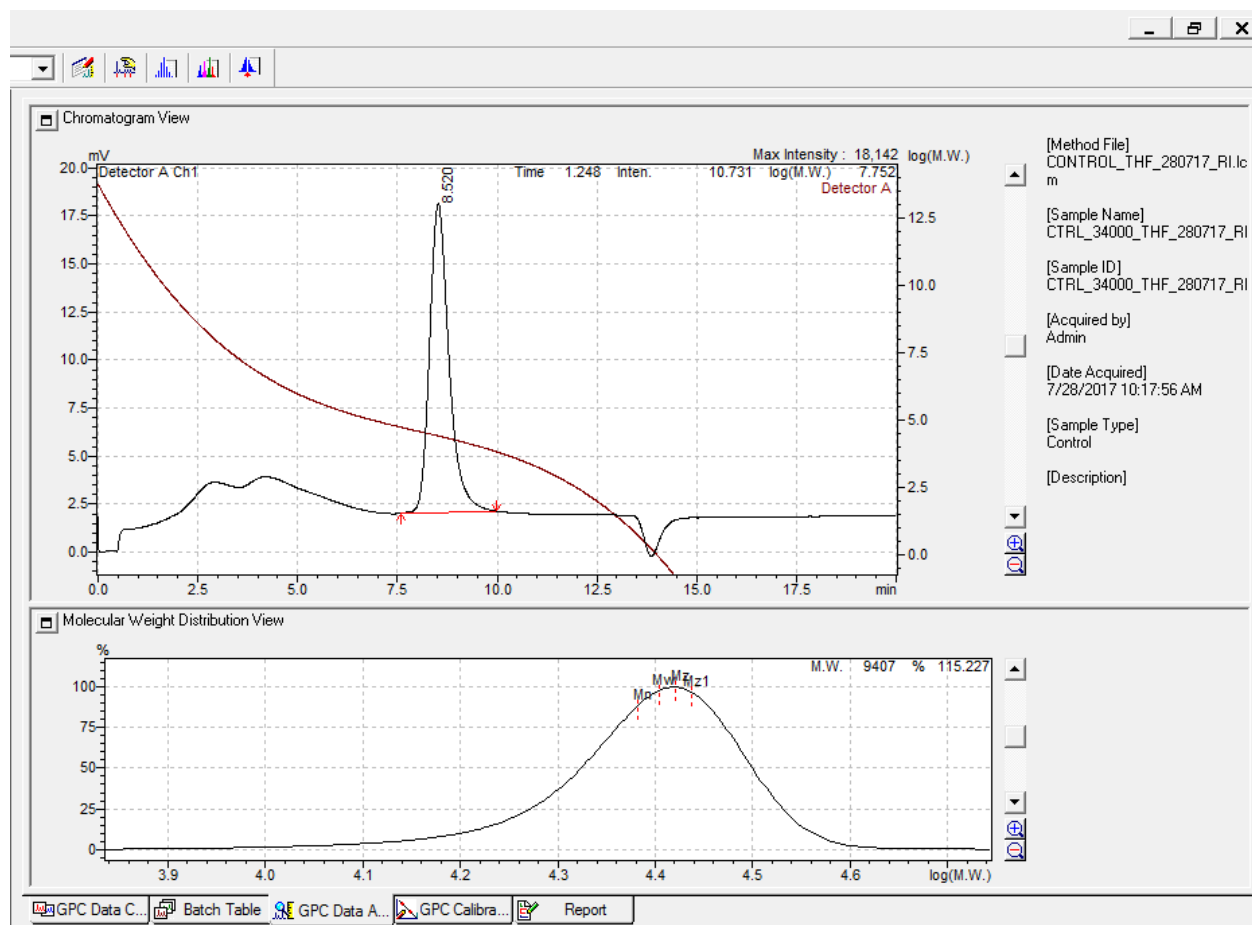


Figure 4.9 Chromatogram view of sample analysis on the LC-Solution software, showing determination of molecular mass of sample utilising calibration curve.

Preparation of samples for GPC analysis

Accurately weigh the sample (usually 5 mg per 2.5 mL solvent).

Dissolve the sample in the solvent being used to run the analysis. Polymers usually take some time to dissolve in a solvent; sonication may aid in dissolution.

Filter sample through 0.22 μm or 0.45 μm syringe filter. Samples should **always** be filtered **prior** to analysis. To inject the sample, move the injection valve into the **load** position. **Only use the glass syringe and blunt needle to inject the sample.** Inject sample until the exhaust tube next to the injection valve releases excess sample. Only turn the valve to **Inject** when you are ready to run the analysis on the sample.



Figure 4.10: Injection valve of the GPC unit where the sample is inserted into the column oven.

Choosing an appropriate column

What does it dissolve in?

Molecular mass separation range? (determine which type of column you need)

Guard column (Pre-column) – must have a guard column, fail safe to protect the main columns.

Column analytical – good resolution

Particle size of column ranges from 3 – 20 µm (low particle sizes are not good – lower flow rate and longer run times)

Things to check on a new column (and also maintenance):

Pressure on new column (if high, polymer may have stuck onto the column)

Plates (fractionation steps) – checking this half height value is the easiest way

Guard column – no plate count, only check the pressure

Pressure

Add guard column only (only to one end from the LC part, the other end is open), make the flow rate 1 mL/min and check the pressure. Should be roughly 70 psi (this is a very low value, the guard column should not have high pressure). If the value is higher than 70 psi then some analyte material may have stuck onto the guard column.

Do this for each column and check the pressure. The main columns will be higher than the guard column, the column with the smallest pore size will have the highest pressure.

Theoretical Plate Count

New column – flush overnight at 0.5 mL/min first and then do the plate count)

Add column to both ends of the GPC system and start the flow at 0.5 mL/min. When adding the column, don't tighten completely. Wait for the solvent to start leaking at the joint and then tighten the column, then follow to the next joint and do the same. Wait for a stable baseline. Make a vial of 2 drops of toluene to 1 mL of solvent (in this case THF) and use this a sample to run through the column. Make the method file for 15 min run time at 1 mL/min flow. Use the toluene peak to determine plate count of the column.

Use the following equation with the toluene peak to determine the number of theoretical plates (N) for column efficiency:

$$N = 5.54 \left(\frac{9.5}{\text{FWHM}} \right)^2$$

where $\text{FWHM} = \text{full width at half maximum}$

Determine the plate count for a new column. Use the same conditions to determine plate count during maintenance. If there is a decrease in the plate count, column efficiency is also decreasing.

Solvent

Changing the solvent: Flush columns overnight with new solvent at 0.5 mL/min.

If there is a metal filter at the end of the solvent line (which goes into the solvent bottle), remove this filter as it may start to corrode and cause issues, such as blockages, in the solvent line.

Filtering the solvent: Filter new solvent through a clean sintered glass filters with 0.2 μm Teflon paper. Sometimes, there is a lot of dust present in the solvent which can cause blockages in the solvent line and increase the pressure in the system.

4.10 UV/Vis Kinetics

UV/Vis spectra were measured on a Shimadzu UV-1650 PC UV-Visible spectrophotometer fitted with a 6-cell cell changer and a Shimadzu CPS-240A electronic temperature controller. Spectra obtained were analysed with the UVProbe Version 2.20 software. Spectra analyses were performed using Scientist software.

4.11 Differential Scanning Calorimetry

Differential scanning calorimetry (DSC) measurements were obtained using a METTLER TOLEDO DSC822e calorimeter with FRS5 detector and auto-sampler. Approximately 5 mg sample masses were used and weighed on a five decimal METTLER XS205 dual-range eletrobalance, then sealed in 40 µL aluminium crucibles. The maximum temperature range for the instrument is between 50°C and 500 °C. Curve analyses were performed using STARe SW 8.10 software.

4.12 Cytotoxicity

4.12.1 Cell Culture

Human cervical cancer cell line (HeLa cell line) were grown in Dulbecco's modified eagle medium (DMEM) supplemented with 10 % fetal calf serum and 1 % penicillin/streptomycin. The cells were incubated with 5 % carbon dioxide present in a humidified atmosphere at 37 °C.

4.12.2 Cytotoxicity Assay

Tests were performed utilising the sulforhodamine B (SRB) assay.³ Monolayer cells were trypsinized (cell dissociation with the use of trypsin) and suspended in 1 mL growth medium. The cell count was adjusted to 0.5×10^5 /mL. Diluted cell suspension (0.1 mL) was added to each well of a 96 well microplate. Plates were incubated for 1 hour in order to allow the cells to adhere to the plate. A range of different concentrations of the polymers **22 – 25** were added to each well (0.1 mL of 0.01 µM to 100 µM). The plates were incubated for 7 days at 37 ° with 5 % carbon dioxide. Trichloroacetic acid (0.05 mL of 50 %) was added to each well and the plates were incubated overnight at 4 °C. The plates were washed under running tap water and dried at 50 °C for 1 hour. SRB stain (0.1 mL) was added to each well and stored in the dark. After 1 hour, the plates were washed with 1 % acetic acid (0.1 mL x 4). The plates were again dried followed by the addition of 10 mM tris(hydroxymethyl) aminomethane buffer (Tris buffer, 0.1 mL) to each of the wells in order to solubilise the dye. The plates were shaken gently for 1 hour and the optical density was measured at 510 nm. The growth inhibition of the polymers **22 – 25** were determined as a percentage of the optical density of the control group. One way ANOVA with Dunnett's post-test was performed using

GraphPad Prism version 5.00 for Windows, GraphPad Software, San Diego, California, USA. Data was fitted to a nonlinear regression versus a normalized response.

Author's note: These were the first cytotoxicity tests performed in-house with newly acquired equipment in the Physical Chemistry laboratory of the UFS.

References

- 1 D. B. G. Williams and M. Lawton, *J. Org. Chem.*, 2010, **75**, 8351–8354.
- 2 F. Moulder, W. F. Stickle and K. D. Bomben, in *Handbook of X-ray Photoelectron Spectroscopy*, ULVAC-PHI, Inc, Enzo, Chigasaki, Japan, 1995, pp. 45, 57, 143.
- 3 V. Vichai and K. Kirtikara, *Nat. Protoc.*, 2006, **1**, 1112–1116.

5

Summary and Future Perspectives

5.1 Summary

This project focussed on the synthesis and characterisation of ferrocenylalkoxy-functionalised polyphosphazene polymers as potential antineoplastic drugs.

A series of known ferrocene-containing alcohols of the type $\text{Fc}(\text{CH}_2)_m\text{OH}$, where $m = 1, 2, 3$ and 4 ; $\text{Fc} = \text{Fe}^{\text{II}}[(\eta^5 - \text{C}_5\text{H}_5)(\eta^5 - \text{C}_5\text{H}_4)]$, **3**, **9**, **13** and **16**, were synthesised by multi-step synthetic routes. The synthesised ferrocene-containing alcohols were converted to sodium ferrocene-containing alkoxide salts, **4**, **10**, **14** and **17**; the required precursor reagents for linking onto the polyphosphazene backbone. Poly(dichloro)phosphazene, **20**, was synthesised utilising a controlled molecular weight living cationic polymerisation reaction. The very labile poly(dichloro)phosphazene, **20**, was refunctionalised to more stable polyphosphazenes including, firstly, the known poly[*bis*(2,2,2-trifluoroethoxy)phosphazene], **21**, in 21.4 % yield as a white powder.

Poly[*tris*(2,2,2-trifluoroethoxy)(ferrocenylalkoxy)phosphazenes], where the carbon alkoxy chain length is 1 (**22**), 2 (**23**), 3 (**24**) and 4 (**25**), were synthesised in yields of 11.6 %, 13.5 %, 12.2 % and 10.3 %, respectively after fractional precipitation. Yields for the ferrocenylalkoxy-containing polyphosphazenes, **22**, **23**, **24** and **25**, were significantly lower than that of poly[*bis*(2,2,2-trifluoroethoxy)phosphazene], **21**, which may be due to the bulky ferrocenylalkoxy groups causing instability in the formation of the polymer. A strong electron-donating power of the $\text{Fc}(\text{CH}_2)_m\text{-}$ group also stabilises the reacting $\text{Fc}(\text{CH}_2)_m\text{O}^-$ - anion, while the $\text{CF}_3\text{CH}_2\text{O}^-$ - anion activated by the electron-withdrawing CF_3 - group.

GPC was used to determine accurate molecular weights of **21** and the newly synthesised poly[*bis*(2,2,2-trifluoroethoxy)(ferrocenylalkoxy)phosphazenes], **22**, **23**, **24** and **25**. The GPC process was new to the physical chemistry group at the UFS and training was received in the laboratory of Prof du Prez at the University of Ghent in Belgium to use this instrument. The molecular weights of the aged samples of poly[*bis*(2,2,2-trifluoroethoxy)phosphazene], **21**, and poly[*tris*(2,2,2-trifluoroethoxy)(ferrocenylalkoxy)phosphazenes], **22**, **23**, **24** and **25**, were determined to be 6307, 3410, 3876, 7421 and 3310, respectively, against poly(methylmethacrylate) (PMMA) standards. Freshly synthesised poly[*tris*(2,2,2-trifluoroethoxy)(ferrocenylbutoxy)

phosphazene], **25**, utilising increasing monomer to initiator ratios (33 : 1; 50 : 1; 100 : 1) were repeated in the physical chemistry laboratory at the UFS, shortly after synthesis and was found to have molecular weights of 126 554, 168 475 and 213 731 daltons, respectively, against polystyrene standards. An extrapolation of these molecular weights to the previously synthesised polymers determined that the initial molecular weight of the freshly synthesised polymer may have been approximately 82 410 daltons. This results demonstated that the shelf-life of the ferrocene-containing polymers do not extend to include 1 year storing times.

Dilute solution viscometry measurements were used to determine the Mark-Houwink parameters in the equation $[\eta] = KM^a$ for poly[*tris*(2,2,2-trifluoroethoxy)(ferrocenylalkoxy)phosphazenes], whereby **a** was determined to be 0.87 and **K** was determined to be 0.0000634 dl/g.

XPS measurements were used to determine surface elemental composition of the synthesised poly[*tris*(2,2,2-trifluoroethoxy)(ferrocenylalkoxy)phosphazenes], **22**, **23**, **24** and **25**. XPS determined empirical formulas were $P_{2.0}N_{2.1}O_{4.2}F_{7.8}C_{9.4}H_xFe_{0.7}$ (theoretical $P_2N_2O_4F_9C_{17}H_{17}Fe$) for **22**, $P_{2.0}N_{2.0}O_{3.4}F_{9.3}C_{5.6}H_xFe_{0.6}$ (theoretical $P_2N_2O_4F_9C_{18}H_{19}Fe$) for **23**, $P_{2.0}N_{2.1}O_{3.7}F_{9.0}C_{6.7}H_xFe_{0.7}$ (theoretical $P_2N_2O_4F_9C_{19}H_{21}Fe$) for **24** and $P_{2.0}N_{2.1}O_{2.3}F_{7.4}C_{3.9}H_xFe_{0.5}$ (theoretical $P_2N_2O_4F_9C_{20}H_{23}Fe$) for **25** (hydrogen is shown as H_x since hydrogen cannot be determined by XPS). The considerably lowered carbon content was considered the result of the decomposition of the ferrocenyl group liberating Fe_2O_3 and volatile carbon species such as free cyclopentadiene upon X-ray irradiation. Structural fluctuations in chemical environments for **22** to **25** were observed by the peak FWHM measurements of the nitrogen and phosphorus photoelectron lines (N1s and P2p) of the polymer backbone. FWHM was observed to be directly proportional to the alkyl chain length on the ferrocenylalkoxy group. Longer alkyl chain lengths in the ferrocenylalkoxy side chains allow for greater flexibility of the polymeric material, therefore allowing more fluctuations of the chemical environments.

An electrochemical study of poly[*tris*(2,2,2-trifluoroethoxy)(ferrocenylalkoxy)phosphazenes], **22**, **23**, **24** and **25**, were carried out. The formal reduction potentials for **22**, **23**, **24**, and **25** were 23.5 mV, -24.5 mV, -35.5 mV, and -51.1 mV at 100 mV/s scan rate respectively. Thus, the formal reduction potential was observed to decrease as the alkyl chain length, **m**, of the ferrocenylalkoxy group increased. Poly[*tris*(2,2,2-trifluoroethoxy)(ferrocenylbutoxy)phosphazene], **25**, therefore required a lower potential in order to oxidise the iron center in the ferrocenyl moiety than poly[*tris*(2,2,2-

trifluoroethoxy)(ferrocenylmethoxy)phosphazene], **22**. Electrochemical reversibility was examined utilising ΔE_p . It was found that as the alkyl chain length, **m**, of the ferrocenylalkoxy group increased, ΔE_p decreased leading to a more electrochemically reversible system at 100 mV/s scan rate. The ΔE_p potentials for **22**, **23**, **24** and **25** were 97, 83, 70 and 70 mV, respectively. Chemical reversibility was examined utilising the ratio of cathodic current over anodic current (i_{pc}/i_{pa}), whereby a value of 1 implies complete chemical reversibility. The i_{pc}/i_{pa} ratios at 100 mV/s for **22**, **23**, **24** and **25** were 0.288, 0.287, 0.676 and 0.839, respectively. Therefore, as the alkyl chain length increased on the ferrocenylalkoxy side group, the i_{pc}/i_{pa} ratios also increased, thereby increasing in chemical reversibility. More flexibility of the ferrocenylalkoxy substituents lead to a more chemically reversible system. An extrapolation of the i_{pc}/i_{pa} ratio versus the alkyl chain length approximates $m = 6$ for a completely chemically reversible ferrocenealkoxy-containing poly(organo)phosphazene.

UV/vis spectroscopy was used to preliminary investigate the rate of hydrolysis of poly[*tris*(2,2,2-trifluoroethoxy)(ferrocenylmethoxy)phosphazene], **22**, into phosphates and ammonia in water/THF solvent mixtures. This reaction was followed kinetically in order to get an indication of the timescale of this process. Pseudo-first-order reaction conditions whereby $[22] = 2.377 \text{ mM}$ and $[\text{H}_2\text{O}] = 13.89 \text{ M}$ (3894 fold excess water) exhibited extremely slow hydrolysis and was not kinetically favourable. A larger excess of water, $[\text{H}_2\text{O}] = 18.51 \text{ M}$, showed that the hydrolysis took place in four separate steps. Firstly, the trifluoroethoxy groups were hydrolysed, followed by the hydrolysis of the ferrocenylmethoxy group. This took place in the first 10 hours. Trifluoroethanol was mostly liberated during the first 3 hours followed by ferrocenylmethanol until ca. 10 hours. Recoiling of the polyphosphazene chain was observed during the third step between 10 and 20 hours. Recoiling was followed in the fourth step by polymer main chain hydrolysis between 20 and 100 hours and was interpreted as the eventual production of phosphates and ammonia. Pseudo-first-order kinetic parameters for step 1, step 2 and step 4 were determined to be $k_{obs} = 2.01 \times 10^{-4} \text{ s}^{-1}$, $1.29 \times 10^{-4} \text{ s}^{-1}$ and $2.6 \times 10^{-6} \text{ s}^{-1}$. This translates into second order rate constants of $k_2 = 1.09 \times 10^{-5} \text{ dm}^3\text{mol}^{-1}\text{s}^{-1}$, $7.00 \times 10^{-6} \text{ dm}^3\text{mol}^{-1}\text{s}^{-1}$ and $1.38 \times 10^{-7} \text{ dm}^3\text{mol}^{-1}\text{s}^{-1}$ respectively when $[\text{H}_2\text{O}]$ concentration = 18.51 M. An excess of 15579 fold water ($[\text{H}_2\text{O}] = 27.78 \text{ M}$) resulted in complete hydrolysis of **22** within 30 hours. Kinetic parameters, k_{obs} and k_2 , were calculated to be $2.92 \times 10^{-5} \text{ s}^{-1}$ and $1.05 \times 10^{-6} \text{ dm}^{-3} \text{ mol s}^{-1}$, respectively under this extreme high water concentration conditions. The results indicated a first-order dependence on polymer concentration but no clear rate-order could be determined for water as k_2 was not constant for different concentrations of water.

DSC was utilised to evaluate thermal properties of poly[*bis*(2,2,2-trifluoroethoxy)phosphazene], **21**, and poly[*tris*(2,2,2-trifluoroethoxy)(ferrocenylalkoxy)phosphazenes], **22**, **23**, **24**, and **25**. Polymer **21** was observed to exhibit thermoplastic properties with indications of thermal cracking of the polymer main chain from cycle 1 to cycle 3 with onset melting temperatures of 68.46 °C to 58.25 °C, respectively. DSC thermograms for polymers **22** – **25** showed thermally silent profiles for cycles 2 and 3. An extensive examination of the thermal profiles during days 2 and 3 showed that the relaxation times for the polymers **22** – **25** were much longer than for **21** and these polymers also exhibited thermoplastic properties. Melting temperatures were determined as 38.3 °C (**22**), 42.4 °C (**23**), 70.1 °C (**24**) and 38.7 °C (**25**). Phase separation between higher and lower molecular mass fractions of polymers **25b** and **25c** was also confirmed whereby the lower molecular mass polymer exhibited a lower onset melting temperature of 37.13 °C (**25c**, $\overline{M}_n = 126\,554$) and higher melting point onsets for the higher molecular mass polymer fraction, 43.43 and 63.83 °C (**25b**, $\overline{M}_n = 168\,475$), respectively.

Cytotoxicity for poly[*tris*(2,2,2-trifluoroethoxy)(ferrocenylalkoxy)phosphazenes], **22**, **23**, **24**, and **25** were performed on the HeLa cervical cancer cell line. The half maximal inhibitory concentration (IC_{50}) values were 18.24 μM (**22**), 40.15 μM (**23**), 58.83 μM (**24**) and 59.09 μM (**25**) and the IC_{50} of cisplatin was observed as 1.21 μM. The polyphosphazenes were successful in acting as a drug delivery system as cytotoxicity was observed. An inversely proportional relationship was observed between the free and polymer-anchored ferrocenylalcohols, whereby the potency of the free ferrocenylalcohols was found to increase with alkyl chain length, **m**, in literature; the anchored ferrocenylalcohols exhibited lower potency with increasing alkyl chain, **m**. This could be attributed to the structure, folding patterns and the hydrolysis kinetic rates of the polymer-drug conjugate, whereby the folding patterns may trap the ferrocenylalkoxy moieties inside hydrophobic pockets and thus inhibiting hydrolysis of the ferrocenylalkoxy side chains. However, a comprehensive hydrolysis kinetic study and further research into the properties of these polymers are required to explain the inverse relationship observed between the IC_{50} values and the increasing alkyl chain length, **m**, in the ferrocenylalkoxy side chains. The IC_{50} values for the free ferrocenylalcohols were directly proportional to the formal reduction potential of the free ferrocenylalcohols. The IC_{50} values for the polymer-anchored ferrocenylalcohols were inversely proportional to the formal reduction potential of the polymer-anchored ferrocenylalcohols.

5.2 Future Perspectives

This study has investigated the use of ferrocenylalkoxy-functionalised polyphosphazene polymers as drug-carriers with chemotherapeutic applications. A large amount of possible related but future research may be performed, building on the foundation that was laid during this study. These may include the following:

1. A full kinetic study may be performed to investigate the influence of a range of variables on the hydrolysis rate, as well as resulting cytotoxicity (IC_{50}) of polymers **22 – 25**. These variables must include temperature, pH influences, solvent mixture compositions, studies to determine activation parameters and ionic strength studies. Different structural architectures are possible with polyphosphazenes (e.g., star, dendrimers, co-block polymers) which may influence rate of hydrolysis and drug release.³ Research into these structural changes is required to investigate the influence thereof for biomedical applications.
2. Previous research into polyphosphazenes containing vitamin substituent side groups were performed.^{1,2} Research may be conducted to synthesise polymer-bearing vitamin substituents as well as the present antineoplastic ferrocenylalkoxy groups. This may enhance treatment options for polyphosphazene drug delivery systems, whereby multiple substituent types on the polymer carrier may maintain healthy cells and enhance cellular responses while treating cancer.¹
3. The unanchored ferrocenylalcohols, especially 4-ferrocenylbutanol, has been shown in literature to exhibit catalytic activity.⁴ Ferrocenylalkoxy-functionalised polyphosphazenes may be researched further by utilising the polyphosphazene polymers as catalytic supports.
4. Polyphosphazenes have also shown potential in polymer membrane fuel cells.⁵ Research into especially ruthenocenylalkoxy-functionalised polyphosphazenes and iridium-ruthenocenyl functionalised polyphosphazenes may provide new materials as polymer membranes in fuel cells.
5. Polyphosphazenes may also be modified to support photodynamic active phthalocyanine derivatives.

This concludes the discussion of the research performed by the author as well as the discussion of the implications of these results in cancer therapy.

M. Govender, 27 Sept 2019

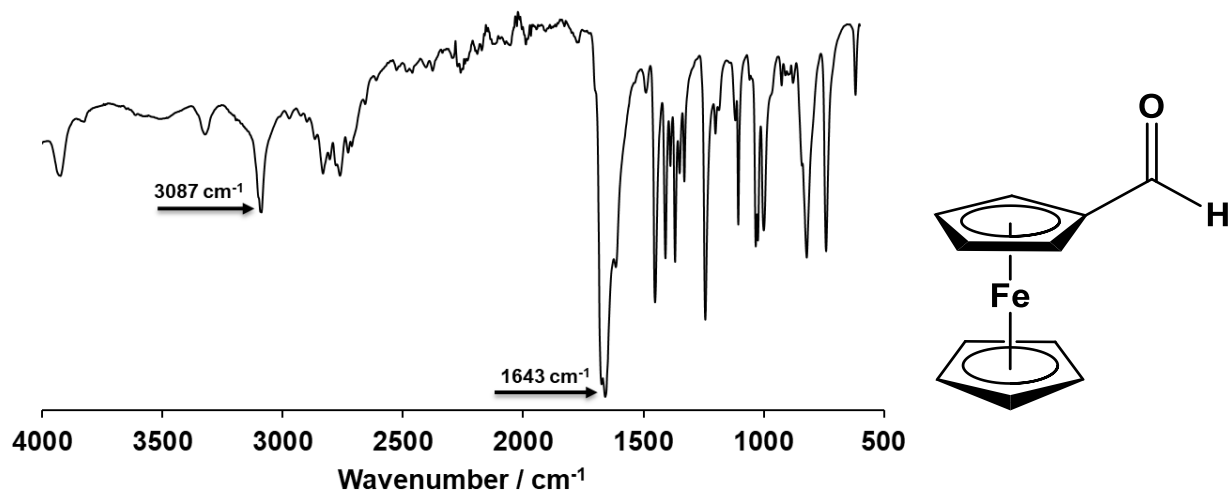
References

- 1 N. L. Morozowich, A. L. Weikel, J. L. Nichol, C. Chen, L. S. Nair, C. T. Laurencin and H. R. Allcock, *Macromolecules*, 2011, **44**, 1355–1364.
- 2 R. F. Shago, J. C. Swarts, E. Kreft and C. E. J. V. Rensburg, *Anticancer Res.*, 2007, **27**, 3431–3433.
- 3 S. Rothemund and I. Teasdale, *Chem. Soc. Rev.*, 2016, **45**, 5200–5215.
- 4 W. L. Davis, R. F. Shago, E. H. G. Langner and J. C. Swarts, *Polyhedron*, 2005, **24**, 1611–1616.
- 5 H. R. Allcock, *Soft Matter*, 2012, **8**, 7521–7532.

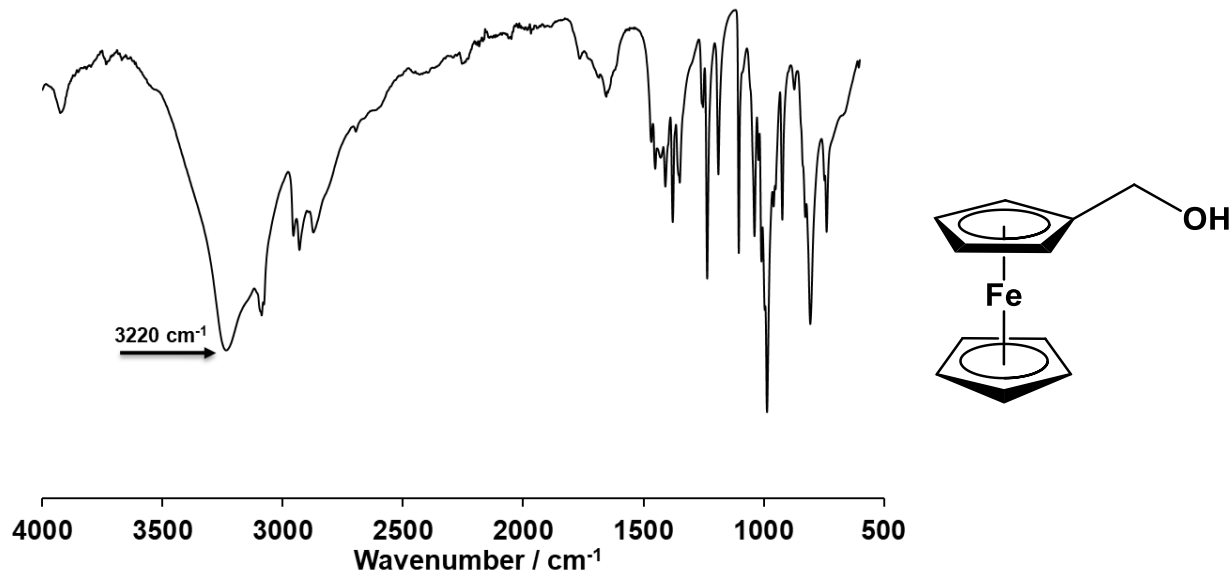
Appendix

IR Spectra

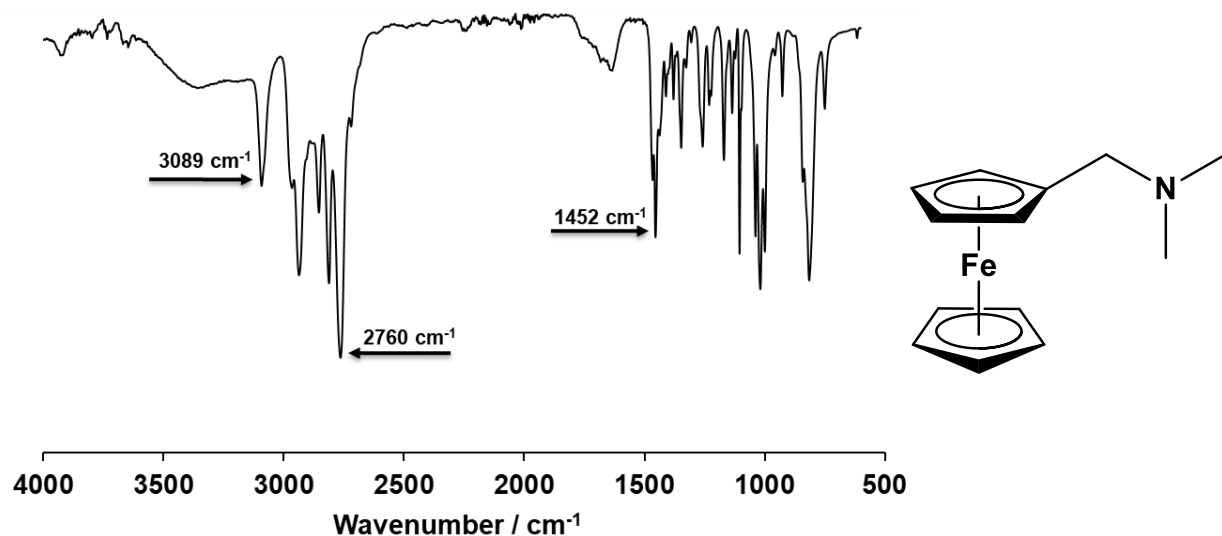
Spectrum 1: Ferrocenecarboxaldehyde, 2



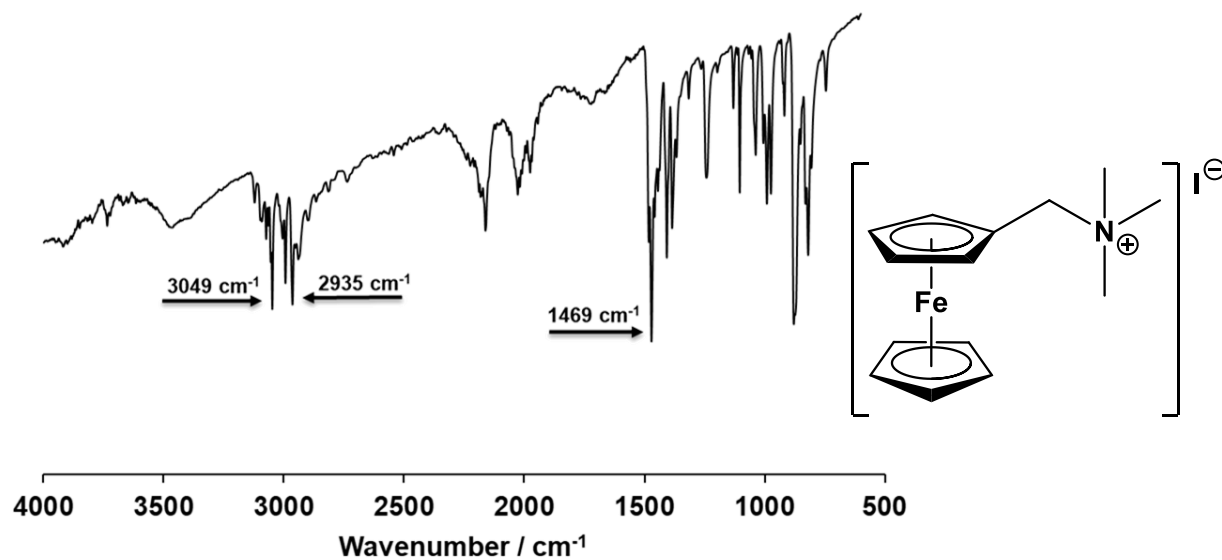
Spectrum 2: 1-Ferrocenylmethanol, 3



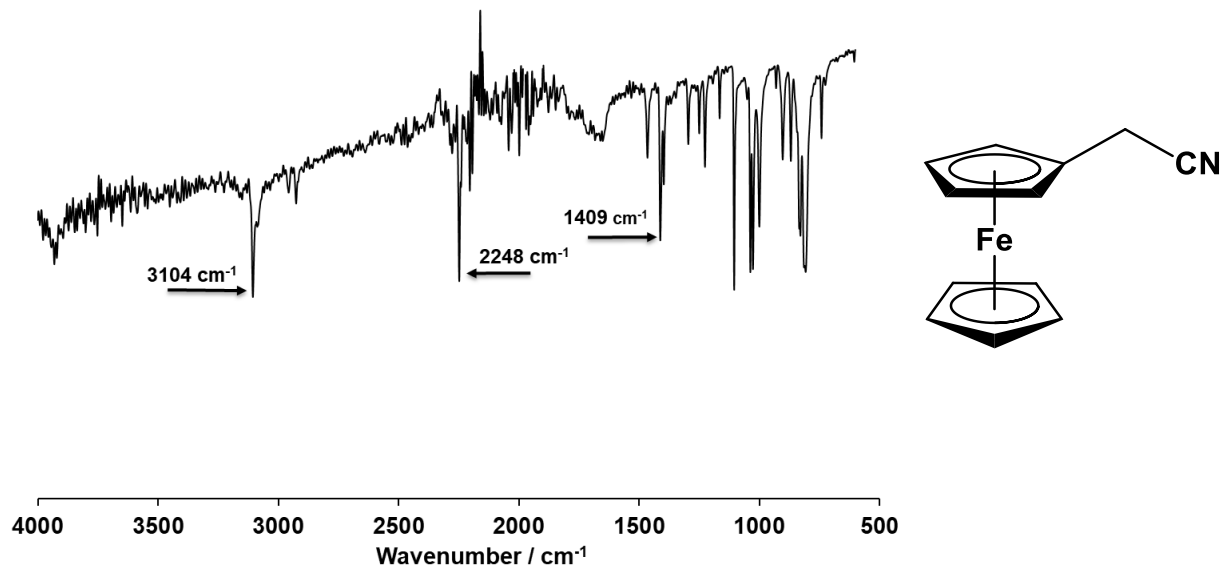
Spectrum 3: *N,N*-Dimethylaminomethylferrocene, 5



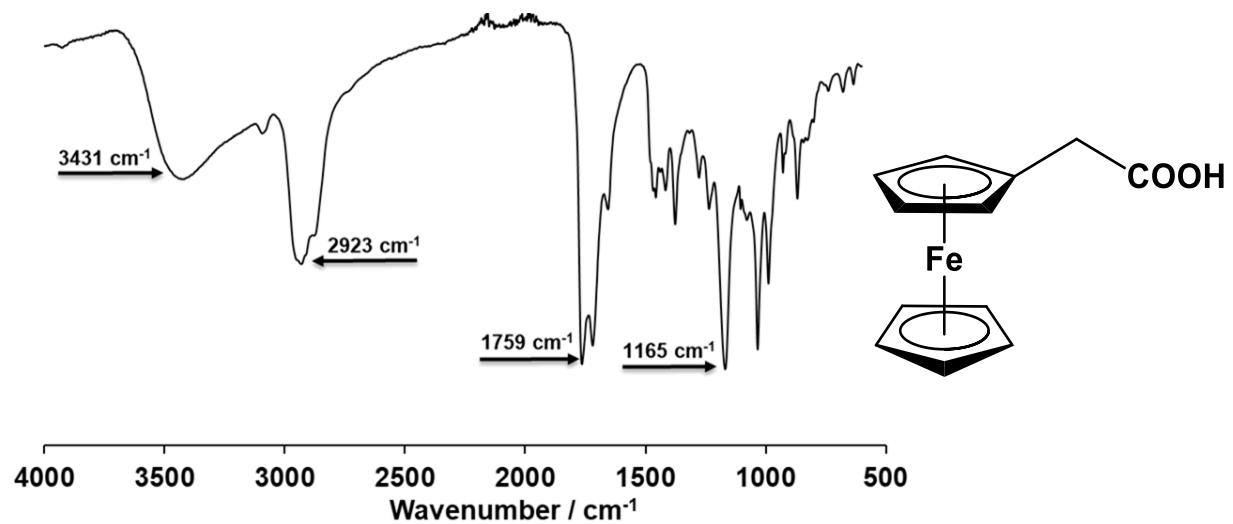
Spectrum 4: *N,N,N*-Trimethylaminomethylferrocene iodide, 6



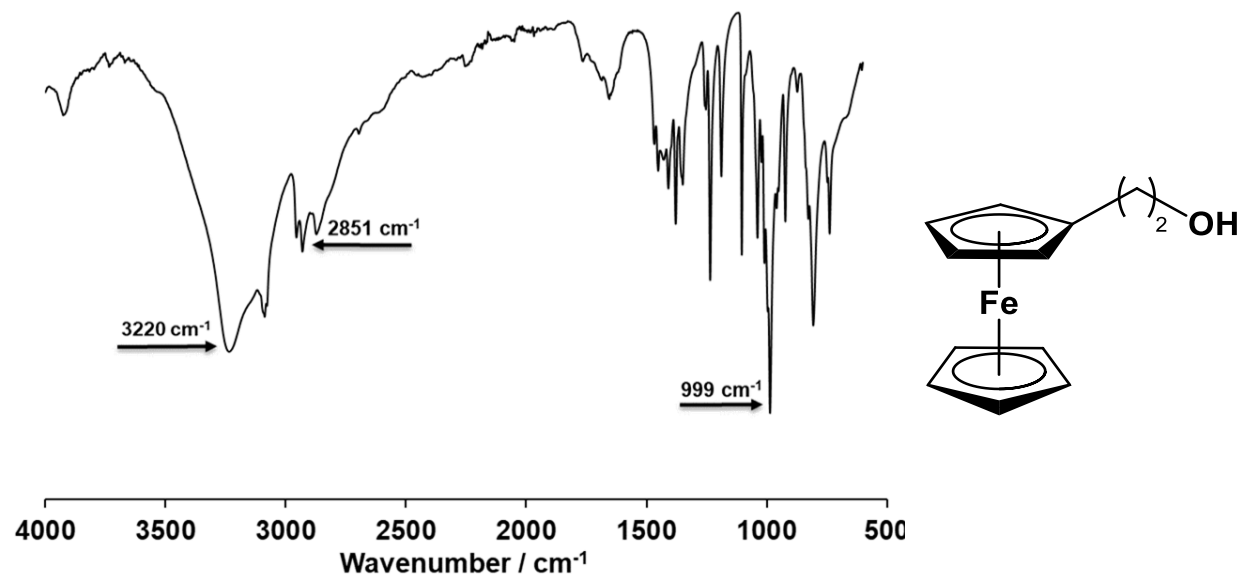
Spectrum 5: Ferrocenylacetonitrile, 7



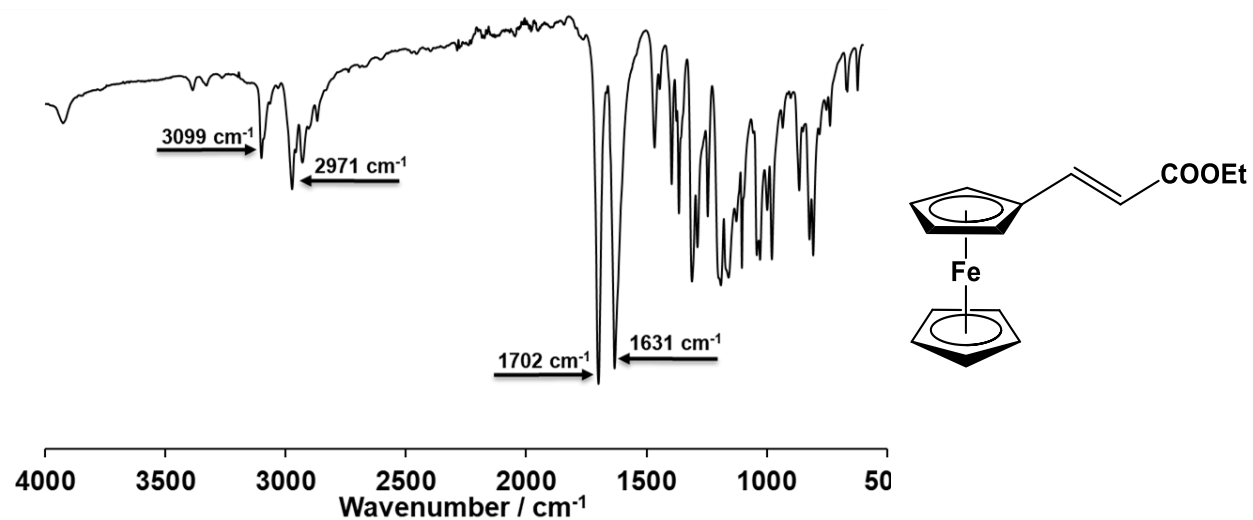
Spectrum 6: 2-Ferrocenylacetic acid, 8



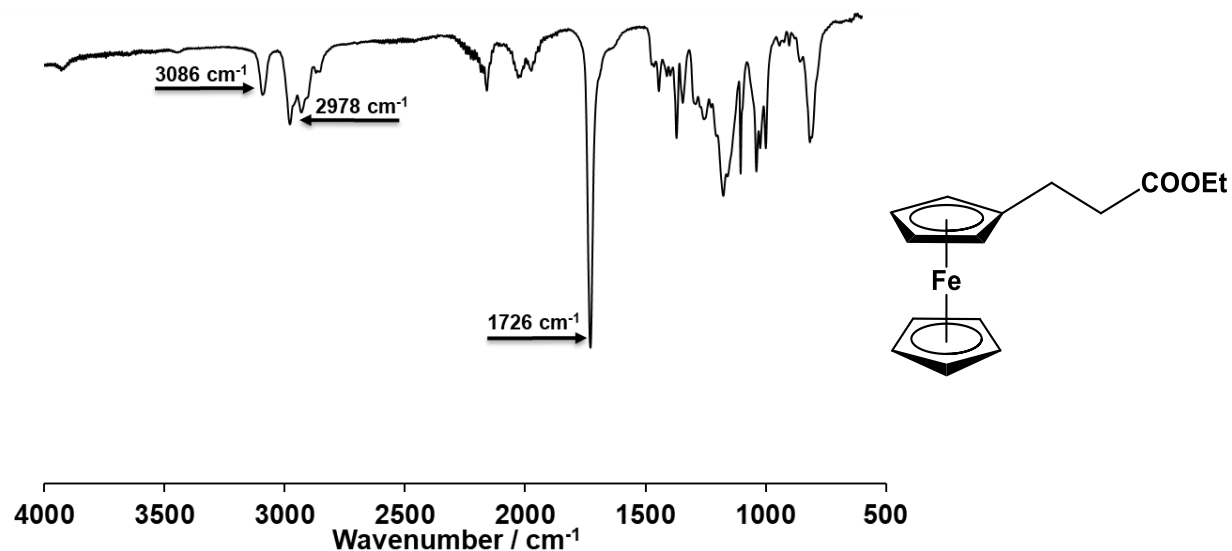
Spectrum 7: 2-Ferrocenylethanol, 9



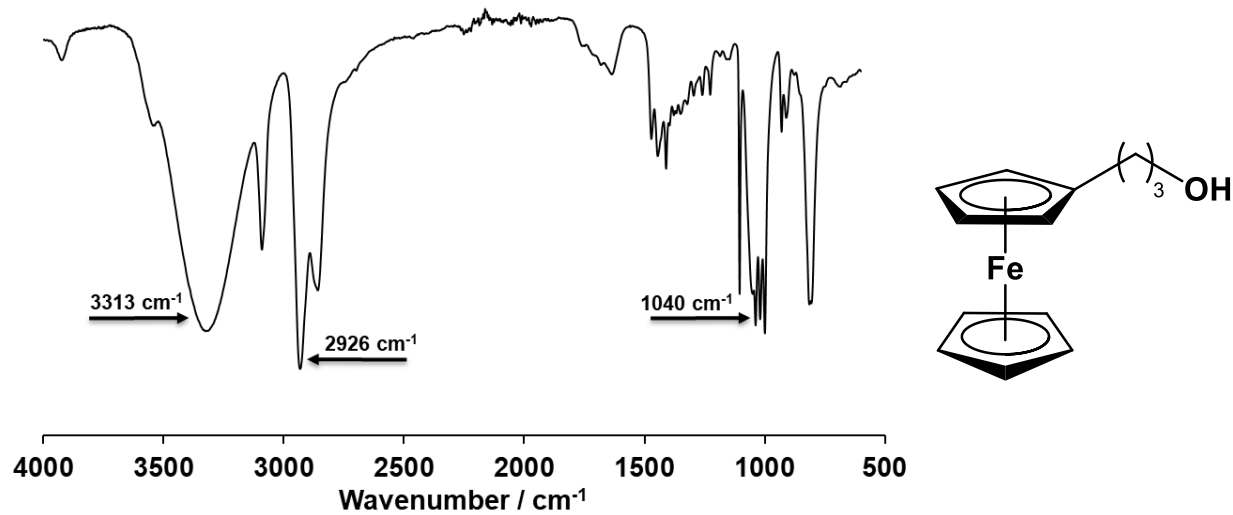
Spectrum 8: Ethyl-3-ferrocenylethenoate, 11



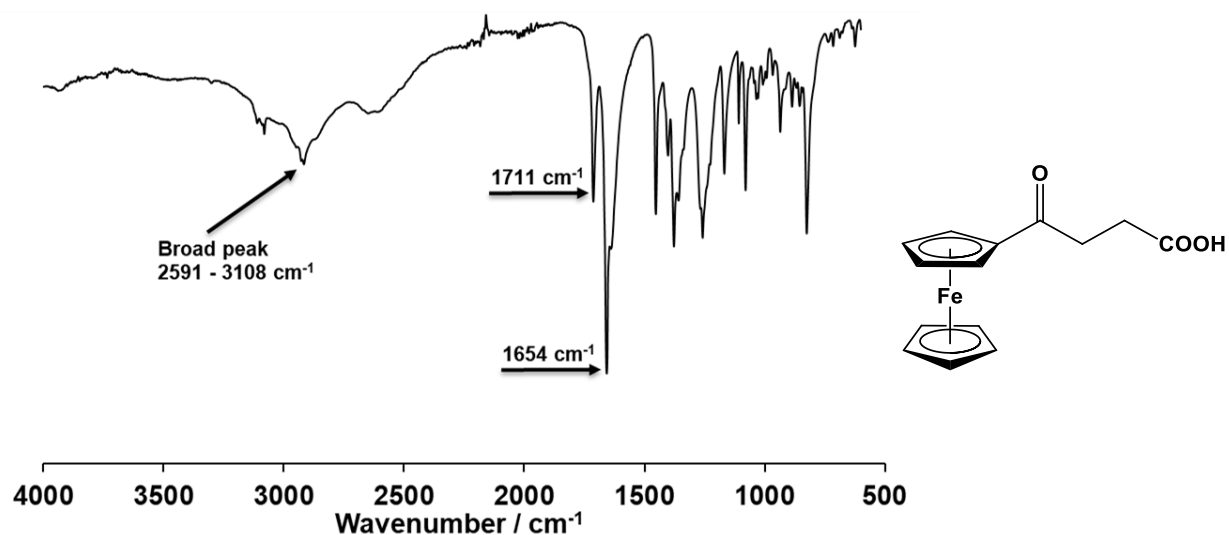
Spectrum 9: Ethyl-3-ferrocenylethanoate, 12



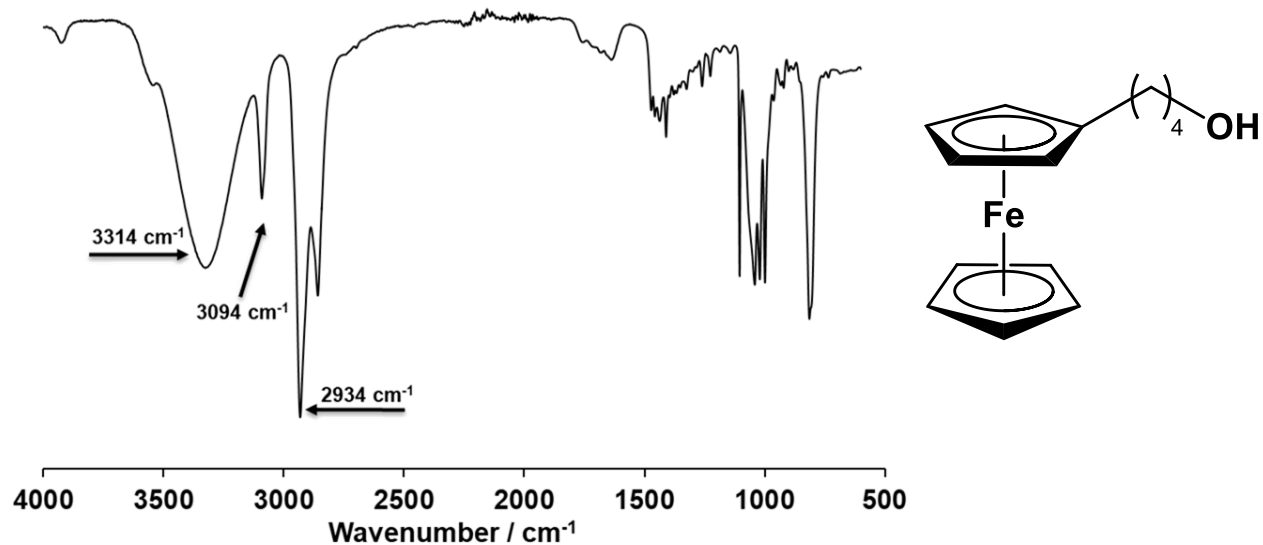
Spectrum 10: 3-Ferrocenylpropanol, 13



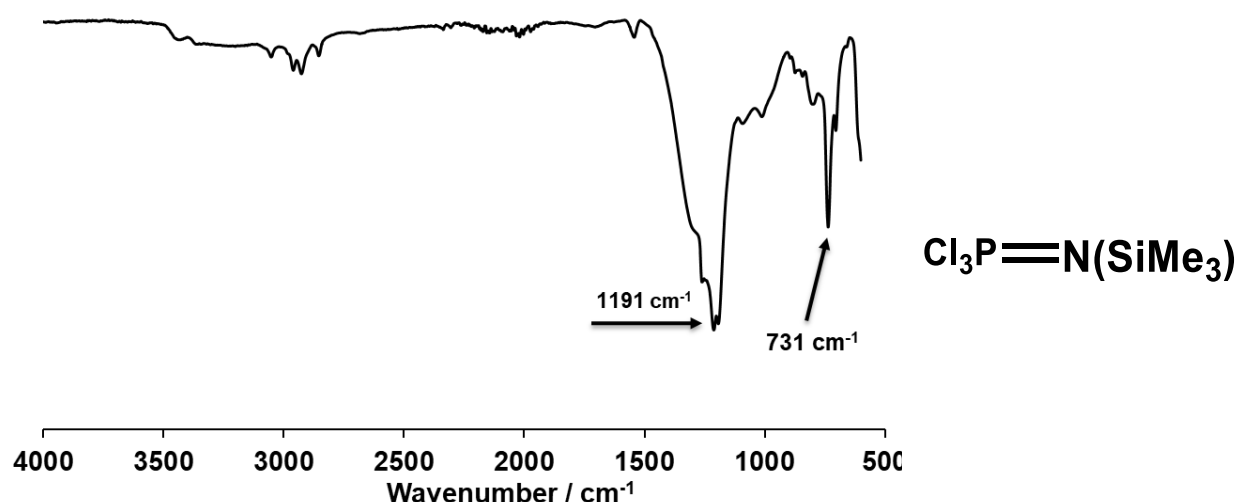
Spectrum 11: 3-Ferrcenoylethylpropionic acid, 15



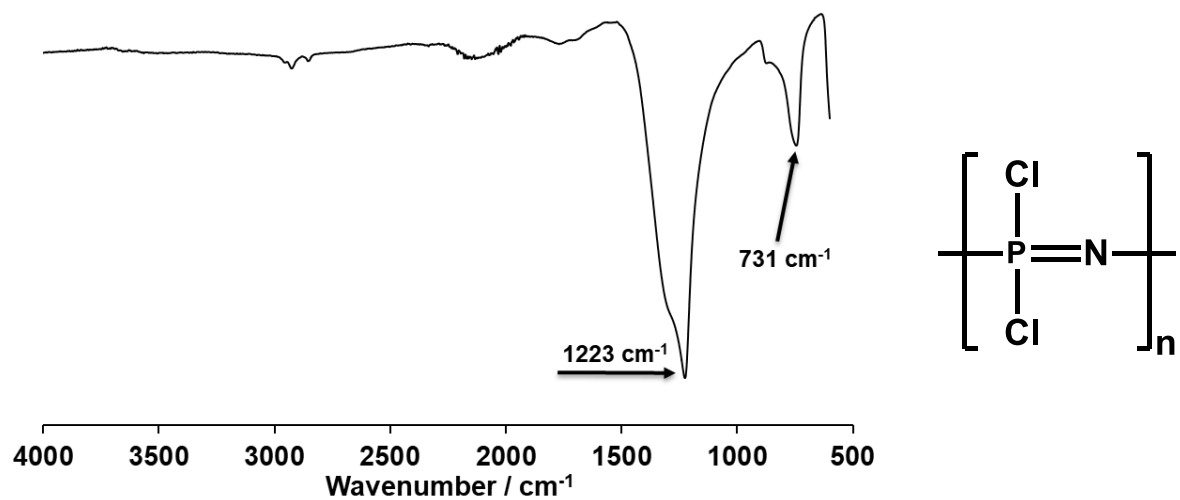
Spectrum 12: 4-Ferrocenylbutanol, 16



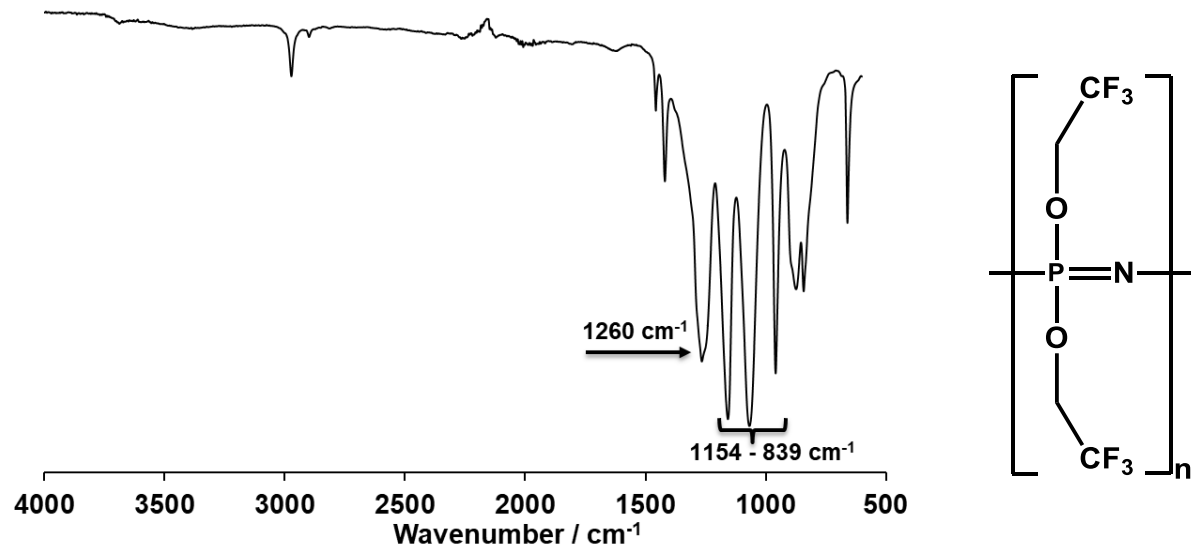
Spectrum 13: Trichloro(trimethylsilyl)phosphoranimine, 19



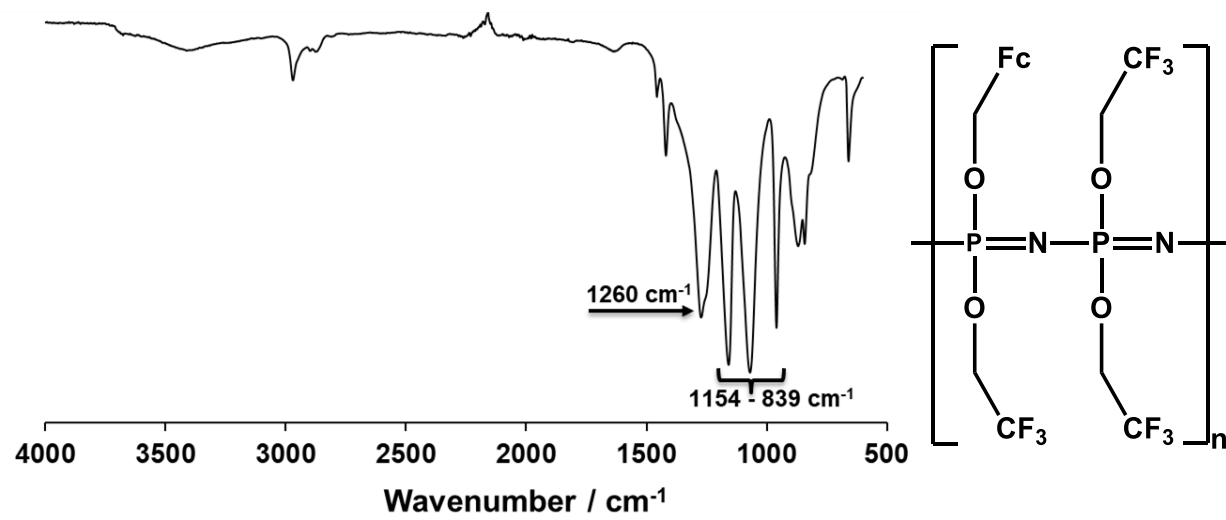
Spectrum 14: Poly(dichlorophosphazene), 20



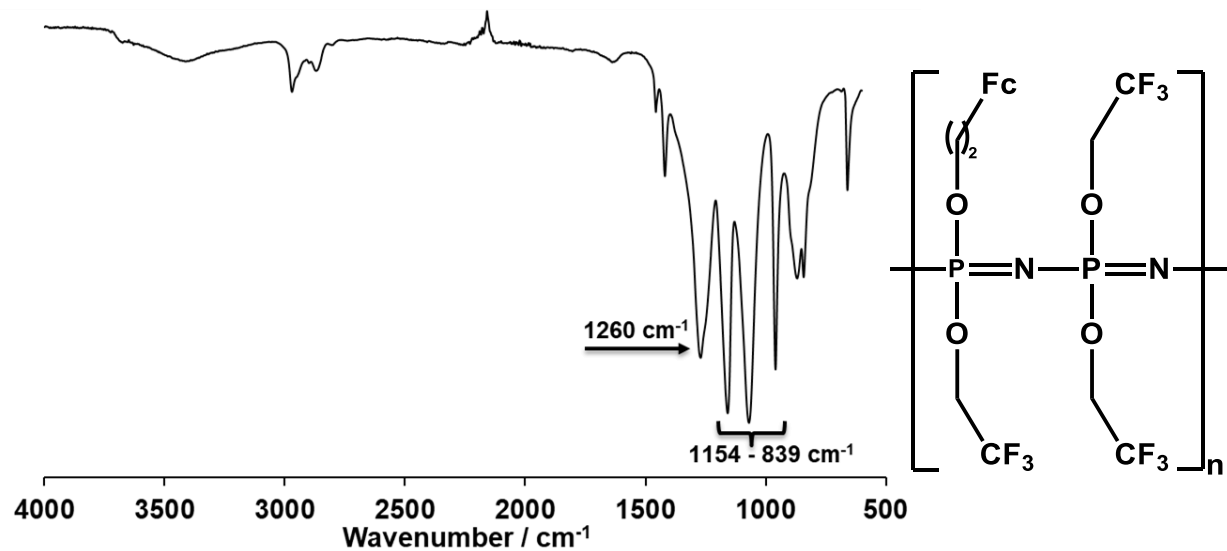
Spectrum 15: Poly[bis(2,2,2-trifluoroethoxy)phosphazene], 21



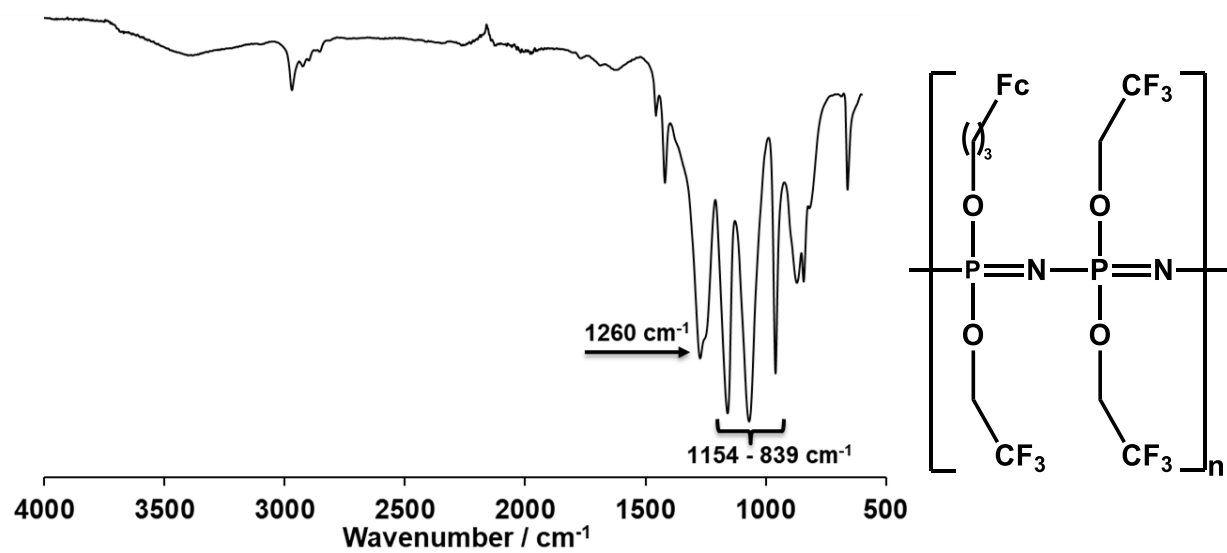
Spectrum 16: Poly[tris(2,2,2-trifluoroethoxy)(ferrocenylmethoxy)phosphazene], 22



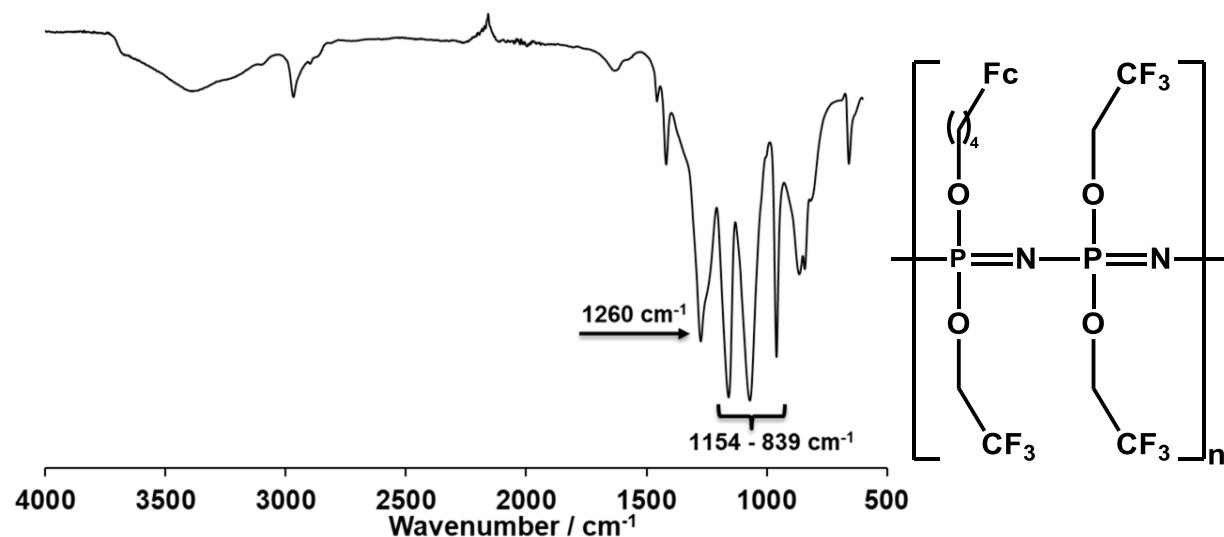
Spectrum 17: Poly[*tris*(2,2,2-trifluoroethoxy)(ferrocenylethoxy)phosphazene], 23



Spectrum 18: Poly[*tris*(2,2,2-trifluoroethoxy)(ferrocenylpropoxy)phosphazene], 24

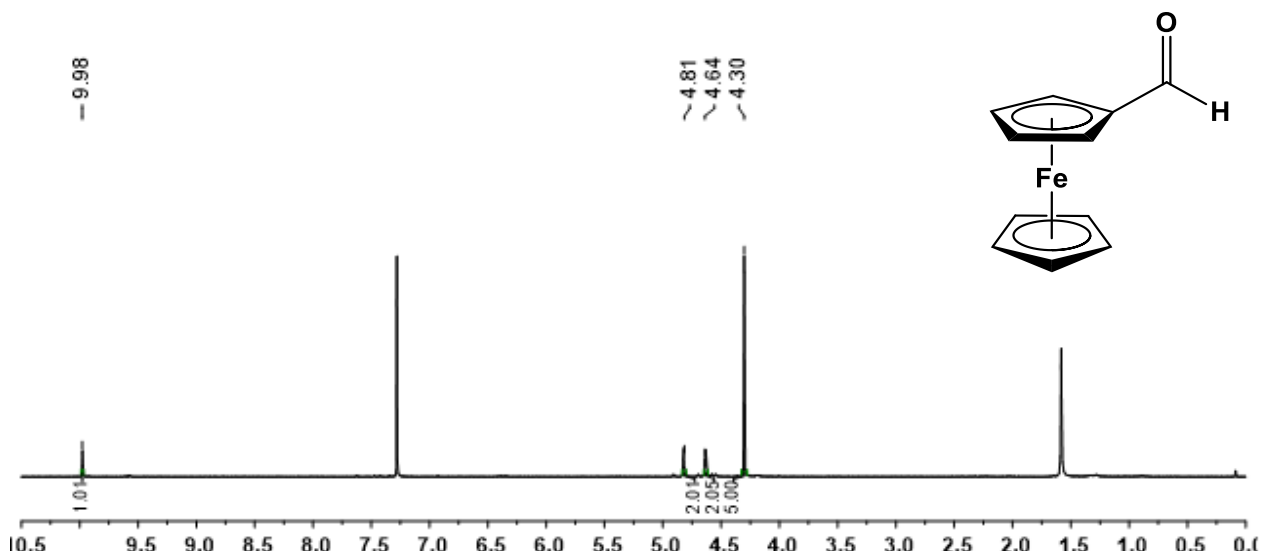


Spectrum 19: Poly[tris(2,2,2-trifluoroethoxy)(ferrocenylbutoxy)phosphazene], 25

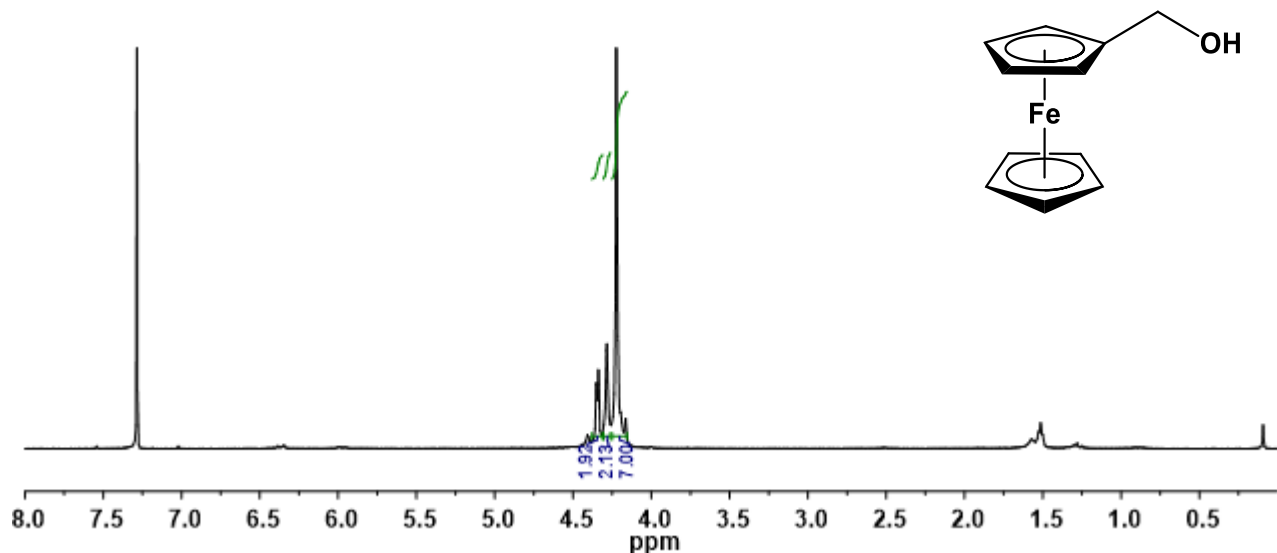


¹H NMR Spectra

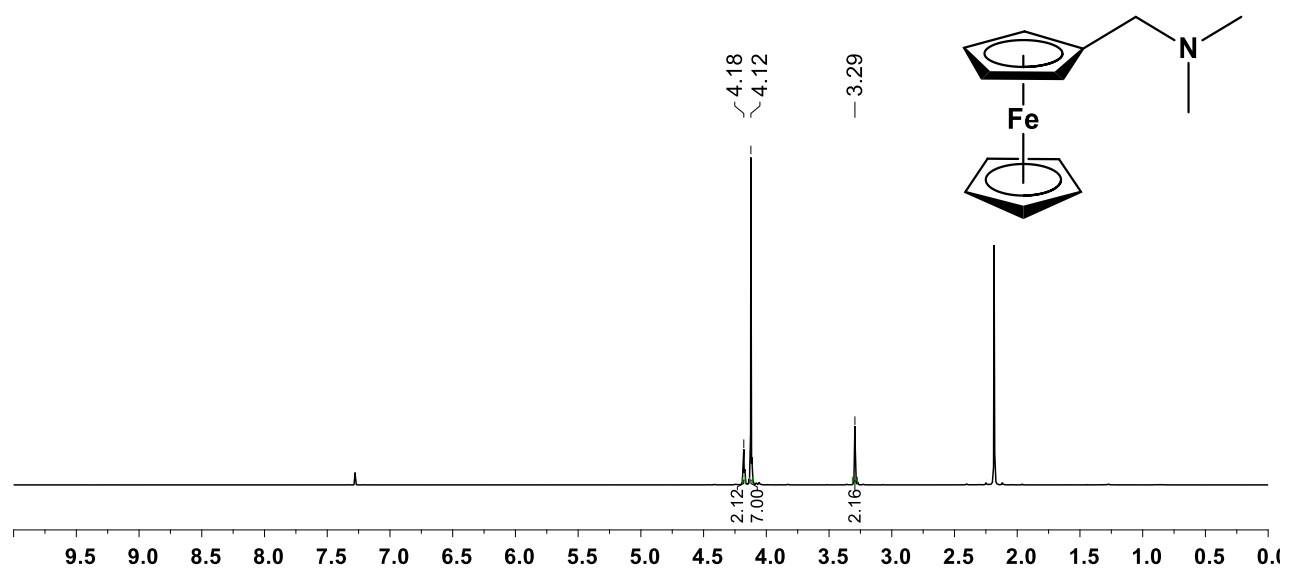
Spectrum 20: Ferrocenecarboxaldehyde, 2



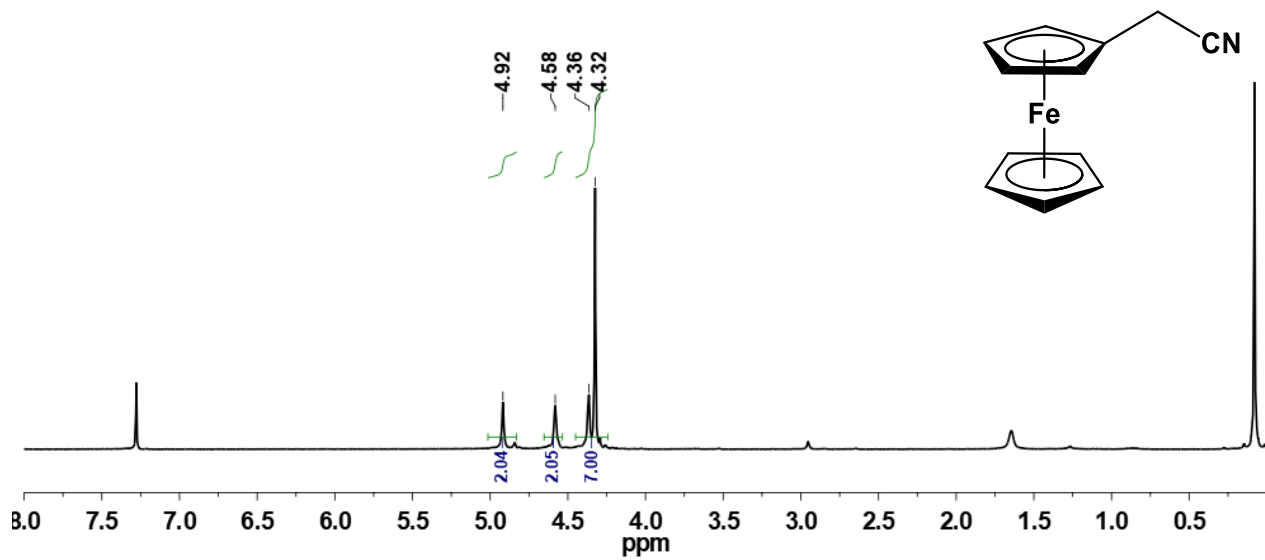
Spectrum 21: 1-Ferrocenylmethanol, 3



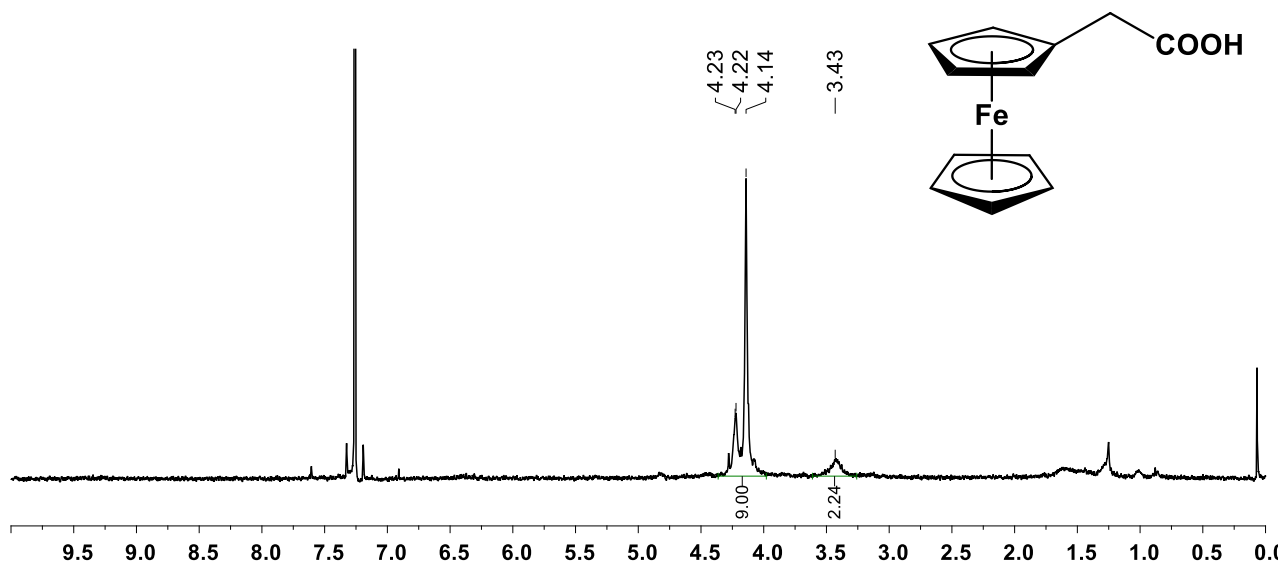
Spectrum 22: *N,N*-Dimethylaminomethylferrocene, 5



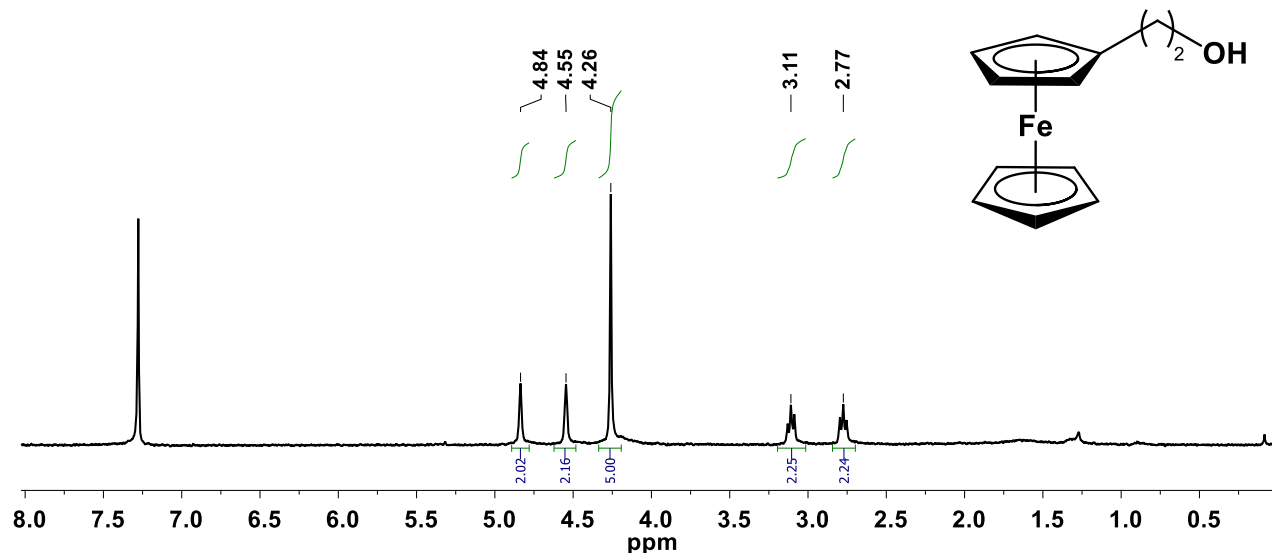
Spectrum 23: Ferrocenylacetonitrile, 7



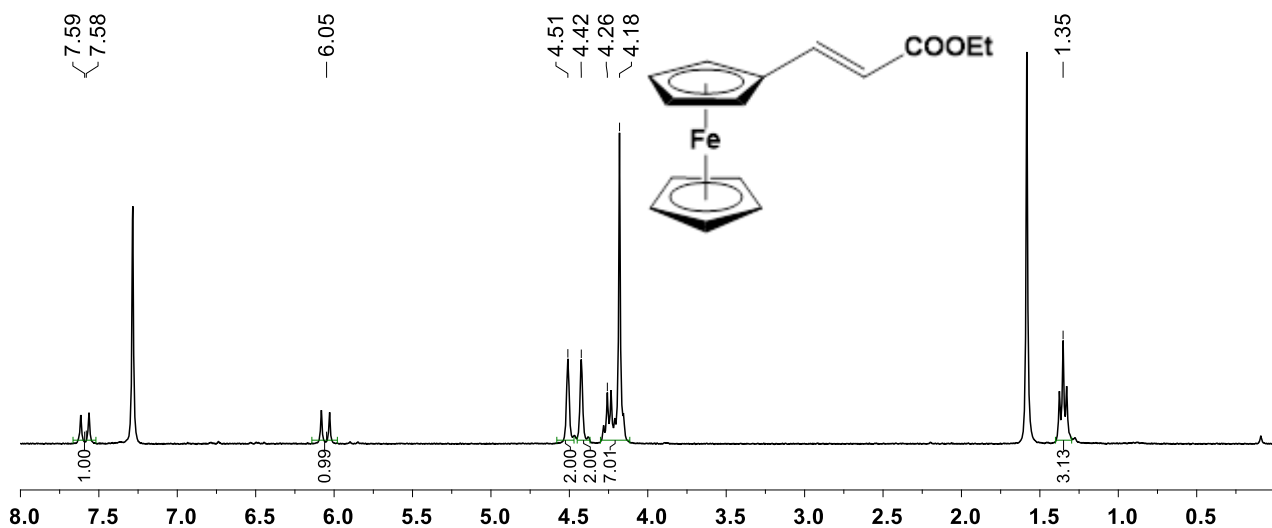
Spectrum 24: Ferrocenylacetic acid, 8



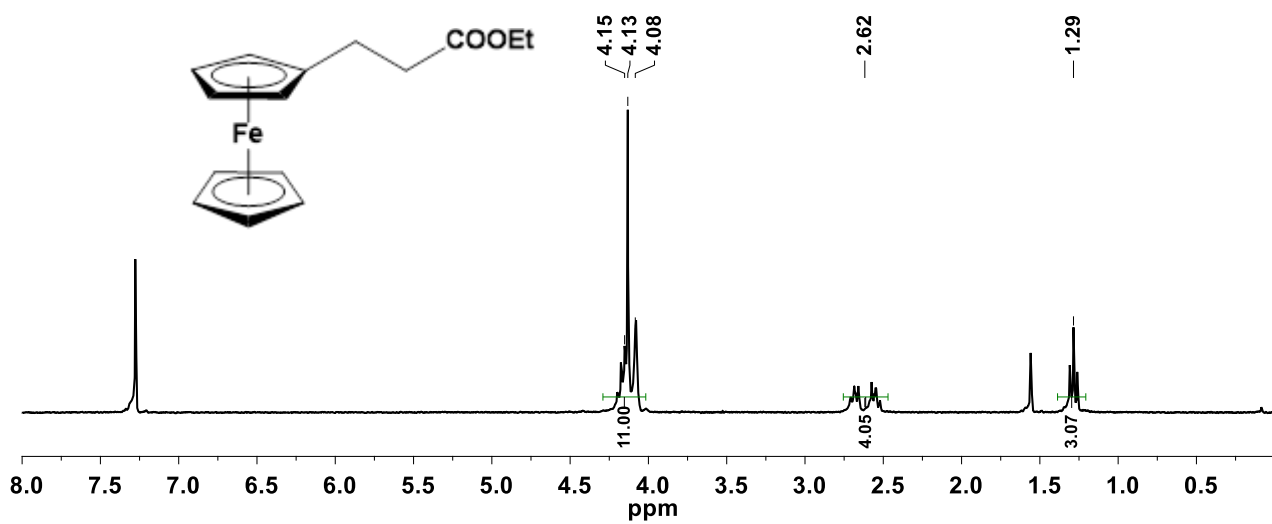
Spectrum 25: 2-Ferrocenylethanol, 9



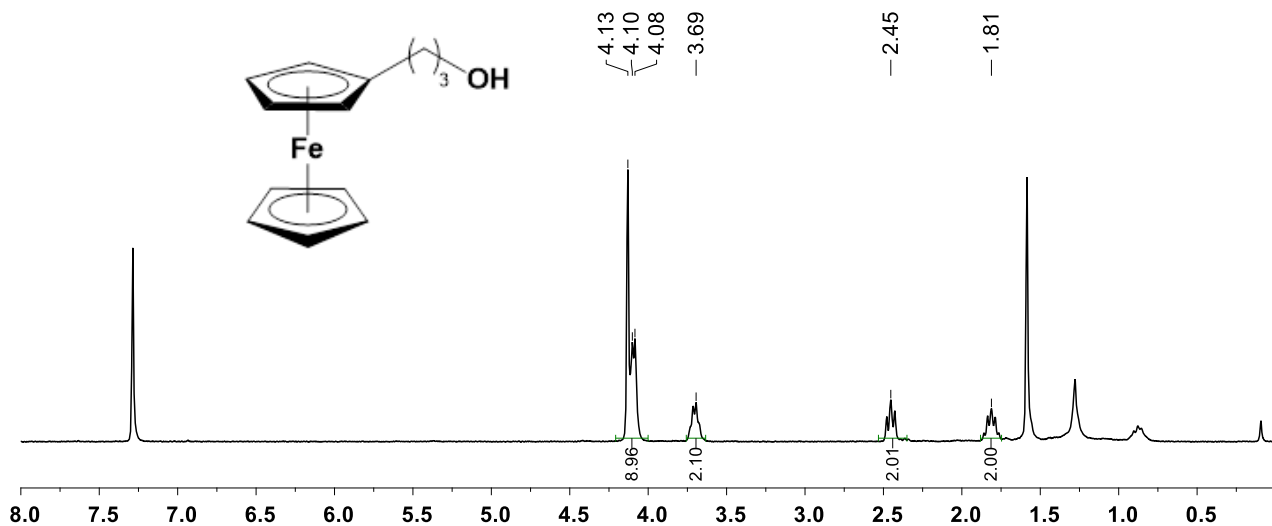
Spectrum 26: Ethyl-3-ferrocenylethenoate, 11



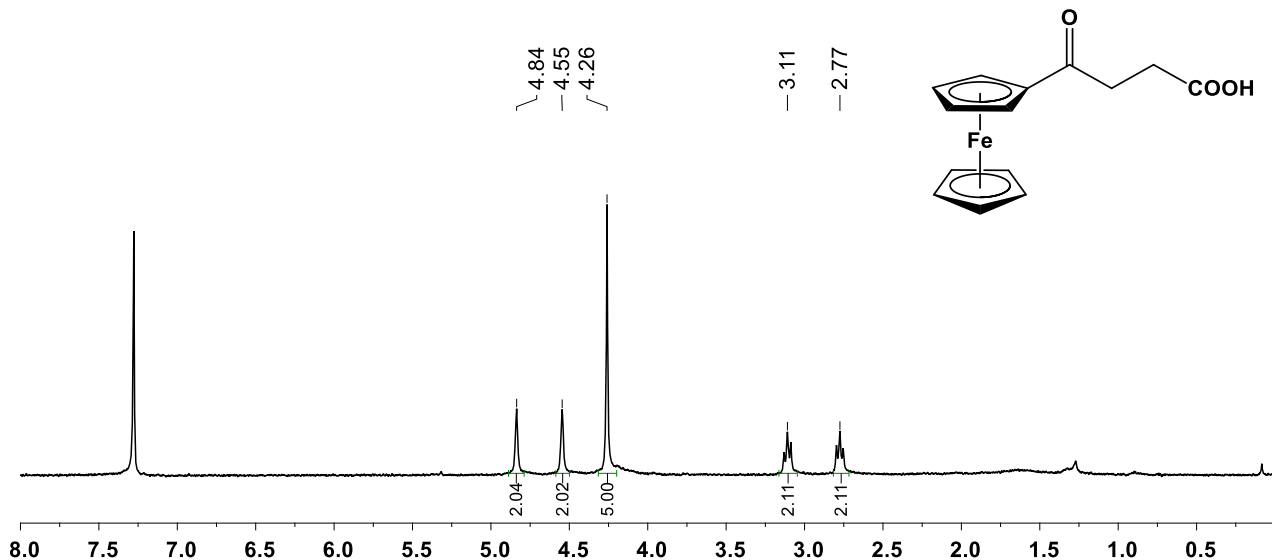
Spectrum 27: Ethyl-3-ferrocenylethanoate, 12



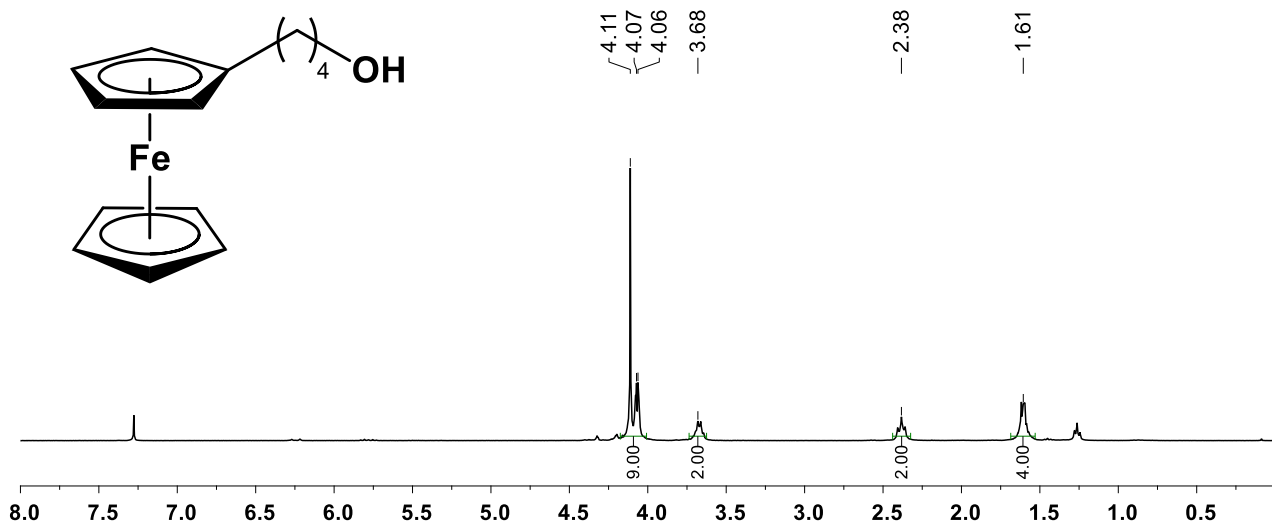
Spectrum 28: 3-Ferrocenylpropanol, 13



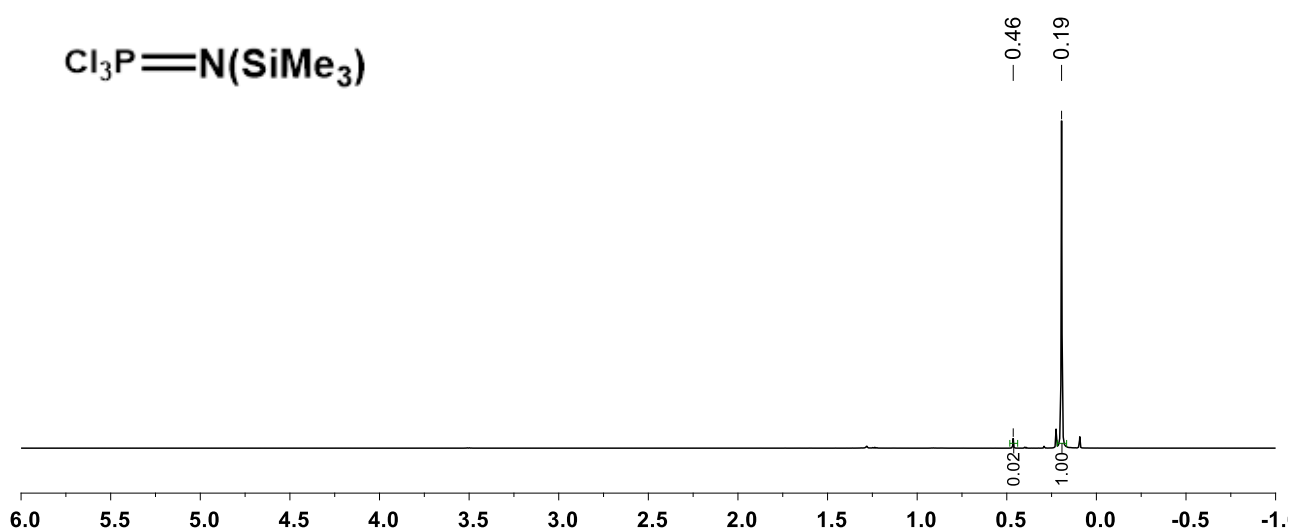
Spectrum 29: 3-Ferrocenoylpropionic acid, 15



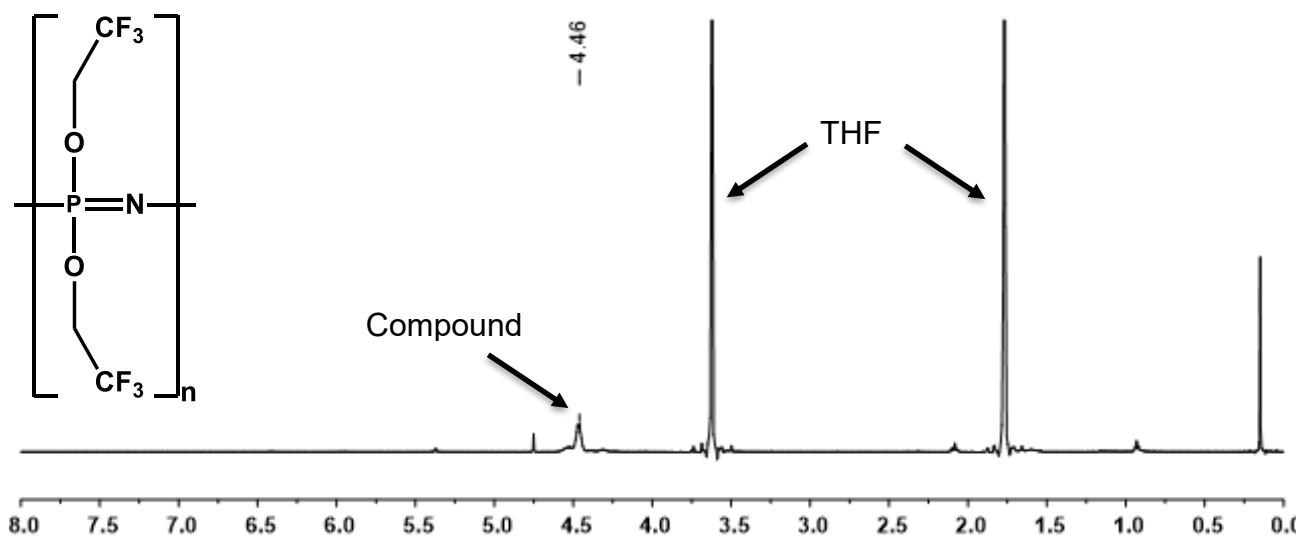
Spectrum 30: 4-Ferrocenylbutanol, 16



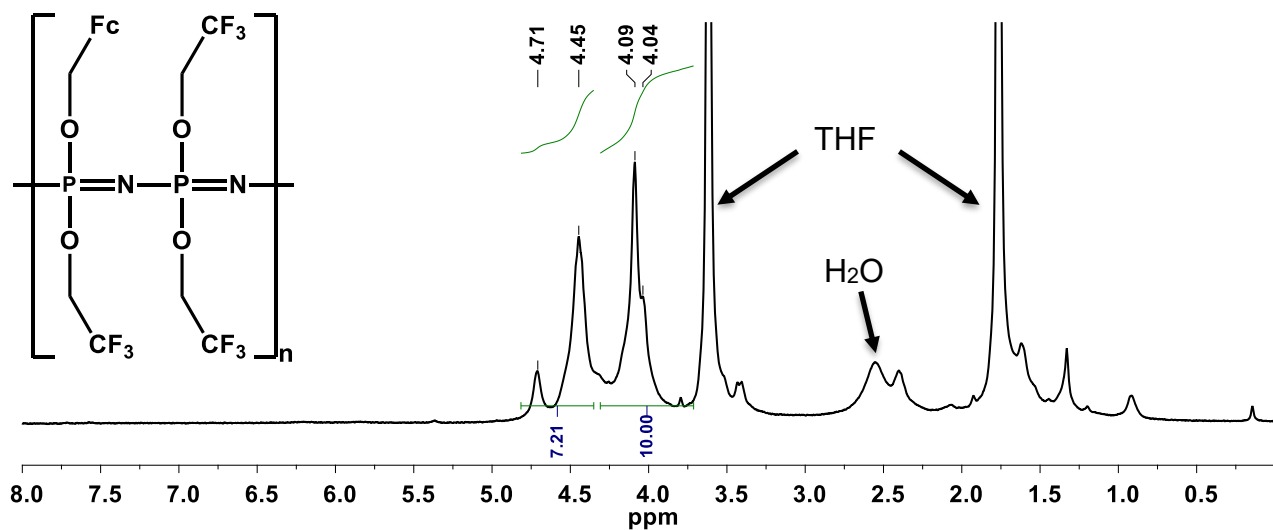
Spectrum 31: Trichloro(trimethylsilyl)phosphoranimine, 19



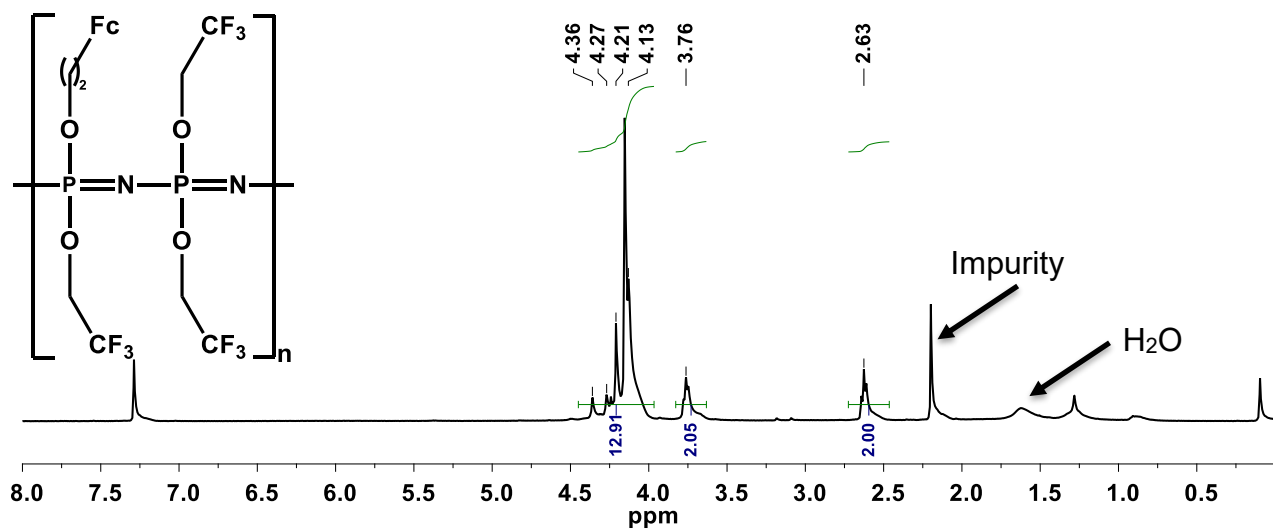
Spectrum 32: Poly[bis(2,2,2-trifluoroethoxy)phosphazene], 21



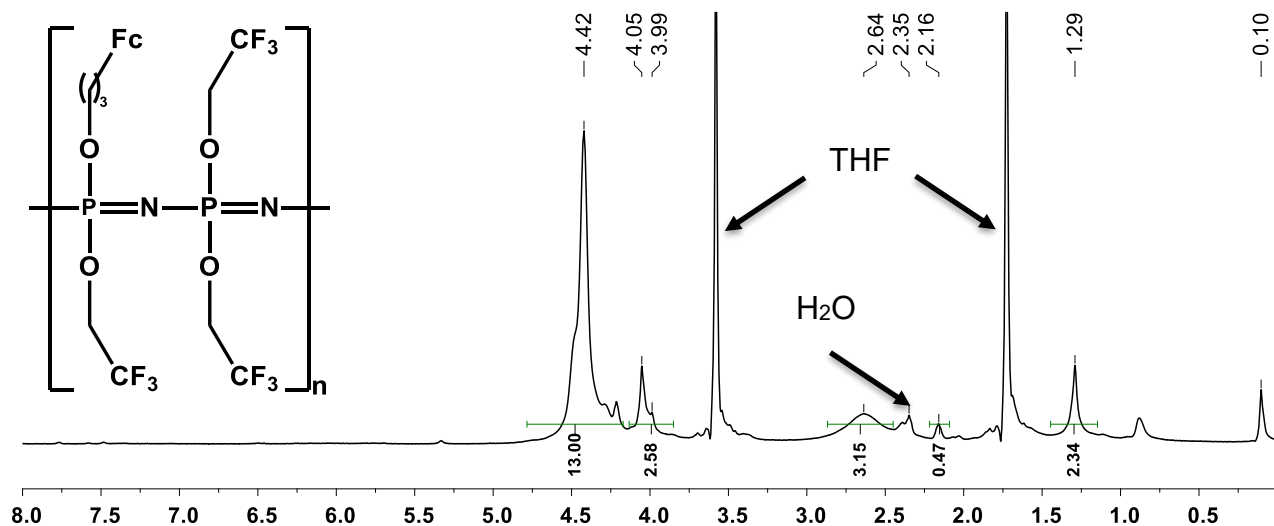
Spectrum 33: Poly[*tris*(2,2,2-trifluoroethoxy)(ferrocenylmethoxy)phosphazene], 22



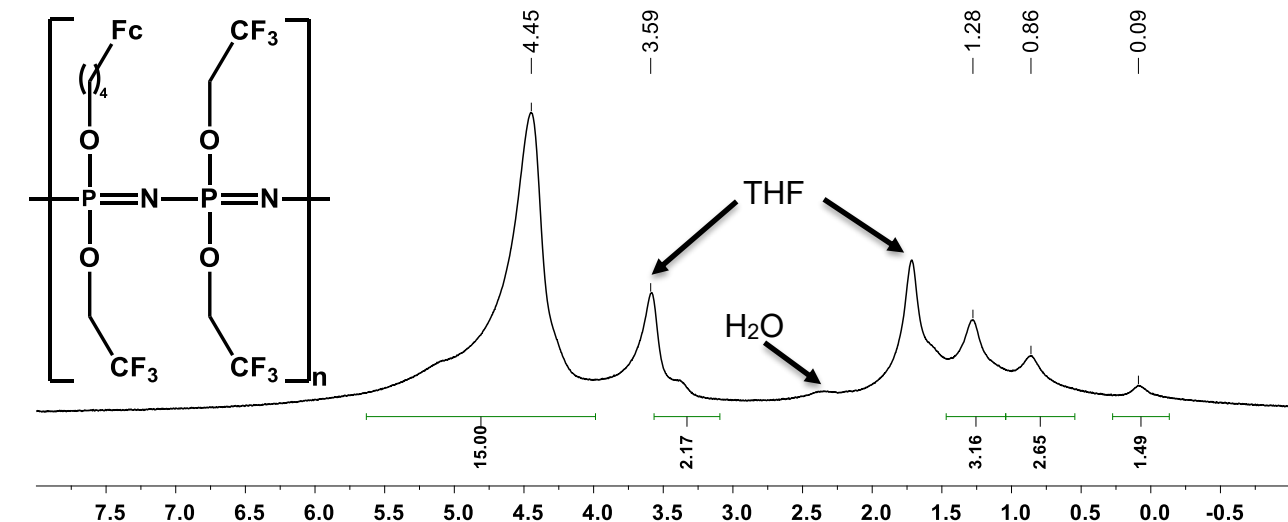
Spectrum 34: Poly[*tris*(2,2,2-trifluoroethoxy)(ferrocenylethoxy)phosphazene], 23



Spectrum 35: Poly[*tris*(2,2,2-trifluoroethoxy)(ferrocenylpropoxy)phosphazene], 24

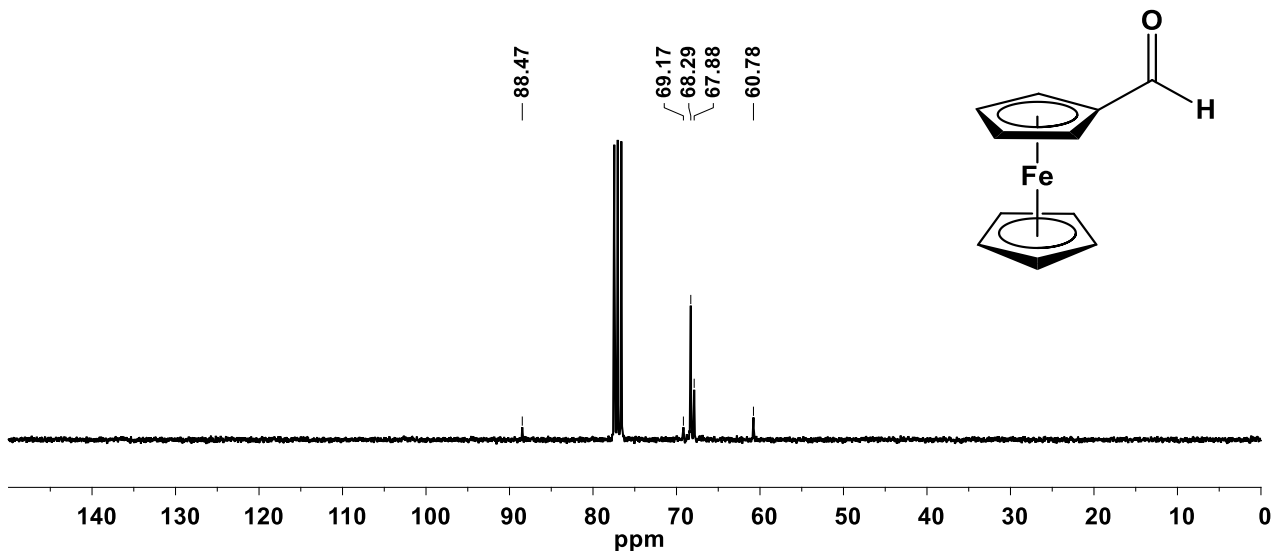


Spectrum 36: Poly[*tris*(2,2,2-trifluoroethoxy)(ferrocenylbutoxy)phosphazene], 25

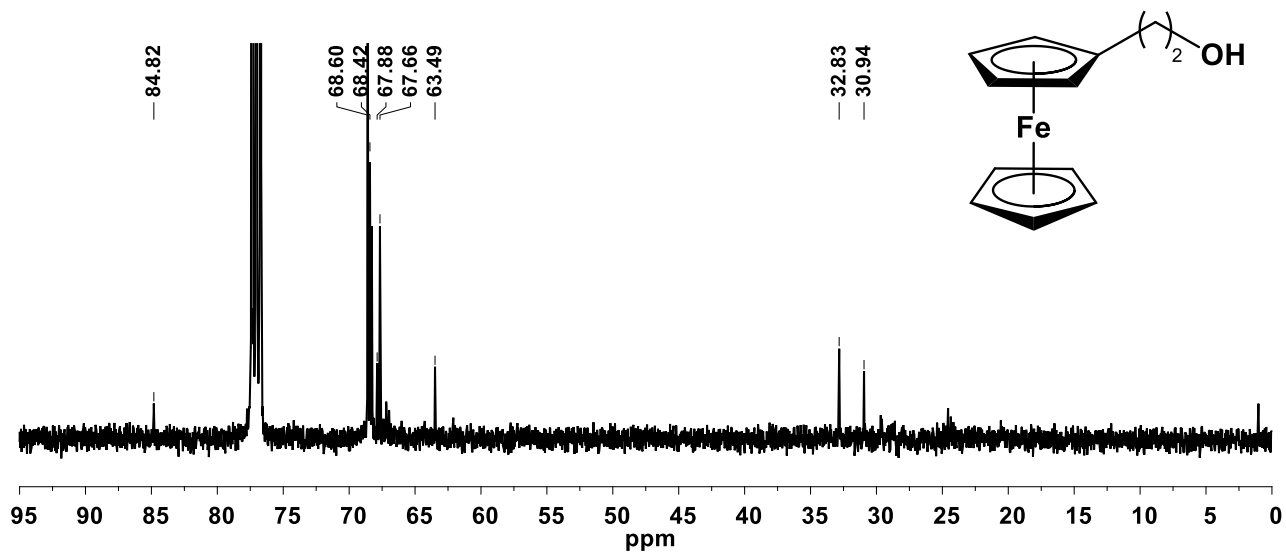


¹³C NMR Spectra

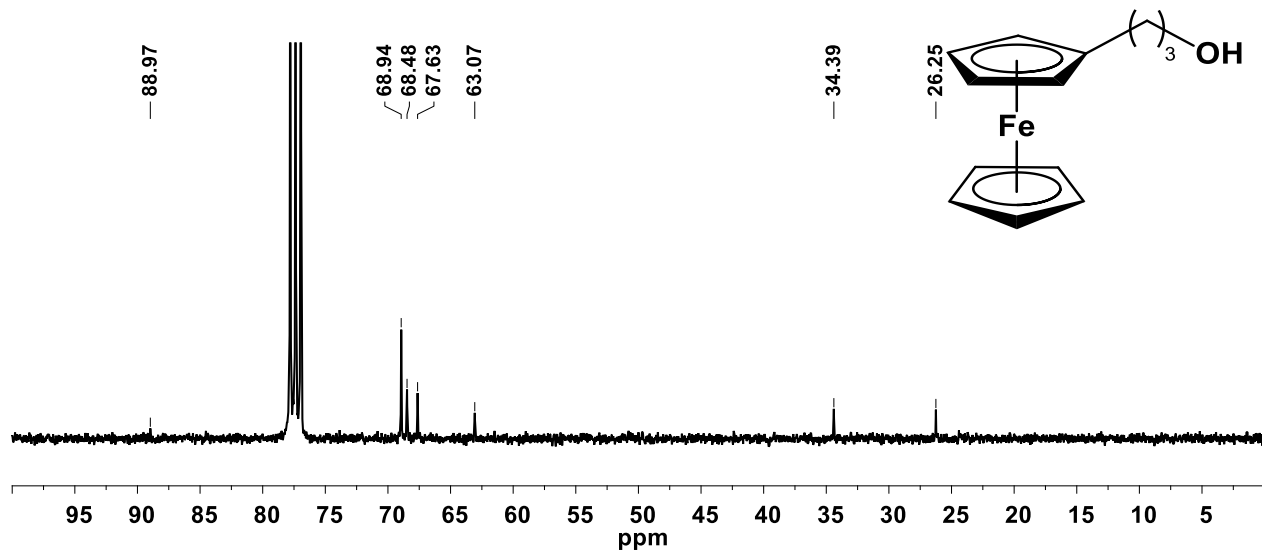
Spectrum 37: 1-Ferrocenylmethanol, 3



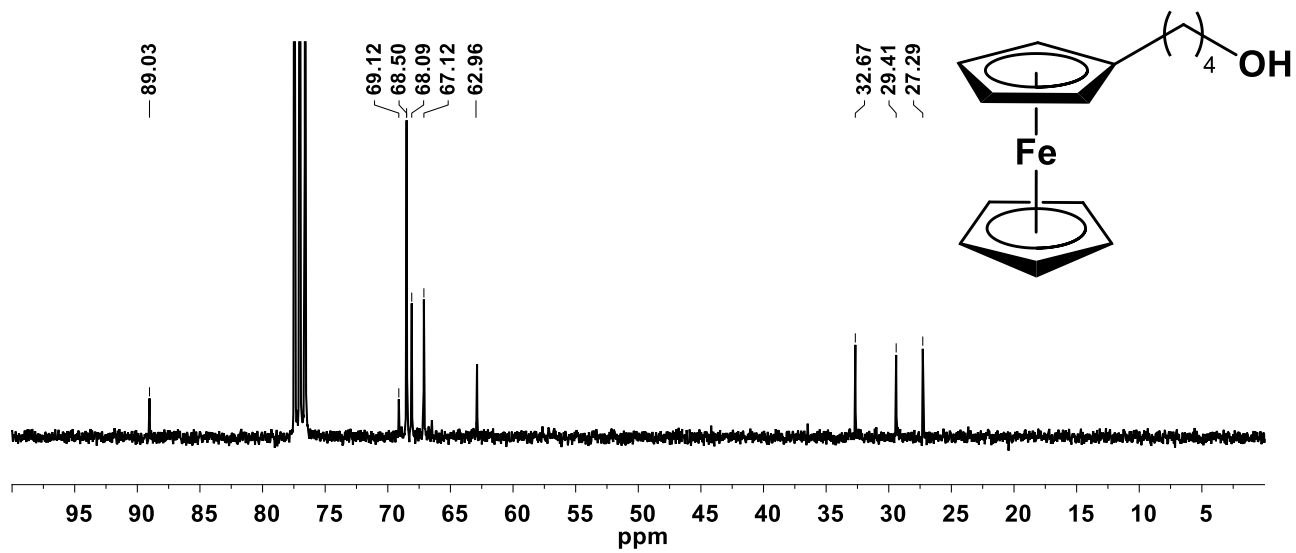
Spectrum 38: 2-Ferrocenylethanol, 9



Spectrum 39: 3-Ferrocenylpropanol, 13

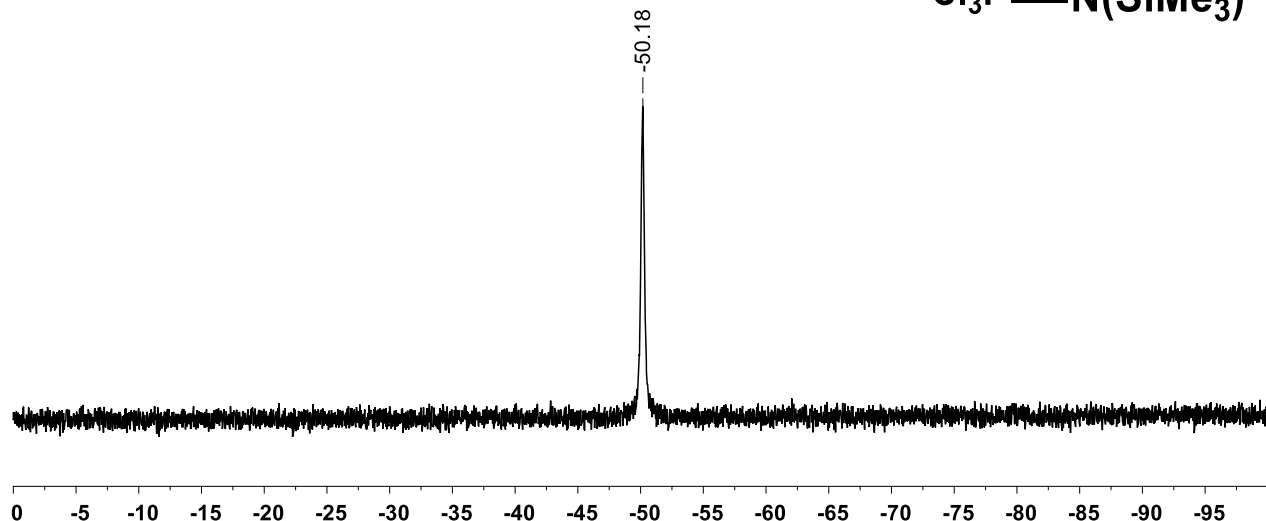


Spectrum 40: 4-Ferrocenylbutanol, 16

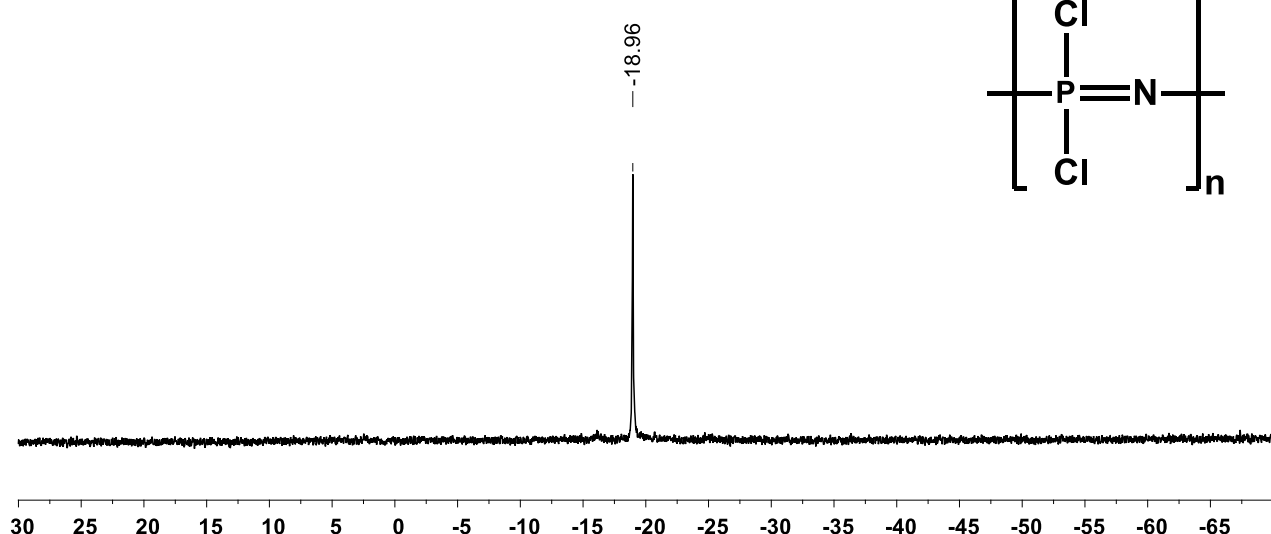
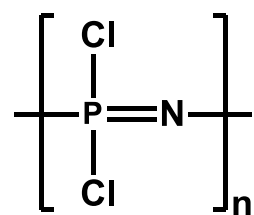


^{31}P NMR Spectra

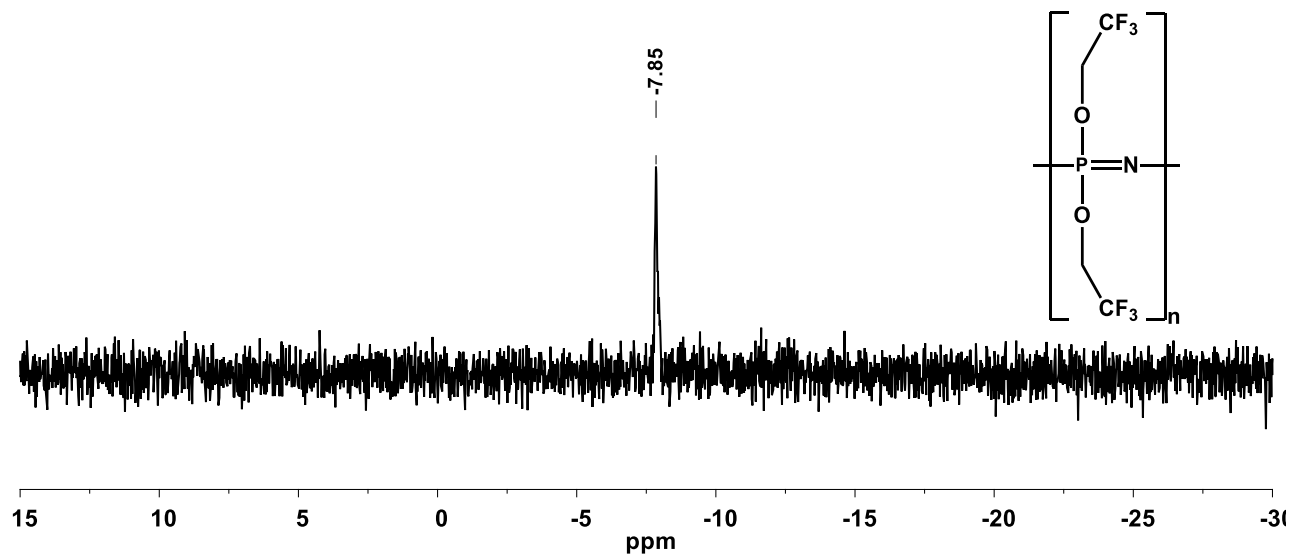
Spectrum 41: Trichloro(trimethylsilyl)phosphoranimine, 19



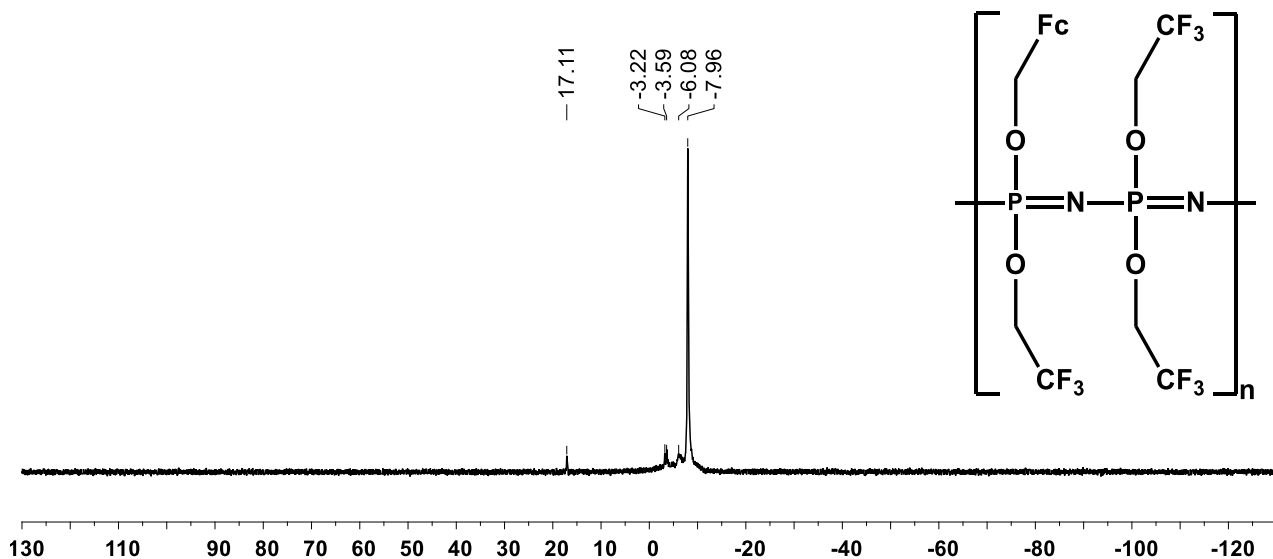
Spectrum 42: Poly(dichlorophosphazene), 20



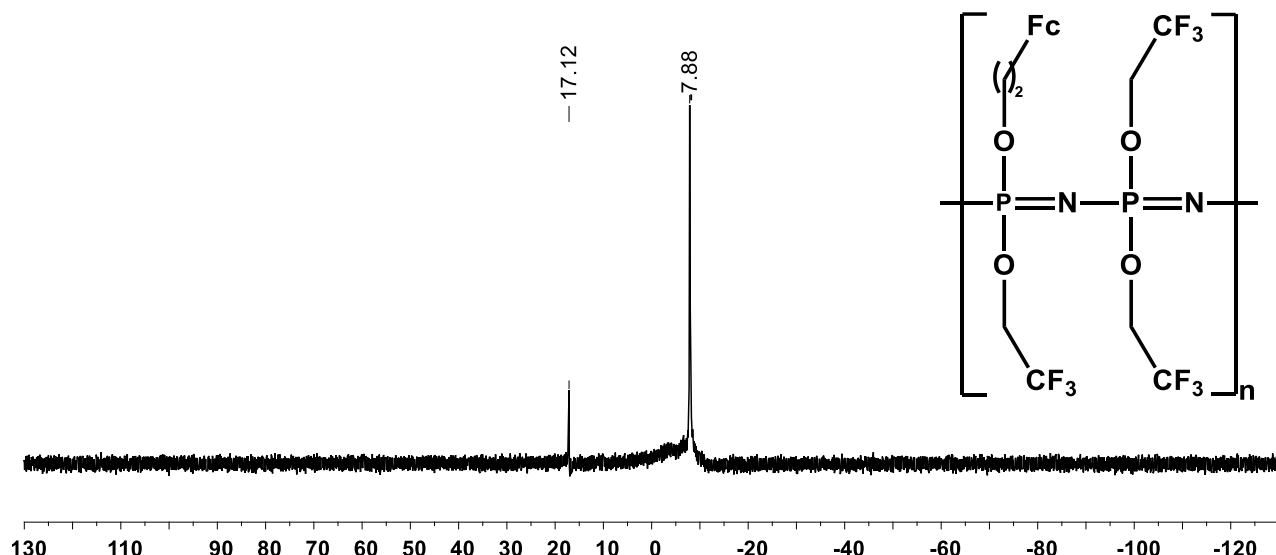
Spectrum 43: Poly[bis(2,2,2-trifluoroethoxy)phosphazene], 21



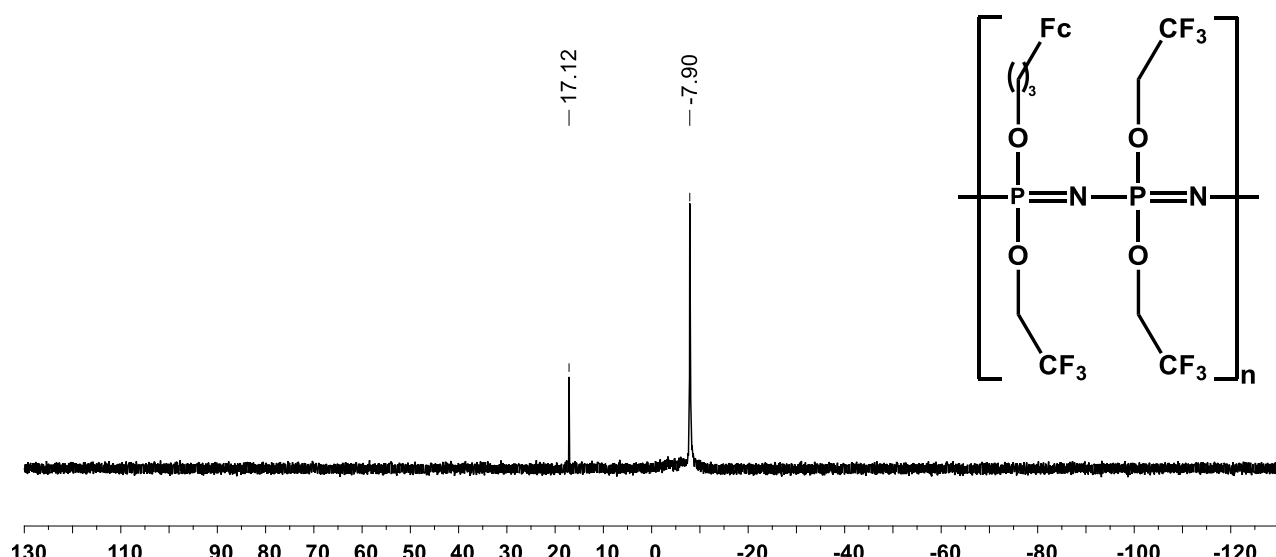
Spectrum 44: Poly[tris(2,2,2-trifluoroethoxy)(ferrocenylmethoxy)phosphazene], 22



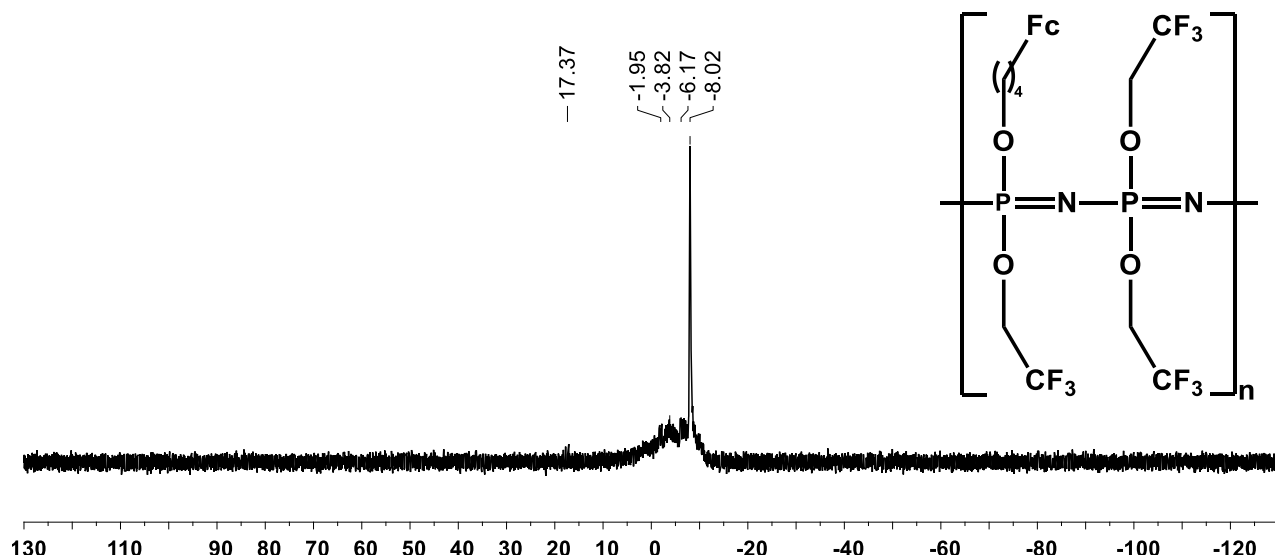
Spectrum 45: Poly[tris(2,2,2-trifluoroethoxy)(ferroncenylethoxy)phosphazene], 23



Spectrum 46: Poly[tris(2,2,2-trifluoroethoxy)(ferrocenylpropoxy)phosphazene], 24

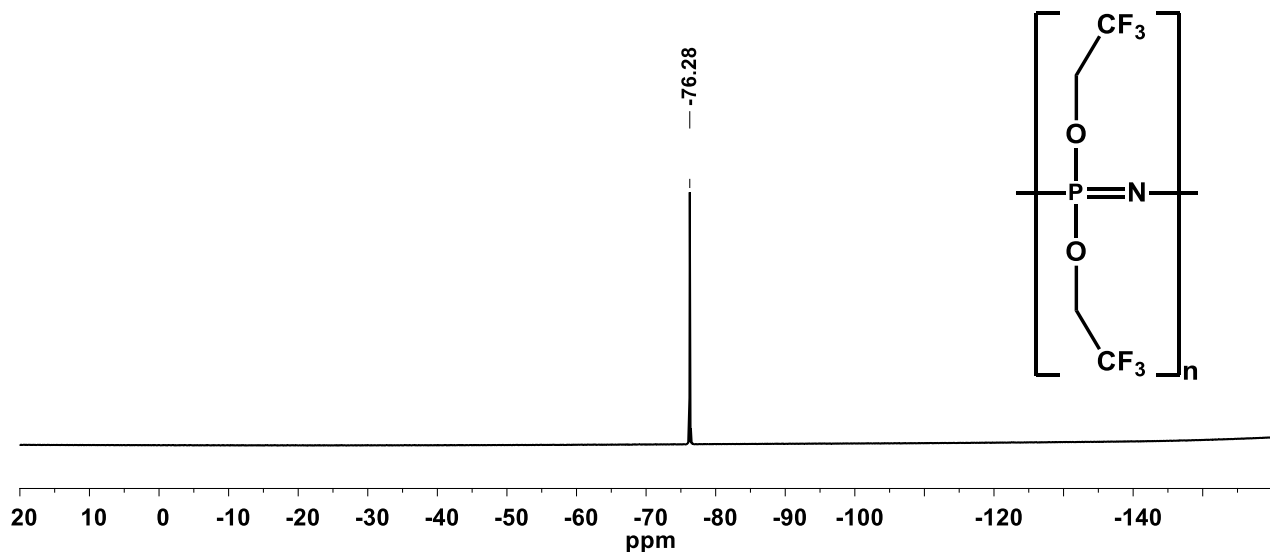


Spectrum 47: Poly[*tris*(2,2,2-trifluoroethoxy)(ferrocenylbutoxy)phosphazene], 25

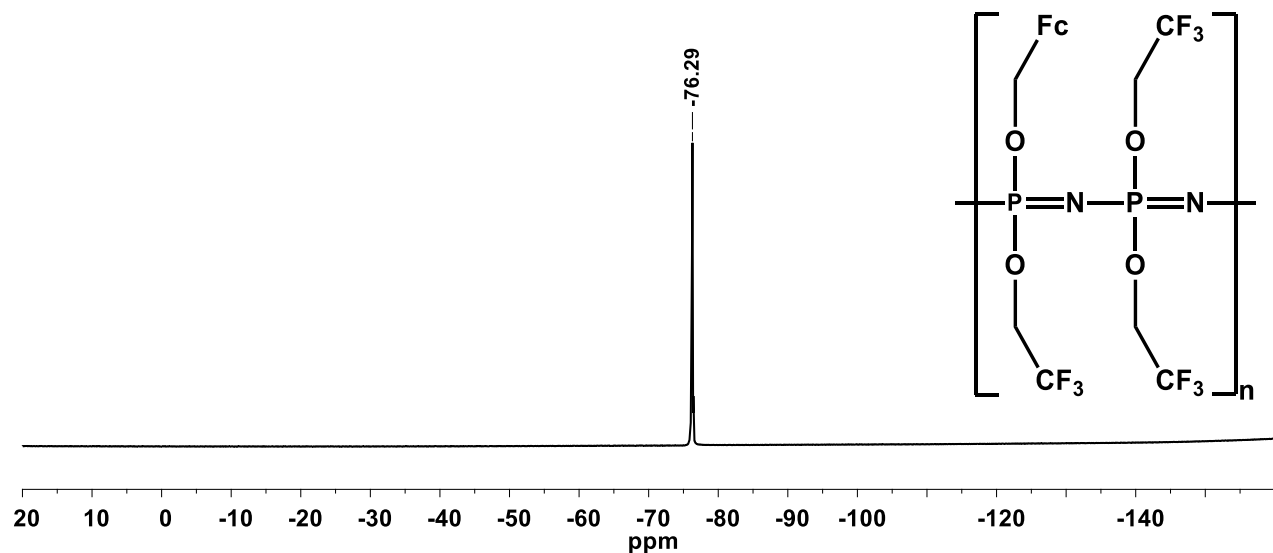


^{19}F NMR Spectra

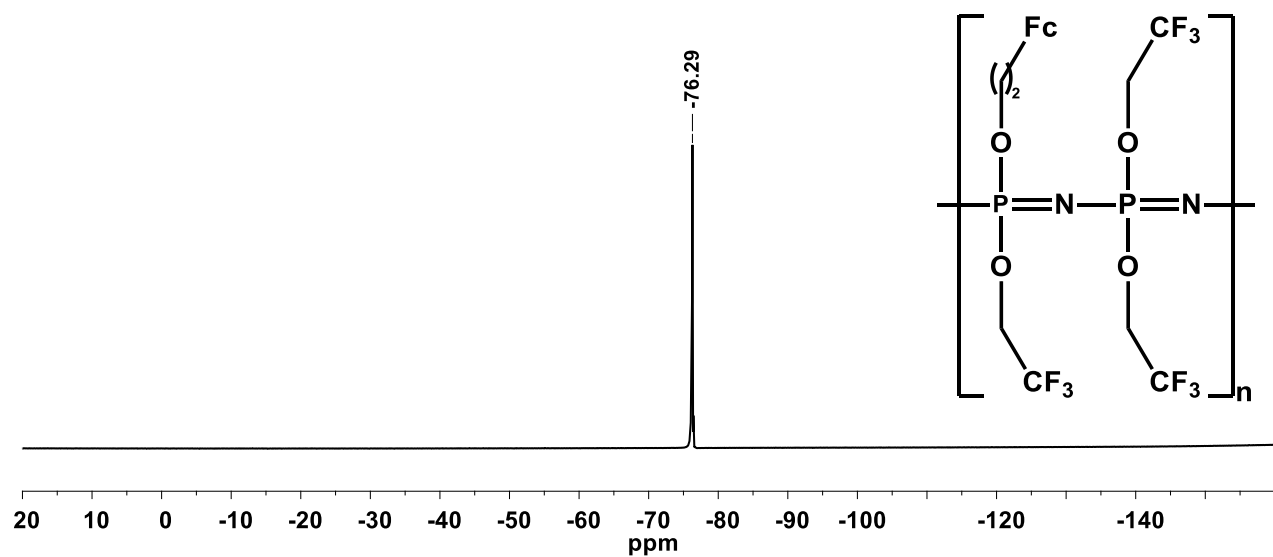
Spectrum 48: Poly[*bis*(2,2,2-trifluoroethoxy)phosphazene], 21



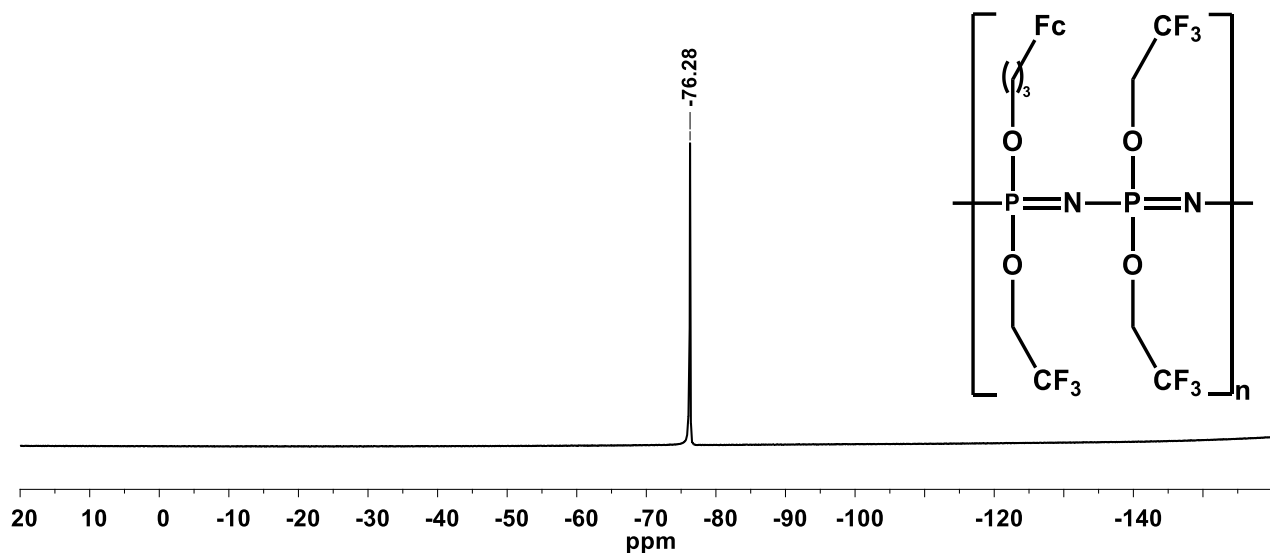
Spectrum 49: Poly[tris(2,2,2-trifluoroethoxy)(ferrocenylmethoxy)phosphazene], 22



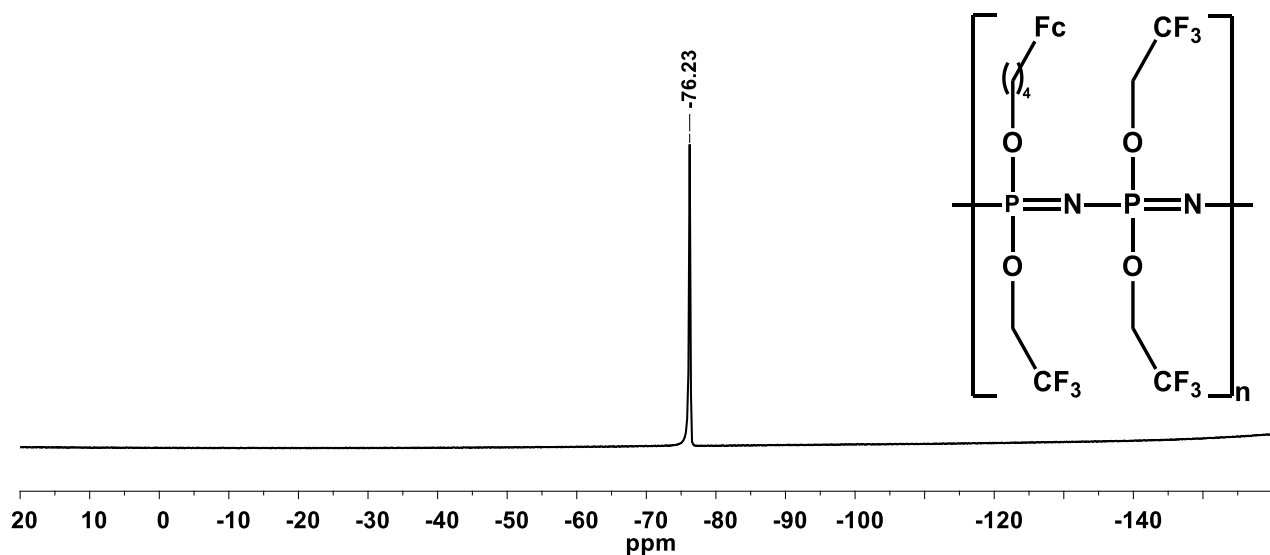
Spectrum 50: Poly[tris(2,2,2-trifluoroethoxy)(ferrocenylethoxy)phosphazene], 23



Spectrum 51: Poly[tris(2,2,2-trifluoroethoxy)(ferrocenylpropoxy)phosphazene], 24

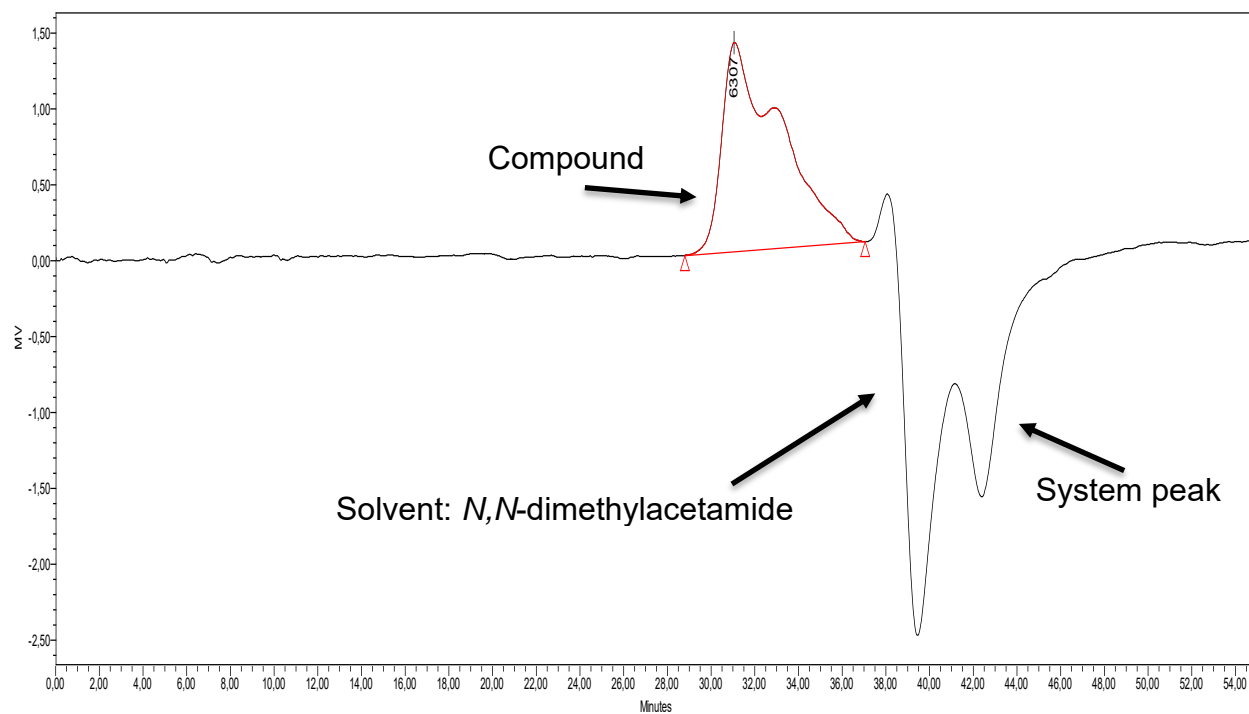


Spectrum 52: Poly[tris(2,2,2-trifluoroethoxy)(ferrocenylbutoxy)phosphazene], 25

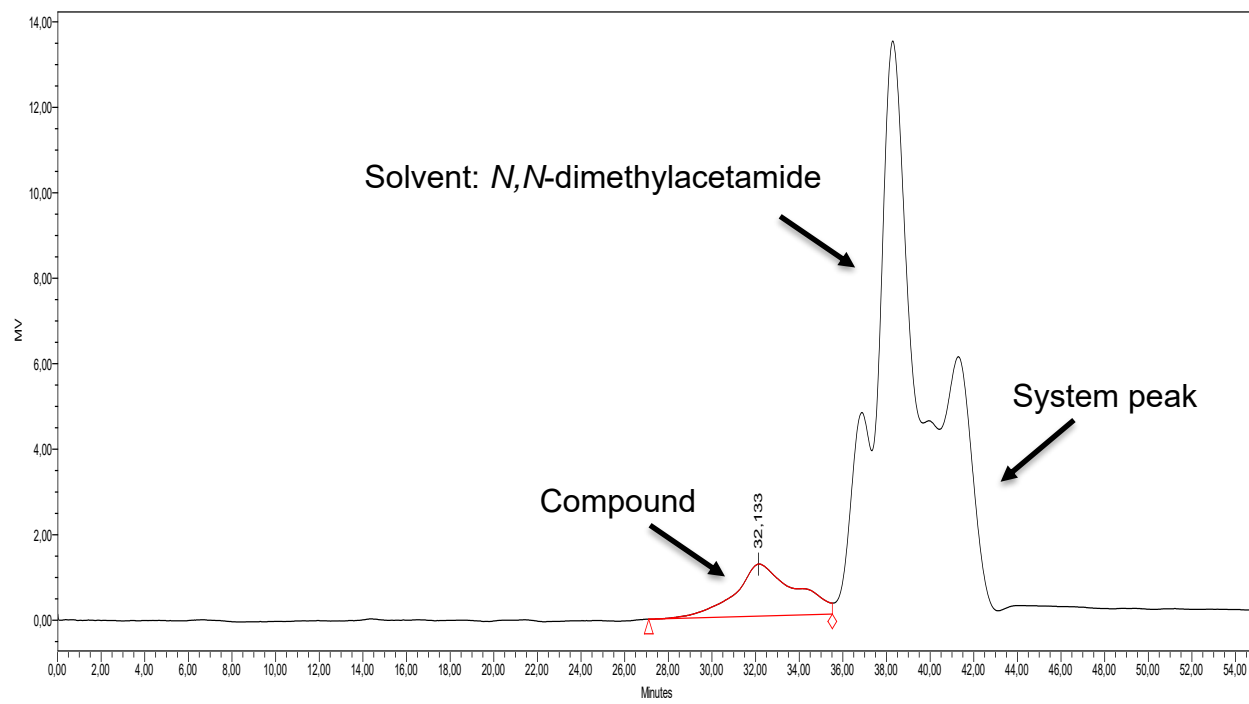


GPC Chromatograms

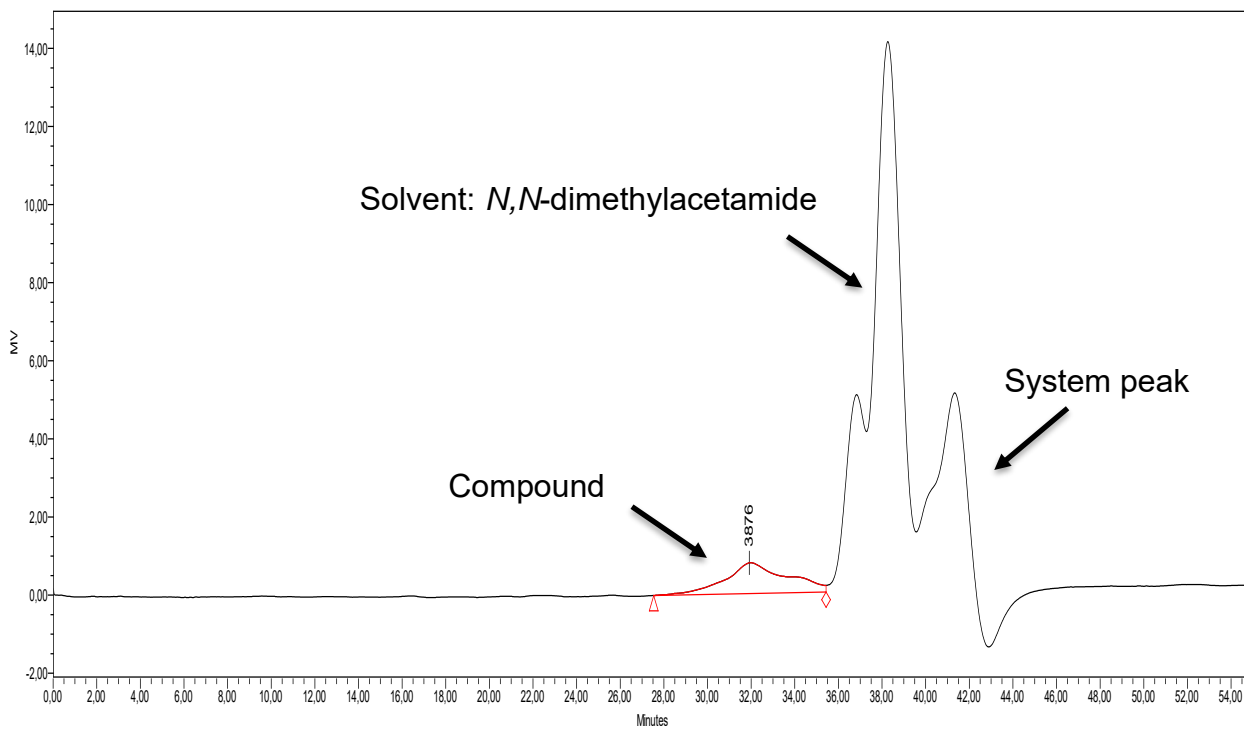
Chromatogram 1: Poly[bis(2,2,2-trifluoroethoxy)phosphazene], 21



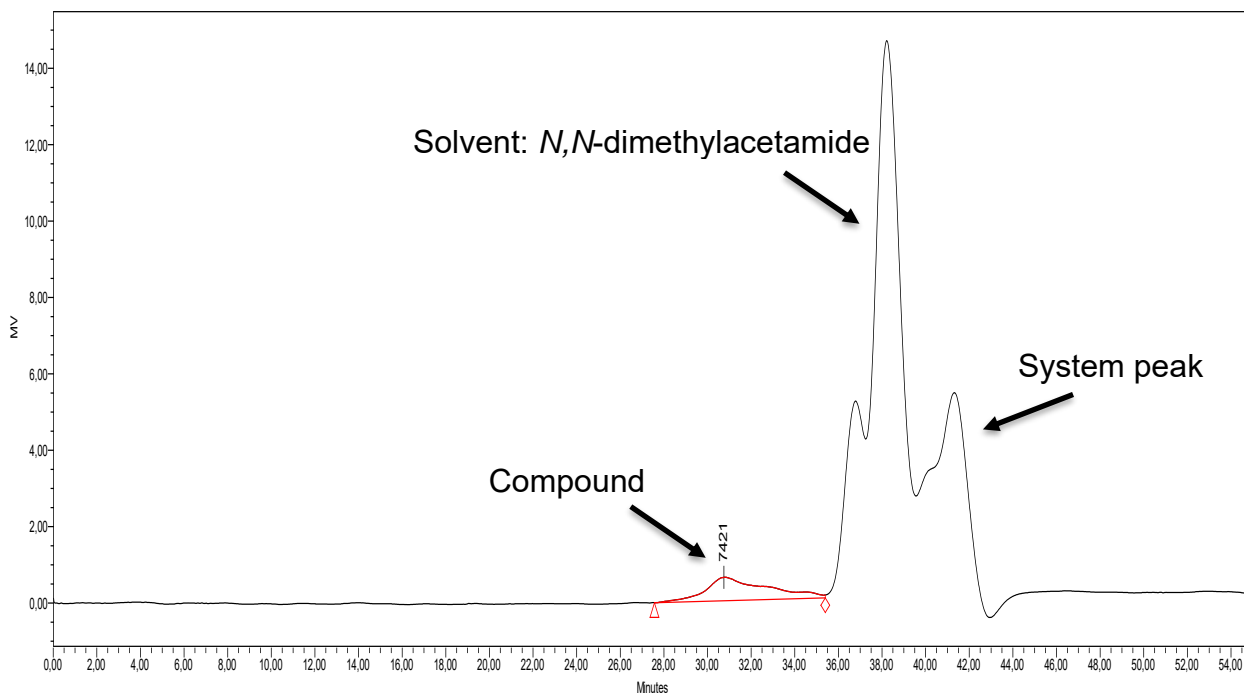
Chromatogram 2: Poly[tris(2,2,2-trifluoroethoxy)(ferrocenylmethoxy)phosphazene], 22



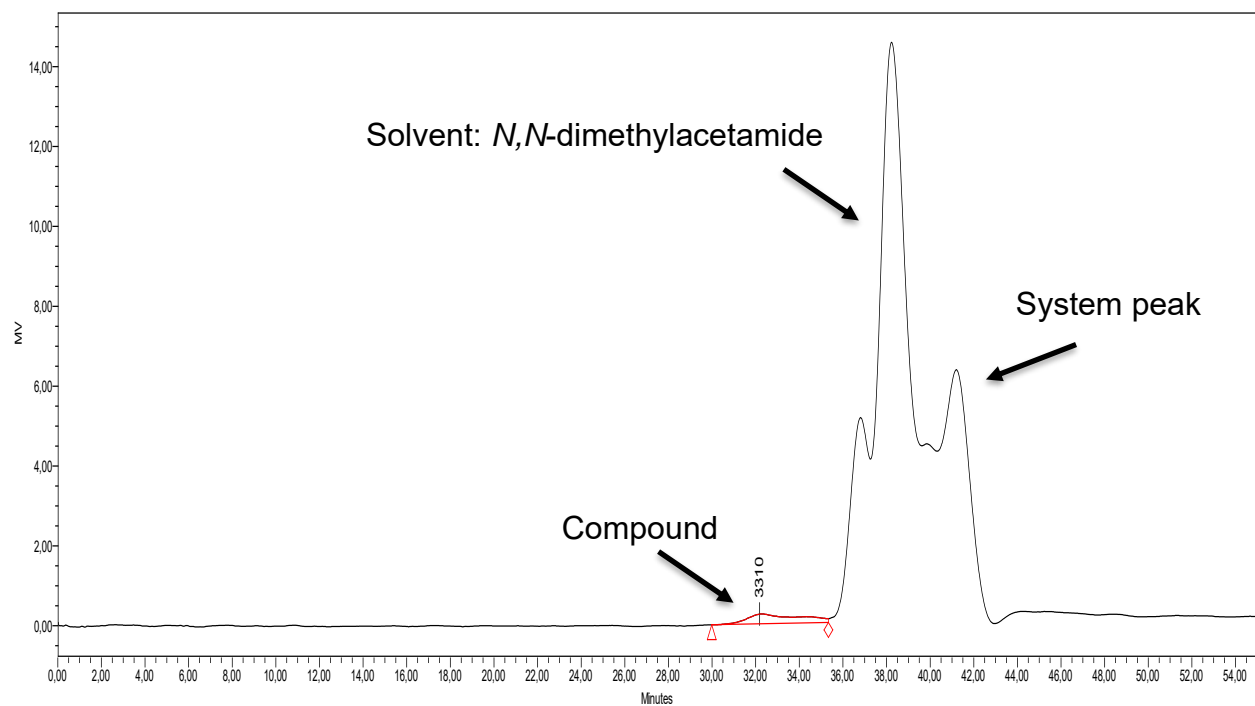
Chromatogram 3: Poly[tris(2,2,2-trifluoroethoxy)(ferrocenylethoxy)phosphazene], 23



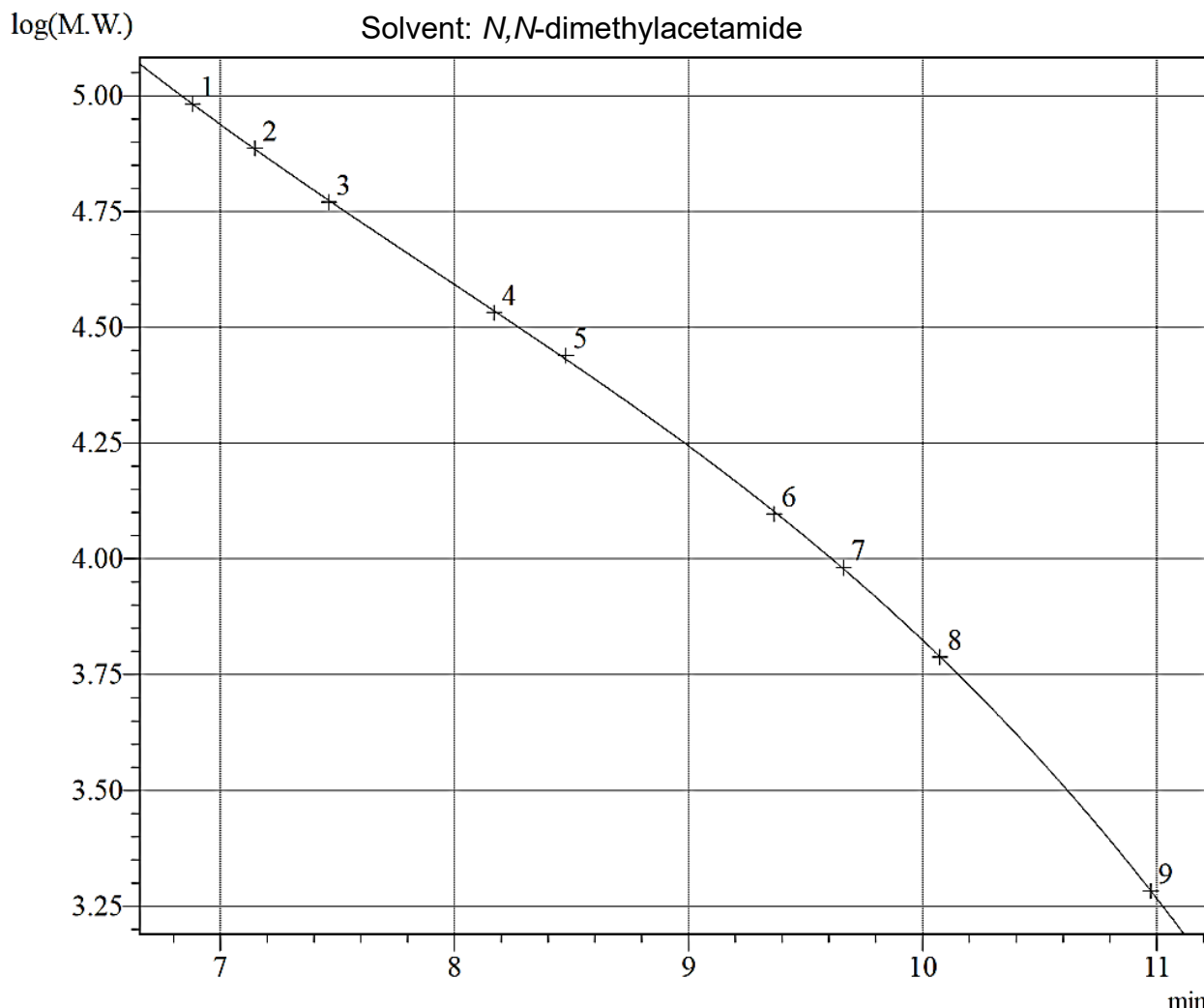
Chromatogram 4: Poly[tris(2,2,2-trifluoroethoxy)(ferrocenylpropoxy)phosphazene], 24



Chromatogram 5: Poly[tris(2,2,2-trifluoroethoxy)(ferrocenylbutoxy)phosphazene], 25

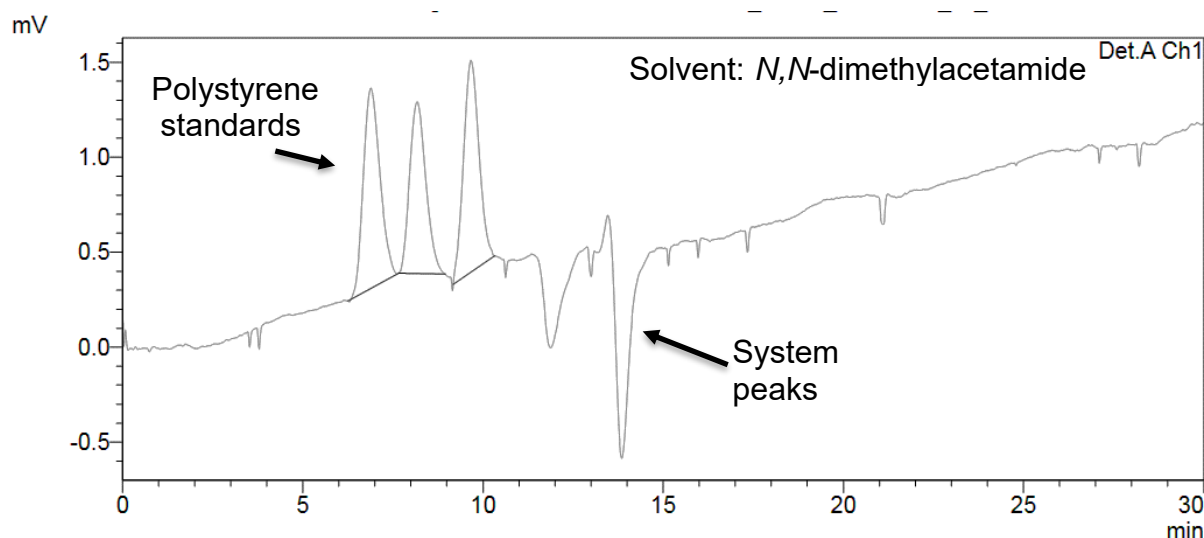
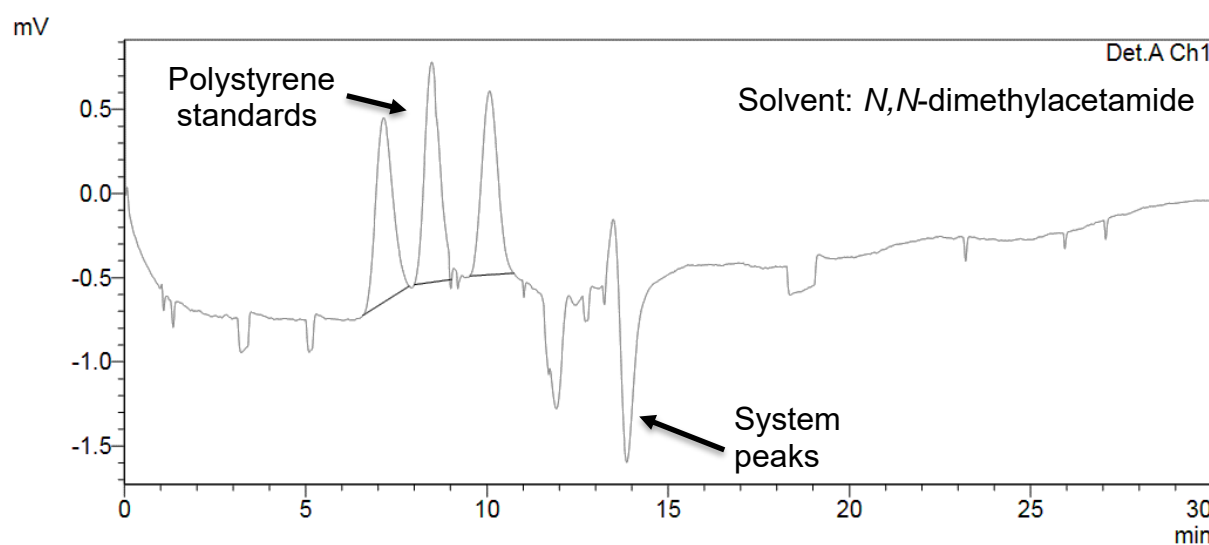
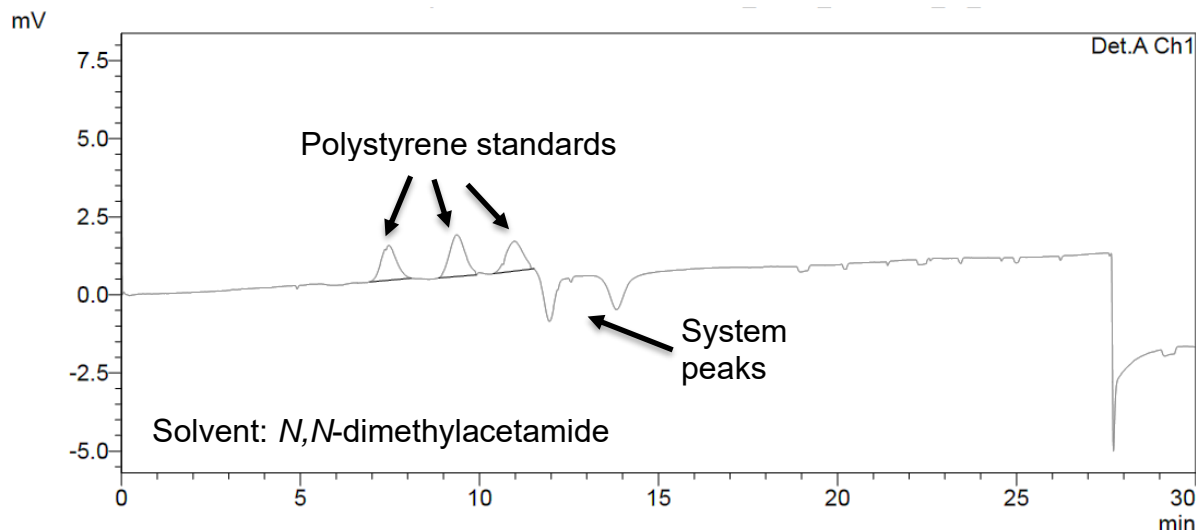


GPC Calibration Curve

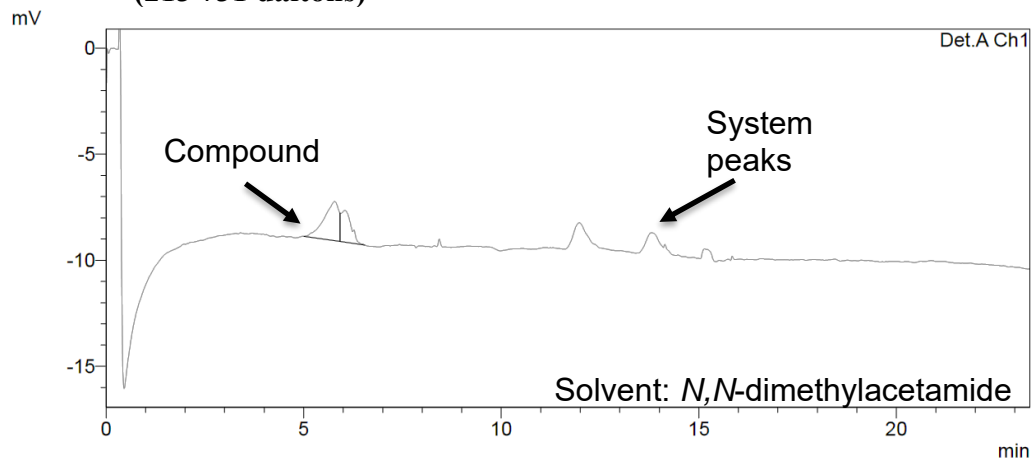


| # | Time(min) | Molecular Weight | Error(%) | Active | Virtual |
|---|-----------|------------------|----------|---------|----------|
| 1 | 6.882 | 96000 | 0.0899 | Enabled | Disabled |
| 2 | 7.147 | 77100 | 0.4971 | Enabled | Disabled |
| 3 | 7.463 | 58900 | -0.9456 | Enabled | Disabled |
| 4 | 8.171 | 34000 | -0.8488 | Enabled | Disabled |
| 5 | 8.476 | 27500 | 1.8449 | Enabled | Disabled |
| 6 | 9.365 | 12500 | -1.2765 | Enabled | Disabled |
| 7 | 9.662 | 9580 | 0.7197 | Enabled | Disabled |
| 8 | 10.074 | 6140 | -0.1789 | Enabled | Disabled |
| 9 | 10.975 | 1920 | 0.0607 | Enabled | Disabled |

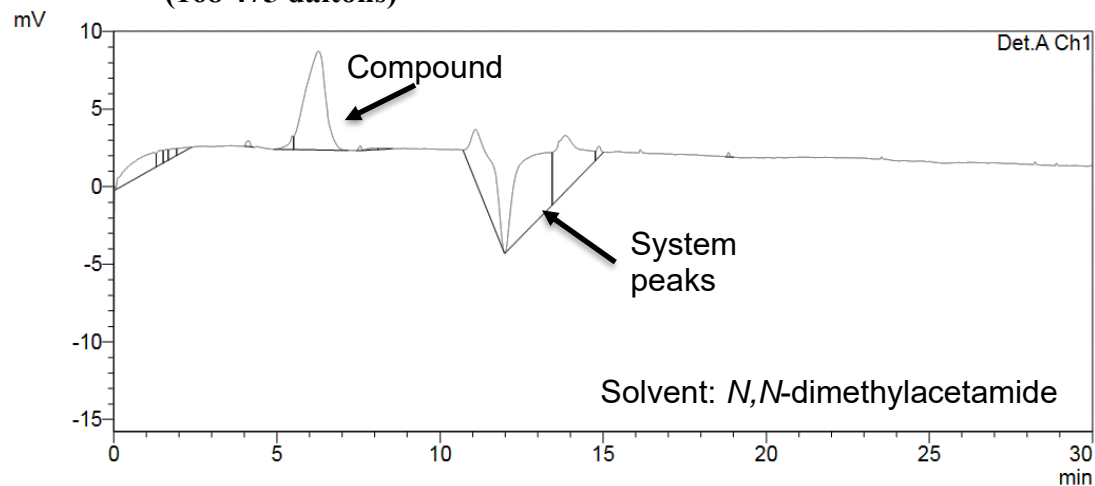
Chromatograms – Polystyrene Standards



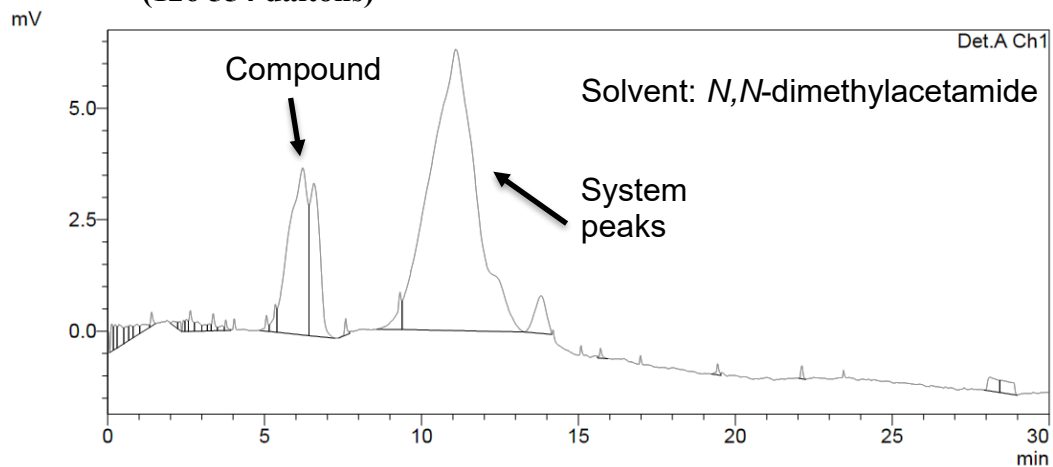
**Chromatogram 6: Poly(2,2,2-trifluoroethoxy)(ferrocenylbutoxy)phosphazene, 25
(213 731 daltons)**



**Chromatogram 7: Poly(2,2,2-trifluoroethoxy)(ferrocenylbutoxy)phosphazene, 25
(168 475 daltons)**

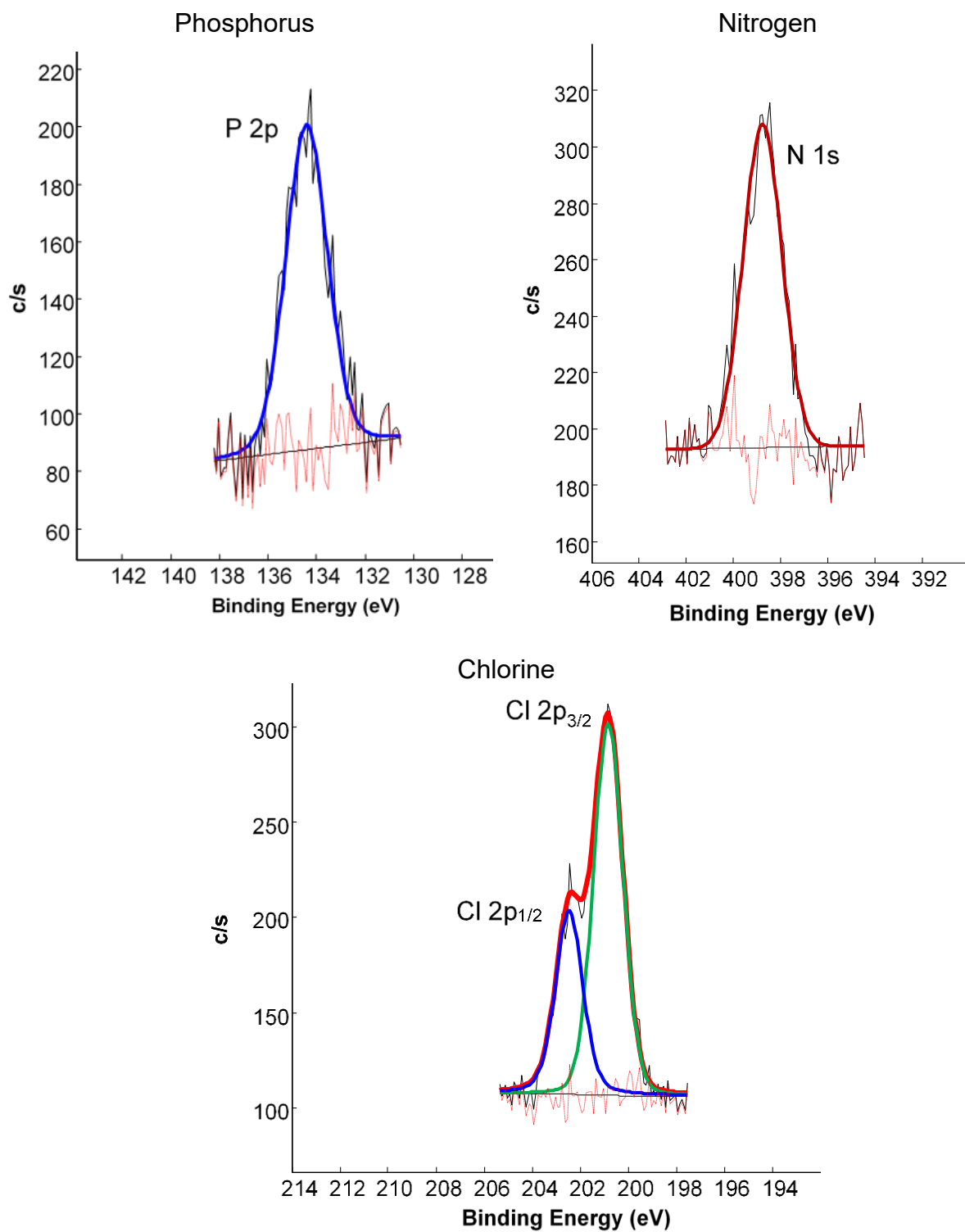


**Chromatogram 8: Poly(2,2,2-trifluoroethoxy)(ferrocenylbutoxy)phosphazene, 25
(126 554 daltons)**

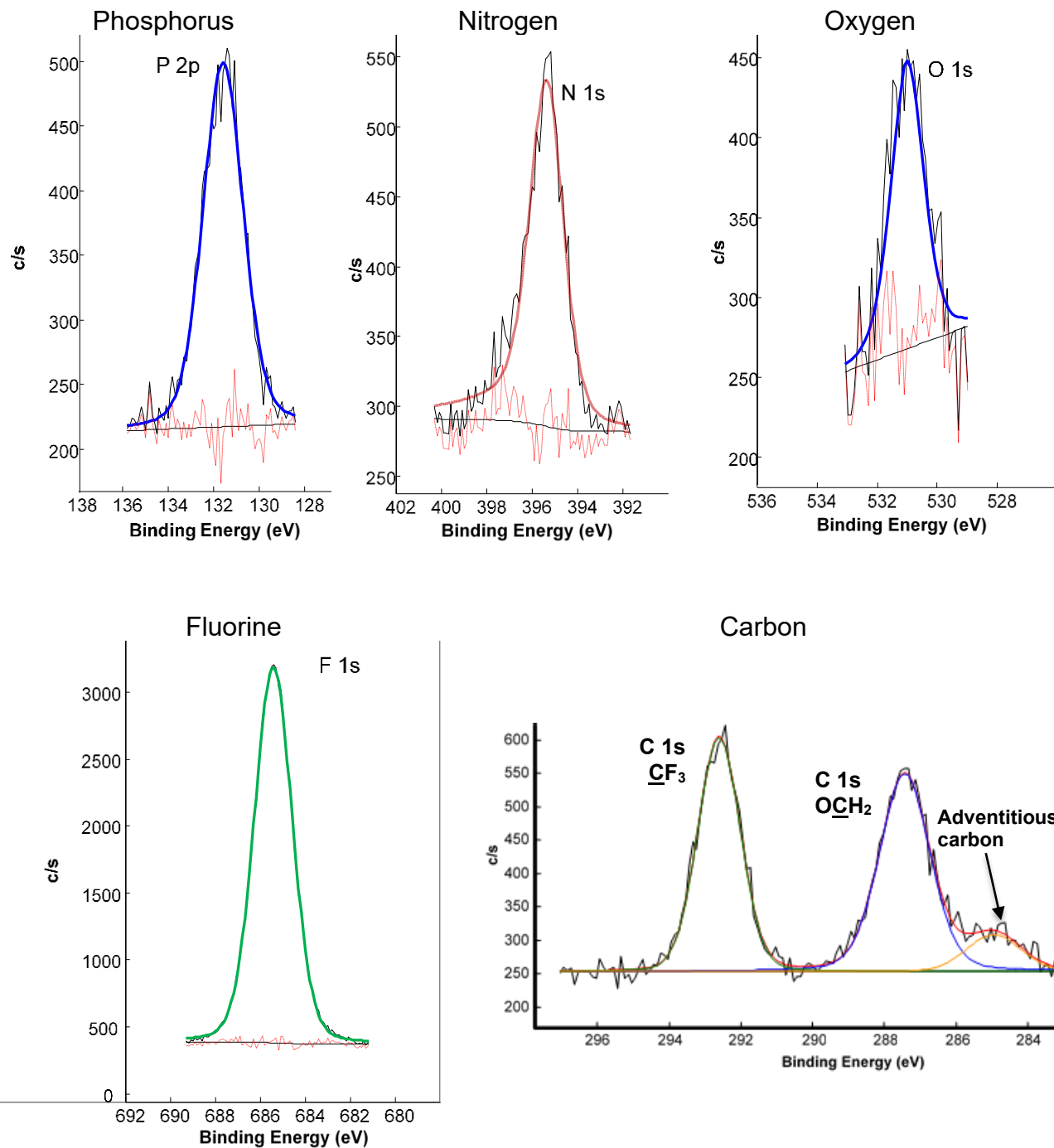


XPS Spectra

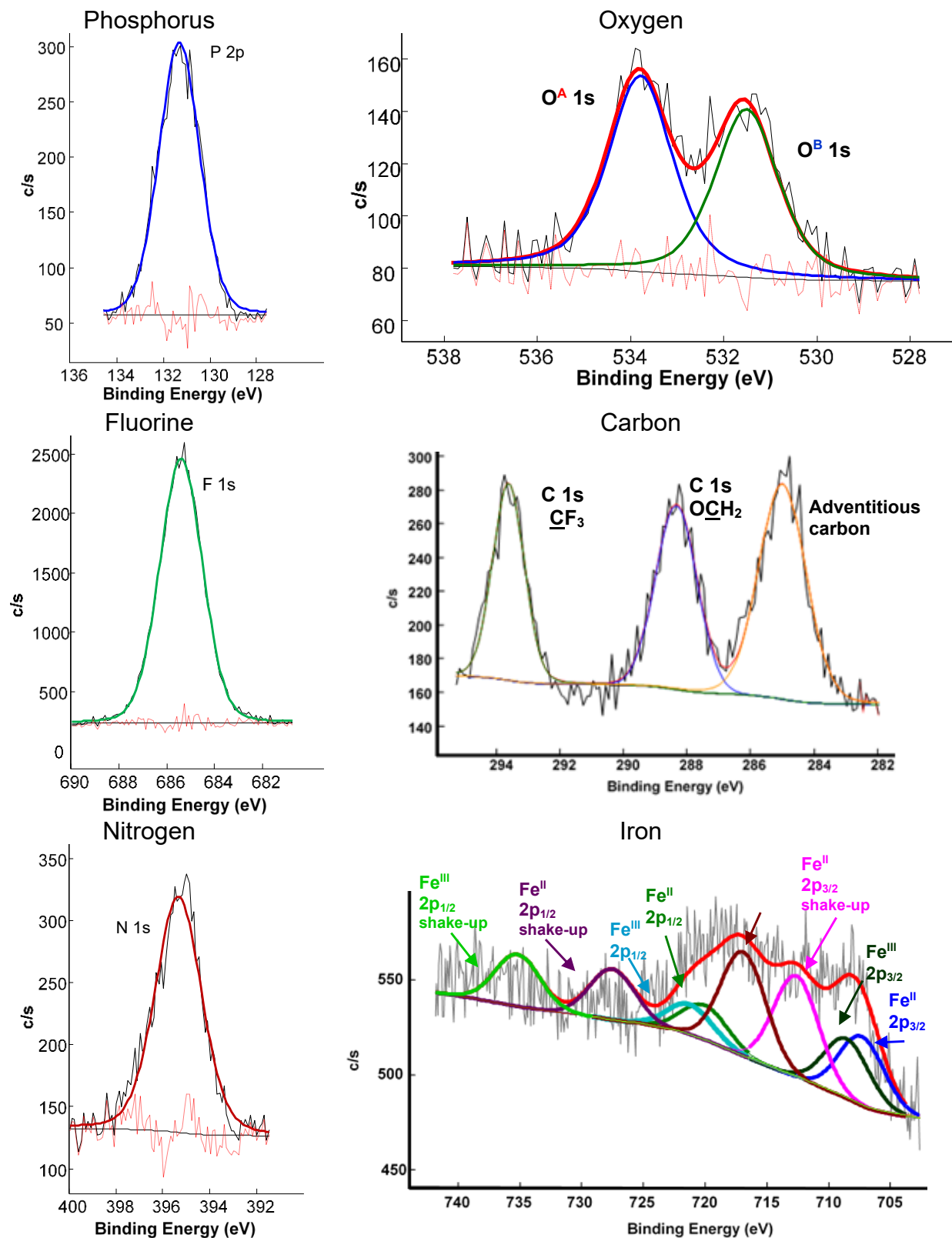
Poly(dichloro)phosphazene, 20



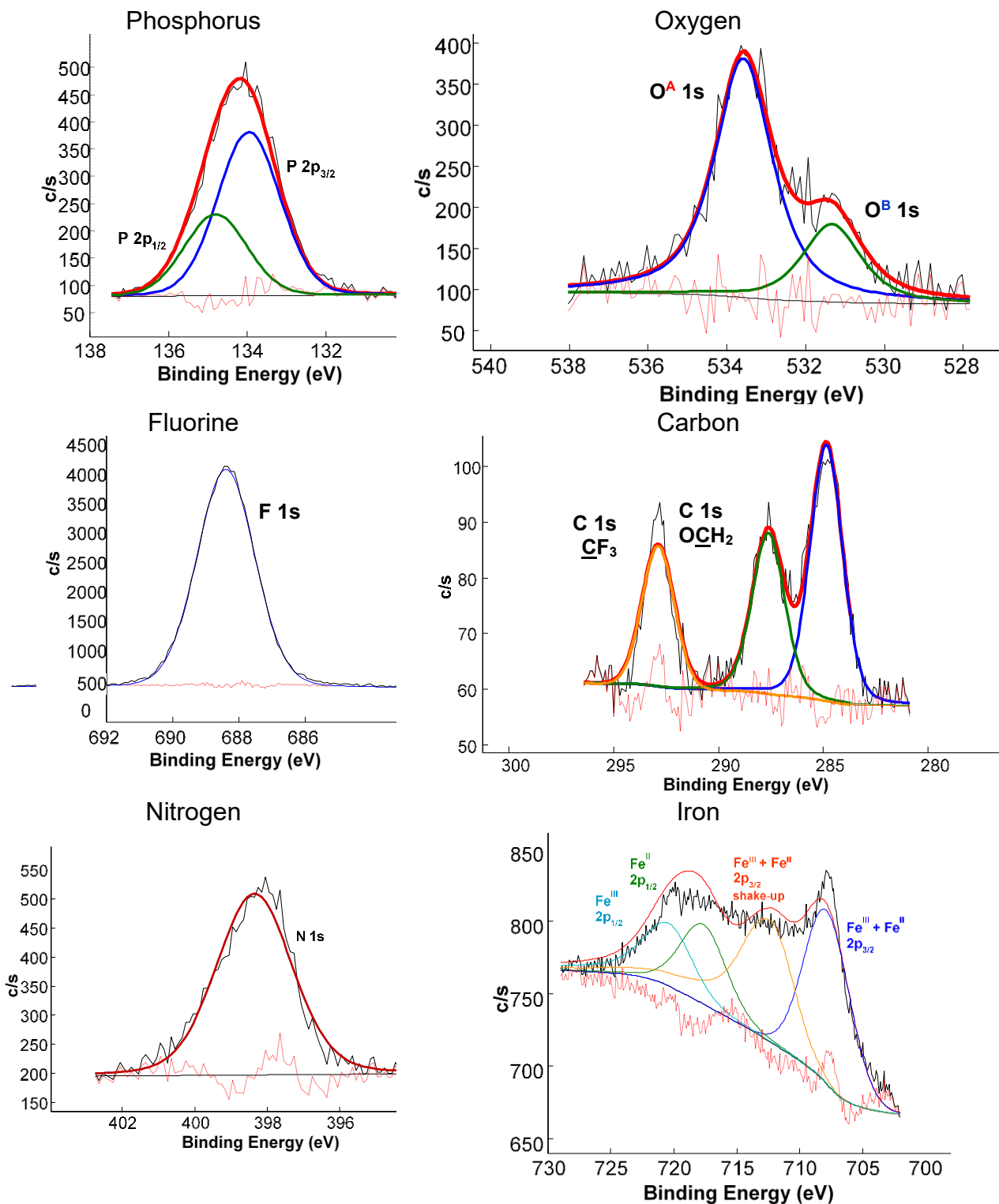
Poly[bis(2,2,2-trifluoroethoxy)phosphazene], 21



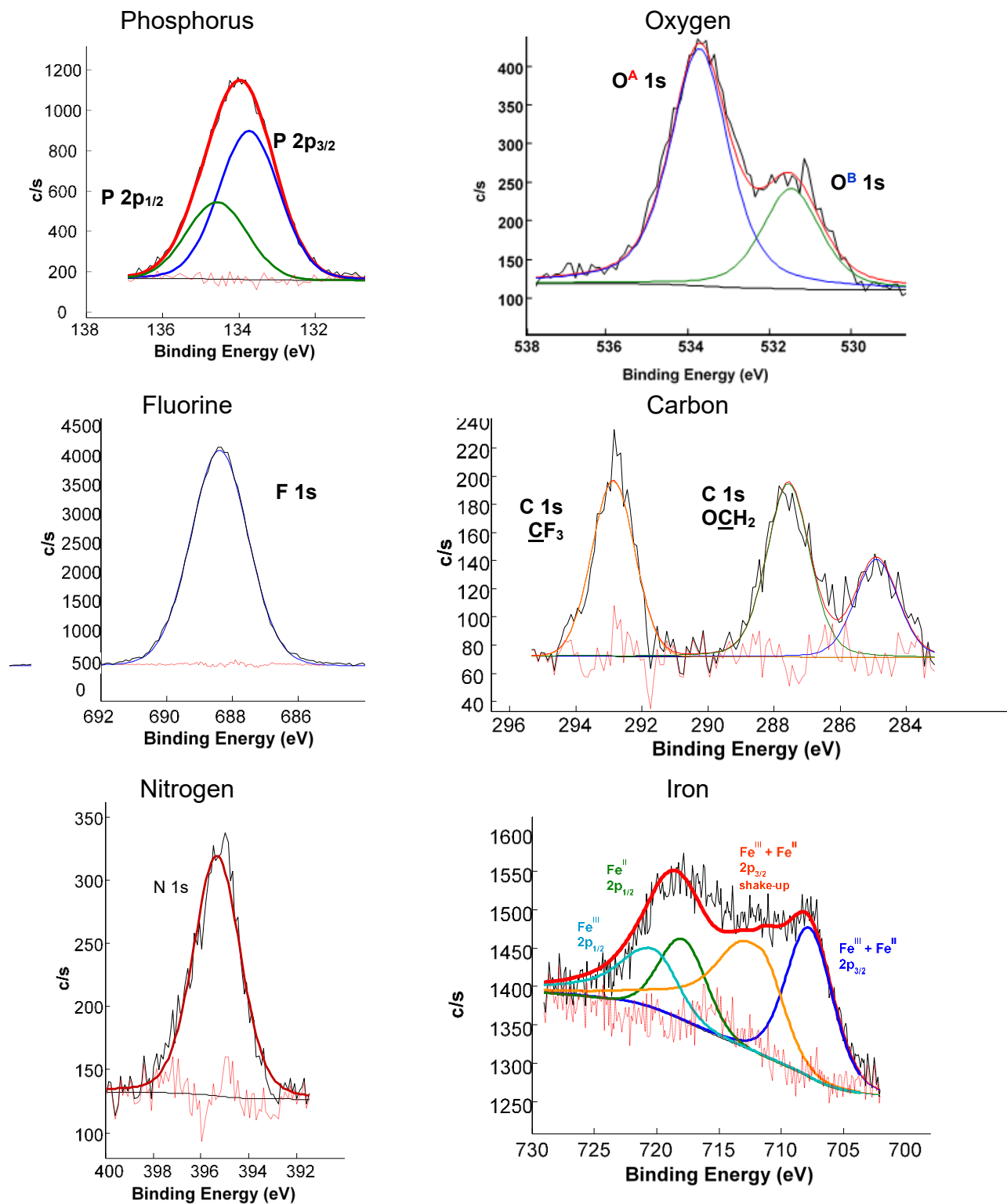
Poly[tris(2,2,2-trifluoroethoxy)(ferrocenylmethoxy)phosphazene], 22



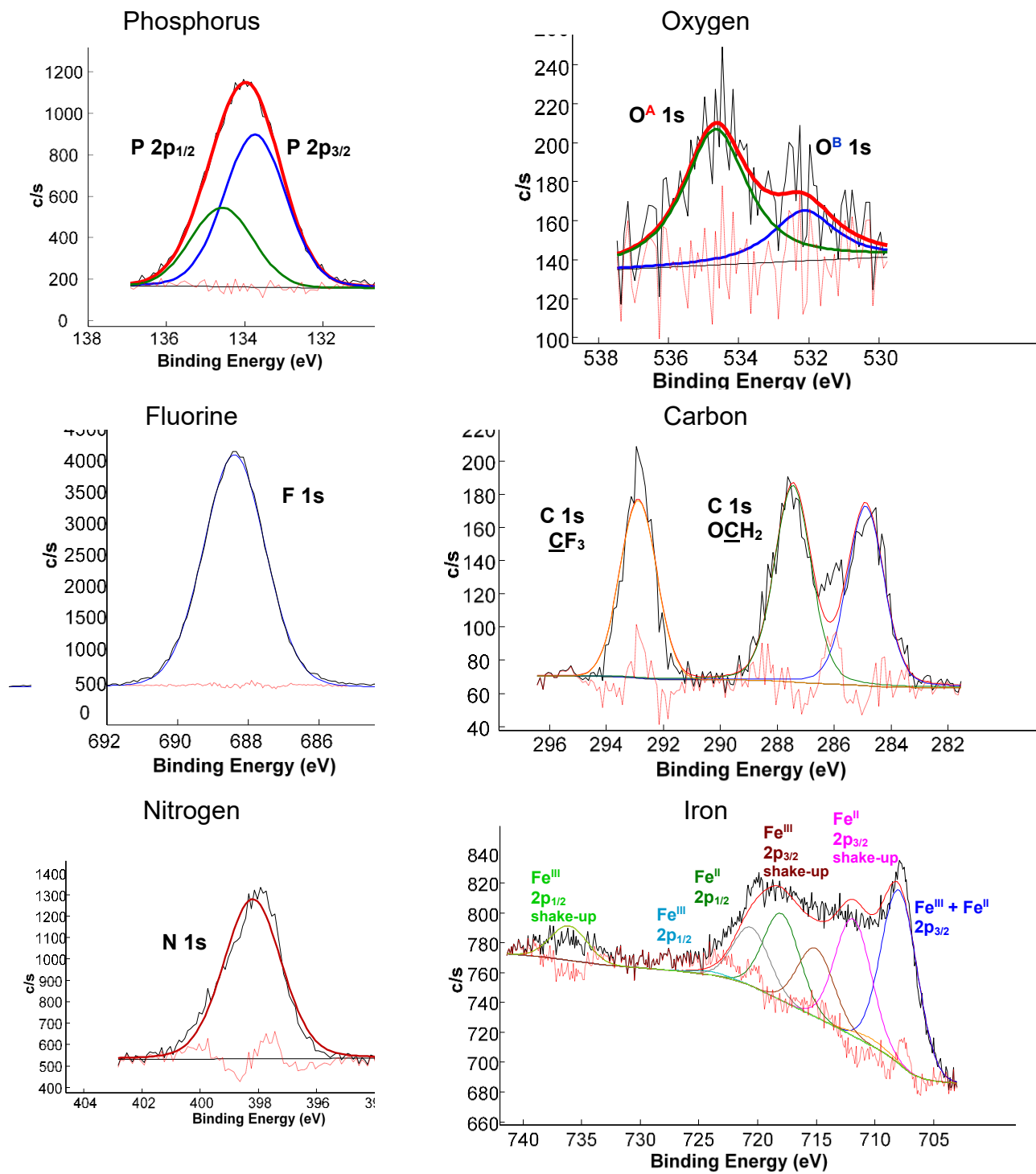
Poly[tris(2,2,2-trifluoroethoxy)(ferrocenylethoxy)phosphazene], 23



Poly[*tris*(2,2,2-trifluoroethoxy)(ferrocenylpropoxy)ferrocene], 24

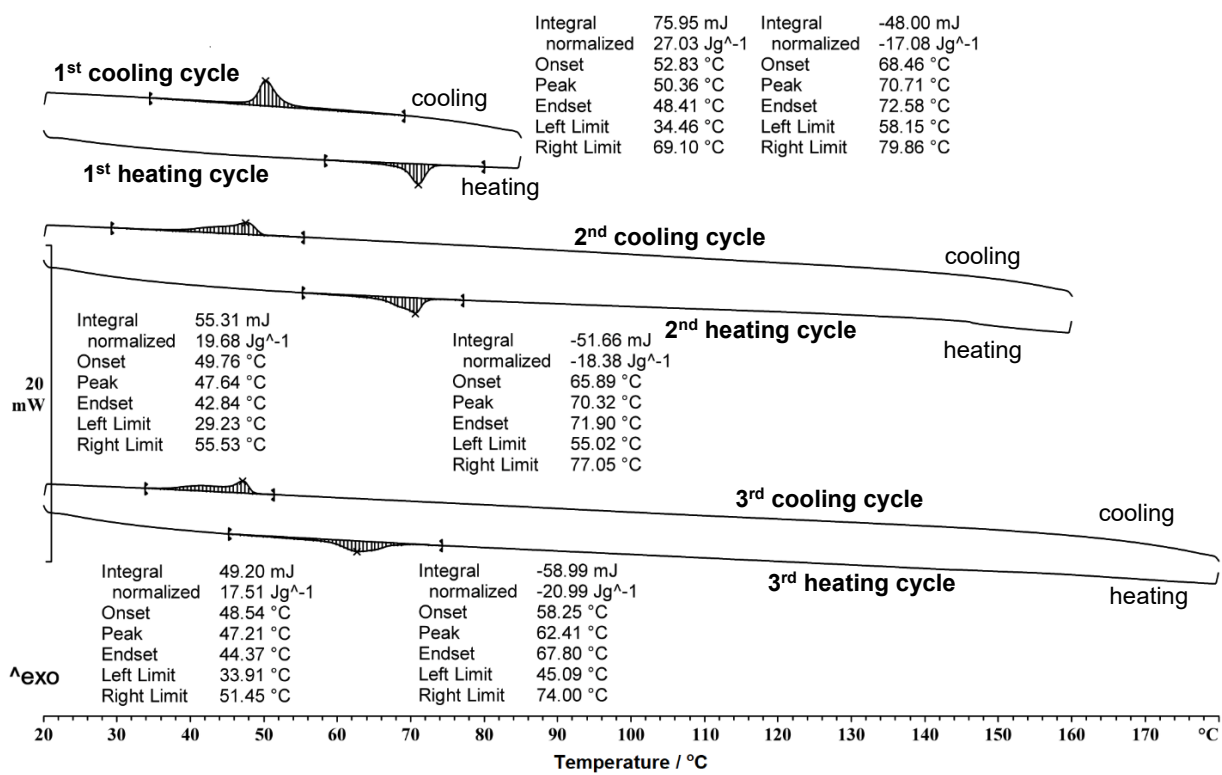


Poly[tris(2,2,2-trifluoroethoxy)(ferrocenylbutoxy)phosphazene], 25

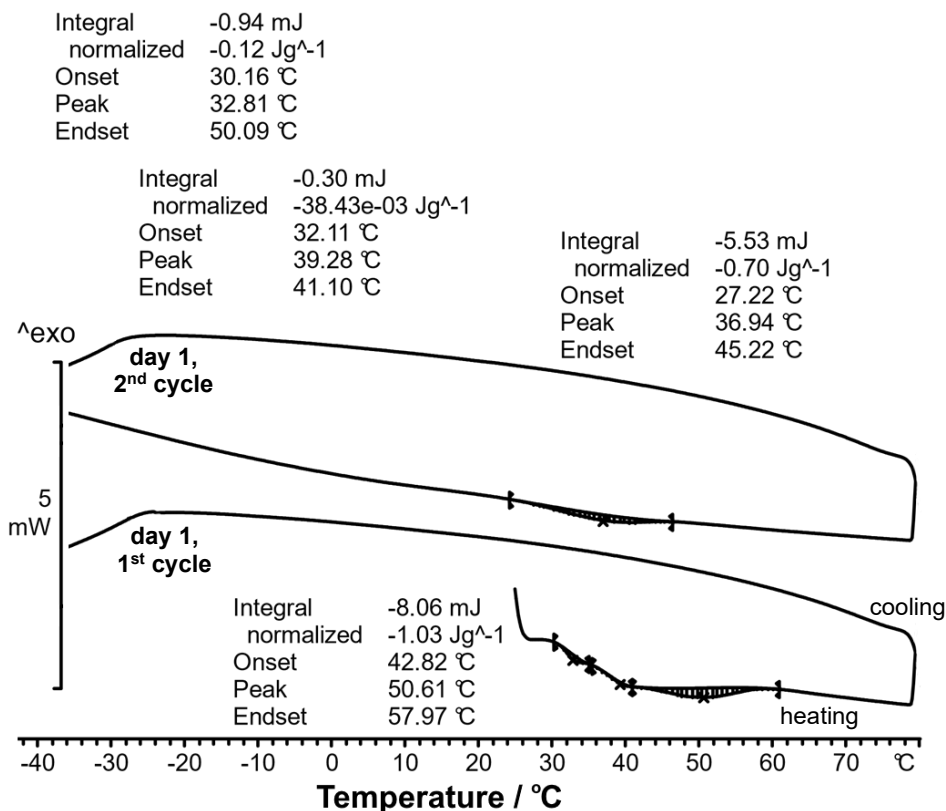


DSC Calorigrams

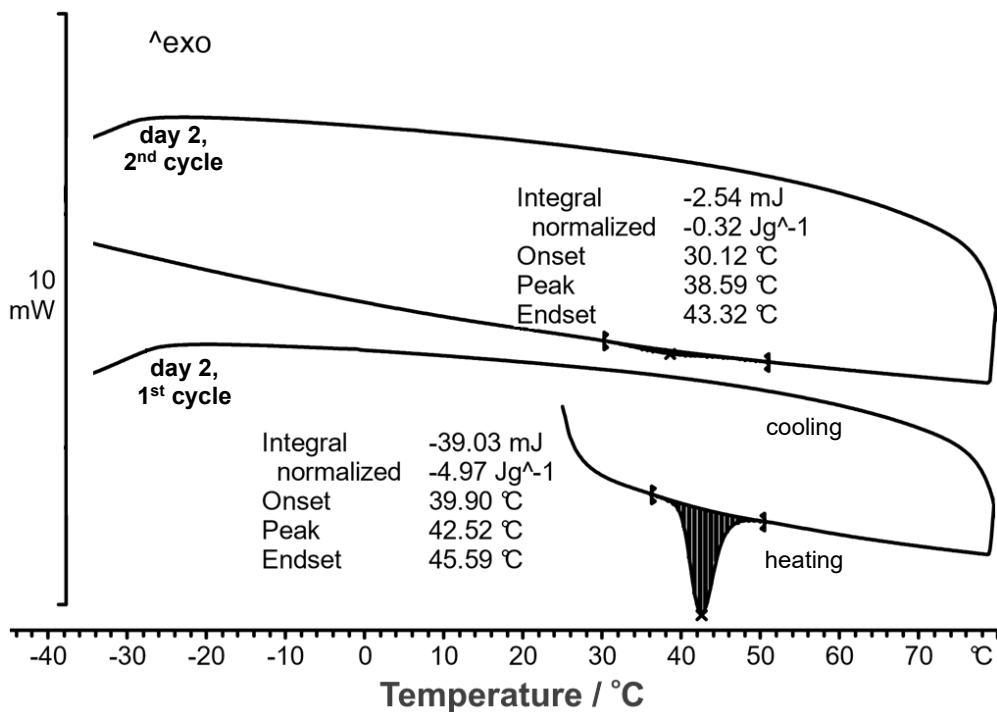
Poly[bis(2,2,2-trifluoroethoxy)phosphazene], 21



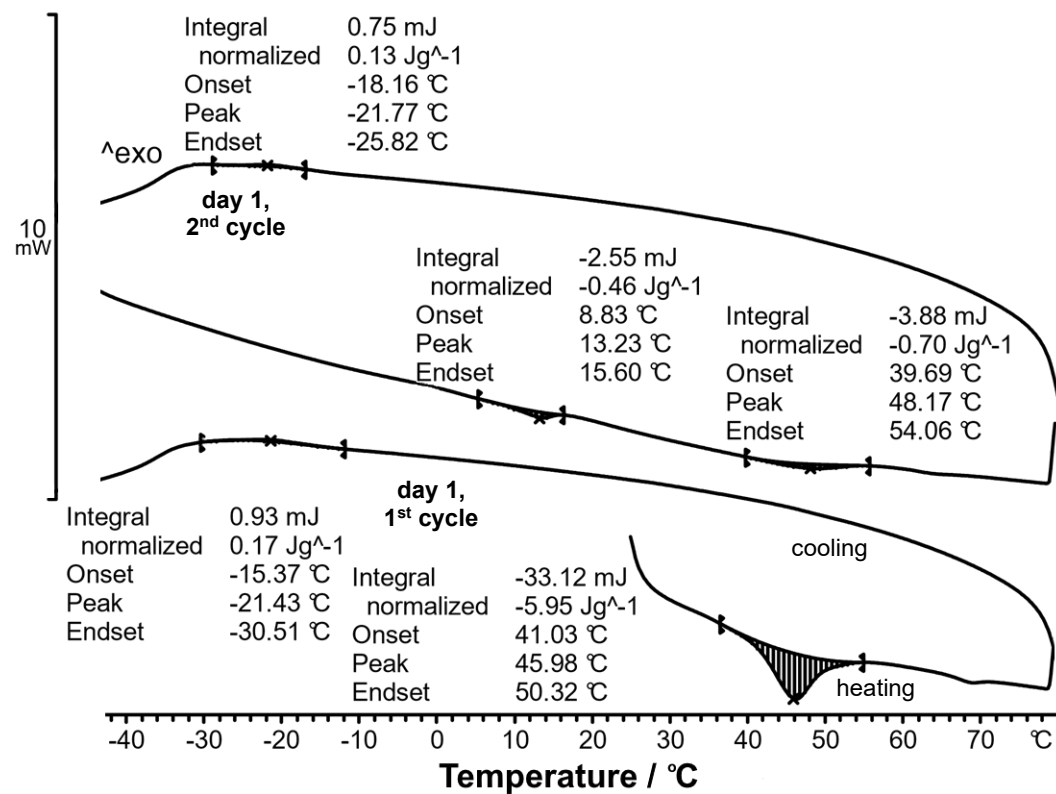
Poly[tris(2,2,2-trifluoroethoxy)(ferrocenylmethoxy)phosphazene], 22 – Day 1



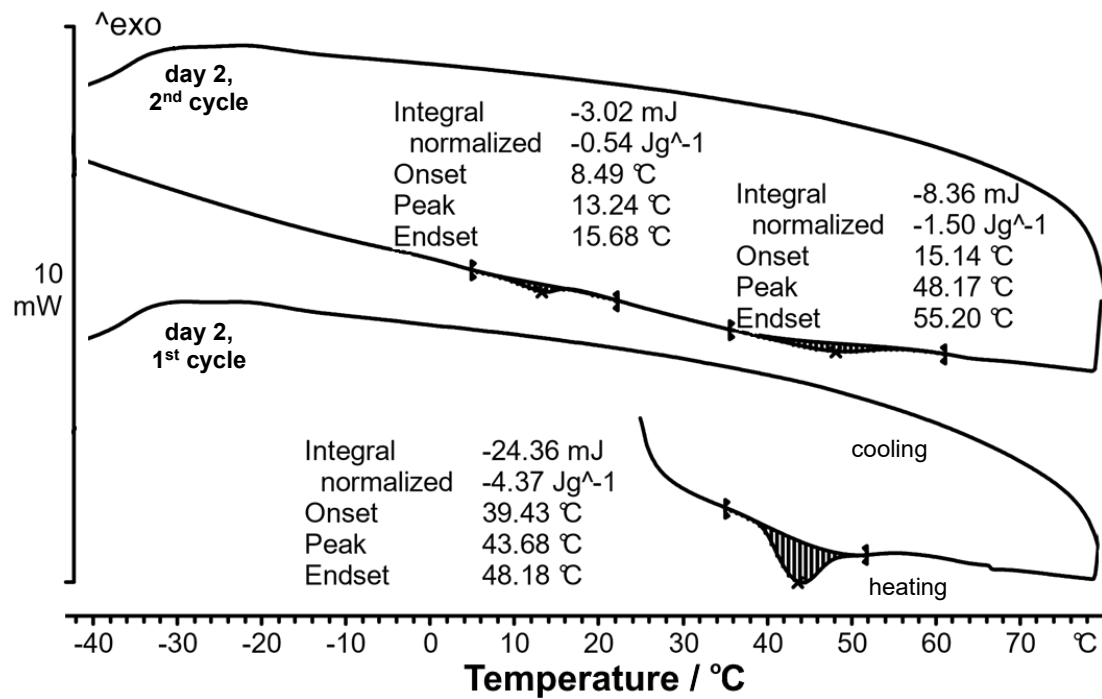
Poly[tris(2,2,2-trifluoroethoxy)(ferrocenylmethoxy)phosphazene], 22 – Day 2



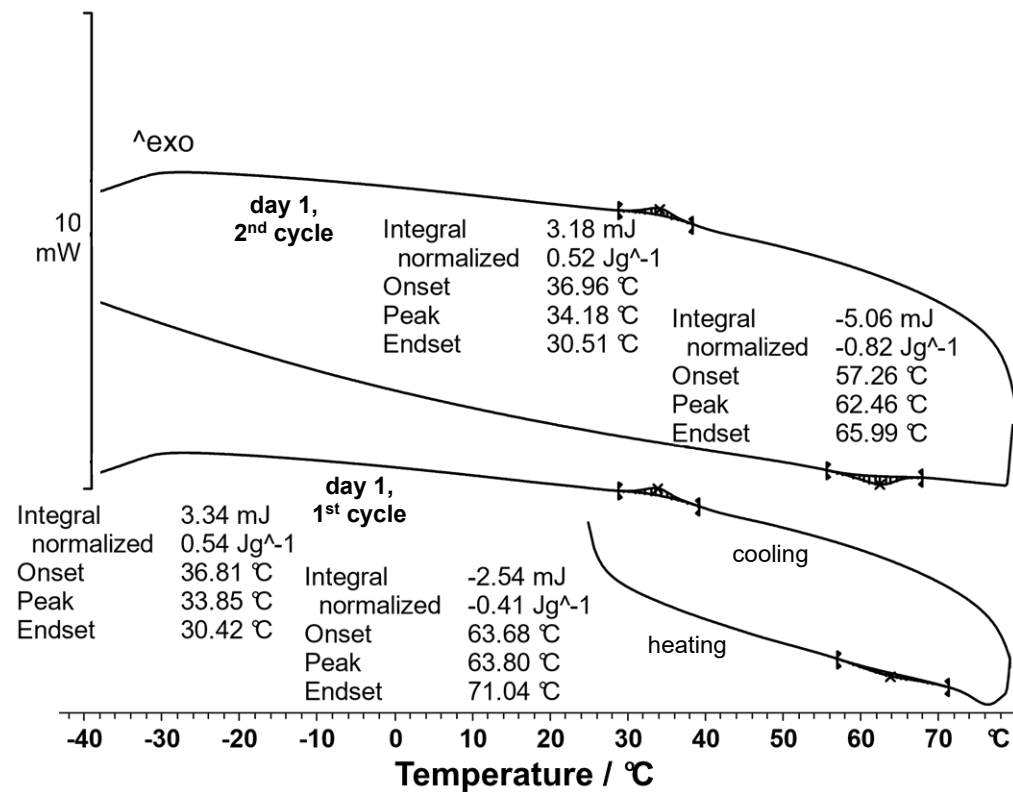
Poly[tris(2,2,2-trifluoroethoxy)(ferrocenylethoxy)phosphazene], 23 – Day 1



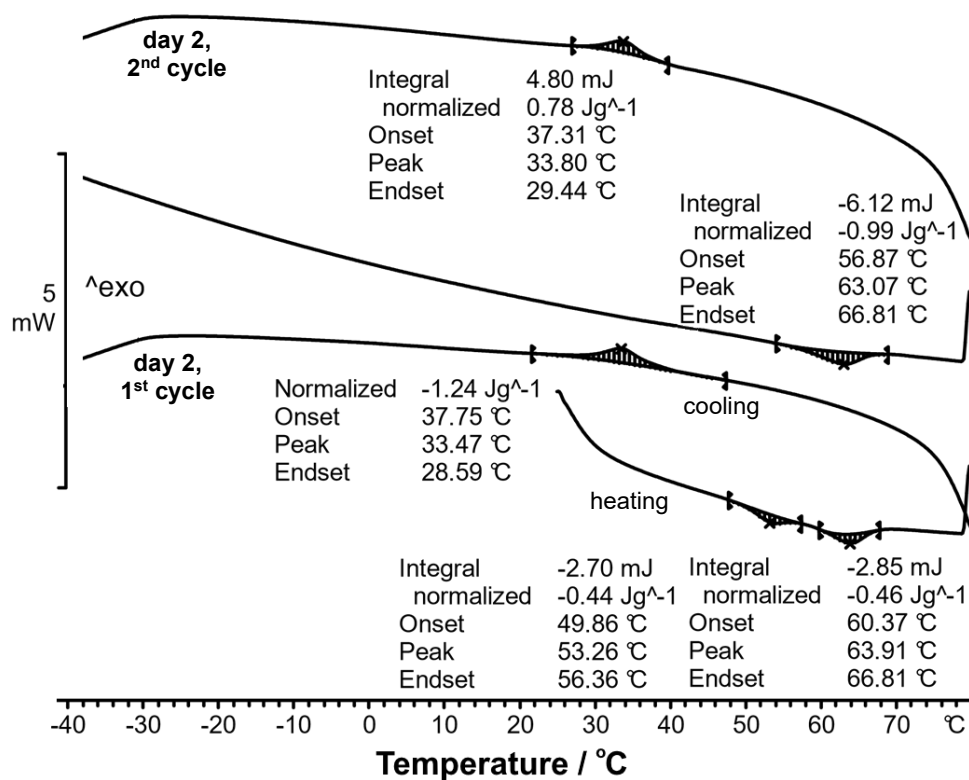
Poly[tris(2,2,2-trifluoroethoxy)(ferrocenylethoxy)phosphazene], 23 – Day 2



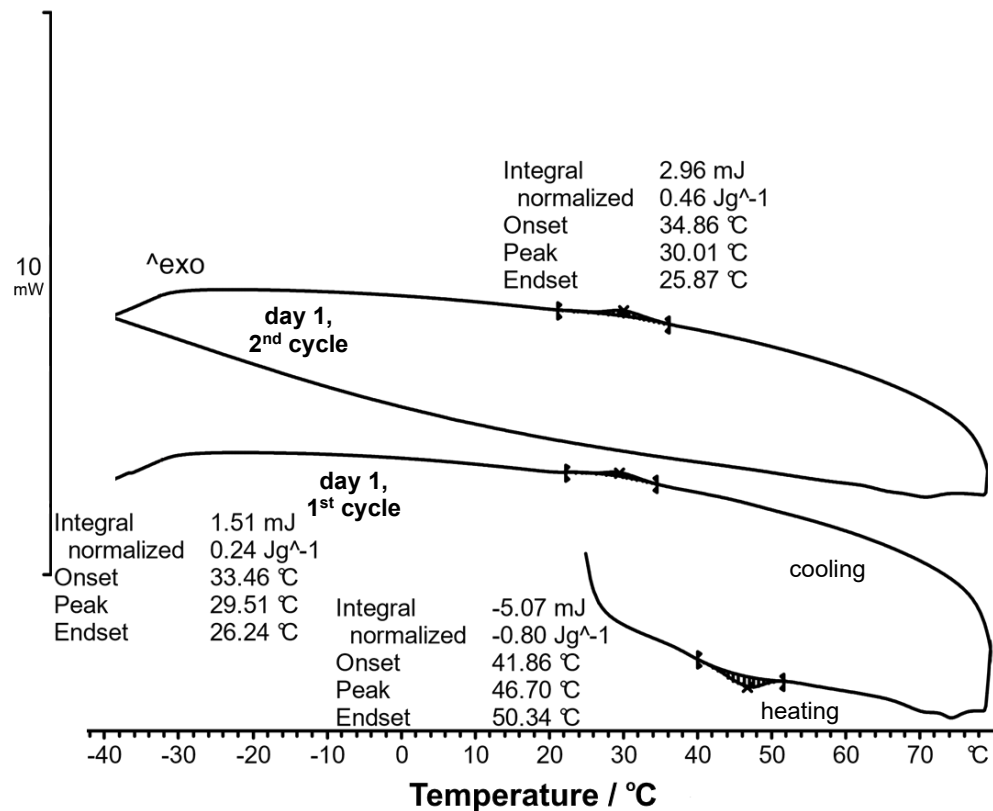
Poly[tris(2,2,2-trifluoroethoxy)(ferrocenylpropoxy)phosphazene], 24 – Day 1



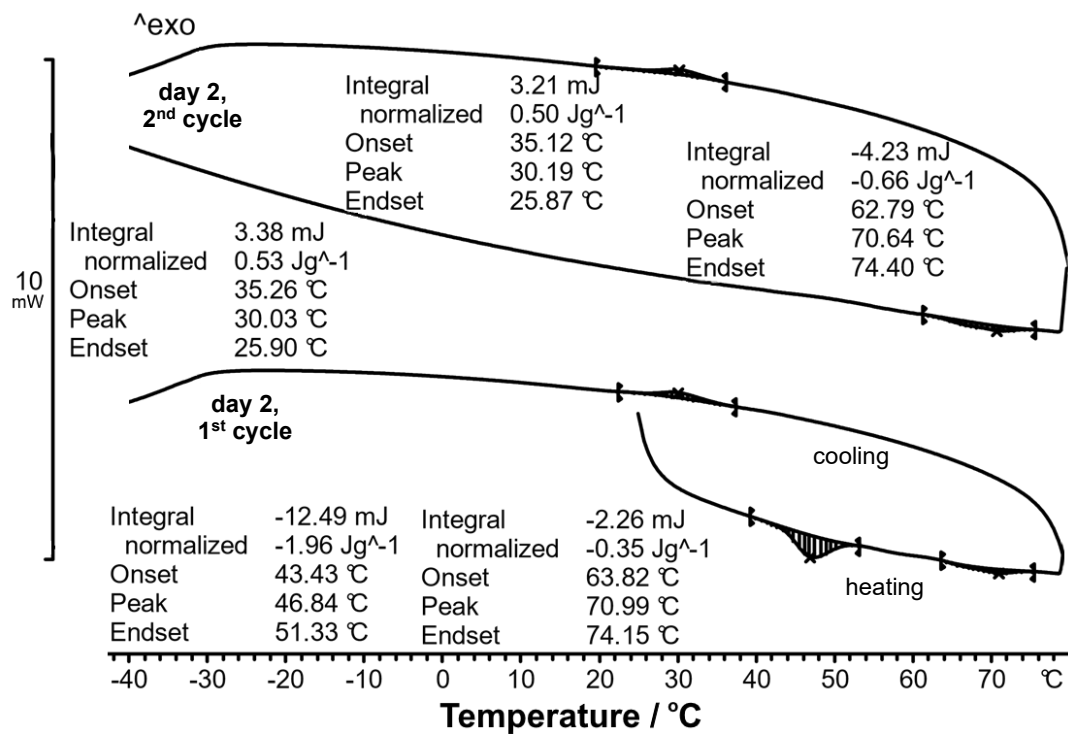
Poly[tris(2,2,2-trifluoroethoxy)(ferrocenylpropoxy)phosphazene], 24 – Day 2



Poly[tris(2,2,2-trifluoroethoxy)(ferrocenylbutoxy)phosphazene], 25 – Day 1



Poly[tris(2,2,2-trifluoroethoxy)(ferrocenylbutoxy)phosphazene], 25 – Day 2



Declaration

I, Maheshini Govender, declare that the thesis hereby handed in for the qualification Philosophiae Doctor in Chemistry at the University of the Free State is my own independent work and that I have not previously submitted the same work for a qualification at/in another university/faculty. I furthermore cede copyright of the thesis in favour of the University of the Free State.

Signed:

Date:
